بسم الله الرحمن الرحيم

Sudan University of Science and Technology (SUST)

College of Graduate Studies

Development of a Simplified Method for Non-Linear Analysis of Tall Buildings

تطوير طريقة مبسطة للتحليل اللاخطي للمباني العالية

A Thesis Submitted in Fulfillment of the Requirements for the Degree of Doctor of Philosophy in Civil Engineering

To the Dept. of Civil Engineering, College of Engineering, (SUST)

By:

Maaz Siddig Ibrahim Mohamed Tom

Supervisor:

Prof. Abdel Rahman Elzubeir Mohamed

November 2016

بسم الله الرحمن الرحيم

* اقرأ باسم ربك الذي خلق * خلق الإنسان من علق

* اقرأ و ربك الأكرم * الذي علم بالقلم * علم

الإنسان مالم يعلم *

صدق الله العظيم

الآيات ١-٥ سورة العلق

ABSTRACT

In this research, a simplified numerical method of static and dynamic, linear and nonlinear analysis of tall buildings is presented. The method is a development and generalization of the moment distribution methods. The first version named the moment transformation method (MT) was based on the rotations as the only degrees of freedom with lateral translations permitted. A computer program named MTProg was developed based on the method. The method is used for the analysis of tall buildings with axial deformations in the vertical members ignored. The method has then been developed to the moment-force transformation method (MFT), which incorporates the axial deformations in the vertical members in order to enable the analysis of super-tall buildings. The programs MFTProg and MFTProgV2 (Nonlinear version) were developed based on MTProg. The global and local second order P-Delta analysis of tall buildings subjected to vertical and horizontal loads were also incorporated by coupling the axial force and the bending moments in each of the vertical members with large lateral displacements at floor levels. Accordingly buckling cases have also been studied. The method was further developed to extract the dynamic properties of tall buildings. Displacements and different structural responses due to dynamic loadings are computed using the proposed method with the response spectrum and the time-history methods for both linear and second order analyses. Validity of the method was established by comparing the results of 2D and 3D buildings with those resulting from reliable finite element packages. The comparisons show that, the results are in good agreement thus verifying the accuracy of the proposed method. The MFT method shows the ability to analyze adequately and very fast tall buildings composed of hundreds of floors that can not be analyzed accurately using the established methods of analysis. The saving in computer storage and computing time provided by MFTProgV2 allow rapid re-analysis of the building to be accomplished in the preliminary analysis and design stages, and in the cases of repeated analysis types such as buckling and dynamic analyses of building. The ease in data preparation and interpretation of final results, compared with finite element packages is one of the main advantages of the method. For all these reasons the developed program MFTProgV2 is recommended to be used for the linear/nonlinear, static/dynamic and stability analyses of tall buildings.

المستخلص:

يعرض هذا البحث طريقة عددية مُبَسَّطة للتحليل الإستاتيكي والديناميكي، الخطي واللاخطي للأبنية العالية. الطريقة هي تطوير وتعميم لطرق توزيع العزوم. الصيغة الأولى هي طريقة نقل العزوم، وفيها استخدمت الدورانات فقط كدرجات حرية مع السماح بالتحركات الجانبية، وتمت حوسبتها بتصميم وتطوير البرنامج (MTProg). وهذه الطريقة يمكن إستخدامها في تحليل المباني التي يمكن تجاهل الإزاحات المحورية في أعضائها الرأسية. وقد طورت الصيغة الأولى لطريقة نقل العزوم و القوى لتأخذ في الإعتبار التشوهات المحورية في الأعضاء الرأسية مما يمكنها من الإستخدام في تحليل المباني شاهقة العلو. تم تطوير البرنامجين MFTProg و MFTProgV2 (النسخة اللاخطية) بناءً على MTProg. ادمجت أيضاً اللاخطية في التحليل، الناتجة عن العلاقة بين العزوم و القوى المحورية في كل من الأعضاء الرأسية في وجود إزاحات جانبية كبيرة، وبناءً على ذلك تمت دراسة الحالات اللازمة للإنبعاجات. تم تطوير الطريقة للقيام بحساب الخواص الديناميكية للمبنى، كما تم حساب الإزاحات وإستجابات المبنى المختلفة للأحمال الديناميكية في الحالتين الخطية واللاخطية، بإستخدام الطريقة المقترحة وبمساعدة طرق التحليل الديناميكية المختلفة كطريقة طيف الإستجابة وطريقة التاريخ الزمني. قورنت النتائج المتحصل عليها بنتائج حصل عليها بإستخدام برامج العناصر المحددة القياسية لمباني ثنائية الأبعاد وأخرى ثلاثية الأبعاد. وقد أثبتت المقارنات أن هنالك توافقاً جيداً بين النتائج يؤكد دقة الطريقة المقترحة. كما أوضحت الطريقة إمكانية إستخدامها بفاعلية في التحليل الدقيق والسريع للمباني شاهقة العلو المكونة من مئات الطوابق والتي يستحيل أو يصعب تحليلها بالطرق القياسية. والتوفير في حجم الذاكرة و في زمن الحل اللذين يوفرهما البرنامج يمكنّان من التحليل السريع والمتكرر للمبنى في مراحل تصميماته الأولية وأيضاً في الحالات التي تحتاج إلى التحليل المتكرر للوصول للحل كما في حالات تحليل الإنبعاجات أو عند حساب الخواص الديناميكية للمبنى. سهولة تجهيز وإدخال المعلومات وإستخراج وعرض النتائج النهائية مقارنة مع طرق العناصر المحددة القياسية يعتبران من المميزات الأساسية للطريقة. لكل هذه الأسباب يوصي بإستخدام البرنامج (MFTProgV2) في التحليل الخطي واللاخطي، والإستاتيكي والديناميكي، ودراسة إستقرارية المباني العالية.

DEDICATION

To the cherished memory of my father.

To my mother, whose prayers supplication gave me support and confidence.

To my patient family, whose forbearance has been incentive to work hard on this research.

To the new generation my kids, Rayyan, Mahmoud, Baddory, Riham and Mohamed, I hope for them good future.

ACKNOWLEDGMENTS

I would like to express my sincere gratitude to:

Prof. Abdel Rahman Elzubeir Mohamed

For his guidance and supervision, patience, encouragement, support and friendly approach towards me throughout the lengthy process of this work.

I wish to thank my wife Eng. Manahil for all the patience and support she has provided.

I am thankful to my dear brother, Automation Engineer Osama, who put me in the right track.

Thanks a lot to my brothers Engineers Aymen, Ahmed Saeed, Amro, Elhadi, Ahmed Norein, for their continuous help and support.

Lastly but not least the individuals whose names are over looked and not mentioned above for every kind of support, help and cooperation in this work.

TABLE OF CONTENTS

LIST OF FIGURES

LIST OF TABLES

CHAPTER ONE

General Introduction

1.1 Introduction

Tall buildings are highly affected by lateral loadings such as wind and earthquake loads. The effects of these lateral forces may be resisted by lateral stiff elements such as shear walls available around elevator shafts and staircases. The unsymmetrical arrangement of the vertical members in the building plan cause twist deformations in the level of the floors plans. In this case the problem becomes more complex and a three dimensional analysis should be carried out instead of the simplified two dimensional analysis. In practice, a full three-dimensional finite element analysis of tall buildings is not simple because of the computer storage problem and the computing time cost factors especially in the design stage when the structure has to be modified several times.

A lot of researches have been conducted in the field of computerized solution of large scale problems with huge numbers of unknowns as the case of three dimensional full finite element model of tall building. Research is also ongoing for the simplification of analyses of tall buildings so as to be carried out with minimum cost. For all these reasons accurate simplified methods of analysis of tall buildings are required.

In most of the simplified methods of analysis, there exist assumptions that lead to wrong results in some of the practical cases. For example methods based on the continuum theory or the equivalent column theory which should always be applied for buildings of equal floor heights, buildings with no set back, cases of contra flexure (zero moments) in the mid of the members, sometimes neglecting the flexural stiffness of the floors, or for very regular structures where the geometric and stiffness characteristics of structural elements are constant throughout the building's height, Bozdogan and Ozturk (2010), Parv and Nicoreac (2012).

A good simplified method must be reliable and supported by physical reality. It must be able to include a wide range of design parameters, such as the positions of a structural member as well as its orientation and dimensions. It should not require large computer storage or long computing time so that a preliminary analysis can be carried out and modified several times before the final design stage.

1.2 Problem Statement

The importance of performing the nonlinear analysis for tall buildings has been pointed out by various researchers, Moghadam and Aziminejad (2004) and Ikago Kohju (2012). If the building to be analyzed is very tall and slender and the axial forces are large or the individual columns are slender, then the lateral displacements become very large and affect the building geometry. This problem results in extra increase of the displacements and stresses, and second order or P-Delta analysis should be carried out, Smith and Coull (1991), Dobson and Arnott (2002).

In some of the available commercial analysis packages, the considerations of the nonlinearity in the static and the dynamic analysis of tall buildings are subjected to several limitations. Examples of these are incorporation of the global geometric stiffness while neglecting the local stress stiffening of the members due to the effects of the axial loads, Dobson and Arnott (2002). Sometimes in some commercial packages there is no possibility to include the effects of geometric nonlinearity during the dynamic analysis mode. In the iterative methods of P-Delta analysis used by most of the analysis packages, the results tend to diverge when the vertical loads tend to reach the critical buckling load at any of the vertical members. Since the critical forces are not known before performing the analysis, the convergence of the results to the correct answers will not be ensured. Also in the design codes, the effects of the nonlinearity are incorporated approximately by modifying some of the design parameters, e.g. amplified moments, as in UBC-97 and ACI 318-14, and, extended effective lengths as in BS8110 (1997). In methods of analysis of tall buildings and in order to include the P-Delta effects, some authors suggest the introduction of an equivalent fictitious member of negative properties, Wilson and Habibullah (1987), Smith and Coull (1991), and this is not acceptable in most of the analysis packages.

As stated above, the analysis of tall buildings needs some simplifications especially in the preliminary analysis and design stages, in order to reduce the large amount of unknowns when using the conventional exact methods of analysis. The problem becomes more severe in the nonlinear analyses (e.g. P-Delta, Buckling, dynamic, time dependant columns shortening), which need extra storage and extra time because most of these methods require several iterations for the results to be converged to final values.

With all these requirements, this work presents development of a simplified method used to analyze two dimensional and three dimensional tall buildings and suitable for the analysis of framed shear walls buildings and for super tall buildings such as tube and outrigger buildings subjected to both vertical and horizontal loading. The proposed method has been developed to incorporate linear and nonlinear static and dynamic analyses. Due to its simplicity, the method greatly saves the effort faced from the difficulties of the data entry and the interpretation of the vast amount of the output results when using the conventional finite elements methods of analysis. The saving in computer storage and computing time provided by the developed program that based on the proposed method, allow rapid re-analysis of the building to be accomplished in the preliminary analysis and design stages, and in the cases of repeated analysis types such as in the buckling and vibration problems. The future use of the proposed simplified method on the more compacted very low memory today's devices (e.g. handhelds, pocket computers and even mobile phones) is also a possibility.

1.3 Objectives

1) To carry out a comprehensive literature review in the field of the linear and nonlinear static and dynamic analysis and elastic stability of tall buildings.
2) To develop a simplified theoretical approach for the linear and nonlinear, static and dynamic analysis of tall buildings.
3) To develop computer programs to be used for advanced analysis of tall buildings easily, both in the data entering and in the interpretation of the output results.
4) To develop an optimized theory, such as a development based on generalization of the simple moment distribution methods, and optimized algorithms used for analysis of tall buildings that can be implemented in very low memory devices, such as pocket PCs and smart phones devices.
5) To verify the accuracy of the results obtained by comparisons with results from known solvers.
6) To demonstrate the capability of the developed theory and programs to analyze accurately tall buildings that are impossible or very difficult to be analyzed by established accurate methods.

1.4 Methodology of Research

The research has been carried out as follows:

1- Literature Review and study of theoretical background.

2- Formulation of the proposed theory.

3- Development of the computer programs based on the formulated theory.

4- Application of the programs for different structures, analysis and verifications of results, and the comments and conclusions.

5- Drawing recommendations for tall buildings analysis and recommendations for future studies.

1.5 Outlines of thesis

The thesis includes the following:

1- Chapter one presents a general introduction.

2- Chapter two presents a literature review of the methods of analysis of tall buildings.

3- Chapter three presents the proposed theory.

4- Chapter four presents the developed computer program.

5- Chapter five presents the program applications and solution of some problems.

6- Chapter six presents two cases study, the results obtained and the analysis and discussion of the results.

7- Chapter seven includes the conclusions and recommendations.

CHAPTER TWO

Literature Review

2.1 Introduction

Simplified methods of static and dynamic analysis for the effects of vertical and horizontal loads on tall building are required, especially in the preliminary design stage when the proposed structural system has to be analyzed several times before the final agreement.

Due to the huge gravity loads and the possible large lateral displacements, the nonlinear analysis should be carried out to adequately design the tall buildings.

In the analysis of large structural systems such as the tall buildings which include huge numbers of unknowns, there arise a lot of difficulties such as:

- The capability of the hardware of the computing machine.
- The machine running time which is proportional to the total number of unknowns.
- The interpretation of the vast amount of the analysis results.
- The need that may arise for new rearrangements or changing of the structural system.

In literature, there are lots of conducted researches, which can be classified into different types of problems formulation and solution methods, such as:

- Simple manual arithmetical methods, e.g. Portal and Cantilever methods.
- Differential equations and Continuum methods of analysis.
- Simplified finite element and matrix methods of analysis.
- Methods of Simplifying the models and Reduction Techniques.

Each one of the mentioned methods is used with limitations and sometimes tailored for a certain type of structural system.

In the following sections the available simplified analysis methods are reviewed and classified.

2.2 Simple Manual Arithmetical Methods

For preliminary design of tall frames, as information regarding stress resultants due to lateral loads is required even before member dimensions are known, the cantilever and portal methods are sought in practice for the specific reason that they do not require cross sectional areas for the analysis. When using these methods of analysis for lateral loads, the analysis for vertical loads can be made in the same way as for the braced frames by using any of the sub-frame methods.

According to Manicka and Bindhu (2011), there are two versions of the portal method. One is the simplified portal method and the other is the improved portal method.

In the simplified portal method, the storey shear is distributed among the columns considering that each of the outer columns resists half the shear resisted by any of the internal columns, and in the improved portal method, the storey shear is distributed among the columns in proportion to the tributary length of the spans between the columns. Manicka et al, proposed an alternative analysis method which they called the Split frame method. The method splits vertically the whole frames into separated simple frames each of one containing only one bay subjected to lateral loads calculated from the dimensions of all the bays. The method gives almost the same answer as that of the improved portal method.

As a conclusion, the cantilever and the simplified and improved portal methods of analysis together with the Split method proposed by Manicka et al, can be used only for analysis of relatively short un-braced portal frames subjected to lateral wind loads or equivalent static seismic loads, also they can’t be used to calculate the dynamic properties of the frames (e.g. natural frequencies and mode shapes), and have no ability to calculate the lateral stiffness of the building frame and therefore the drift and the lateral displacements of the frame.

2.3 Differential Equations and Continuum Methods of Analysis

Based on the continuum theory, the researchers developed and solved approximately miscellaneous types of problems, ranging from a very simple problem used to distribute the lateral loads between the vertical members in a relatively short building, up to the analysis of a more complicated tube and outrigger structural systems used in the ultra tall buildings. The type of the problems also can be classified ranging from a simple static problem up to a more complicated dynamic one, used to calculate the dynamic properties of the building such as the vibration frequencies and their corresponding mode shapes.

Following are some researches and developments based on these types of analyses:

Jaeger, Mufti and Mamet (1973), proposed an analytical theory for the analysis of tall three dimensional multiple shear wall buildings. The basis of their theory was the continuum approach in which the floors of the building are replaced by an equivalent continuous medium. Their results were compared with data obtained by the finite element method and experiments conducted on a seven storey multiple, shear wall model.

A Simplified method was presented by Coull, Bose and Abdulla Khogali (1982), used for the analysis of bundled tube structures subjected to lateral loads. In the method, the rigidly-jointed perimeter and interior web frame panels were replaced by equivalent orthotropic plates. The force and stress distributions in the substitute panels were assumed to be represented by polynomial series in the horizontal coordinates, the coefficients of the series being functions of the height only. The unknown functions were determined from the principle of the least work. By incorporating simplifying assumptions regarding the form of stress distribution in the frame panels, the structural behavior was reduced to the solution of a single second-order linear differential equation, enabling closed-form solutions to be obtained for the standard load cases, and solutions were obtained from design curves.

A simplified approximate analysis of lateral load distribution in structures composed of different assemblies was presented by Coull and Tag Eldeen Husein (1983). The load distribution on each assembly was assumed to be represented by a polynomial in the height coordinate, together with a concentrated interactive force at the top. A set of

flexibility influence coefficients, relating the deflection at any level to any particular load component, was established for each assembly, the continuum approach was used to analyze individual assemblies. By making use of the equilibrium and compatibility equations at any desired set of reference levels, the load distribution on each assembly was determined. Good results were achieved for regular structures by using no more than about six reference levels.

As an alternative a simplified analysis of shear-lag in framed-tube structures with multiple internal tubes was presented by Lee, Guan and Loo (2000). In their work a simple numerical modeling technique was proposed for estimating the shear-lag behavior of framed-tube systems with multiple internal tubes. The system was analyzed using an orthotropic box beam analogy approach in which each tube is individually modeled by a box beam that accounts for the flexural and shear deformations, as well as the shear-lag effects. The method idealizes the tube(s)-in-tube structure as a system of equivalent multiple tubes, each composed of four equivalent orthotropic plates capable of carrying loads and shear forces. The numerical analysis so developed was based on the minimum potential energy principle in conjunction with the variational approach. The shear-lag phenomenon of such structures was studied taking into account the additional bending stresses in the tubes. Structural parameters governing the shear-lag behavior in tube(s)-in-tube structures were also investigated through a series of numerical examples. The method results were verified through the comparisons with a 3-D frame analysis program.

An approximate hand-method for seismic analysis of asymmetric building structure having constant properties along its height was presented by Meftah, Tounsi and El Abbas (2007). The method used the continuum technique and D'Alembert's principle to derive the governing equations of free vibration and the corresponding eigenvalue problem. By applying the Galerkin technique, a generalized method was proposed for the free vibration analysis. Simplified formulae were given to calculate the circular frequencies and internal forces of a building structure subjected to earthquakes. The accuracy of the method was demonstrated by a numerical example, in which the results obtained were compared with finite element package.

A method for lateral stability analysis of wall-frame buildings including shear deformations of walls was presented by Bozdogan and Ozturk (2010). Their study presented an approximate method based on the continuum approach and transfer matrix method. In the method, the whole structure was idealized as an equivalent sandwich beam which includes all deformations. The effect of shear deformations of walls was taken into consideration and incorporated in the formulation of the governing equations. Initially the stability differential equation of this equivalent sandwich beam was presented, and then shape function for each storey was obtained by the solution of the differential equations. By using boundary conditions and stability storey transfer matrices obtained by shape functions, system buckling load were calculated. To verify the presented method, four numerical examples were solved. The results of the samples demonstrated the comparison between the presented method and the other methods given in the literature.

Also Bozdogan and Ozturk (2010), presented a Vibration analysis method of asymmetric shear wall structures using the transfer matrix method. In the method the whole structure was assumed as an equivalent bending-warping torsion beam. The governing differential equations of equivalent bending-warping torsion beam were formulated using the continuum approach and were posed in the form of a simple storey transfer matrix. By using the storey transfer matrices and point transfer matrices, which take into account the inertial forces, the system transfer matrix was obtained. Natural frequencies were calculated by applying the boundary conditions. The structural properties of the building may change in the proposed method. A numerical example were solved and presented by means of a program written in MATLAB to verify the proposed method. The results obtained were compared with other valid method given in the literature.

Bozdogan (2011), developed a differential quadrature method (DQM). In his work, free vibration analysis of wall-frame structures were studied. A wall-frame structure was modeled as a cantilever beam and the governing differential equations were solved using the (DQM). At the end of the study, a sample taken from literature was solved and the results were evaluated in order to test the convenience of the method.

A simplified method for high-rise buildings was developed by Takabatake (2012). In his work an analytical theory for doubly symmetric frame-tube structures was established by applying ordinary finite difference method to the governing equations proposed by the one-dimensional extended rod theory. Takabatake, claims that his theory can be usable in the preliminary design stages of the static and dynamic analyses for a doubly symmetric single or double frame-tube with braces in practical use, and it would be applicable to hyper high-rise buildings, e.g. over 600m in the total height, because the calculation is very simple and very fast. Also the approximate method for natural frequencies of high-rise buildings was presented in the closed-form solutions and it was stated to be necessary for seismic retrofitting of existing high-rise buildings subject to earthquake wave included relatively long period.

Another simplified method for nonlinear dynamic analysis of shear-critical frames is developed by Guner and Vecchio (2012). In their work, an approach was presented by which a static analysis method can be modified for a dynamic load analysis capability in a total-load secant-stiffness formulation, and a nonlinear static analysis method was developed for the performance assessment of plane frames. The primary advantage of the method is its ability to represent shear effects coupled with axial and flexural behaviors through a simple modeling approach. In the study, the method was further developed to enable a dynamic load analysis. Among the developed and implemented formulations there are an explicit three-parameter time-step integration method, based on a total-load secant-stiffness formulation, and dynamic increase factor formulations for the consideration of strain rates. The method was applied to eleven previously tested specimens, subjected to impact and seismic loads, to examine its accuracy, reliability, and practicality. The method was found to simulate the overall experimental behaviors. Strengths, peak displacements, stiffness, damage, and failure modes and vibrational characteristics were calculated.

An approach to static analysis of tall buildings with a combined tube-in-tube and outrigger-belt truss system subjected to lateral loading was presented by Jahanshahi, Rahgozar and Malekinejad (2012). The method was presented a technique for static analysis of the system while considering shear lag effects. In the process of replacing the

discrete structure with an elastically equivalent continuous one, the structure was modeled as two parallel cantilevered flexural-shear beams that are constrained at the outrigger-belt truss location by a rotational spring. Based on the principle of minimum total potential energy, simple closed form solutions were derived for stress and displacement distributions. Standard load cases were considered. The formulas proposed in the method were compared to a finite element computer package. Results obtained from the proposed method for 50 and 60 storey tall buildings were compared to those obtained using SAP2000.

A "Global structural analysis of central cores supported tall buildings compared with FEM" was presented by Prav and Nicoreac (2012). The focus of their article was to present an approximate method of calculation based on the equivalent column theory. By applying the geometrical and stiffness characteristics of the structure the displacements in the two directions, the rotation of the structure, critical load, shear forces, bending moments for each resisting element and the torsional moment of the structure may be determined. The results obtained using the approximate method was compared with the results obtained using an exact calculation based on Autodesk Robot Structural Analysis and ANSYS 12.1. The equivalent column theory is an approximate method used for comparing and checking the results obtained by the Finite Element Method (FEM).

2.4 Simplified Finite Element and Matrix Methods of Analysis

Simplified methods of solution for the two and three dimensional frames based on the matrix and finite element methods of analysis were developed.

In Macginely and Choo (1990) and Ghali et al (2009), a two dimensional analysis based on building composed of parallel assemblies and on the shear wall frame interaction system were presented. A three dimensional analysis of shear walls structures was proposed by Ghali et al. In their method, the total degrees of freedom were reduced to three per each floor. The global stiffness matrix was constructed from all shear walls, with the assumptions of the rigid diaphragm and neglection of the floor out of plane stiffness. The external lateral loads were applied at the assumed origin, the global

displacements were obtained and the local displacements and stresses were calculated accordingly.

A two-level finite element technique of constructing a frame super-element was created by Leung and Cheung (1981), to reduce the computational effort for solving large scale frame problems. The ordinary finite element method was used first to yield matrices for the beam members. Then the nodal displacements of all the nodes were related to those of a small number of selected joints (master nodes) in the frame by means of global finite element interpolating functions. Thus the frame was considered as a super-element connected to other elements by means of the master nodes. The accuracy of solution may be improved either with finer subdivision or by taking more master nodes inside each super-element.

Also Leung (1983) presented another method, for the analysis of plane frames by microcomputer. The method was based on the assumptions that, the distribution of the vertical and rotational displacements at the nodes of a story is characterized by the concept of distribution factors which are relative nodal displacements. The distribution factors were allowed to vary from floor to floor and were determined by using three floors at a time. These are calculated once only for floors having identical members. By means of the distribution factors, the number of degrees of freedom was reduced to three at any one floor. Therefore, it was possible for a micro-computer to handle a large number of stories without difficulty. The resulting displacements and internal forces were compared with full finite element analyses for a number of cases even with sudden changes of stiffness.

The two dimensional method was further generalized by Leung (1985) to solve three dimensional frames. It was also based on the fact that the deformation pattern at the nodes of a particular floor may be predetermined before loading. These relative displacements were called distribution factors which govern the distribution of displacements. A number of free parameters were determined in the global analysis from the applied loading. These parameters were called mixing factors. The linear combinations of the distribution factors with mixing factors as weighting factors give the actual displacements at the nodes. Structural idealizations of coupled shear walls by

beams and columns were recommended. In order to improve the results another three additional sets of global distribution factors were introduced by Leung (1988) to account for the uneven elongation (shortening) of the columns having unevenly distributed stiffness along the height and across the floor plane. The total number of unknowns per floor was reduced. Using the concept of the two-level finite-element method, the global distribution factors of the building frame were obtained. The global and local distribution factors together predicted the lateral and torsion deflections and internal nodal displacements accurately.

In a similar manner, Wong and Lau (1989), presented a simplified finite element for analysis of tall buildings. It was based on the assumption that the warping displacement modes of a floor and the differences between neighboring floors are mainly determined by the local structural characteristics. Once the warping modes are determined, these modes are taken as the basis of generalized coordinates. Then, the problem can be reduced to a formulation in which only the rigid body displacements and the warping generalized coordinates of each floor are unknown. Results obtained from the examples show that the simplified analysis method was satisfactory in displacements as well as in internal forces when suitable warping modes from a multi-storey sub-model are chosen. The authors claimed that the proposed simplified finite element method using a multi-storey sub-model one-floor-unknown scheme is inexpensive and is able to yield sufficiently good results for practical design purposes. The method can also be generalized to solve dynamic problems.

A finite strip analysis method was developed by Swaddiwudhipong, Lim and Lee (1988). The method was presented for the analysis of coupled frame-shear wall buildings subjected to lateral loads. Appropriate displacement functions of admissible class were adopted such that the problem is uncoupled and can be conveniently solved term by term. Although this uncoupling property is valid only when the building is uniform throughout its height, the method was extended to buildings with non-uniform section by employing the concept of equivalent uniform section. Several numerical examples were presented to show the accuracy and validity of the proposed scheme. The method required a small

core storage and short computing time and suitable for implementation on any of the personal computers commonly available in most engineering design offices.

Giovanni (2009), in his PhD thesis dissertation showed the different types of the structural condensations which can be used in the structures simplification, and these were, the static condensation, the dynamic condensation (Guyan's reduction method) and the exact dynamic condensation method developed by Leung (1978). Leung method efficiently reduces the order of dynamic matrices without introducing further approximation by representing the passive co-ordinates in terms of the active ones exactly. The resulting frequency dependent eigenvalue problem is solved by a combined technique of Sturm sequence and subspace iteration. The method is a condensation method in dynamic economization and dynamic substructure analysis and it converges to the natural modes of interest always, even for the extreme case that the natural modes of the overall structure are multiple and very close to the partial modes of its substructures, a case when the normal methods fail.

A method for lateral static and dynamic analyses was presented by Bozdogan (2011). The study presented an approximate method which was based on the continuum approach and one dimensional finite element method to be used for lateral static and dynamic analyses of wall-frame buildings. In the method, the whole structure was idealized as an equivalent sandwich beam which includes all deformations. The effect of shear deformations of walls was considered and incorporated in the formulation of the governing equations. Initially the differential equations of the equivalent sandwich beam were written and the shape functions and stiffness matrix were obtained by solving the differential equations. For static and dynamic analysis the lateral forces and masses were applied on the storey levels. Angular frequency and modes were obtained by using system mass and system stiffness matrices. Numerical examples were solved using MATLAB to verify the presented method.

2.5 Methods of Simplifying the Models and Reduction Techniques

The simplification of the modeling can be treated in the structural analysis stage in order to reduce and simplify the problem solution. The reduction technique can be classified in the following types:

1. Symmetry and anti-symmetry of the building plan
2. Two-dimensional model of non-twisting structures.
3. Two-dimensional models of structures that translate and twist.
4. Lumping Techniques which can be classified into lateral lumping and vertical lumping
5. Wide-column and deep-beam analogies.

In the work of Akis (2004), the main purpose of the study was to model and analyze the non-planar shear wall assemblies of shear wall-frame structures. Two types of three dimensional models, for open and closed section shear wall assemblies, were developed. Those models were based on conventional wide column analogy, in which a planar shear wall was replaced by an idealized frame structure consisting of a column and rigid beams located at floor levels. The rigid diaphragm floor assumption was also taken into consideration. The connections of the rigid beams were released against torsion in the model proposed for open section shear walls. For modeling closed section shear walls, in addition to that the torsional stiffness of the wide columns were adjusted by using a series of equations. Several shear wall-frame systems having different shapes of non-planar shear wall assemblies were analyzed by static lateral load, response spectrum and time history methods where the proposed methods were used. The results of those analyses were compared with the results obtained by using common shear wall modeling techniques.

A simplified finite element modeling of multi-storey buildings was proposed by Li, Duffield and Hutchinson (2008). The study discussed how to substructure different parts of a multi-storey building with cubes having equivalent stiffness properties. As a result, the mesh density of the whole building is reduced significantly and the computational time and memory normally consumed by such complex structural dimensions and material properties will also be reduced. The simplified analysis results of a high-rise frame structure with a concrete core were used to explore the reliability of the proposed method. In the study a typical 32-storey high-rise building was modeled with one storey blocks. Force-Displacement relationship calibration was carried out to find the proper simplified cubic model. According to the study, the equivalent cubic method was not suitable for dynamic analysis. Further investigation focusing on the overall behavior of

the structural model built using the equivalent cubic method needs to be conducted to ensure the connection properties between floors work correctly.

2.6 Miscellaneous Researches Conducted to Study and Improve the Structural Systems of the Tall Buildings

Otani (1979), showed that, the nonlinear analysis of a reinforced concrete building is difficult because inelastic deformation is not confined at critical sections, but spreads throughout the structure and because stiffness of the reinforced concrete is dependent on a strain history. The paper reviewed the behavior of reinforced concrete members and their sub-assemblies observed during laboratory tests. Then different hysteresis and analytical models of reinforced concrete members were reviewed, and their application to the simulation of building model behavior was discussed. In the paper the behavior of reinforced concrete buildings, especially under earthquake motion, was briefly reviewed. Otani concluded that, his method is useful and reliable, when a structure can be idealized as plane structures, but more research required to understand the effect of slabs, gravity loads, and biaxial ground motion on nonlinear behavior of a three-dimensional reinforced concrete structure.

A study conducted by Moghadam and Aziminejad (2004), for the interaction of torsion and P-Delta effects in tall buildings", evaluated the importance of asymmetry of building on the P-Delta effects in elastic and inelastic ranges of behavior. The contributions of lateral load resisting system, number of stories, degree of asymmetry, and sensitivity to ground motion characteristics were assessed. In the study four buildings with 7, 14, 20 and 30 story were designed based on typical design procedures, and then their elastic and inelastic static and dynamic behavior, with and without considering P-Delta effects, were investigated. Each building was considered for 0%, 10%, 20% and 30% eccentricity levels. The results indicated that the type of lateral load resisting system played an important role in degree that torsion modifies the P-Delta effects. It was also shown that although in the elastic static analyses, torsion always magnified the P-Delta effects, but the same not always true for dynamic analyses. The results of dynamic analyses also showed high level of sensitivity to ground motion characteristics.

The main results of the study were as follows:

1. In the elastic static analyses, effect of P-Delta always is increasing, as number of stories of buildings or their eccentricity increased.
2. In the elastic or inelastic dynamic analyses, the effects of P-Delta sometimes increased the response and sometimes decreased the responses.
3. “Importance of interaction of torsion and P-Delta effect” mainly depends on the type of lateral load resisting system of building. The results indicated that the type of lateral load resisting system played an important role in degree that torsion modifies the P-Delta effects. It was concluded that the characteristics of lateral load resisting system had far more importance compared with the number of stories in building.
4. It was seen that the effects of P-Delta is quite sensitive to ground motion characteristics such as the frequency content of earthquake. In inelastic analyses, the sensitivity is still important but less than the elastic dynamic cases. In general, the sensitivity to ground motion increased, as the eccentricity increased.
5. In elastic or inelastic dynamic analyses, increase in eccentricity caused change in the effect of P-Delta. The change is very important in elastic analyses and is somewhat less important in inelastic analyses. However, the variation is not have a constant increasing or decreasing trend. One of the reasons is the fact that with increase in the eccentricity, the mass moment of inertia has not increased in all cases.

A nonlinear finite element analysis of tall buildings was presented by Marsono and Wee (2006). The structural behaviors and mode of failure of reinforced concrete tube in tube tall building via application of computer program namely COSMOS/M were presented. Three dimensional quarter model was carried out and the method used for the study was based on non-linearity of material. A substantial improvement in accuracy was achieved by modifying a quarter model leading deformed shape of overall tube in tube tall building to double curvature. The ultimate structural behaviors of reinforced concrete tube in tube tall building were achieved by concrete failed in cracking and crushing. The model presented in the paper put an additional recommendation to practicing engineers in conducting non-linear finite element analysis (NLFEA) quarter model of tube in tube type of tall building structures.

The findings of the study were summarizing as follow:

1. The quarter model was capable to perform non-linearity behavior up to ultimate limit state.

2. Modified boundary condition by assigning restraint at *X*-direction at all slab edges, fully restraint at wall bottom ends was considered appropriate in generating a double curvature profile as expected in tube in tube model.

3. NLFEA in tube in tube building performed well using non-linear concrete stress-strain curve up to 32 steps of non-linearity and yields the ultimate behavior of tall building.

4. Modified quarter model, which included the full configuration of shear wall, was found to be appropriate in modeling the tube in tube tall building as quarter section. Thus, the behavior of coupling beams was successfully presented out.

A study conducted by Bayati, Mahdikhani and Rahaei (2008) presented to optimize the use of multi-outriggers system to stiffen tall buildings. They stated that "in modern tall buildings, lateral loads induced by wind or earthquake forces are often resisted by a system of multi-outriggers". An outrigger is a stiff beam that connects the shear walls to exterior columns. When the structure is subjected to lateral forces, the outrigger and the columns resist the rotation of the core and thus significantly reduce the lateral deflection and base moment, which would have arisen in a free core. During the last decades, numerous studies have been carried out on the analysis and behavior of outrigger structures. But the question remained that how many outriggers system are needed in tall buildings? The paper presented the results of an investigation on drift reduction in uniform belted structures with rigid outriggers, through the analysis of a sample structure built in Tehran's Vanak Park. Results showed that using optimized multi-outriggers system can effectively reduce the seismic response of the building. In addition, the results showed that a multi-outriggers system can decrease elements and foundation dimensions.

Jameel et al (2012), were carried a research to optimize structural modeling for tall buildings. They were concluded that it is a common practice to model multi-storey tall buildings as frame structures where the loads for structural design are supported by beams and columns. Intrinsically, the structural strength provided by the walls and slabs are neglected. The consideration of walls and slabs in addition to the frame structure modeling shall theoretically lead to improved lateral stiffness. Thus, a more economic structural design of multi-storey buildings can be achieved. In their research, modeling

and structural analysis of a 61-storey building were performed to investigate the effect of considering the walls, slabs and wall openings in addition to frame structure modeling. Sophisticated finite element approach was adopted to configure the models, and various analyses were performed. Parameters, such as maximum roof displacement and natural frequencies, were chosen to evaluate the structural performance. It was observed that the consideration of slabs alone with the frame modeling may have negligible improvement on structural performance. However, when the slabs are combined with walls in addition to frame modeling, significant improvement in structural performance can be achieved.

In the research, different combinations of structural components of multi-storey buildings were modeled to investigate the optimum design solution. Static as well as free vibration analyses were carried out aiming at evaluating the structural performance and responses.

The following conclusions were drawn from the research:

1. Among the applied modeling concepts, (frame, wall, slab) is recommended for economical design.
2. (Frame, wall, slab) modeling provides higher lateral stiffness and lower shear and moment as compared with conventional frame and (frame, slab) modeling, which is an expected trend.
3. The size of the structural member or the steel reinforcement in (frame, wall, slab) modeling can be reduced, while satisfying the safety and serviceability requirement.
4. Wall openings, which would reduce lateral stiffness of a structure, should be taken into consideration in structural analysis.
5. To fully understand the significance of walls and slabs in modeling and analysis of multi-storey buildings, more modeling with a different plan view arrangement (such as anti-symmetrical, non-symmetrical or more complex building shapes) were recommended.
6. Further extensive study can be performed to generalize the effect of wall openings, by modeling with different percentages of wall openings.
7. In the research, besides eigenvector analysis, only equivalent static analysis was performed.

Static pushover analysis and response spectrum analysis could also be performed to further investigation of the response of multi-storey buildings under seismic loading conditions.

A seismic analysis of building with and without shear wall was studied by Chandurkar and Pajgade (2013). They were concluded that, in the seismic design of buildings, reinforced concrete structural walls, or shear walls, act as major earthquake resisting members, providing an efficient bracing system and offer great potential for lateral load resistance. The properties of these seismic shear walls dominate the response of the buildings, and therefore, it is important to evaluate the seismic response of the walls appropriately. In their study, main focus was to determine the solution for shear wall location in multi-storey building. Effectiveness of shear wall has been studied with the help of four different models. One model was bare frame structural system and other three models are dual type structural system. An earthquake load was applied to a building of ten stories located in zone II, zone III, zone IV and zone V. Parameters like Lateral displacement, story drift and total cost required for ground floor were calculated in both the cases replacing column with shear wall.

The conclusions of the paper were:

From all the conducted analyses, they observed that in 10 story building, constructing building with shear wall in short span at corner was economical as compared with other models. From this it can be concluded that large dimension of shear wall is not effective in 10 stories or below 10 stories buildings. It was observed that the shear wall was economical and effective in high rise building. Also observed that:

1. Changing the position of shear wall will affect the attraction of forces, so that wall must be in proper position.
2. If the dimensions of shear wall are large then major amount of horizontal forces are taken by shear wall.
3. Providing shear walls at adequate locations substantially reduces the displacements due to earthquake.

2.7 Review to the Moment Transformation Method

The Moment Transformation method (MT) was presented by Ibrahim (2013), and Ibrahim and Mohamed (2013). The method was used firstly to simplify the analysis of the continuous beams and sub frames connected by a single or double upper and lower columns at the joints, same as the direct moment distribution procedure but with different formulation.

The no-shear moment distribution (sometimes also known as the cantilever moment distribution), is based on the concept of distribution of the sway fixed end moments without changing the sway-moment equation during the distribution procedure, Ghali and Neville (1978).

The concept of the direct moment distribution was suggested by Lin, [Williams (2009)], as a means of eliminating the iteration required in the standard moment distribution procedure. Several alternative methods have also been developed for the direct distribution of moments, e.g. the precise moment distribution (some times called the coefficient of restraints), Reynolds and Steedman (1999).

Then the method was used to solve the problems of the single post connected by horizontal members and subjected to lateral forces, and permitted to sway freely such as in the substitute frame method. In this type of analysis, the concept of the no-shear moment distribution is applied.

The method has then been developed and generalized to solve the wall-frame interaction problems, and also developed to solve the more complex two dimensional, and three dimensional multi-bay multi-floor buildings with irregular arrangement and orientation of the vertical members and subjected to both vertical and horizontal loads.

A computer program (MTProg) has been developed based on Visual Basic Environment and implemented for the method.

2.8 Summary

The exact solution for tall buildings is very expensive in terms of time and computer storage. For this reason the need for simplified methods of analysis is arise.

The simplified methods of analysis always require some assumptions e.g.

(a) Neglection of the axial deformations.

(b) The in-plane rigid body movement.

(c) Assumption of the contra-flexural points in the middle of the columns and the beams.
(d) Assumption of equal floor heights.
(e) Assumption of uniform properties throughout the building height.

This is mainly shown in the continuum methods of analysis. The results obtained by the continuum methods are less accurate when compared with the solutions obtained by the simplified matrix based methods, especially if the walls are not symmetrical or the members stiffnesses are largely different from each other, or if there is a setback in the building as this affects the locations of the contra-flexure points. Analysis methods based on simplified matrix and finite elements analysis give relatively accurate solutions.

Simplifications of the models, such as the optimized modeling schemes proposed by Akis (2004), assist in analyzing the tall buildings with a lesser cost and effort.

Therefore, a simplified method of analysis that is based on reasonable assumptions is required, in order to reach a more simple and accurate solution when compared with the exact methods. In this research, such a simplified method is proposed and verified.

CHAPTER THREE

The Moment-Force Transformation Method Theory

3.1 Introduction

In simplified analysis methods of tall buildings, the following assumptions are widely used and are found to be reasonable for the majority of building structures:

(1) The floors are rigid in their own plane. The whole structural assembly in each floor moves as a rigid body in the horizontal direction. The structural stiffness matrix is formed under the assumption that all frames are connected at each floor level by a diaphragm, which is rigid in its own plane. Due to the high in-plane stiffness, the lateral loads are transferred to the columns and shear walls through these diaphragms.

(2) The out-of-plane stiffness of the floor can either be neglected or incorporated approximately into corresponding equivalent beams.

In three dimensional analyses, there are some factors that influence how fast results can be obtained and how accurate they are. The most important factors are the amount of required data, computer running time and the vast output results that should be interpreted. These should be optimized in such a way that sufficient results can be obtained by entering lesser data and having a relatively short computing time. The computer running time is mostly affected by the total number of degrees of freedom in the system. Generally it may be decreased by:

(a) A reduction in the total number of elements used in the analysis and,

(b) The use of elements having the least degrees of freedom.

3.2 Reduction of Total Degrees of Freedom by Considering Rotations Only

Instead of considering the whole degrees of freedom and applying all the forces directly in the joints, the problem can be reduced to a system that includes only the rotational degrees of freedom and fixed end moments. The known methods using such assumptions are the slope deflection method, the ordinary moment distribution method, the no-shear moment distribution and the successive sway correction method.

3.3 Analysis of Structural Systems using rotational degrees of freedom

Any structural system subjected to both vertical and/or horizontal loads can be split into two loading systems (a) and (b), as shown in Figure 3.1. This simplifies the problem and reduces the total degrees of freedom to only rotational degrees of freedom. System (a) is a system in which the lateral degrees of freedom are released and the rotations are completely restrained by the fixed moments for all the joints in the structure. The system is used to calculate the fixed-end moments due to the external loading, the fixed moments produced from the carryover moments and the transformed moments. System (b) is a system with all the translational and rotational degrees of freedom released and used for the released moments (the balancing moments).

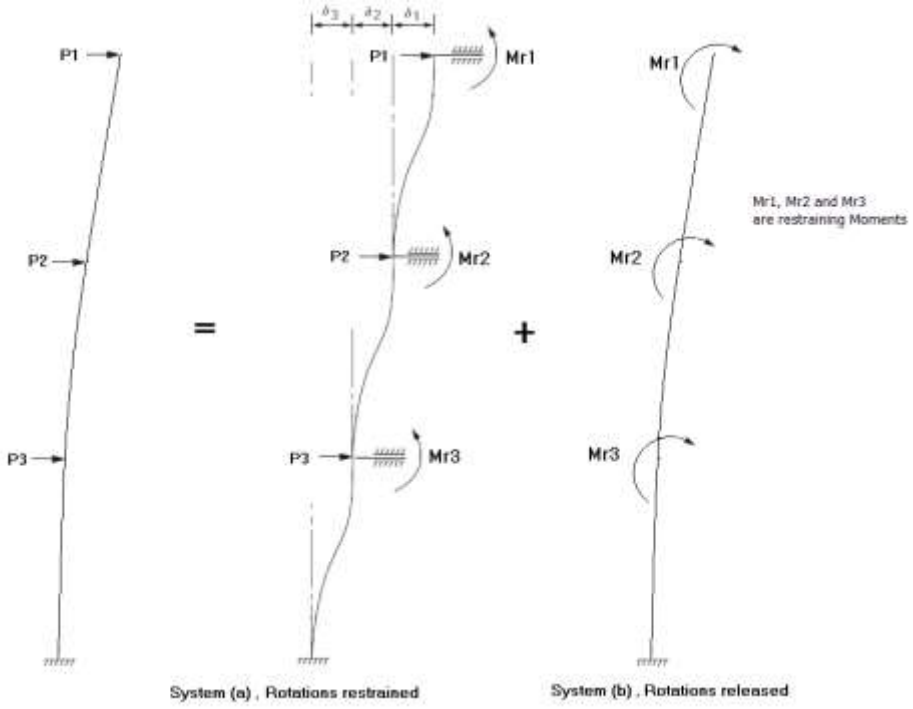

Figure 3.1: Single post model

The released or the balancing moments, which are the reverse of the restraining moments of the structural system (a), will be applied as concentrated moments in the joints of the structural system (b). The induced moments e.g. the carryover moments and the transformed moments are considered as fixed moments and should be applied again in the structural system (a).

Appendix A1 shows an example illustrates the use of the two loading systems.

The example yields the following two important notes:

(1) The joints rotations can be that obtained only from the structural system (b), as the structural system (a) has no rotations at the joints.

(2) The total translations of the joints are produced from the two structural systems by superimposing the translations obtained from each system.

Based on the illustrated two structural systems concept, the moment distribution and the moment transformation procedures are illustrated as shown in Appendix A2 and A3.

3.4 Sway Fixed-End Moments

In order to obtain the sway fixed end moments in the vertical members, let us consider the structure shown in Figure 3.2, which shows an intermediate storey in a multi-bay plane frame subjected to horizontal loads at floor levels. Assume that the frame is allowed to sway without joint rotation. Neglecting the axial deformations in the horizontal members, the top ends of all the columns in one storey translate relative to their bottom ends by the same amount *D*. This sway induces end-moments and shearing forces in all the columns. For equilibrium, the sum of the shearing forces in the columns of one storey must be equal to the sum *P* of the horizontal forces acting on all the higher floors; thus *P* and the column end-moments are related by:

$$P = \frac{1}{h}\sum M \qquad ...(3.1)$$

Where the summation is for the end-moments *M* at top and bottom of all the columns in the given storey, and *h* is the floor height, Ghali and Neville (1978).

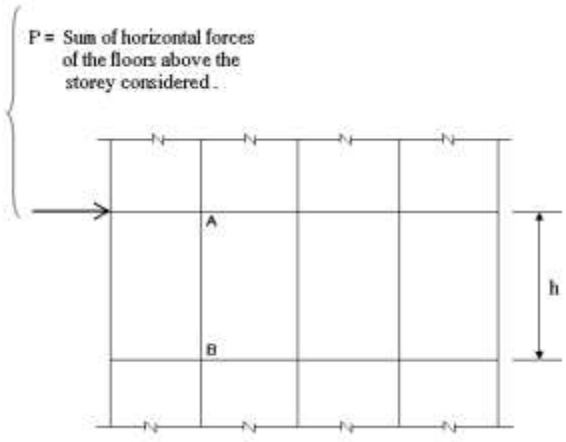

Figure 3.2: Intermediate storey of a multistory frame

3.5 The Moment Transformation method

3.5.1 Column of two members

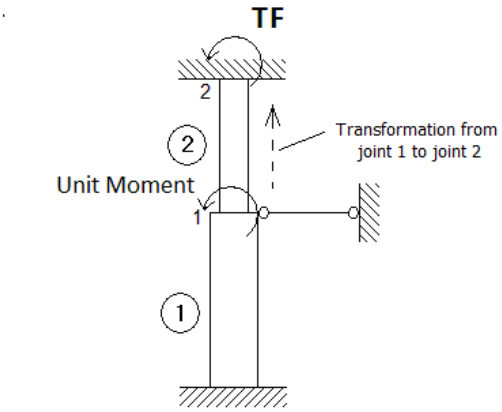

Figure 3.3: Transformation of Moment

Referring to Figure 3.3, and using the displacement method of analysis, the equivalent rotational stiffness S_e of the two members 1 and 2 at joint 2, and the transformation factor *TF* for the moment transformed from joint 1 to joint 2, are given as follows:

$$S_e = \left[S_2 - \frac{t_2{}^2}{(S_1 + S_2)} \right] \qquad \ldots(3.2)$$

$$TF = \frac{-t_2}{(S_1 + S_2)} \qquad \ldots(3.3)$$

where:

S_i is the rotational stiffness of member # *i*.

t_i is the carryover moment of the member # *i*.

3.5.2 Generalization of the Method to Two and Three Dimensional Multi-storey buildings

Instead of transformation from joint to joint through members, as in the case of the two columns, Figure 3.3, the system now is composed of multiple bays and multiple floors as in Figure 3.4, and the transformation will be carried out through the floors from top to bottom and from bottom to top.

Instead of the joints, the transformation in this case will be carried out from one level to another level, Ibrahim (2013).

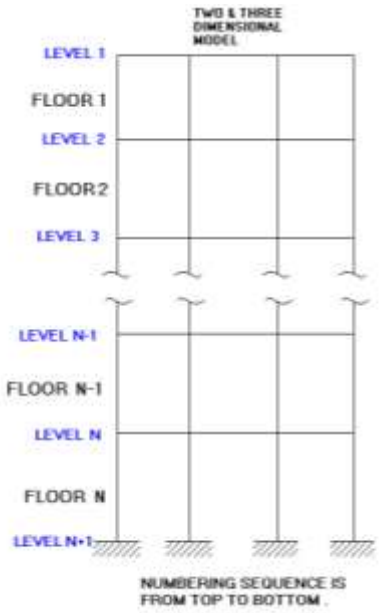

Figure 3.4: Multi-Storey 2D or 3D Building

The transformation procedure is generalized and given in a matrix form as shown in the following sections.

3.5.3 Equivalent stiffness matrix and moment transformation factors matrix

Moments Transformation procedure from top to bottom,

$[SR] = [\,NN\,]_i \quad , \ (\text{if } i = 1)$ …(3.4a)

$[SR] = [\,NN\,]_i + [GG]_{i-1} \quad , \ (\text{if } i \neq 1)$ …(3.4b)

$[AA] = [A]_i + [SR]$ …(3.5)

$[FF]_i = -[\,BC\,]^T{}_i \ [AA]^{-1}$ …(3.6)

$[GG]_i = [A]_i + [FF]_i \ [BC]_i$ …(3.7)

where;

$[\,NN\,]_i$, is the Over All Rotation Stiffness Matrix of the Level # i .

$[GG]_{i-1}$, is the Equivalent Rotation Stiffness Matrix of The Floor # i-1 .

$[A]_i$, is the Condensed Rotation Stiffness Matrix of The Floor # i .

$[\,FF\,]_i$, is the Transformation Factors Matrix of The Floor # i .

$[BC]_i$, is the Carryover Moments Matrix of The Floor # i .

$[BC]^T{}_i$, is the Transpose of The Carryover Moments Matrix of The Floor # i .

$[GG]_i$, is the Equivalent Rotation Stiffness Matrix of The Floor # i .

The same procedure can be carried out for transformation from bottom to top.

3.5.4 Total Transformation Factors matrix from one level to a far level

The total transformation factors matrix is calculated as follows:

$$[\ FT\ ]_{K\rightarrow K+2} = [\ FT\ ]_{K\rightarrow K+1}\ \ [\ FF\ ]_{K+1\rightarrow K+2} \qquad \ldots(3.8)$$

where:

$[\ FT\ ]_{K\rightarrow K+1}$, is the total transformation factors matrix used to transform the moments at level # K toward the level # $K+1$.

$[\ FT\ ]_{K\rightarrow K+2}$, is the total transformation factors matrix used to transform the moments at level # K toward the level # $K+2$.

$[\ FF\ ]_{K+1\rightarrow K+2}$, is the Transformation Factors Matrix of Floor between level #$K+1$ and level $K+2$.

3.5.5 Transformation of the moments from level # *j* to level # *i*

Transformation of the moment vectors from level j to level i can be carried out as shown in Equation 3.9.

$$\{\ MT\ \}_i = \{\ MT\ \}_i + [\ FT\ ]_{j\rightarrow i}\ \{\ MT + MB + MS\ \}_j \qquad \ldots(3.9)$$

Figure 3.5, shows the arrangement of the fixed ends moments at the level # i.

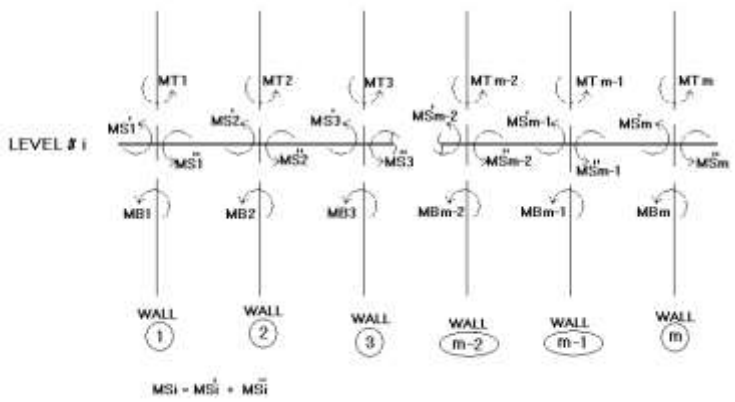

Figure 3.5: Moments of the Concerned Level

3.5.6 The joints rotations and the final moments at each level

The rotations and the moments at the joints of the level # i are calculated as shown below:

The rotation of all the joints of level # i is given as follows:

$$\{\ ROT\ \}_i = -[KT]_i^{-1}\ \{\ MTOT\ \}_i \qquad \ldots(3.10)$$

$$[\ KT\ ]_i = [\ KT\ ]_i + [\ KB\ ]_i + [\ KS\ ]_i \qquad \ldots(3.11)$$

$$\{ MTOT \}_i = \{ MT \}_i + \{ MB \}_i + \{ MS \}_i \quad \ldots(3.12)$$

Final moments of the level # *i*:

$$\{ MTf \}_i = \{ MT \}_i + [KT]_i \{ ROT \}_i \quad \ldots(3.13a)$$

$$\{ MBf \}_i = \{ MB \}_i + [KB]_i \{ ROT \}_i \quad \ldots(3.13b)$$

$$\{ MSf \}_i = \{ MS \}_i + [KS]_i \{ ROT \}_i \quad \ldots(3.13c)$$

where:

$[KT]_i$, is the total stiffness matrix at the level # i .

$\{ MTOT \}_i$, is the total moments vector at level # i .

$\{ ROT \}_i$, is the rotations of the joints vector at the level # i .

$\{ MT \}_i$, is the original and the transformed moments vector just above the level # i .

$\{ MB \}_i$, is the original and the transformed moments vector just below the level # i .

$\{ MS \}_i$, is the original moments vector at the beams ends of the level # i .

$\{ MTf \}_i$, is the final moments vector just above the level # i .

$\{ MBf \}_i$, is the final moments vector just below the level # i .

$\{ MSf \}_i$, is the final moments vector at the beams ends of the level # i .

3.5.7 The condensed Stiffness and the Carryover Moment for single member

The rotation stiffness for single post subjected to side sway with no shear produced can be obtained as follows:

Figure 3.6: Rotation and Translation DOF s of a Single Member

The two DOFs are shown in Figure 3.6 and the corresponding system matrix equation is as follows:

$$\begin{pmatrix} S_{11} & S_{12} \\ S_{21} & S_{22} \end{pmatrix} \begin{Bmatrix} D_1 \\ D_2 \end{Bmatrix} = \begin{Bmatrix} F_1 \\ F_2 \end{Bmatrix} \quad \ldots(3.14)$$

In order to obtain the condensed stiffness matrix, substitute for $F_1 = S^*$, $F_2 = 0$, $D_1 = 1$, $D_2 = D$ in equation 3.14, yields

$$\begin{pmatrix} S_{11} & S_{12} \\ S_{21} & S_{22} \end{pmatrix} \begin{Bmatrix} 1 \\ D \end{Bmatrix} = \begin{Bmatrix} S^* \\ 0 \end{Bmatrix} \qquad \ldots(3.15)$$

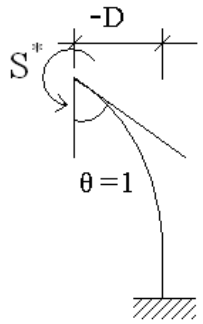

Figure 3.7: Condensed rotation Stiffness with Translation Permitted

where S^* is the condensed stiffness or rotation stiffness with translation not prevented. The matrix Equation 3.15 contains the following two equations:

$$S_{11} + S_{12} \,.\, D = S^* \qquad \ldots(3.16a)$$

$$S_{21} + S_{22} \,.\, D = 0 \qquad \ldots(3.16b)$$

From equation (3.16b)

$$D = - S_{22}^{-1} \,.\, S_{21} \qquad \ldots(3.17)$$

Substitute equation (3.17) into equation (3.16a), gives:

$$S^* = S_{11} - S_{12} \,.\, S_{22}^{-1} \,.\, S_{21} \qquad \ldots(3.18)$$

These relations can be formulated in a general matrix form as shown below:

$$\begin{pmatrix} [S_{11}] & [S_{12}] \\ [S_{21}] & [S_{22}] \end{pmatrix} \begin{Bmatrix} [\,I\,] \\ [\,D\,] \end{Bmatrix} = \begin{Bmatrix} [\,S^*\,] \\ [\,0\,] \end{Bmatrix} \qquad \ldots(3.19)$$

where:

[I] : Identity matrix .

[0] : Null matrix .

[D] : Displacement matrix corresponding to the condensed stiffness matrix .

[S_{ij}] : Sub-Matrices of the main matrix .

[S^*] : The condensed rotation stiffness matrix .

Equation (3.17) and (3.18) becomes as follows:

$[D] = -[S_{22}]^{-1} . [S_{21}]$ …(3.20)

$[S_{11}^*] = [S_{11}] - [S_{12}] . [S_{22}]^{-1} . [S_{21}]$ …(3.21)

For a single member, shown in Figure 3.6, the stiffness matrix of the two degrees of freedom in the general form, is as follows:

$$\begin{pmatrix} S & (S + t)/L \\ (S + t)/L & 2*(S + t)/L^2 \end{pmatrix}$$

Considering bending deformation and neglecting shear deformations, the stiffness matrix will be as shown below:

$$[S] = \begin{pmatrix} 4EI/L & 6EI/L^2 \\ 6EI/L^2 & 12EI/L^3 \end{pmatrix}$$

Using equation (3.17) and equation (3.18):

$D = -(6EI/L^2)/(12EI/L^3) = -0.5L$

$S^* = 4EI/L - (6EI/L^2)^2/(12EI/L^3) = 4EI/L - 3EI/L = EI/L$

where:

S^* is the condensed rotation stiffness with the lateral sway permitted.

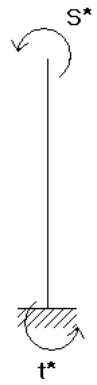

Carry Over Moment

Figure 3.8: Carryover Moment for a Single Member

For equilibrium of the post:

$t^* = -S^*$ …(3.22)

Where: t^* is the carryover moment corresponding to the condensed rotation stiffness S^*.

The lateral loads are applied in terms of side sway fixed moments with no rotation of the joints permitted.

The final moments and the rotation at each joint is obtained directly by the transformation method from which we can get the joint lateral displacements and the shear forces in all members.

3.5.8 The condensed Stiffness and the Carryover Moments matrices for two members

The previous procedure that used to obtain the condensed stiffness for a single member subjected to side sway is now generalized to a bundle of members. To simplify the presentation we consider a system of two vertical members (columns or walls),

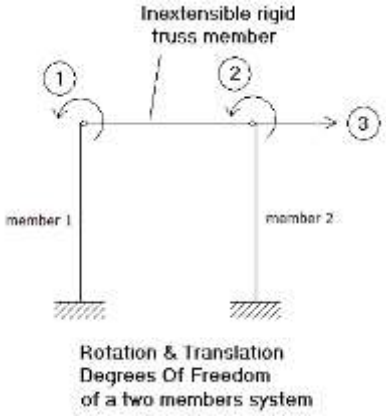

Figure 3.9: Rotations and Translation DOF s of a two Members System

The system equation corresponding to the three degrees of freedom shown in Figure 3.9 including the condensed rotation stiffness matrix with the translation of the joints permitted is as shown below:

$$\left(\begin{array}{cc|c} S_{11} & S_{12} & S_{13} \\ S_{21} & S_{22} & S_{23} \\ \hline S_{31} & S_{32} & S_{33} \end{array}\right) \left\{\begin{array}{c|c} \begin{bmatrix} 1 & 0 \\ 0 & 1 \end{bmatrix} & \\ \hline [\, D_1 & D_2 \,] \end{array}\right\} = \left\{\begin{array}{c|c} \begin{bmatrix} S_{11}^* & S_{12}^* \\ S_{21}^* & S_{22}^* \end{bmatrix} & \\ \hline [\, 0 & 0 \,] \end{array}\right\} \quad \ldots(3.23)$$

Applying equation (3.20) shown in the previous illustration, we get the displacements corresponding to the condensed stiffness matrix:

$$[\, D_1 \;\; D_2 \,] = -\,[\, S_{33}]^{-1}\, [\, S_{31} \quad S_{32} \,] = -\,[\, (S_{31}/\, S_{33}) \quad (S_{32}/\, S_{33}) \,]$$

$$= \; [\, -(S_{31}/\, S_{33}) \quad -(S_{32}/\, S_{33}) \,] \qquad \ldots(3.24)$$

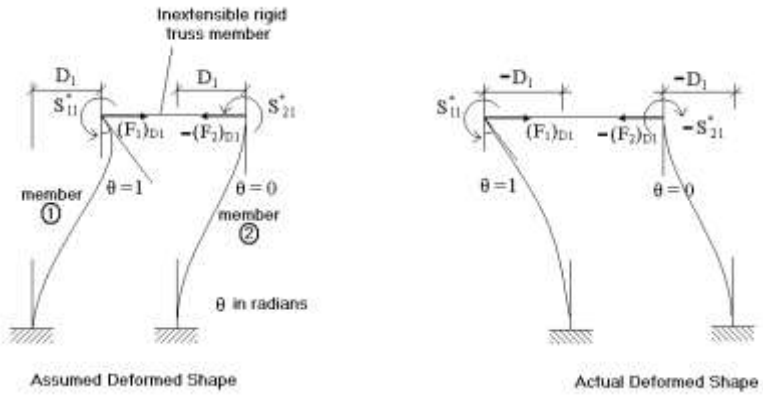

Figure 3.10: Condensed Stiffness Coefficient Corresponding To Displacement *D1*

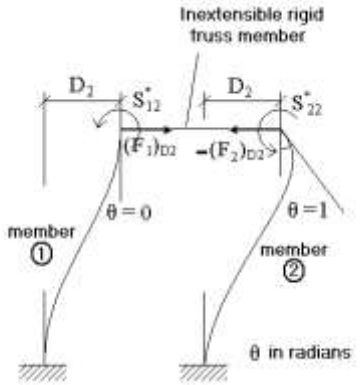

Figure 3.11: Condensed Stiffness Coefficient Corresponding to Displacement *D2*

From equation (3.21) the condensed rotation stiffness matrix is:

$$\begin{pmatrix} S_{11}^* & S_{12}^* \\ S_{21}^* & S_{22}^* \end{pmatrix} = \begin{pmatrix} S_{11} - S_{13}.\, S_{33}^{-1}\, .S_{31} & S_{12} - S_{13}.\, S_{33}^{-1}\, .S_{32} \\ S_{21} - S_{23}.\, S_{33}^{-1}\, .S_{31} & S_{22} - S_{23}.\, S_{33}^{-1}\, .S_{32} \end{pmatrix} \quad \ldots(3.25)$$

The internal interaction force is obtained from the local stiffness matrix of the member that free in one end and fixed in the other end, the considered degrees of freedom are the rotation and the translation of the free end, as shown below:

$$\begin{pmatrix} S_i & (S_i + t_i)/L \\ (S_i + t_i)/L & 2(S_i + t_i)/L^2 \end{pmatrix} \begin{Bmatrix} 1 \\ D_j \end{Bmatrix} = \begin{Bmatrix} S^*_{ij} \\ (F_i)_{Dj} \end{Bmatrix} \text{ (For } i = j \text{)} \quad \ldots(3.26)$$

and,

$$\begin{pmatrix} S_i & (S_i + t_i)/L \\ (S_i + t_i)/L & 2(S_i + t_i)/L^2 \end{pmatrix} \begin{Bmatrix} 0 \\ D_j \end{Bmatrix} = \begin{Bmatrix} S^*_{ij} \\ (F_i)_{Dj} \end{Bmatrix} \text{ (For } i \neq j \text{)} \quad \ldots(3.27)$$

where:

S_i & t_i are the ordinary rotation and carryover moment of member # *i* respectively.

D_j is the displacements corresponding to the stiffness configuration #*j*.

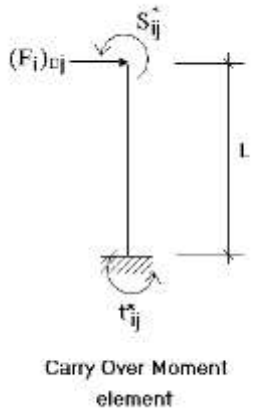

Figure 3.12: Carryover Moment Coefficient t^*_{ij}

For equilibrium of the member shown in Figure 3.12, the carryover moment matrix element t^*_{ij} can be calculated as follows:

$$t^*_{ij} = - S^*_{ij} + (F_i)_{Dj} * L \qquad \ldots(3.28)$$

3.6 The Moment-Force Transformation Method

The moment transformation (MT) method was developed to analyze moderate tall buildings neglecting the axial deformations in the vertical members. In this research the MT method has been further developed to the Moment-Force Transformation (MFT) method, which included the axial deformation in the vertical members in the analysis. The two methods are used for linear static analysis of tall buildings. The algorithm of the moment transformation program MTProg has been further developed to the moment-force transformation program MFTProg.

In the moment distribution methods, the moments are distributed between the end joints of each individual member. In the moment transformation (MT) method the distributions are carried out for a coupled group of moments at the same time from one level toward the next level. Using this stream or bundle of distribution, permits the axial deformation (shortening/elongation) of the vertical members to be incorporated in the analysis.

3.6.1 Consideration of the axial deformations in the vertical members

In this part, the axial deformation in the vertical members is incorporated in the analysis. The procedure start using a single post composed of different members and then

generalized to any system composed of multiple vertical members. To simplify the presentation a post composed of two elements is considered as shown in Figure 3.13.

The stiffness matrix for each individual member is as follows:

$$\begin{pmatrix} K & -K \\ -K & K \end{pmatrix} \quad \text{or} \quad \begin{pmatrix} K & t \\ t & K \end{pmatrix}$$

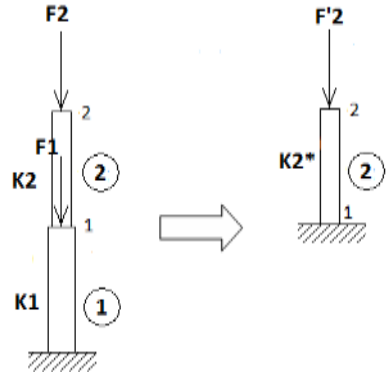

Figure 3.13: Column of two segments

Where: K is the axial stiffness ($K= EA/L$) and $t=-K$ = carryover force (Similar to the carryover moment). The carryover moment or force, actually are the moment or the force reactions of the restrained far end of the member.

The matrix equation of the structural system shown in Figure 3.13 is as follows:

$$\begin{pmatrix} K1+K2 & -K2 \\ -K2 & K2 \end{pmatrix} \begin{Bmatrix} D1 \\ D2 \end{Bmatrix} = \begin{Bmatrix} F1 \\ F2 \end{Bmatrix} \qquad \ldots(3.29)$$

Where:

K1 and *K2* are the axial stiffnesses of the members 1 and 2 respectively.

F1 and *F2* are forces acting at joints 1 and 2 respectively.

D1 and *D2* are the axial displacements of the joints 1 and 2 respectively.

From which:

$(K1+K2)\ D1-K2\ D2 = F1$ …(3.30)

$-K2\ D1+K2\ D2 = F2$ …(3.31)

From equation 3.30

$$D1 = \frac{K2}{K1+K2} D2 + \frac{F1}{K1+K2} \qquad \ldots(3.32)$$

Substituting from equation 3.32 into 3.31 and rearranging, yields:

$$(\frac{K1.K2}{K1+K2})D2 = F2 + (\frac{K2}{K1+K2})F1 \qquad \ldots(3.33)$$

or

$$K2^{*}.D2 = F2 + TF.F1 \qquad \ldots(3.33a)$$

where

$$K2^{*} = (\frac{K1.K2}{K1+K2}) \qquad \ldots(3.34)$$

$$TF = \frac{K2}{K1+K2} \qquad \ldots(3.35)$$

*K2**: is the equivalent axial stiffness replacing the two members 1 and 2, in the place of member 2.

TF: is the factor used to transform the axial force from joint 1 to joint 2.

The form of the produced equation is similar to the moment transformation equations, so that the axial stiffness can be introduced in the transformation procedure together with the rotational stiffness.

For multiple vertical members, the axial stiffnesses of the vertical members are coupled with the transverse stiffness of the beams in the case of the two dimensional analyses and by the whole transverse (out of plane) stiffness of the floor slab in the case of the three dimensional analyses.

The transformation of the moment and the force from joint (1) to joint (2) is carried out as shown in the following steps:

(1) Restraining of joint (2).

(2) Application of the force (*F1*) at joint (1).

(3) Finding the force reaction (*R*) at joint (2).

(4) Reversing the reaction (*R*) to get active force (*F'21=-R*).

The reaction (*F'21*) is part of the force (*F1*) , and is given by:

$F'_{21} = a.F_1$ …(3.36)

Where: *a = TF*

The equivalent stiffness of the two members is match with the equation used to calculate the equivalent axial stiffness of (*n*) members. The equivalent stiffness of (*n*) members is obtained from:

For axial force, *F*, acting at the top of a vertical cantilever composed of members connected in series, the total displacement is equal to the summation of all the member's displacements:

$D_{tot} = D1 + D2 + \ldots + Dn$

$$\frac{F}{Ke} = \frac{F}{k1} + \frac{F}{k2} + \ldots + \frac{F}{Kn}$$

Or;

$$\frac{1}{Ke} = \frac{1}{k1} + \frac{1}{k2} + \ldots + \frac{1}{Kn} \qquad \ldots(3.37)$$

The axial displacements for a three segments column were calculated using the force transformation method is presented in Appendix A4.

3.6.2 Multi-Bay Multi-Storey Buildings

By combining the moments and the forces transformation procedures, the moment-force transformation procedure can be generalized to calculate the equivalent stiffness matrix and the transformation factors matrix of tall building.

3.6.3 Condensed Stiffness and Carryover Matrix for Multiple Vertical Members including axial deformations

Considering a system of two vertical members, Figure 3.14, the stiffness matrix equation corresponding to the three degrees of freedom 1,2 and 3, as before, is condensed into degrees of freedom 1 and 2, as follows:

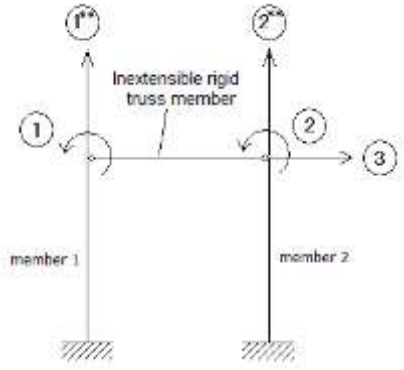

Figure 3.14: Rotations and Translations DOF s of a Two Vertical Members System

$$\begin{pmatrix} S_{11} & S_{12} & S_{13} \\ S_{21} & S_{22} & S_{23} \\ S_{31} & S_{32} & S_{33} \end{pmatrix} \begin{Bmatrix} 1 & 0 \\ 0 & 1 \\ D_1 & D_2 \end{Bmatrix} = \begin{Bmatrix} S_{11}^* & S_{12}^* \\ S_{21}^* & S_{22}^* \\ 0 & 0 \end{Bmatrix} \quad \ldots (3.38)$$

As in the moment transformation method, the internal interaction force, $(F_i)_{Dj}$ is obtained from the different rotational stiffness configurations and hence the elements of the carryover moments matrix, t^*_{ij}, are calculated from equation 3.39:

$$t_{ij}^* = -S_{ij}^* + (F_i)_{Dj}.L \qquad \ldots(3.39)$$

Where; L is the floor height.

Since the axial stiffness of the vertical members are uncoupled with each other and also uncoupled with the rotational and the lateral translation stiffness of the members, then the axial stiffness of each member can be added to the condensed rotational stiffness, S^*_{ij}, of the members after the condensation procedure. Similarly, the axial force carryover elements are also added to the carryover matrix.

3.7 Second order P-Delta analysis of tall buildings

By coupling of the moments and the axial forces in each of the vertical members for large lateral displacements at the floors levels during the moment-force transformation procedure, the second order P-Delta effects are directly included in the analysis and structural instability with reference to overall buckling or failure of individual members is also studied.

3.7.1 Condensed Stiffness and Carryover Matrices for Multiple Vertical Members, including P-Delta effects

Considering a system of two vertical members, Figure 3.15, the stiffness matrix equation 3.38, corresponding to the three degrees of freedom 1, 2 and 3, are condensed into 1 and 2, as follows:

The translational stiffness S_{33} (Equation 3.38), is a summation of the translational stiffness (S_T) of each vertical member including its global P-Delta effect (i.e. $-P/L$, where P is the axial force in the vertical member), as shown in Figure 3.16. The effect of the local p-delta in any member may be incorporated by using the Euler stability functions where the rotational stiffness, S, and the carryover moment, t, of the member, are

trigonometric functions of axial compression forces for positive *P* values, or hyperbolic functions of axial tension forces for negative *P* values, Ghali et al. (2009).

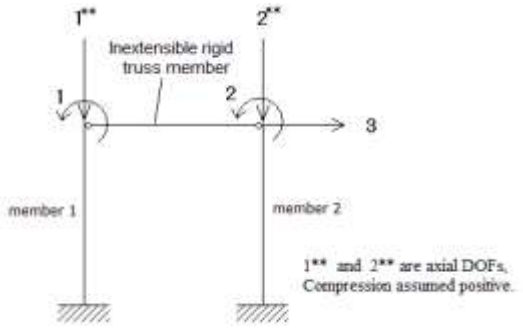

Figure 3.15: Rotations and Translations DOFs of Two Vertical Members System, (with large displacements)

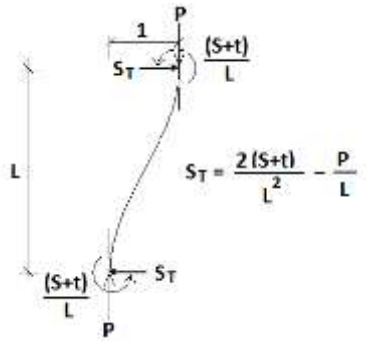

Figure 3.16: Translational Stiffness of a member including P-Delta effect

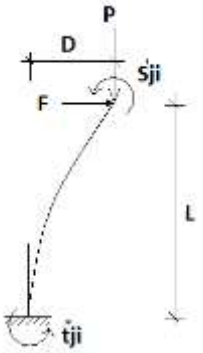

Figure 3.17: Carryover moment including P-Delta effect

The lateral displacement, D, and the internal interaction force, *F*, Figure 3.17, are obtained from the different rotational stiffness configurations and hence the elements of the carryover moment matrix, including the P-Delta effects, are calculated from equation 3.40:

$$t^*_{ji} = -S^*_{ji} + F.L + P.D \qquad \ldots (3.40)$$

3.7.2 Linear-displacement assumptions

In the case of the linear-displacement assumption, the end rotational stiffness *S* and the carryover moment *t* of a beam element are assumed not to be affected by the axial load. The affected term is the lateral stiffness S_T, as shown in equation 3.41:

$$S_T = \frac{2(S+t)}{L^2} - \frac{P}{L} \qquad \ldots(3.41)$$

For beam element with shear deformations considered, the ordinary end rotational stiffness and the carryover moment are given, as follows:

$$S = \frac{(4+\alpha)}{(1+\alpha)}\frac{EI}{L} \qquad \ldots(3.42)$$

, and $t = \frac{(2-\alpha)}{(1+\alpha)}\frac{EI}{L}$ $\ldots(3.43)$

Where

$$\alpha = \frac{12EI}{Ga_r L^2}$$

And, for members with shear deformations neglected stiffness factors are:

$S = \frac{4EI}{L}$, and $t = \frac{2EI}{L}$

The term $(-\frac{P}{L})$ is the linear geometric stiffness of the beam element affecting the lateral stiffness.

The term geometric stiffness is introduced so that the stiffness matrix has a different name from the mechanical stiffness matrix, which is based on the physical properties of the element. The geometric stiffness exists in all structures but it becomes important only if it is large compared to the mechanical stiffness of the structural system, Wilson (2000).

3.7.3 Cubic-displacement assumptions

In the case of a beam element with bending properties in which the deformed shape is assumed to be a cubic function caused by the rotations φ*i* and φ*j* at the beam ends, additional moments *Mi* and *Mj* are developed. Considering the cubic function, the force-displacement relationship is given by Equation 3.44, Wilson (2000):

$$\begin{bmatrix} F_i \\ M_i \\ F_j \\ M_j \end{bmatrix} = \frac{-P}{30L}\begin{bmatrix} 36 & 3L & -36 & 3L \\ 3L & 4L^2 & -3L & -L^2 \\ -36 & -3L & 36 & -3L \\ 3L & -L^2 & -3L & 4L^2 \end{bmatrix}\begin{bmatrix} v_i \\ \phi_i \\ v_j \\ \phi_j \end{bmatrix} \quad \text{or, } \mathbf{F}_G = \mathbf{k}_G\mathbf{v}$$

…(3.44)

The well-known elastic force deformation relationship for a prismatic beam neglecting shear deformations is:

$$\begin{bmatrix} F_i \\ M_i \\ F_j \\ M_j \end{bmatrix} = \frac{EI}{L^3}\begin{bmatrix} 12 & 6L & -12 & 6L \\ 6L & 4L^2 & -6L & -2L^2 \\ -12 & -6L & 12 & -6L \\ -6L & -2L^2 & -6L & 4L^2 \end{bmatrix}\begin{bmatrix} v_i \\ \phi_i \\ v_j \\ \phi_j \end{bmatrix} \quad \text{or, } \mathbf{F}_E = \mathbf{k}_E\mathbf{v}$$

…(3.45)

Therefore, the total stiffness matrix, **k***T*, of the beam element is as follows:

k*T* = **k***E* + **k***G* …(3.46)

where;

k*E* is the elastic (mechanical) stiffness matrix, and **k***G*, is the geometric stiffness matrix. So, to account for the cubic displacement function, it is only required to incorporate the total rotational stiffness and the carryover moment including the terms shown circled in the geometric and the mechanical stiffness matrices, therefore:

$$S = \frac{4EI}{L} - \frac{4PL}{30} \qquad \ldots(3.47)$$

, and $$t = \frac{2EI}{L} + \frac{PL}{30} \qquad \ldots(3.48)$$

If shear deformations are considered in both the geometric and mechanical stiffness matrices, the rotational stiffness and the carryover moment become as follows:

$$S = \frac{(4+\alpha)}{(1+\alpha)}\frac{EI}{L} - \frac{P(2L/15 + L\alpha/6 + L\alpha^2/12)}{(1+\alpha)^2} \qquad \ldots(3.49)$$

, and

$$t = \frac{(2-\alpha)}{(1+\alpha)}\frac{EI}{L} + \frac{P(L/30 + L\alpha/6 + L\alpha^2/12)}{(1+\alpha)^2} \qquad \ldots(3.50)$$

The translational stiffness S_T, can directly be obtained by maintaining the equilibrium of the element.

$$S_T = S_{33} = \frac{2(S+t)}{L^2} - \frac{P}{L} \qquad \ldots(3.51)$$

Considering bending deformations only,

$$S = \frac{4EI}{L} - \frac{4PL}{30}, \text{ and } \quad t = \frac{2EI}{L} + \frac{PL}{30}$$

$$S_T = \frac{12EI}{L^3} - \frac{6P}{30L} - \frac{P}{L} = \frac{12EI}{L^3} - \frac{36P}{30L}$$

S_T is the summation of the elements shown squared in the geometric and mechanical stiffness matrices.

3.7.4 Euler Stability Functions

The rotational stiffness and the carryover moment for a member subjected to an axial force P, are shown in Figure 3.18.

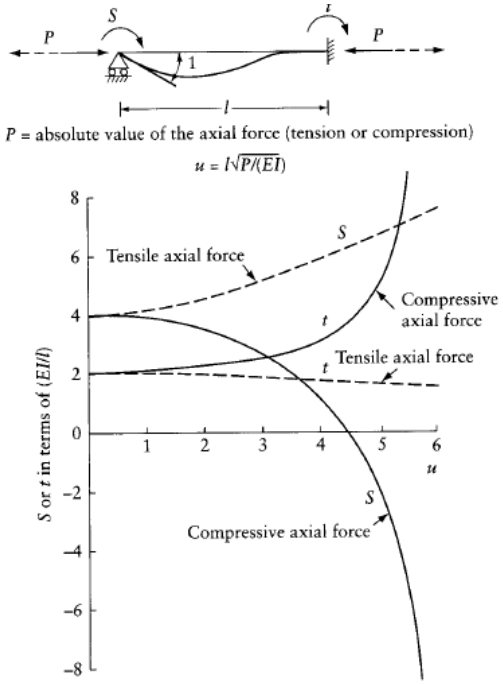

Figure 3.18: End-rotational stiffness and carryover moment for a prismatic member subjected to an axial force

For member subjected to axial compression, *S* and *t* are given as follows, Ghali and Neville (1978):

$$S = \frac{u(s-uc)}{(2-2c-us)}\frac{EI}{l} \qquad \ldots (3.52)$$

, and

$$t = \frac{u(u-s)}{(2-2c-us)}\frac{EI}{l} \qquad \ldots (3.53)$$

Where:

$s = \sin u$, $c = \cos u$, $u = l\sqrt{P/(EI)}$

For member subjected to axial tension, *S* and *t* are given as follows:

$iu = l\sqrt{-P/(EI)}$, $i = \sqrt{-1}$

$\sinh u = -i \sin iu$, $\cosh u = \cos iu$

$$S = \frac{u(u\cosh u - \sinh u)}{(2-2\cosh u + u\sinh u)}\frac{EI}{l} \qquad \ldots (3.54)$$

, and

$$t = \frac{u(\sinh u - u)}{(2-2\cosh u + u\sinh u)}\frac{EI}{l} \qquad \ldots (3.55)$$

Where:

$u = l\sqrt{P/(EI)}$, *P*: the absolute value of the axial tension force

If shear deformation is considered, the rotational stiffness and the carryover moment are adjusted as follows:

$$S = [\frac{(4+\alpha)}{4(1+\alpha)}]\frac{u(u\cosh u - \sinh u)}{(2-2\cosh u + u\sinh u)}\frac{EI}{l} \qquad \ldots (3.56)$$

, and

$$t = [\frac{(2-\alpha)}{2(1+\alpha)}]\frac{u(\sinh u - u)}{(2-2\cosh u + u\sinh u)}\frac{EI}{l} \qquad \ldots (3.57)$$

3.8 The level rotation-translation stiffness

The level rotation and rotation-translation stiffness matrices used in all the transformation methods presented in Ibrahim (2013), and in this research is calculated using the four node rectangular plate finite element presented by Ghali and Neville (1978), and beams members used to represent the different floor beams and also the rigid parts of the slabs or beams intersecting with the wide shear walls.

The displacement function used in the formulation was a polynomial with twelve generalized coordinates as shown below:

$$w = A_1 + A_2.x + A_3.y + A_4.x^2 + A_5.x.y + A_6.y^2 + A_7.x^3 + A_8.x^2.y + A_9.x.y^2 + A_{10}.y^3 + A_{11}.x^3.y + A_{12}.x.y^3 \quad \ldots(3.58)$$

The rotation or the rotation-translation stiffness matrices are calculated after constructing the whole stiffness matrix of the floor and assigning the different shear walls, by applying a unit rotation in each of the two principal directions and unit translation of each shear wall with all the other directions restrained. The corresponding calculated support reactions are then arranged systematically to form the required level stiffness matrix. At the same time during the construction of the level stiffness matrix, another three matrices corresponding to the translation and the two rotations of all the floor joints are constructed. The elements of these matrices are constructed from the same applied unit rotations and translation that are used in the level stiffness matrix construction. After finalizing the transformation procedure, the vertical translation and rotations of all the joints in any floor level can be obtained directly by multiplying each of the three matrices by the rotation and translation vector of the corresponding level. By using the calculated translation and rotations of all the floor joints, the deformed shape of the floor can be plotted, and the stress contour can be calculated and plotted.

3.9 The Lateral Joints Displacements and the Shear Forces in the Vertical Members

By using the calculated rotations and the final moments in any member calculated using the transformation methods. The shear forces and the joint transverse displacements can, then, be calculated by using the following procedure;

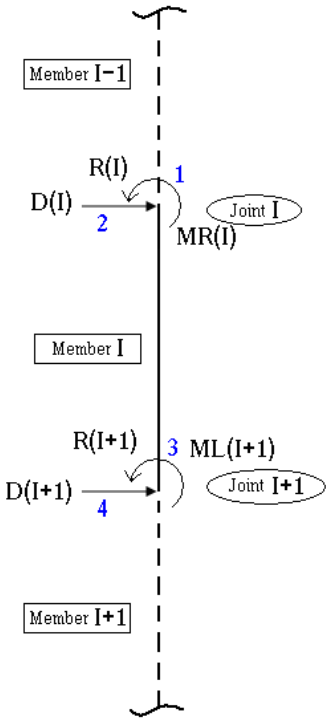

Figure 3.19: Degrees of Freedom of the Two Ends of Member # I

The system equation 3.59, corresponding to the member with the degrees of freedom, shown in Figure 3.19 is as follows:

$$\begin{bmatrix} S & (S+t)/L & t & -(S+t)/L \\ (S+t)/L & 2*(S+t)/L^2 & (S+t)/L & -2*(S+t)/L^2 \\ t & (S+t)/L & S & -(S+t)/L \\ -(S+t)/L & -2*(S+t)/L^2 & -(S+t)/L & 2*(S+t)/L^2 \end{bmatrix} \begin{Bmatrix} R(I) \\ D(I) \\ R(I+1) \\ D(I+1) \end{Bmatrix} = \begin{Bmatrix} MR(I) \\ VR(I) \\ ML(I+1) \\ VL(I+1) \end{Bmatrix} \quad \ldots(3.59)$$

Where

$S = [(4+\alpha)/(1+\alpha)].(EI/L)$ *and* $t = [(2-\alpha)/(1+\alpha)].(EI/L)$, $\alpha = (12EI)/(G.a_r.L^2)$

From the first row:

$R(I)*S+(S+t)/L*D(I)+t*R(I+1)-(S+t)/L*D(I+1)=MR(I)$

$D(I)$ is obtained as:

$D(I)=[(MR(I)-R(I)*S-t*R(I+1)+(S+t)/L*D(I+1)]L/(S+t)$

$$D(I)=[MR(I)-R(I)*S-t*R(I+1)]*L/(S+T)+D(I+1) \quad \ldots(3.60)$$

The numbering sequence is from top to bottom, and the displacement at the bottom is fixed, i.e. the displacement $D(N+1)$ =0, where N is the number of floors.

The other displacements are obtained by reverse order from bottom to top, i.e. from floor number N up to floor number 1.

The shear force is calculated directly from the calculated moments $MR(I)$ and $ML(I+1)$, and also can be cross checked as follows :

After calculating the whole displacements $D(1)$ to $D(N)$, the shear forces at the two ends can be calculated from the second and fourth rows of the matrix equation 3.59 as follows:

$$VR(I) = (S+t)/L*R(I)+ 2*(S+t)/L^2*D(I)+(S+t)/L*R(I+1)-2*(S+t)/L^2*D(I+1)$$

and;

$$VL(I+1) = -(S+t)/L*R(I)- 2*(S+t)/L^2*D(I)-(S+t)/L*R(I+1)+2*(S+t)/L^2*D(I+1) \quad \ldots(3.61)$$

$$= -VR(I)$$

3.10 Concluding Remarks on the transformation methods

The transformation methods simplify the 2D and 3D analysis of tall buildings in three ways, summarized as follows:

- The typical floors are analyzed only once, by condensation of the floor degrees of freedom (DOFs) into only the supported DOFs with all the other remaining DOFs translating and rotating freely.
- In 3D analyses, the considered DOFs in the vertical members are only two principal rotations in each floor level, as manipulated in the (MT) method, which can be reasonably used for moderate tall buildings or shear wall structures with negligible axial deformations in the vertical members. But for super tall buildings with the axial deformation in the vertical members dominant (e.g. tube and outrigger systems), (MFT) method can be used with one translational DOF added to each of the vertical members in each floor level, to represent their axial deformations. Hence, with some modifications in stiffness and carryover moment, the second order analysis can be incorporated with no extra cost.
- The solution for the unknowns are carried out in each floor level separately by use of the calculated equivalent rotational-translational stiffness matrices and balancing the fixed and the transformed moments and forces in the concerned level.

Appendix A5, presents a further optimization of the transformation procedure and a new faster subroutine developed and implemented in the program MFTProgV2.

3.11 Modal Analysis using the Transformation Methods

3.11.1 Introduction

As described by Clough and Penzien (1995), the mode displacement super-position method provides an efficient means of evaluating the dynamic response of structures. The response analysis for the individual modal equations requires very little computational effort, and in most cases only a relatively small number of the lowest modes of vibration need be included in the superposition. The mathematical models developed to solve practical problems in structural dynamics range from very simplified systems having only a few degrees of freedom (e.g. determinant method) to highly sophisticated finite element models including hundreds or even thousands of degrees of freedom in which as many as a relatively very few modes may contribute significantly to the response. To deal effectively with these practical problems, much more efficient means of vibration analysis are needed than the determinant solution procedure.

The basic concept is explained first with reference to the simplest application, the evaluation of the fundamental (or first mode) shape and frequency of an *N* degree of freedom system. Using the original dynamic matrix force, iteration will converge to the first mode properties.

3.11.2 Fundamental Mode Analysis

The use of iteration to evaluate the fundamental vibration mode of a structure is a very old concept that was originally called the Stodola method. The starting point of this formulation is the statement of the un-damped free vibration equations of motion given by equation 3.62:

$$kv_n = \omega_n^2 m v_n \qquad \ldots(3.62)$$

Equation 3.62 expresses the fact that in an un-damped free vibration, the inertial forces induced by the motion of the masses, *m*, must be equilibrated by the elastic forces resulting from the system deformations.

This equilibrium will be satisfied only if the displacements $\boldsymbol{v_n}$ are in the shape of the n^{th} mode of vibration and are varying harmonically at the n^{th}-mode frequency $\boldsymbol{\omega_n}$.

The inertial forces are that shown in the right hand side of Equation 3.62. Expressing the inertial forces as:

$$f_{In} = \omega_n^2 m v_n \qquad \ldots(3.63)$$

The displacements resulting from these forces may be calculated by solving the following static deflection problem:

$$v_n = k^{-1} f_{In} \qquad \ldots(3.64)$$

Or,

$$v_n = \omega_n^2 k^{-1} m v_n \qquad \ldots(3.65)$$

The matrix product in this expression summarizes the dynamic properties of the structure. It is called the *dynamic* matrix, and denoted as:

$$D = k^{-1} m \qquad \ldots(3.66)$$

Therefore, Equation 3.65, becomes:

$$v_n = \omega_n^2 D v_n \qquad \ldots(3.67)$$

In the conventional methods, the flexibility matrix of the structure could be obtained easily by inversion of the stiffness matrix (i.e. $\boldsymbol{k^{-1}}$), it will also be derived by applying a unit load to each degree of freedom successively and the deflections resulting from these unit loads represent the flexibility influence coefficients. In the transformation methods, the first option is not possible because the method has no direct lateral degrees of freedom, and the unit load option is used to calculate the flexibility matrix. Therefore, multiplying the flexibility matrix by the mass matrix yields the dynamic matrix.

The Stodola method can be demonstrated as follows: first computing the inertial forces corresponding to any assumed shape, then computing the deflections resulting from those forces, computing again the inertial forces due to the computed deflections. Repeating the procedure yields the correct shape vector and the corresponding vibration frequency.

. The concept is well illustrated in Figure 3.20.

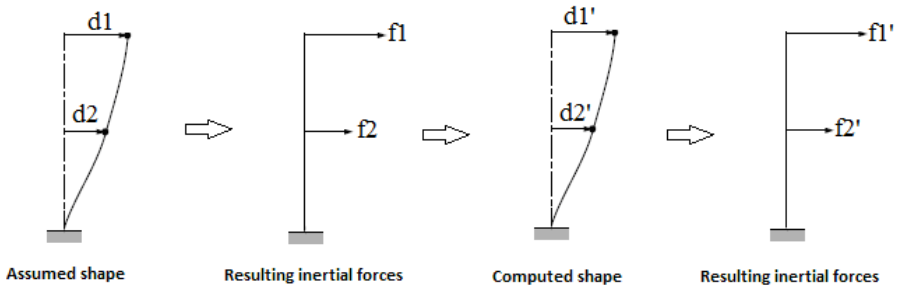

Figure 3.20: Physical interpretation of Stodola iteration sequence.

Using the original dynamic matrix (***D=k*$^{-1}$*m***), the Stodola iteration process must converge to the first mode shape. The contributions of the higher modes to the displacements vector can be made as small as desired by iterating for a sufficient number of cycles; thus the procedure converges to the first mode shape.

3.11.3 Analysis of Higher Modes

I- Second Mode Analysis

In the vibration theory, the proof of the convergence of the matrix iteration procedure to the first mode of vibration also suggests the manner in which matrix iteration can be used to evaluate higher modes as well.

The way of obtaining the second mode properties is by introducing a matrix called the *sweeping* matrix (***S₁***) used to purify the current shape vector from any first mode contribution, Clough and Penzien (1995):

$$S_1 \equiv I - \frac{1}{M_1}\phi_1\phi_1^T m \qquad \ldots(3.68)$$

Where:

M₁ is the first mode generalized mass = $\emptyset_1^T m\, \emptyset_1$

Ø₁ is the shape vector of the first mode.

m is the mass matrix.

Thus, if this component is removed from the assumed shape, the vector which remains may be said to be *purified*: This purified vector will now converge toward the second mode shape in the iteration process. The matrix iteration procedure can now be formulated with this sweeping matrix so that it converges toward the second mode of vibration. In this case, the equations used in the iteration procedures can be written which state that a second mode trial shape which contains no first mode components will converge toward the second mode.

Multiplying the dynamic matrix by the sweeping matrix yields a new dynamic matrix, (***D₂=DS₁***), which eliminates the first mode component from any trial shape and thus automatically converges toward the second mode. When ***D₂*** is used, the second mode analysis is entirely equivalent to the first mode analysis procedures.

It is clear that the first mode must be evaluated before the second mode can be determined by this method.

Instead of modifying the dynamic matrix by using the sweeping matrix, the alternative procedure used in the Transformation methods is to modify the mass matrix using the sweeping matrix to get a new purified mass matrix ($\boldsymbol{m_2=mS_1}$) (which may not be a diagonal matrix as $\boldsymbol{m}$). Instead of using the flexibility matrix, the solver of the transformation method is used here by receiving the inertial applied loads produced from the trial shape vector and producing a new corrected shape vector. This approach (based on Stodola method) is better compared with the direct iteration method where the flexibility matrix should by constructed by applying unit loads at all the directions of the degrees of freedom (i.e. *N* loading conditions). Using this modified approach yields a fast solution because the needed mode shapes are very few compared with the large amount of the whole degrees of freedom, especially in the very large systems such as the super-tall buildings.

The approach can be used also for the coupled mass matrices (e.g. consistent mass matrix or purified mass matrix), because the applied inertial forces are a vector produced from the multiplication of the vibration frequency, the mass matrix and the trial displacements vector. These multiplications result in an inertial load vector containing only one column.

II- Analysis of Third and Higher Modes

The same sweeping process can be extended to purify a trial vector of both the first and second mode components, with the result that the iteration procedure will converge toward the third mode. Hence this modified dynamic matrix $\boldsymbol{D_3}$, or the modified mass matrix $\boldsymbol{m_3}$, performs the function of sweeping out first and second mode components from the recent trial vector, and thus produces convergence toward the third mode shape. The process can be extended successively to the analysis of higher modes of the system in turn. The most important limitation of this procedure is that all the lower mode shapes must be calculated before any given higher mode can be evaluated.

The general form of the sweeping matrix is as follows:

$$S_n \equiv S_{n-1} - \frac{1}{M_n}\phi_n\phi_n^T m \qquad \ldots(3.69)$$

Where:

$\boldsymbol{M_n}$ is the n^{th} mode generalized mass = $\varnothing_n^T m\, \varnothing_n$

$\boldsymbol{Ø_n}$ is the shape vector of the nth mode.

$\boldsymbol{m}$ is the mass matrix.

3.11.4 Inverse Iteration (Stodola Concept) using the Transformation Method

In the previous discussions of matrix iteration, the improvement in calculated shape achieved during each cycle of iteration is obtained by simply multiplying the vector for the preceding cycle by the dynamic matrix $\boldsymbol{D=k^{-1}m}$. For this reason the procedure is called direct iteration. Because the method is based on the flexibility version of the dynamic matrix, it converges toward the shape of the lowest vibration mode, as is necessary as a general tool for structural dynamics. The major disadvantage of this procedure is that the flexibility matrix is fully populated, and this leads to computational inefficiency in comparison with what can be achieved by operating with the narrowly banded stiffness matrix. But direct iteration with the stiffness based dynamic matrix $\boldsymbol{E=m^{-1}k}$ is not appropriate because it will converge to the highest mode shape. Also the dynamic matrix $\boldsymbol{E}$ is not narrowly banded even though both $\boldsymbol{k}$ and $\boldsymbol{m}$ are. For these reasons another alternative technique is considered.

Inverse iteration is the preferred method for taking advantage of the narrow banding of the stiffness matrix. Because it is applied inversely, it converges toward the lowest mode shape. In order to retain the narrow banding of $\boldsymbol{k}$, the dynamic matrix $\boldsymbol{E}$ is never formed. Instead, the mass matrix is combined with the assumed displacement vector to obtain an inertial load vector. Then the stiffness based simultaneous equations of equilibrium are solved to obtain the improved displacement vector. As in the direct iteration method, the initial displacement vector will be assumed then the inertial forces due to harmonic motions with this shape are calculated. However, noting that the effect of the frequency will be removed subsequently by the normalization step, in this formulation the frequency is assumed to be unity and the resulting inertial forces are formed. Now the improved displacement vector resulting from the action of these forces is obtained by solving the equilibrium equations of the structure subjected to these forces. One way to solve these equations would be to calculate the flexibility matrix by inversion of the stiffness matrix ($\boldsymbol{f = k^{-1}}$) and to multiply the inertial forces by the produced flexibility matrix. This procedure actually would be entirely equivalent to the direct iteration

analysis and would be inefficient because of the need to invert and then multiply by a fully populated flexibility matrix. In the inverse iteration procedure, the equilibrium equations are solved after first using Gauss elimination method to decompose the stiffness matrix to the Lower (***L***) and Upper (***U***) triangular matrices. The simultaneous solution then is carried out in two fast direct and backward substitution steps.

As was described, this derived vector then is normalized by dividing by its largest element to obtain the improved first mode shape that is the final result of the first iteration cycle. It is important to note that the narrow banded character of the stiffness matrix ***k*** is retained in the triangular matrices ***L*** and ***U***. Consequently the efficiency of this inverse displacement analysis is greatly enhanced relative to the flexibility matrix formulation used with direct iteration. Because the only difference between this inverse iteration procedure and the previously described direct iteration lies in the more efficient Gauss decomposition technique used to calculate the derived displacement vector, the entire earlier description of direct matrix iteration is equally applicable to inverse iteration if the equation that was used previously to calculate the displacements vector is replaced by the simultaneous equation solution described above. However, even though this difference may appear to be minor, the tremendous computational advantage of inverse iteration must not be overlooked, especially when the system being analyzed has a large number of degrees of freedom.

In principle, the inverse iteration procedure can be combined with sweeping matrix concept to obtain a more efficient method for calculating the second and higher modes of vibration, as discussed before.

Repeated calculation of the displacements is very fast using the Transformation method, thus the method is proposed to be used as a simple alternative of the inverse iteration method.

As a conclusion, the un-damped free vibration equation that expresses the equilibrium between the vibration inertial forces and the elastic resisting forces will be adopted here as the basic eigenproblem. Because the dynamic matrix ***D*** contains both the flexibility and the mass properties of the structure, each cycle of the iteration solution for the mode shapes involves merely multiplication by ***D*** as in the direct iteration method or solving for the displacements as in the inverse iteration method, followed by normalization

(scaling) which is accomplished by dividing the improved displacement vector by its largest element in order to isolate the vibration frequency and obtain the new trial vector. This iteration procedure converges toward the lowest mode shape because the eigenvalue is in the denominator of the eigenproblem equation.

3.12 Buckling Analysis by Matrix Iteration (Vianello Method)

As for the vibration problem, the matrix iteration procedure for evaluating eigenvalues and eigenvectors is applicable also when axial forces act in the members of the structure, Clough and Penzien (1995). For any specified condition of axial loading, a similar equation may be formulated as:

$$v_1^{(1)} = \omega_1^2 \bar{D} v_1^{(0)} \qquad \ldots(3.70)$$

In which

$$\bar{D} = \bar{k}^{-1} m \qquad \ldots(3.71)$$

Where $\bar{k} = k - k_{G0}$ is the combined stiffness matrix, taking account of the geometric stiffness effect k_{G0}. The vibration mode shapes and frequencies can be determined by iteration, as if they are without axial loads. The effect of compressive axial forces is to reduce the stiffnesses of the members of the structure, thus tending to reduce the frequencies of vibration. In the limiting (buckling) case, the vibration frequency goes to zero, and the static eigenvalue equation takes the form

$$(k - \lambda_G k_{G0}) \hat{v} = 0 \qquad \ldots(3.72)$$

Pre-multiplying equation 3.72 by $(1/\lambda_G)\bar{f}$ gives

$$\frac{1}{\lambda_G} \hat{v} = G \hat{v} \qquad \ldots(3.73)$$

In which

$$G = \bar{f} k_{G0} \qquad \ldots(3.74)$$

Where, $\bar{f}$ is the flexibility matrix of the syatem.

Equation 3.74 has the same form as the vibration eigenvalue equations and may be solved by the same type of iterative procedure. The eigenvalues which permit nonzero values of

$\hat{v}$ to be developed are the buckling loads, which are represented by the values of the load parameter λ_G. Thus, if a trial shape for the first buckling mode is designated $v_1^{(0)}$, the iterative process is indicated by

$$\frac{1}{\lambda_{G0}} v_1^{(1)} = G v_1^{(0)} \qquad \ldots(3.75)$$

When the iterative procedure is used to evaluate buckling modes in this way, it is named the *Vianello method*, Clough and Penzien (1995). The matrix iteration analysis of buckling is identical in principle and technique to the iteration analysis of vibration. Even the orthogonality conditions can also be used in evaluating the higher buckling modes but generally only the lowest mode of buckling is of interest, and there is little need to consider procedures for evaluating higher buckling modes.

The influence of geometric stiffness on the vibration frequency of the structure can also be calculated by matrix iteration, but if the critical load value is reached, the vibration frequency will be zero. However, for any value of a smaller portion of critical loads, a corresponding frequency can be determined. Then the geometric stiffness is given by substituting this value into the expression for $\boldsymbol{k_{Go}}$. The elastic stiffness of the column is obtained and the combined stiffness matrix which takes account of the axial force effects is formulated by subtracting the geometric stiffness from the elastic stiffness. Finally, the vibration analyses could be carried out by iterating with a modified dynamic matrix calculated from the flexibility matrix produced from the inverse of the combined stiffness matrix.

Vianello method can also be formulated using the transformation method in order to calculate the buckling loads of buildings. By applying the transformation method, the linear displacement approximation can be directly used in the formulation of the geometric stiffness matrix. This approach can be directly applied in the case of two dimensional problems, because the geometric stiffness can be easily formulated using the total loads at each floor. The problem becomes more complicated in the case of three dimensional analysis of a buildings subjected to lateral loads producing twist rotations in the floor levels, because some of the terms in the geometric stiffness matrix depend on the axial loads in the individual vertical members. This can be solved with continuous corrections of the axial forces in the geometric stiffness matrix during the iterations

procedure. As for the vibration analysis, inverse iteration or Stodola concept can also be modified and incorporated in the Vianello buckling analysis.

In the two dimensional analysis, a parabolic shape is taken as a reasonable first guess for the first mode buckled shape.

To illustrate the analysis using Vianello method, assume a cantilevered column with 3 concentrated weights of magnitudes from top to bottom equal to N_1, N_2 and N_3 respectively, and segments lengths *l1*, *l2* and *l3*. When the linear-displacement approximation is used, the geometric stiffness of this cantilevered column is given as:

$$k_{G0} = \begin{bmatrix} \frac{N_1}{l_1} & \frac{-N_1}{l_1} & 0 \\ \frac{-N_1}{l_1} & \frac{N_1}{l_1} + \frac{N_2}{l_2} & \frac{-N_2}{l_2} \\ 0 & \frac{-N_2}{l_2} & \frac{N_2}{l_2} + \frac{N_3}{l_3} \end{bmatrix} \qquad \ldots (3.76)$$

For the torsional effects, the analysis is carried out as for the fictitious column illustrated by Smith and Coull (1991), which is located at the centroid of the total gravity loading above the concerned story. As illustrated by Smith and Coull, this column should be incorporated in the model to cater for the torsional P-Delta effect. The column has a negative torsional constant calculated from:

$$\frac{1}{h_i}\sum[P_{ij}(d_{yij}^2 + d_{xij}^2)] = \frac{1}{h_i}P_i r_i^2 = \frac{-GJ_i}{h_i} \qquad \ldots(3.77)$$

In which P_{ij} is the gravity load in column or wall j in story i, d_{yij} and d_{xij} are its Y and X distances from the center of gravity loading in story i, and r_i is the radius of inertia of the total load P_i about the center.

Using same concept as in Equation 3.77, the coordinate origin of the proposed program MFTProgV2 is located at the center of the total gravity loadings. The inertias are calculated approximately for each column or wall from the axial forces in column or wall computed from linear elastic analysis of the whole frame.

In MFTProgV2, if the column or wall is oriented in the building plane, the column or wall coordinates should be transformed to the coordinates corresponding to the principal axes of the column or wall as shown in Figure 3.21.

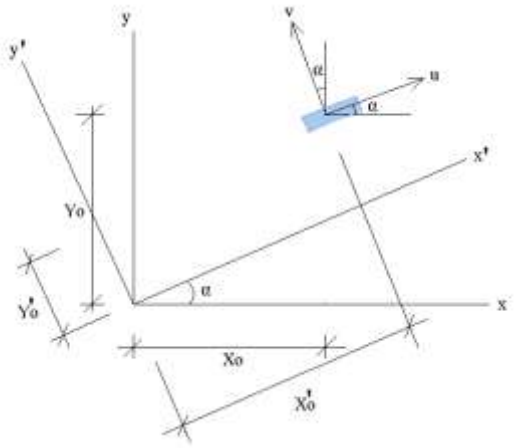

Figure 3.21: Transformation of coordinates for orient column

With reference to Figure 3.21, the new coordinates considered in the inertia calculations are obtained using the following transformation matrix equation:

$$\begin{Bmatrix} x_0' \\ y_0' \end{Bmatrix} = \begin{bmatrix} \cos\alpha & \sin\alpha \\ -\sin\alpha & \cos\alpha \end{bmatrix} \begin{Bmatrix} x_0 \\ y_0 \end{Bmatrix} \qquad \ldots(3.78)$$

The inertia part in the 3D building geometric stiffness matrix is constructed using the same arrangement as the loads parts, as shown in equation 3.76.

3.13 The Improved Vianello Method

Buckling analysis using Vianello method and the transformation method uses the linear-displacement function. The method can be improved by adjusting the end rotational stiffness and the carryover moment of the member by incorporating the axial load multiplied by the calculated buckling factor, using the Euler stability functions or the cubic shape function. The procedure is repeated until reaching a negligible difference between the last two buckling factors. The procedure should be carried out for each buckling mode after sweeping out the buckling matrix. The results converge towards the exact value faster than in the cases of the incremental and the bisection methods.

In this research, the proposed improved Vianello method is used in MFTProgV2 instead of the conventional eign solution as that used in the advanced buckling analysis solver of STAAD shown in Appendix E.

3.14 The conventional buckling incremental method

The elastic critical loads of plane frame can be obtained using the flow chart shown in Figure 3.22 which is based on the method described by Coates et al (1990). Illustration of

the method is shown in Appendix B. The method involves repeated stiffness method analysis of the structure at progressively increasing load factors. As shown by Coates et al (1990), the stiffness matrix ***Ks*** of a stable structure has the property of positive-definiteness, and a test for this property can be performed at each load level. As soon as a load factor is used for which ***Ks*** ceases to be positive-definite and becomes singular it is known that the critical load has been reached. The test applied is to the determinant of the matrix which should be positive until singularity when it becomes zero, but in practice exact singularity cannot be obtained and the sign becomes negative corresponding to a state of unstable equilibrium.

The determinant is used here as a convenient quantity for which a standard computer library routine is likely to be developed, but an alternative is presented in the end of this section.

An alternative to the use of eignvalues in checking singularity in a stability analysis if a Choleski solution is used, is to observe the sign in the square-rooting operation required for the calculation of diagonal terms in the decomposed matrix. For a positive-definite matrix these signs should all be positive, but one term will become negative as soon as the singular condition is passed. The method has the advantage that, apart from examining terms as they are calculated, no additional operations are required, but has the disadvantage that it provides no information from which mode shapes can be calculated.

3.15 Buckling Analysis using the transformation method

The incremental subroutine described in section 3.14 above is modified to be incorporated in the transformation method. The transformation method uses the rotational degrees of freedom in place of the lateral translational one. For this reason, the rotational stiffness is used to examine the singularity, as illustrated in Appendix C.

As shown in Appendix C, the condensed translation and rotation DOFs produce the same results. This fact, results in a generalized rule used in the buckling analysis by using the transformation method. In this case the minimum determinant of all the floors rotational stiffness matrices is used to examine the singularity.

I. Because in structural analysis the determinate of the stiffness matrix can be very large or very small (in stability analysis), the natural logarithm of the determinate is calculated and used instead of the determinant.

II. Although the algorithm is originally designed for plane frame, it is developed and used in both the 2D and 3D analyses.

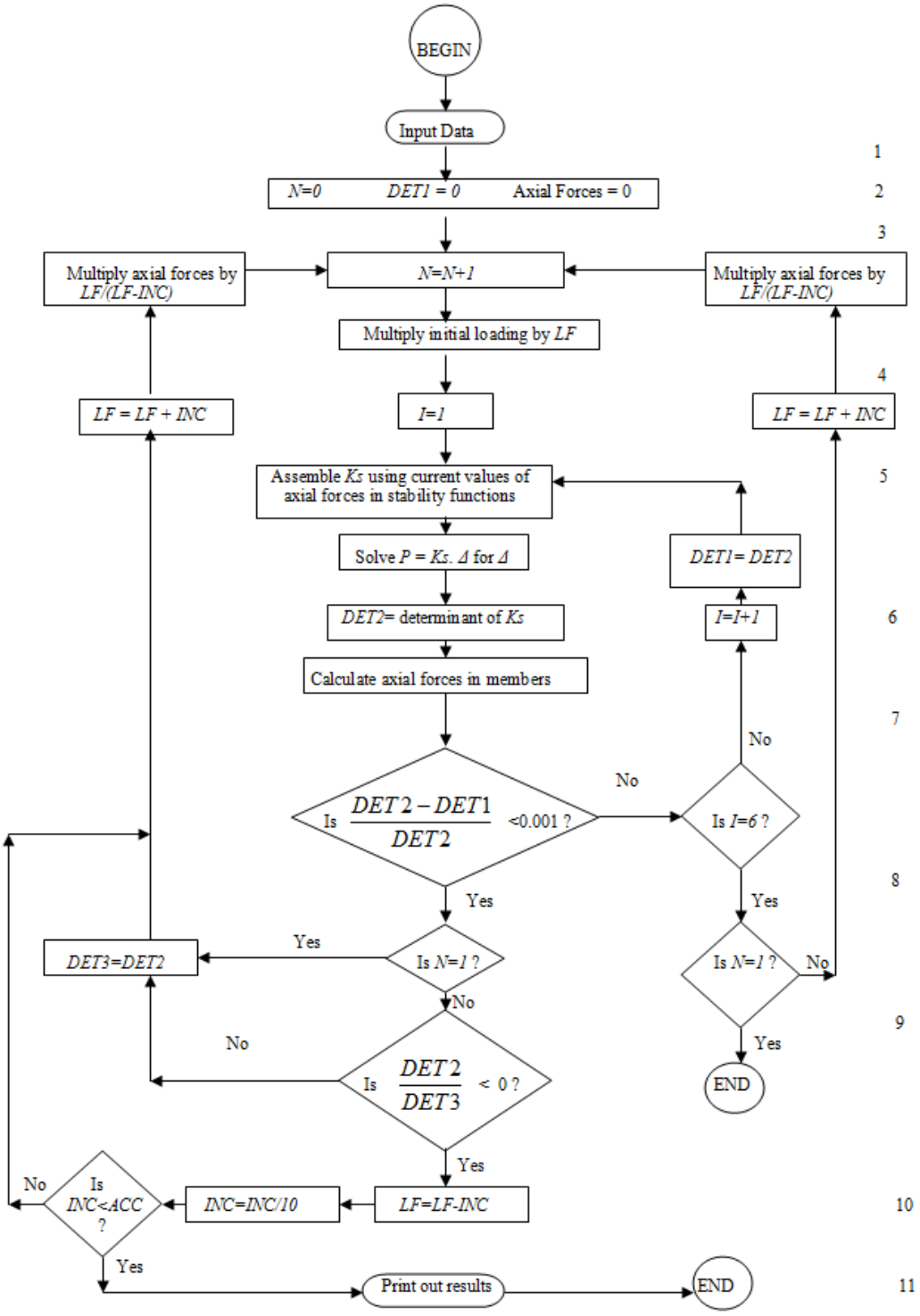

Figure 3.22: Flow chart for elastic critical loads of plane frame

3.16 Buckling Analysis using the transformation method with the aid of the bisection method

The sequence of the basic Solver in STAAD, shown in Appendix D, was followed partially in the proposed program MFTProgV2. The procedure followed in MFTProgV2 is as follows: 1) Linear static analysis based on the provided external loading is carried out. 2) Calculate member axial forces. These forces are used to calculate the rotational stiffness and the carryover moments, and are adjusted at each trial. Both the large delta effects and the small delta effects are calculated. 3) MFTProgV2 starts an iterative procedure with a buckling factor (*LF*) estimate of 1.0. If that *LF* causes buckling, then a new, lower *LF* estimate (new *LF* = previous *LF/2*) is used in the next trial. If the *LF* does not cause buckling, then a higher *LF* estimate (new *LF* = previous *LF**2*) is used. 4) After a few iterations, MFTProgV2 will have the largest *LF* that did not cause buckling (lower bound) and the lowest *LF* that did cause buckling (upper bound). Then each trial will use a *LF* estimate that is halfway between the current upper and lower bounds for *LF* (bisection method). 5) After the default iteration limit is reached or the maximum iteration limit is reached or when two consecutive *LF* estimates are within 0.1% of each other; then the iteration is terminated. 6) Result for this analysis is based on the average of the two values.

3.17 Review to the earthquake design response spectra

Earthquake is irregular ground motion and time-dependant acceleration function. The response spectrum can simplify the analysis by providing a graphic representation of the maximum response of a damped single-degree-of-freedom (SDOF) mass-spring system with continuously varying natural periods to a given ground excitation. By solving the equation of motion of the system, the relative displacement can be obtained. For any input acceleration, the solution will yield the maximum absolute value of the relative displacement u, termed the spectral displacement S_d, which will be a function of natural frequency, ω (or period) and damping factor, Smith and Coull (1991).

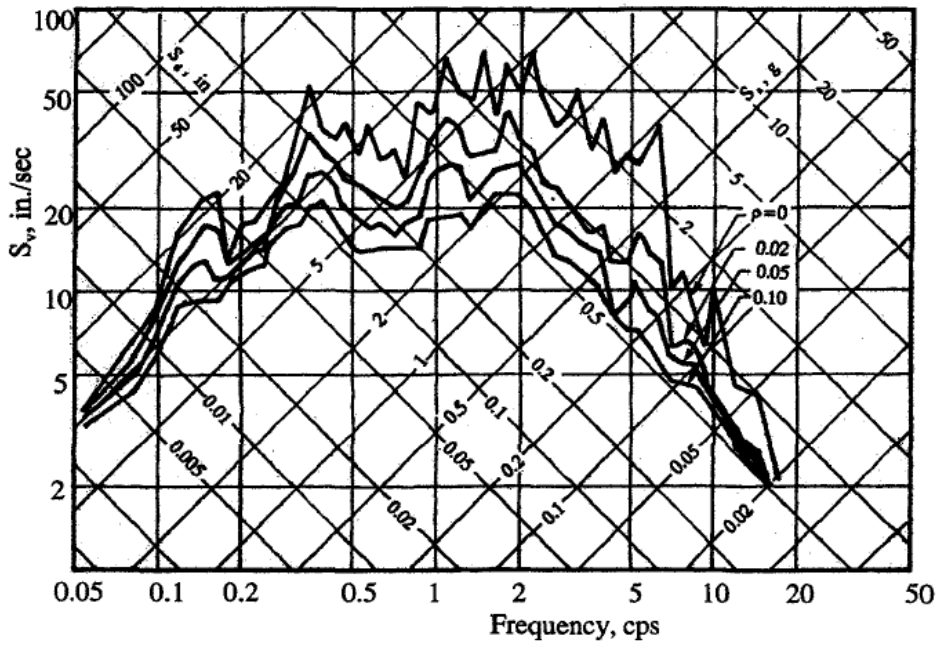

Figure 3.23: Response spectra. El Centro earthquake, N-S direction, Smith and Coull (1991)

The maximum pseudo relative velocity S_v, and maximum absolute pseudo acceleration S_a are then given by:

$S_v = \omega S_d$ …(3.79)

$S_a = \omega^2 S_d$ …(3.80)

The pseudo acceleration is identical to the maximum acceleration when there is no damping, which, for normal levels of structural damping, is practically the same as the maximum acceleration, Smith and Coull (1991).

As a result of the relationships described in the equations, the complete response spectrum may be represented on a plot of the form shown in Figure 3.23. The response spectra shown refer to the El Centro earthquake of May 1940. N-S direction, Smith and Coull (1991), and are for different damping factors. Although the actual response spectra for earthquake motions are quite irregular, they have the general shape of a trapezoid when plotted in tripartite logarithmic form as shown in Figure 3.24. For design purposes, the actual response spectrum is normally smoothed to produce a curve that consists only of straight line portions, as shown in Figure 3.24, Cheng (2001).

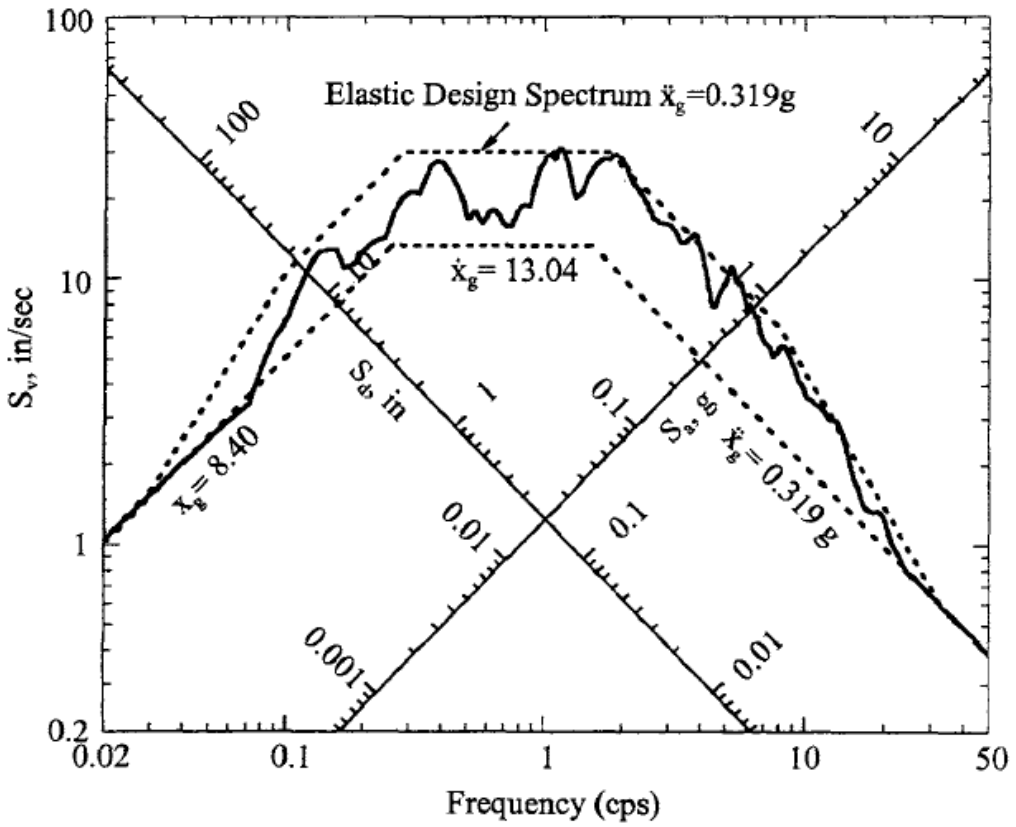

Figure 3.24: Idealized design response spectrum, Cheng (2001)

With the response spectra method, if the natural frequency of a structure is calculated, and the damping ratio is estimated, the important design parameters such as the maximum displacement and maximum acceleration can be obtained directly from the response spectrum diagram. Using the modal method of analysis, the peak response of any building to the design earthquake can be easily obtained.

3.17.1 Modal analysis procedure

To avoid solving the coupled dynamic equations of motion simultaneously, the modal methods of analysis can be used to determine all displacements that define the motions of the structure. The method employs the superposition of a limited number of modal peak responses, as determined from a prescribed response spectrum, and with appropriate modal combination rules it will yield results that compare closely with those from a time-history analysis, Smith and Coull (1991).

This method of analysis is based on the fact that for certain forms of damping that are reasonable approximations for many buildings, the equations of motion can be uncoupled

so that the response in each natural mode of vibration can be calculated independently of the others.

The advantage of this method is that an independent analysis can be made of a single-degree-of-freedom system for each natural mode of vibration. The response generally needs to be determined for only the first few modes since the total response to earthquake is primarily due to the lowest modes of vibration. Sufficiently accurate design values of forces and deformations in tall buildings could be achieved by combining no more than about six modes in each component direction. Three would probably be sufficient for medium-rise buildings, Smith and Coull (1991).

The earthquake response is obtained by combining the contributions of all the modes of vibration involved. And this can be used to give a complete time-history of the structural actions. However, only the evaluation of the peak response is of importance in design, and this may be derived directly from the design response spectrum.

3.17.2 Design response spectrum analysis

Since in the modal analysis the response of the structure in each mode of vibration is derived from a single-degree-of-freedom system, the maximum response in that mode can be obtained directly from the earthquake design response spectrum.

The maximum response in the N^{th} mode can be expressed in terms of the ordinates of the displacement S_d, Pseudo velocity S_v and pseudo acceleration S_a, which correspond to the frequency ω_n and damping ratio β_n. The three quantities are related by:

$S_a = \omega\, S_v = \omega^2 S_d$ …(3.81)

Expressed in terms of the modal participation factor γ_n the maximum values of the modal response quantities then become:

Maximum modal displacement:

$\bar{Y}_n = \gamma_n S_{dn}$ …(3.82)

Maximum displacement at jth floor:

$\bar{u}_{jn} = \gamma_n S_{dn} \varphi_{jn}$ …(3.83)

φ_n is the n^{th} modes of vibration and φ_{nj} is the ordinate of the n^{th} at the floor j.

Maximum value of equivalent lateral force at j^{th} floor P:

$$\bar{P}_{jn} = \gamma_n S_{an} m_j \varphi_{jn} \qquad \ldots(3.84)$$

Where, m_j is the mass at the level j.

The modal participation factor γ_n is given by:

$$\gamma_n = \frac{L_n}{M_n} \qquad \ldots(3.85)$$

Where, $L_n = \sum_{i=1}^{N} m_i \varphi_{in}$, and the modal mass $M_n = \sum_{i=1}^{N} m_i \varphi_{in}^2$

In the equations, a bar above a particular variable is used to denote the maximum value of the quantity concerned.

The maximum values of the internal forces in the building, particularly the story shear and moments, are then obtained by a static analysis of the structure.

The maximum modal response can thus be expressed in terms of the displacements or accelerations, evaluated for the particular frequency and damping ratio for the mode, from the design response spectrum.

The total response R of the building to earthquake motions is the sum of the individual responses r of the natural modes. However, the maximum total response R is not generally equal to the absolute sum of the maximum modal responses, r, since they will not normally occur simultaneously. Such a sum would, however, give an upper bound to the maximum likely total response.

A more realistic design estimate of the maximum response is to combine the modal maxima according to the square root of the sum of squares (SRSS) method, Smith and Coull (1991).

$$\bar{R} = \sqrt{(\sum \bar{r}_n)^2} \qquad \ldots(3.86)$$

The maximum values of displacements, inter-story drifts, story shears, and moments may all be evaluated using the SRSS method.

This formula will generally give realistic estimates of peak response for structures in which the natural frequencies of vibration are well separated, a property that is usually valid for idealized building structures in which lateral displacements in one plane are considered (2D analysis). If this is not the case, and some natural frequencies are so close that the motions may be coupled together, a more realistic combination, such as the

complete quadratic combination method (CQC), should be undertaken, Smith and Coull (1991).

It is necessary to consider only the modes that contribute most to the response of the structure. Since most of the energy of vibration is contained in the lower modes of vibration. A convenient rule is to include a sufficient number of modes, *r*, so that an effective modal mass, *e*, of at least 90% of the total mass of the building is represented by the modes chosen, Smith and Coull (1991), that is,

$$e = \frac{\sum_{n=1}^{r} \gamma_n L_n \,/100}{\sum_{j=1}^{N} m_j} \geq 90 \qquad \ldots(3.87)$$

3.17.3 SRSS Modal Combination Method

The SRSS method can be expressed as

$$x^k = \sqrt{\sum_{n=1}^{N} (x^k)_n^2}; \qquad \ldots(3.88)$$

N = number of modes considered

In which superscript k represents the k^{th} degree of freedom of the structural system. This method of combination is known to give a good approximation of the response for frequencies distinctly separated in neighboring modes, Cheng (2000).

3.17.4 CQC Modal Combination Method

In general, the CQC method may offer a significant improvement in estimating maximum structural response. The CQC combination is expressed as:

$$x^k = \sqrt{\sum_{i=1}^{N}\sum_{j=1}^{N} x_i^k \alpha_{ij} x_j^k} = \left[\sum_{i=1}^{N} (x_i^k)^2 + \sum_{j=1(j\neq i)}^{N}\sum_{i=1}^{N} x_i^k \alpha_{ij} x_j^k\right] \qquad \ldots(3.89)$$

$$i,j = 1 - N$$

Where: α_{ij} is called the cross-correlation coefficient, indicating the cross-correlation between modes i and j. α_{ij} is a function of model frequency and damping ratio of a structure, and can be expressed as:

$$\alpha_{ij} = \frac{8\rho^2(1+q)q^{3/2}}{\left(1-q^2\right)^2 + 4\rho^2 q(1+q)^2} \qquad \ldots(3.90)$$

$q=P_j/P_i$

The correlation coefficient diminishes when q is small, i.e. p_i and p_j are distinctly separate natural frequencies, particularly when damping is small, such as $\rho = 0.05$ or less. The CQC method is significant only for a narrow range of q. Note that when α_{ij} is small, the second term of equation 3.89 can be neglected; consequently CQC is reduced to SRSS, Cheng (2000).

3.18 The time history analysis method

The dynamic loading resulting from blast, gusts of wind, or seismic forces is generally irregular. In such case the equation of motion has to be solved numerically, and a solution in exact form can be obtained only if some idealized loading is used to represent the true loading. Analysis for a general dynamic loading resulting from time-dependant effect is accomplished by considering the loading as a sequence of impulse loads, and integrating for the effect of these impulses to obtain the system response. This integration can either be carried out in closed form, if the load function is fairly simple, or numerically, if the function is complex.

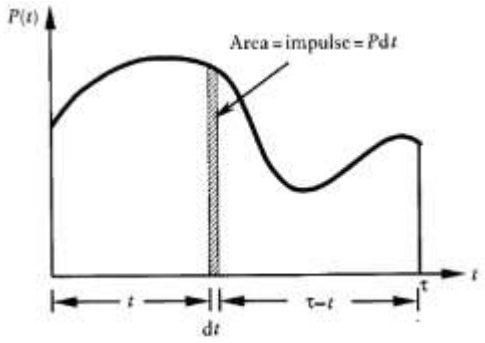

Figure 3.25: General force-time relation

For a damped single-degree-of-freedom system subjected to a randomly varying time-dependant force, *P(t)*, as shown in Figure 3.25, the response to the total force can be evaluated as the cumulative action of the individual increases.

When initial displacement and velocity are zero, the final displacement at time τ caused by the impulse applied at earlier time t is equal to:

$$D_\tau = \frac{1}{\omega_d m}\int_0^\tau P e^{-\beta(\tau-t)} \sin(\omega_d \tau - \omega_d t)dt \qquad \ldots(3.91)$$

$$\beta = \frac{c}{2m}$$

Where

c = damping coefficient

m = lumped mass

$$\omega_d = \omega\sqrt{1-\zeta^2}$$

$$\zeta = \frac{\beta}{\omega}$$

ζ = damping ratio, ω_d = damped natural frequency

This integration represents the displacement response of a single-degree-of-freedom system subjected to a regular or irregular time-dependant force.

This type of integration is named Duhamel's superposition integral (or convolution integral). It can be easily evaluated numerically using step-by-step methods of integration to give the required displacement, Ghali et al (2009).

In this research, numerical and analytical methods are developed. The numerical method was developed first and verified using simple problems. It was seen that the numerical method is not efficient in the analysis using real problems such as in the case of solving for seismic time-dependant forces e.g. El Centro earthquake (www.vibrationdata.com). With 31.2 seconds duration of the earthquake and 0.02 seconds time step, the total segments of linear problem is about 1560 segments. The need for a more efficient method arises, and a close form solution was developed and used in all the verification works.

3.18.1 Time history problem, the proposed numerical solution

Figure 3.26, shows a linear relation between two ordinates of time-dependant loading with multiple of segments. Each segment start and end times are measured from a reference time 0. The numerical integration is carried out for each segment by division to a number of sub-segments. The effects are summed starting from the earlier segment, to give the total displacement at the end of the time duration.

With reference to Figure 3.26, the total displacement is given using equation 3.91 as follows:

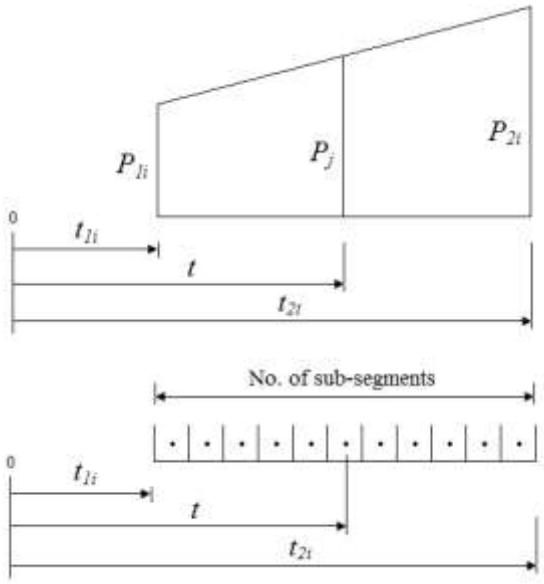

Figure 3.26: Numerical Solution of time history linear loadings between ordinates

$$D_\tau = \frac{1}{\omega_d m}\sum_{i=1}^{N}\sum_{j=1}^{n} P_j e^{-\beta(\tau-t)} \sin(\omega_d \tau - \omega_d t)\Delta t \qquad \ldots(3.92)$$

Where:

t_{1i} is the start time of the loading segment number *i*.

t_{2i} is the end time of the loading segment number *i*.

P_{1i} is the loading at the start of the loading segment number *i*.

P_{2i} is the loading at the end of the loading segment number *i*.

$$\Delta t = \frac{(t_{2i} - t_{1i})}{n} \qquad \ldots(3.93)$$

$$t = t_{1i} + \frac{\Delta t}{2} \qquad For\ j=1 \qquad \ldots(3.94)$$

$$t = t + \Delta t \qquad For\ j>1 \qquad \ldots(3.95)$$

$$P_j = P_{1i} + \frac{(P_{2i} - P_{1i})}{(t_{2i} - t_{1i})}(t - t_{1i}) \qquad \ldots(3.96)$$

N = No. of segments between any two readings.

n = number of sub-segments in each segment (can be increased for more accurate solution).

Where;

t is the time at the mid of the sub-segment *j* within the loading segment number *i*.

P_j is the loading ordinate at the mid of the sub-segment j within the loading segment number i at time t.

3.18.2 Time history problem, the proposed closed-form solution

The linear relation between the two forces of any two adjacent points is introduced in equation 3.91 as follows. The integration is carried out for each segment and the total displacement is obtained by the summation as shown in the following equations:

$$D_\tau = \frac{1}{\omega_d m}\int_0^\tau P e^{-\beta(\tau-t)} \sin(\omega_d \tau - \omega_d t)dt$$

$$D_\tau = \frac{1}{\omega_d m}\int_0^\tau P e^{-\beta\tau} e^{\beta t}[\sin(\omega_d \tau)\cos(\omega_d t) - \sin(\omega_d t)\cos(\omega_d \tau)]dt$$

$$D_\tau = \frac{1}{\omega_d m}\sum_{i=1}^{N}\{\int_{t1i}^{t2i}(P_{1i}t + P_{2i}) e^{-\beta\tau} e^{\beta t}[\sin(\omega_d \tau)\cos(\omega_d t) - \sin(\omega_d t)\cos(\omega_d \tau)]dt\}$$

$$= \frac{e^{-\beta\tau}}{\omega_d m}\sum_{i=1}^{N}\{\int_{t1i}^{t2i}(P_{1i}t + P_{2i}) e^{\beta t}[\sin(\omega_d \tau)\cos(\omega_d t) - \sin(\omega_d t)\cos(\omega_d \tau)]dt\}$$

$$D_\tau = \frac{e^{-\beta\tau}}{\omega_d m}\sum_{i=1}^{N}\{\sin(\omega_d \tau)P_{1i}\int_{t1i}^{t2i} te^{\beta t}\cos(\omega_d t)dt + \cos(\omega_d \tau)P_{1i}\int_{t1i}^{t2i} te^{\beta t}\sin(\omega_d t)dt$$

$$+ \sin(\omega_d \tau)P_{2i}\int_{t1i}^{t2i} e^{\beta t}\cos(\omega_d t)dt + \cos(\omega_d \tau)P_{2i}\int_{t1i}^{t2i} e^{\beta t}\sin(\omega_d t)dt\ \} \quad \ldots(3.97)$$

Where: N is the number of segments.

t is the time within the loading segment number i.

P is the loading ordinate within the loading segment number i at time t.

Equation 3.97, includes the following forms of integrations, which are carried out and used to formulate the closed-form solution for the total displacement due to the time history applied loads or, acceleration acting in the building base.

$$I_1 = \int x e^{bx} \cos gx.dx \qquad \ldots(3.98)$$

$$I_2 = \int x e^{bx} \sin gx.dx \qquad \ldots(3.99)$$

$$I_3 = \int e^{bx} \cos gx.dx \qquad \ldots(3.100)$$

$$I_4 = \int e^{bx} \sin gx.dx \qquad \ldots(3.101)$$

The integrations are carried out for equations 3.98 to 3.101 using integration by parts and are as shown below:

$$I_3 = \frac{[e^{bx}(g \sin gx + b \cos gx)]}{g^2 + b^2} \qquad \ldots(3.102)$$

$$I_4 = \frac{[e^{bx}(b \sin gx - g \cos gx)]}{g^2 + b^2} \qquad \ldots(3.103)$$

$$I_1 = \frac{[e^{bx}(xg \sin gx + xb \cos gx) - bI_3 - gI_4]}{g^2 + b^2} \qquad \ldots(3.104)$$

$$I_2 = \frac{[e^{bx}(-xg \cos gx + xb \sin gx) - bI_4 + gI_3]}{g^2 + b^2} \qquad \ldots(3.105)$$

The final displacement is related to a single-degree-of-freedom system, and for multi-degrees-of-freedom systems, the coupled differential equations of motion need uncoupling using the modal methods as shown in the following sections.

3.18.3 The normal coordinates system

In derivation of the equation of motion of a forced un-damped system in coordinates $\{D\}$, the stiffness matrix $[S]$ in the equation is generally not a diagonal matrix. The equations become uncoupled if both the mass matrix $[m]$ and the stiffness matrix $[S]$ are diagonal matrices.

Transformation of the n coordinates $\{D\}$ into another system with the same number of coordinates $\{\eta\}$, is given by:

$\{D\} = [\varnothing]\{\eta\}$ …(3.106)

Where $[\varnothing]$ is the transformation matrix. This gives an equation of motion in which both $[m]$ and $[S]$ are transformed into $[M]$ and $[K]$ which are generally diagonal matrices and hence the equations of motion become uncoupled.

The coordinates $\{\eta\}$ are called normal coordinates, Ghali et al (2009).

The generalized [M] and [K] matrices transformed to the normal coordinates, and the transformed force, $\{L\}$, are:

$[M]= [\emptyset]^T [m] [\emptyset]$ …(3.107)

$[K]= [\emptyset]^T [S] [\emptyset]$ …(3.108)

$\{L\}= [\emptyset]^T \{P\}$ …(3.109)

Using the orthogonality relationships, the transformation matrix [$\emptyset$] can be formed by the eign vectors of the considered modes.

The uncoupled form of the equation of motion is useful when considering response to time-dependent forces. It makes it possible to determine the response in each normal mode separately as an independent system with one degree of freedom, The displacement $\{\eta\}$ are then transformed to the displacement $\{D\}$. Equation 3.106 superimposes the modes to obtain the total displacement.

3.18.4 Response of structures to ground motion

In an analysis of seismic effects, the response of structures is determined due to a given motion of the supports rather than due to the application of external forces. The support motion may be described by an acceleration-time curve obtained from records of previous earthquakes, as in El Centro earthquake.

The effect of the support motion is the same as that a force $(-\ddot{u}_s\, m)$ acting on the building. The equations of motion are solved for the normal displacements $\{\eta\}$, and the final displacements $\{D\}$ are obtained using equation 3.106.

3.18.5 Structural response history using the transformation method

The previous sections determine time history displacements in the directions of the respective degrees of freedom. In this section a procedure is adopted for the calculations of the different structural responses due to the already obtained displacements, by using the transformation method. In the conventional methods the calculated time history displacements are applied as prescribed displacements in the directions of the lateral degrees of freedom and the structural responses are obtained accordingly. In the transformation method these lateral degrees of freedom do not exist and the adopted procedure to calculate the structural responses is based on distributing the fixed-end moments produced from the time history displacements. The responses include the internal stresses in the different members, the local displacements and the supports reactions.

Calculation of the time history responses of the structure, in the existence of the given displacements, can be carried out using one of two different ways based on the following cases:

Case (1): If the time history records are less than the structure total degrees of freedom, the structural responses can be obtained by applying the known displacements in the structure and calculating the induced fixed-end moments in the vertical members, then the structure analyzed, and the structural responses can be directly obtained for each time ordinate.

Case (2): If the time history records are much greater than the total degrees of freedom, as in the El Centro earthquake records, it is more efficient to construct a structural response matrix built from successively applying unit displacements at the different degrees of freedom and obtaining the partial different structural responses due to the unit displacements. Thus, the final responses can be obtained by multiplying the structural responses matrix by the known displacements vector at the concerned time.

The theory is illustrated firstly for 2D analysis and then generalized to the 3D analysis. In the 2D analysis, calculation of the structural responses using the transformation methods can be carried out using the following procedure:

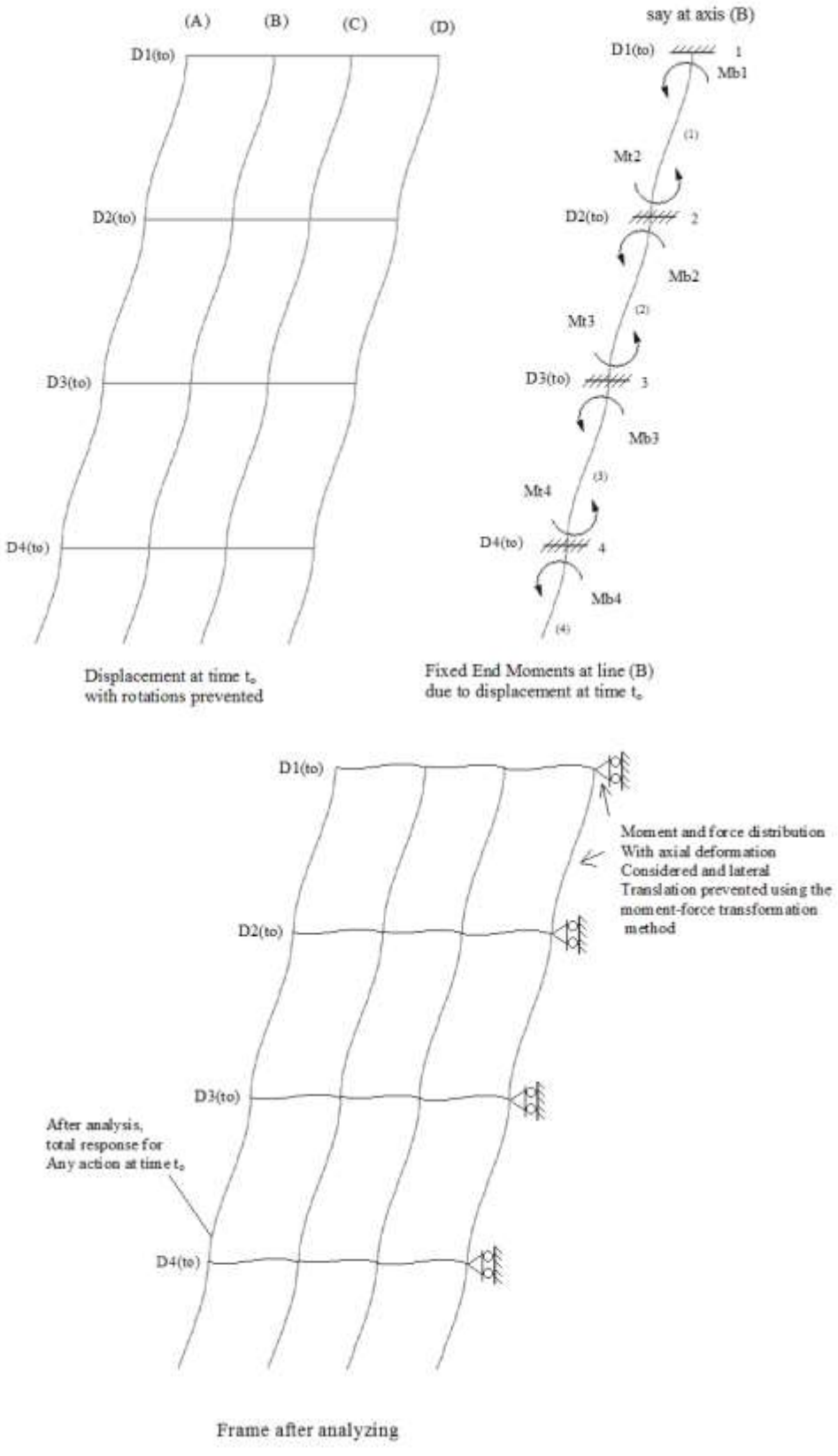

Figure 3.27: Total structural response due to displacements at time t_o

For Case (1), with reference to Figure 3.27:

(1) Apply all the displacements set at any time t_o, at the respective DOFs, keep all the rotations of the DOFs restrained.

(2) Calculate the fixed-end moments in all the vertical members produced from the displacements set at time t_o, using the following equations:

$$Mb_i = +[\frac{(S+t)}{L}]_i[D_i(t_o) - D_{i+1}(t_o)] \quad \ldots(3.110)$$

$$Mt_{i+1} = Mb_i \quad \ldots(3.111)$$

Where:

$D_i(t_o)$ = Displacement of joint i, at time t_o.

$D_{i+1}(t_o)$ = Displacement of joint $i+1$, at time t_o.

S = Rotational stiffness.

t = Carryover moment.

Mb_i = Fixed Moment in member i, just below joint i.

Mt_{i+1} = Fixed Moment in member i, just above joint $i+1$.

(3) Analyze the frame by distributing the calculated fixed-end moments using the moment-force transformation method with the axial deformation of the vertical members considered. Use in the analysis, the ordinary rotational stiffnesses and the carryover moments of the members, with the joints laterally restrained to be prevented from extra translations, using the matrices shown below (shear deformations considered in the elements):

Assuming 5 vertical members:

The condensed rotational stiffness matrix of the group is a diagonal uncoupled matrix composed of the rotational stiffness of the individual vertical members and is given as follows:

$$[S^*] = \begin{bmatrix} [\frac{(4+\alpha)}{(1+\alpha)}\frac{EI}{L}]_1 & 0 & 0 & 0 & 0 \\ 0 & [\frac{(4+\alpha)}{(1+\alpha)}\frac{EI}{L}]_2 & 0 & 0 & 0 \\ 0 & 0 & [\frac{(4+\alpha)}{(1+\alpha)}\frac{EI}{L}]_3 & 0 & 0 \\ 0 & 0 & 0 & [\frac{(4+\alpha)}{(1+\alpha)}\frac{EI}{L}]_4 & 0 \\ 0 & 0 & 0 & 0 & [\frac{(4+\alpha)}{(1+\alpha)}\frac{EI}{L}]_5 \end{bmatrix} \quad \ldots(3.112)$$

And the carryover moment matrix of the group is also a diagonal uncoupled matrix composed of the carryover moment of the individual vertical members and is given as follows:

$$[t^*] = \begin{bmatrix} [\frac{(2-\alpha)}{(1+\alpha)}\frac{EI}{L}]_1 & 0 & 0 & 0 & 0 \\ 0 & [\frac{(2-\alpha)}{(1+\alpha)}\frac{EI}{L}]_2 & 0 & 0 & 0 \\ 0 & 0 & [\frac{(2-\alpha)}{(1+\alpha)}\frac{EI}{L}]_3 & 0 & 0 \\ 0 & 0 & 0 & [\frac{(2-\alpha)}{(1+\alpha)}\frac{EI}{L}]_4 & 0 \\ 0 & 0 & 0 & 0 & [\frac{(2-\alpha)}{(1+\alpha)}\frac{EI}{L}]_5 \end{bmatrix} \quad \ldots(3.113)$$

Where: $\alpha = \dfrac{12EI}{Ga_r L^2}$

(4) Obtain from the analysis results, the total responses for any action (e.g. shear, moment, axial force), due to the applied displacements set at the concerned time.

In the analysis, it is worthwhile to note that:

A- The equivalent stiffness and the transformation factors matrices may be calculated only once and used several times for the different displacements sets, in order to accelerate and optimize the calculations.

B- The response matrix can include many responses at the same time (e.g. base shear, overturning moment, moment in one column, rotation in the member end or axial deformation.)

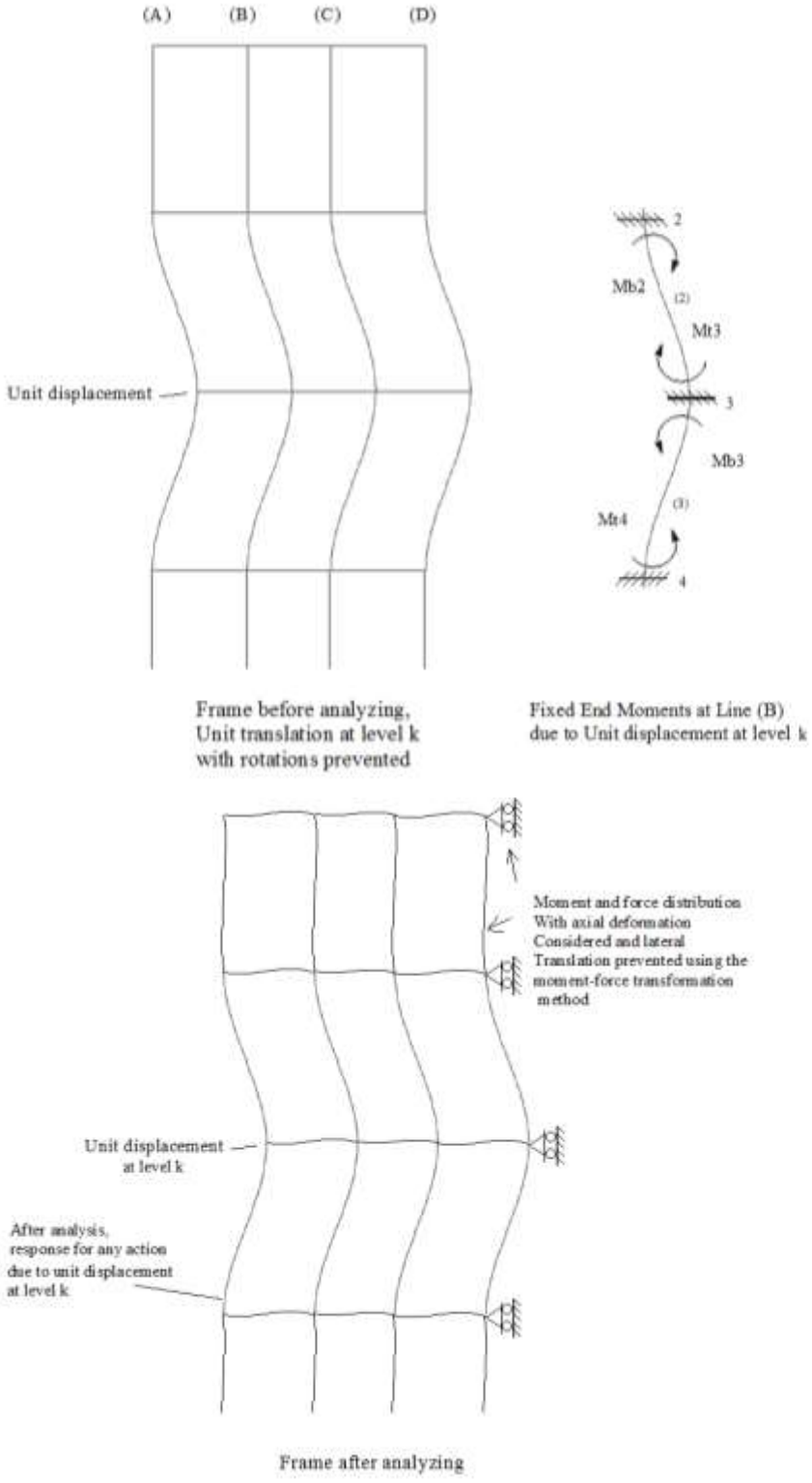

Figure 3.28: Partial structural response due to unit displacement at level *k*

For Case (2), with reference to Figure 3.28:

(1) Apply unit displacement at the first DOF with all the joints in the other levels remain in positions. The rotations of all the joints should be restrained.

(2) Calculate the fixed-end moments in the vertical members produced from the unit displacement, at joint *i*, for the affected members *i* and *i-1* as follows:

For unit displacement at joint *i*, the affected members are member *i* and member *i-1*
And the induced fixed-end moments are:
For member *i-1*:

$$Mb_{i-1} = -[\frac{S+t)}{L}]_{i-1} \quad , (i \neq 1) \qquad \ldots(3.114)$$

$$Mt_i = Mb_{i-1} \qquad \ldots(3.115)$$

For member *i*:

$$Mb_i = +[\frac{S+t)}{L}]_i \qquad \ldots(3.116)$$

$$Mt_{i+1} = Mb_i \qquad \ldots(3.117)$$

(3) Analyze the frame by distributing the calculated fixed-end moments using the moment-force transformation method with the axial deformation of the vertical members considered. Use in the analysis, the ordinary rotational stiffnesses and the carryover moments of the members, with the joints laterally restrained to be prevented from extra translations, using the same matrices as in case (1).

(4) Obtain from the analysis results, the partial response due to the applied unit displacement.

(5) Repeat steps 1 to 3 with the next degree of freedom, until finishing all the degrees of freedom.

(6) Use the constructed structural response matrix, that contains all the required responses, and multiply the matrix by the displacements set vector at any concerned time t_o, to get the complete response at that time.

In the analysis, the notes presented for Case (1) are also apply for Case (2).

In the 3D analysis, for the two cases, the displacement sets in case (1) or the unit displacements in case (2), will be applied in the building global coordinates directions. The global displacements are then transformed to obtain the local displacements of the vertical members using equation 3.118 as follows:

$$\begin{Bmatrix} u_i \\ v_i \\ rw_i \end{Bmatrix} = \begin{bmatrix} \cos\alpha & \sin\alpha & X_0\sin\alpha - Y_0\cos\alpha \\ -\sin\alpha & \cos\alpha & X_0\cos\alpha + Y_0\sin\alpha \\ 0 & 0 & 1 \end{bmatrix} \begin{Bmatrix} x \\ y \\ rz \end{Bmatrix} \quad \ldots(3.118)$$

And the same steps used in the 2D analysis to obtain the structural responses are carried out also in the 3D analysis.

3.19 Response spectrum analysis using the transformation method

The illustrated procedure discussed in section 3.17 is directly used in the proposed program MFTProgV2. The lateral response forces obtained using the spectra curve, are calculated for each mode and applied directly on the structure. The transformation procedure is carried out and the required response for each mode is calculated. The total responses are calculated using the methods of combinations (namely SRSS and CQC).

3.20 The Mass matrix

The mass matrix for any lumped mass in any floor of 3D model, considering the responses in the two horizontal coordinates *x* and *y* and neglecting the vertical inertia force and the rotary inertias about axes *x* and *y* which are very small and can be eliminated, is given as follows:

$$[M] = \begin{bmatrix} m_x & 0 & -m_x Y_{ms} \\ & m_y & m_y X_{ms} \\ symm & & m_x Y_{ms}^2 + m_y X_{ms}^2 \end{bmatrix} \quad \ldots(3.119)$$

And for the i^{th} floor with *L* lumped masses. The mass matrix is:

$$[M_i]=\begin{bmatrix} \sum_{j=1}^{L} m_{xj} & 0 & \sum_{j=1}^{L}(-m_{xj}Y_{msj}) \\ & \sum_{j=1}^{L} m_{yj} & \sum_{j=1}^{L}(m_{yj}X_{msj}) \\ symm & & \sum_{j=1}^{L}(m_{xj}Y_{msj}^2+m_{yj}X_{msj}^2) \end{bmatrix} \quad \ldots(3.120)$$

If the coordinate origin is chosen to coincide with the total masses center, then the mass matrix becomes a diagonal matrix, which will simplify the problem solution, and the final simplified mass matrix becomes:

$$[M_i]=\begin{bmatrix} \sum_{j=1}^{L} m_{xj} & 0 & 0 \\ & \sum_{j=1}^{L} m_{yj} & 0 \\ symm & & \sum_{j=1}^{L}(m_{xj}Y_{msj}^2+m_{yj}X_{msj}^2) \end{bmatrix} \quad \ldots(3.121)$$

3.21 Column Shortening Calculations for Reinforced and Composite Concrete Structures

A procedure for calculation of time dependent column shortening in tall building by using the transformation method is proposed as a future study. A brief illustration shows the efficiency of the procedure is presented in Appendix F.

CHAPTER FOUR

Computer Program MFTProgV2

4.1 Introduction

In this chapter the program MFTProgV2 (Nonlinear version) developed on the basis of the proposed theory and presented in this research, is described briefly.

4.2 Description of the Program MFTProgV2

The computer programs have been written in Visual Basic 6 and are developed based on the transformation methods presented in chapter three and in Ibrahim (2013), and can be used in any personal computer. The program utilizes graphical user interface (GUI) both in the data input and output modes.

Flow charts illustrate the general algorithm of the moment-force transformation procedure, extraction of the dynamic properties of the building and the buckling analysis using the bisection method described in section 3.16, are shown in Figures 4.1-a to 4.3-c.

Same as the previous versions, MTProg and MFTProg, the program MFTProgV2 includes two modes of analysis:

1- Two dimensional analyses. 2- Three dimensional analyses.

The layout of the program is shown in Figure 4.4. The two and three dimensional analysis modes buttons are shown in the figure, with different buttons used in the two analysis modes.

4.2.1 The two Dimensional analysis

This type of analysis is used to solve problems of portal frames, coupled shear walls (Walls with openings), symmetrical frames subjected to symmetrical loadings with absence of floors twist rotations.

Pressing the two dimensional button results in showing the multi-page form shown in the Figure 4.5

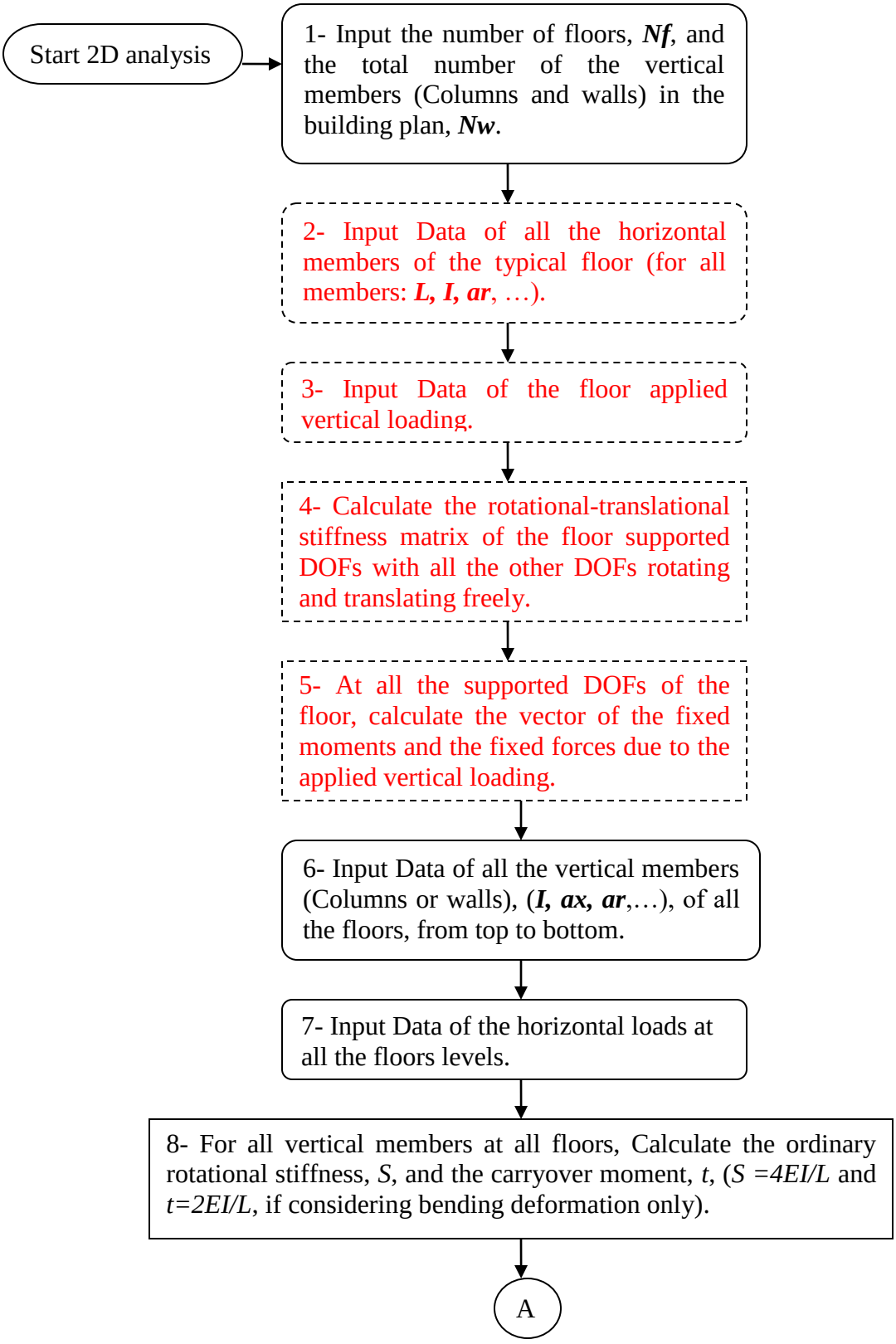

Figure 4.1-a: Flow chart of the moment-force transformation main solver

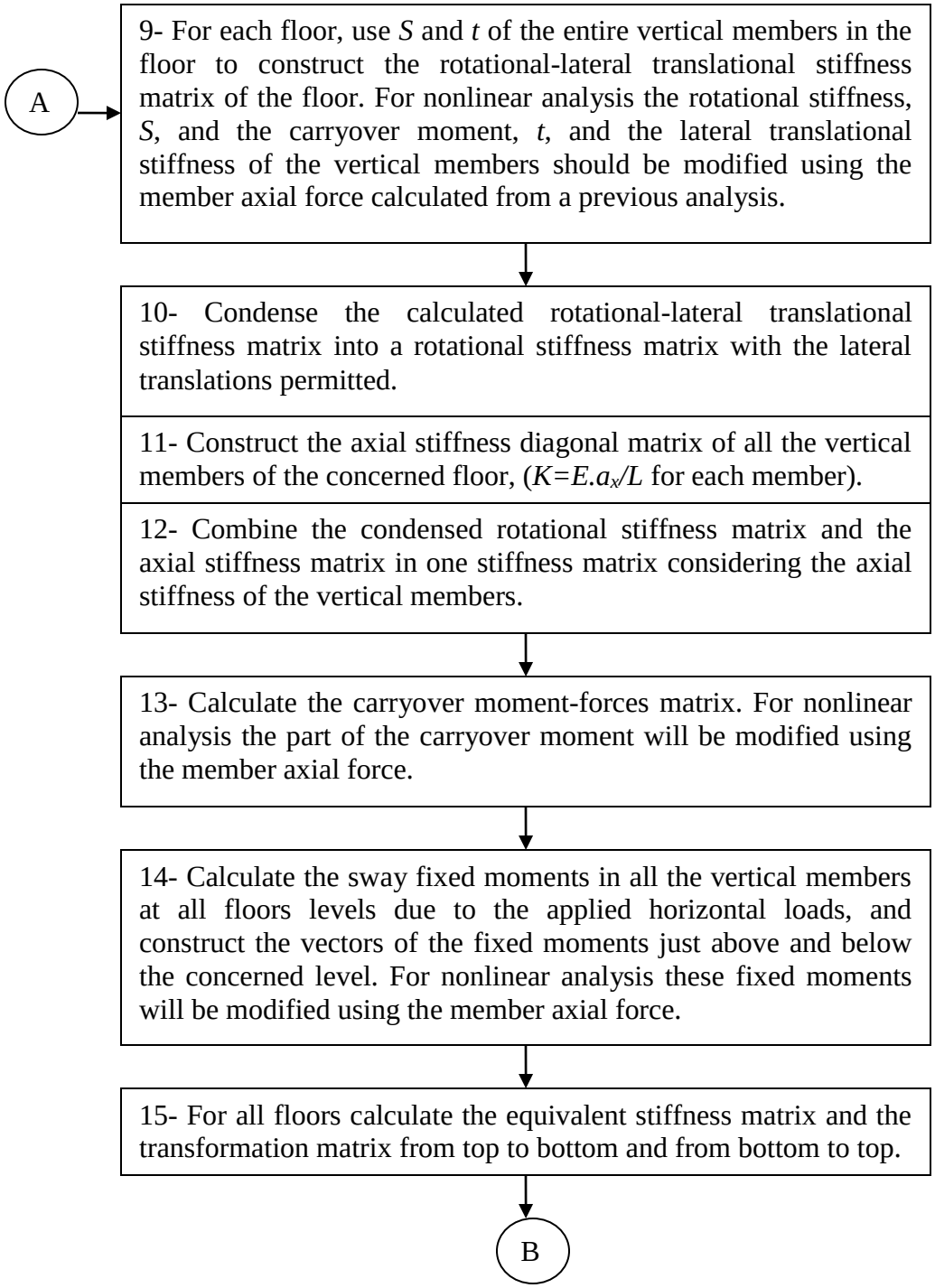

Figure 4.1-b: Flow chart of the moment-force transformation main solver

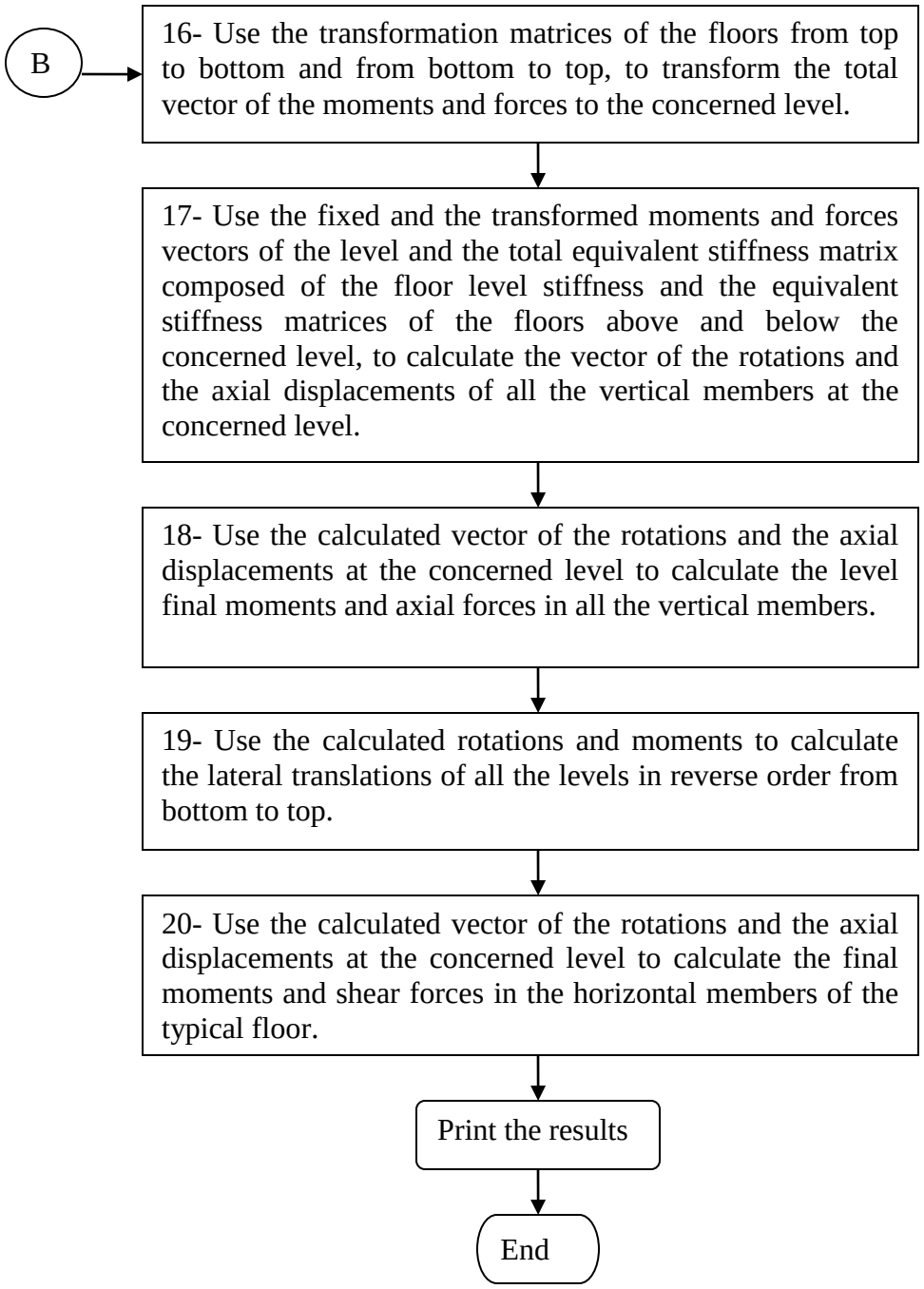

Figure 4.1-c: Flow chart of the moment-force transformation main solver

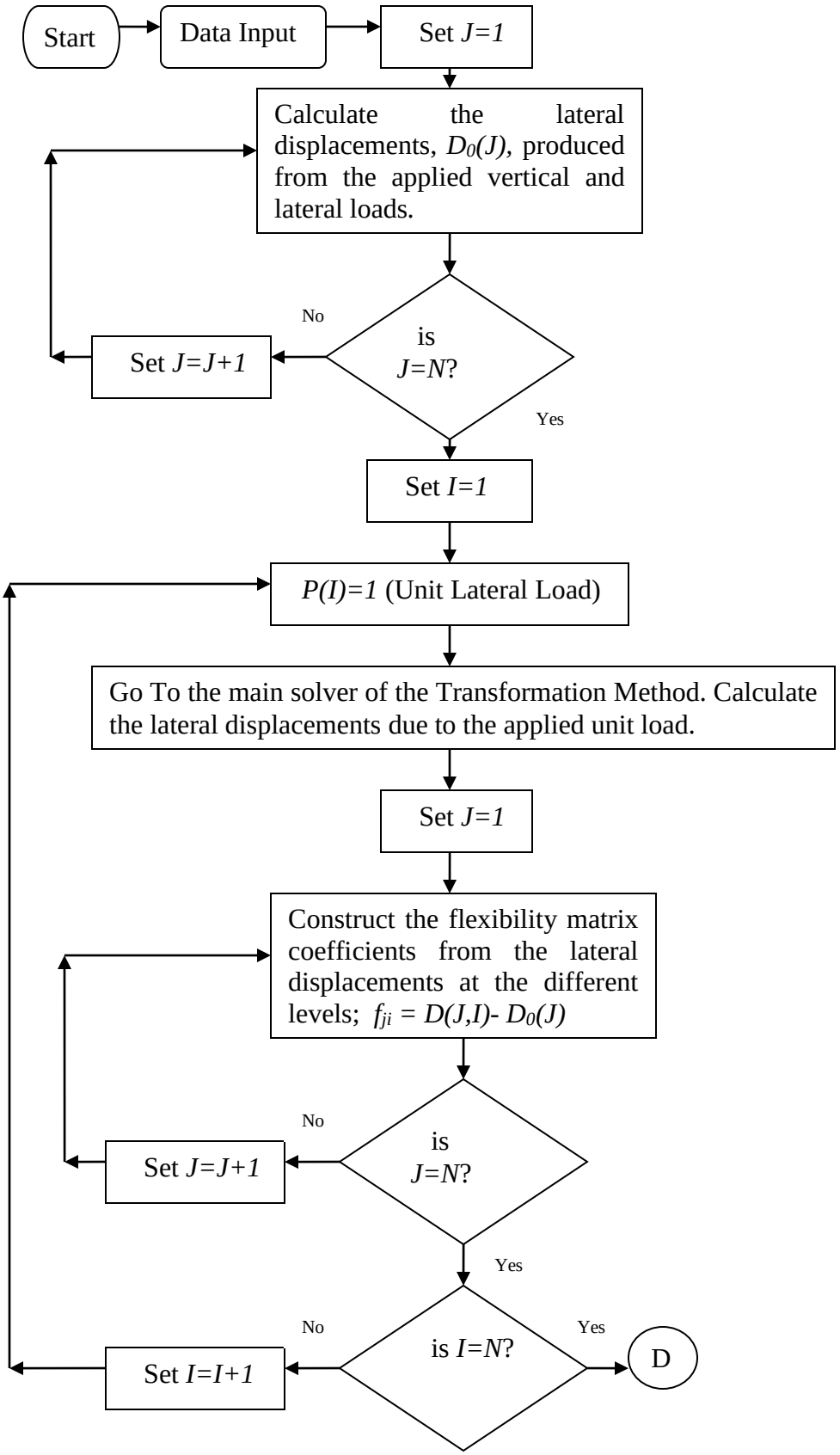

Figure 4.2-a: Flow chart of dynamic properties extraction of 2D frames

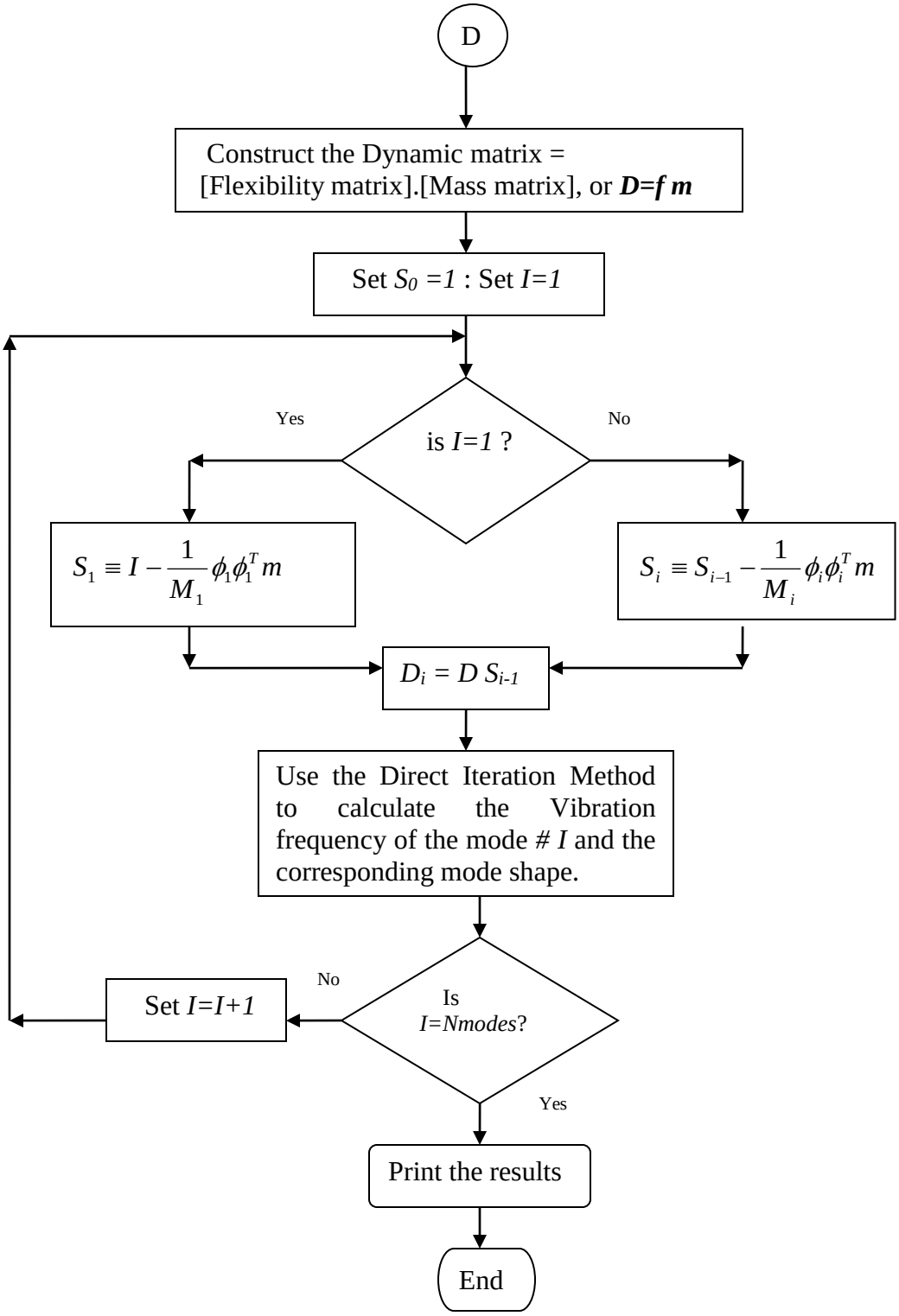

Figure 4.2-b: Flow chart of dynamic properties extraction of 2D frames

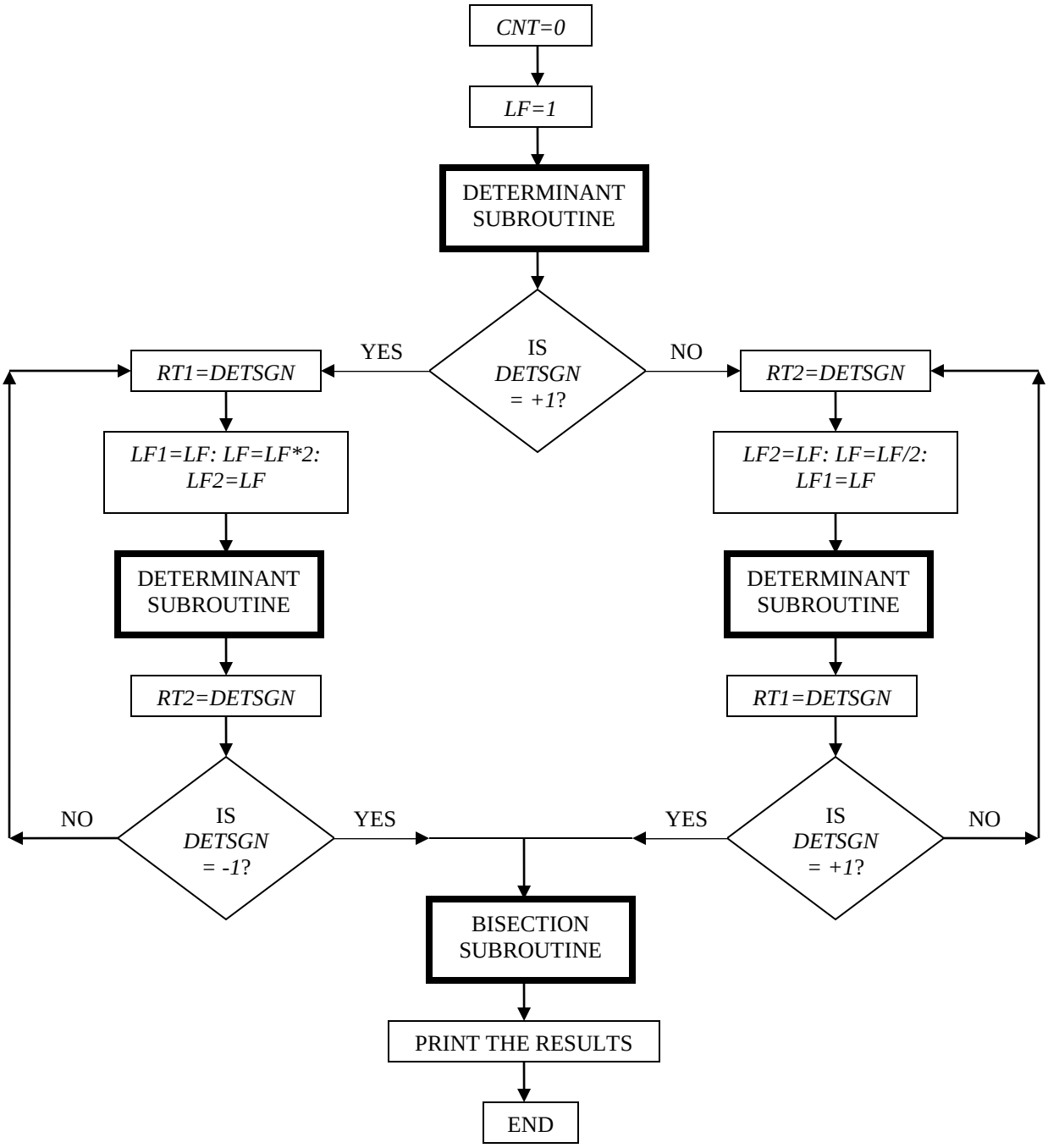

Figure 4.3-a: Flow Chart of the proposed buckling analysis solver

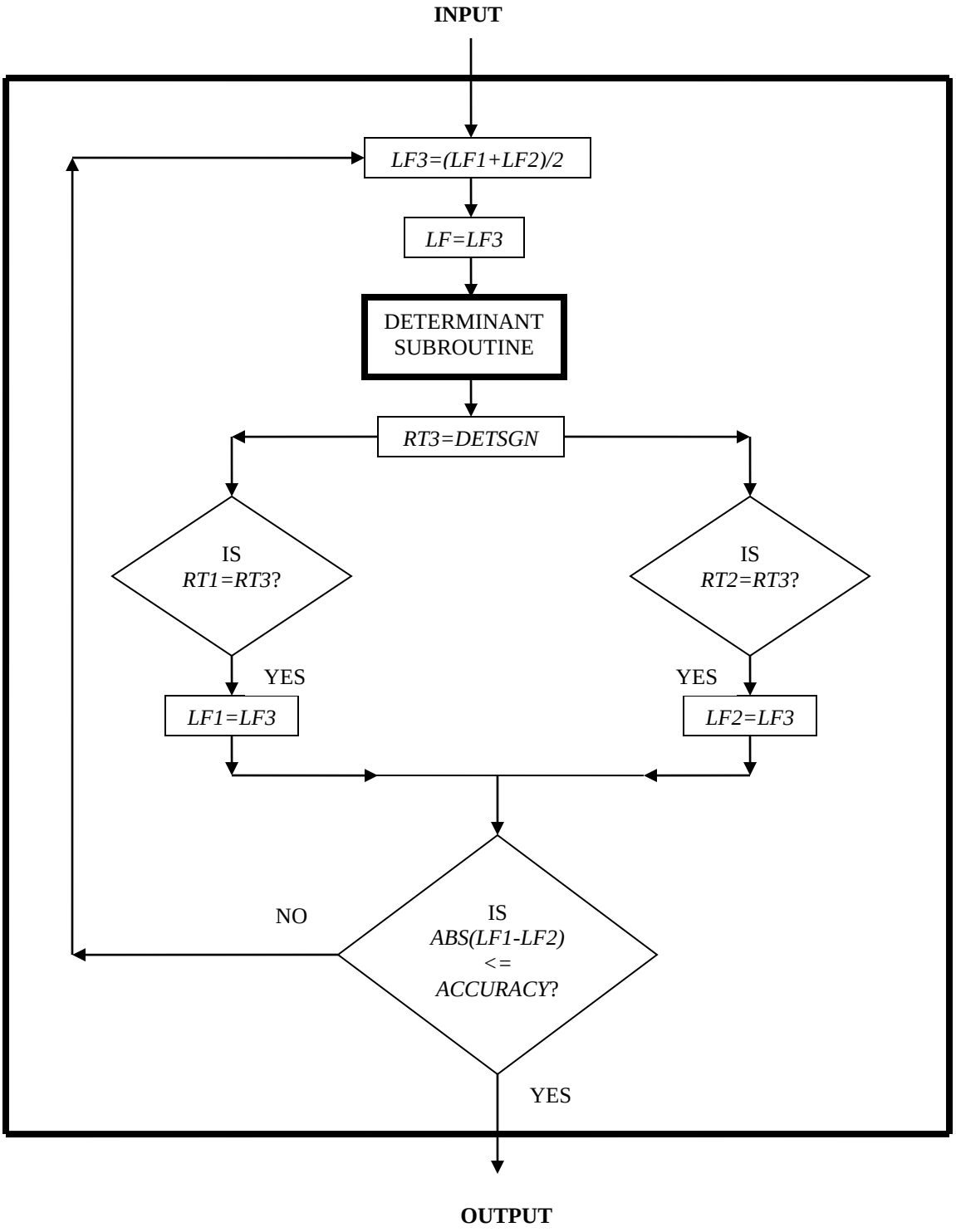

Figure 4.3-b: Flow Chart of the bisection subroutine

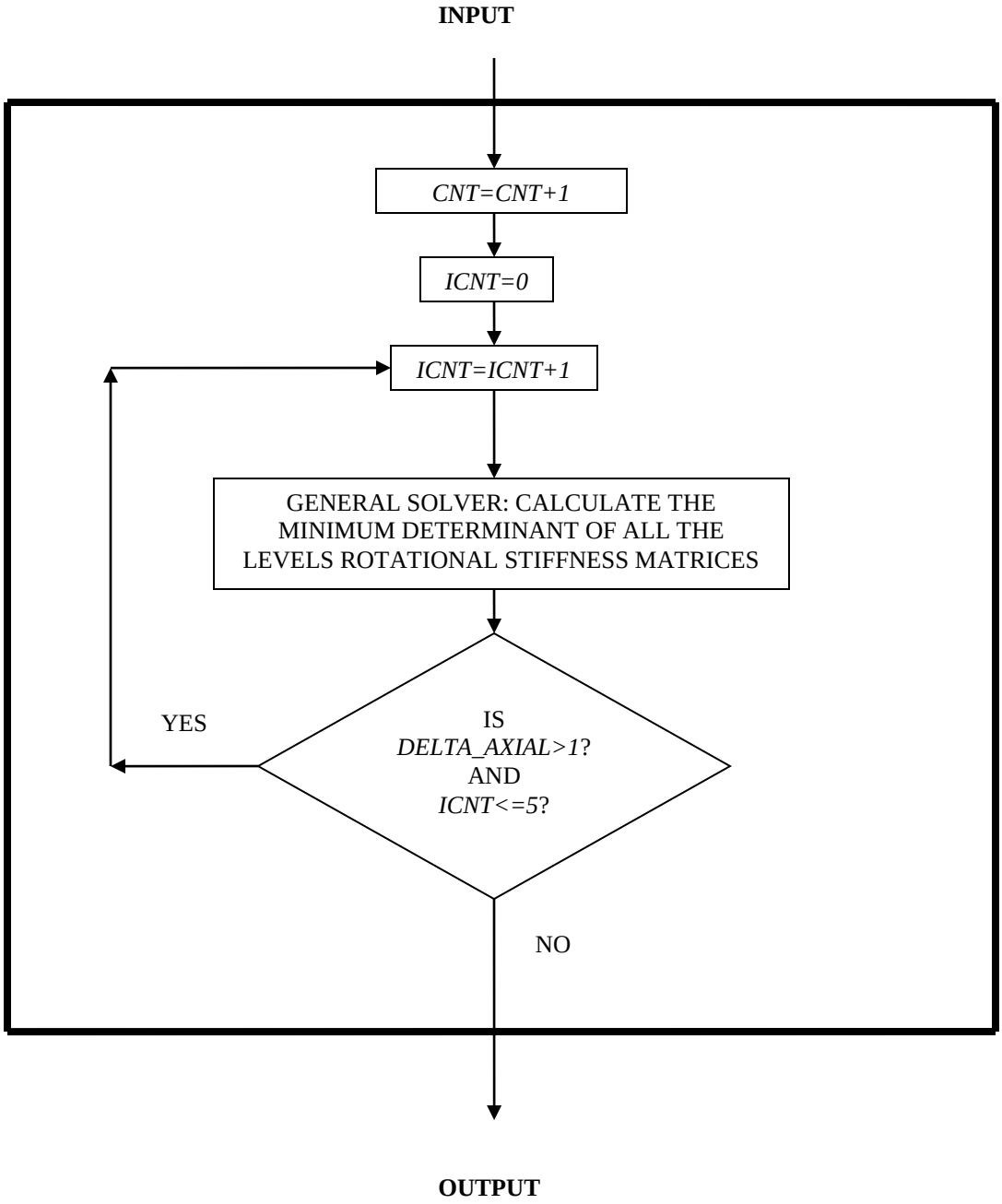

Figure 4.3-c: Flow Chart of the determinant subroutine

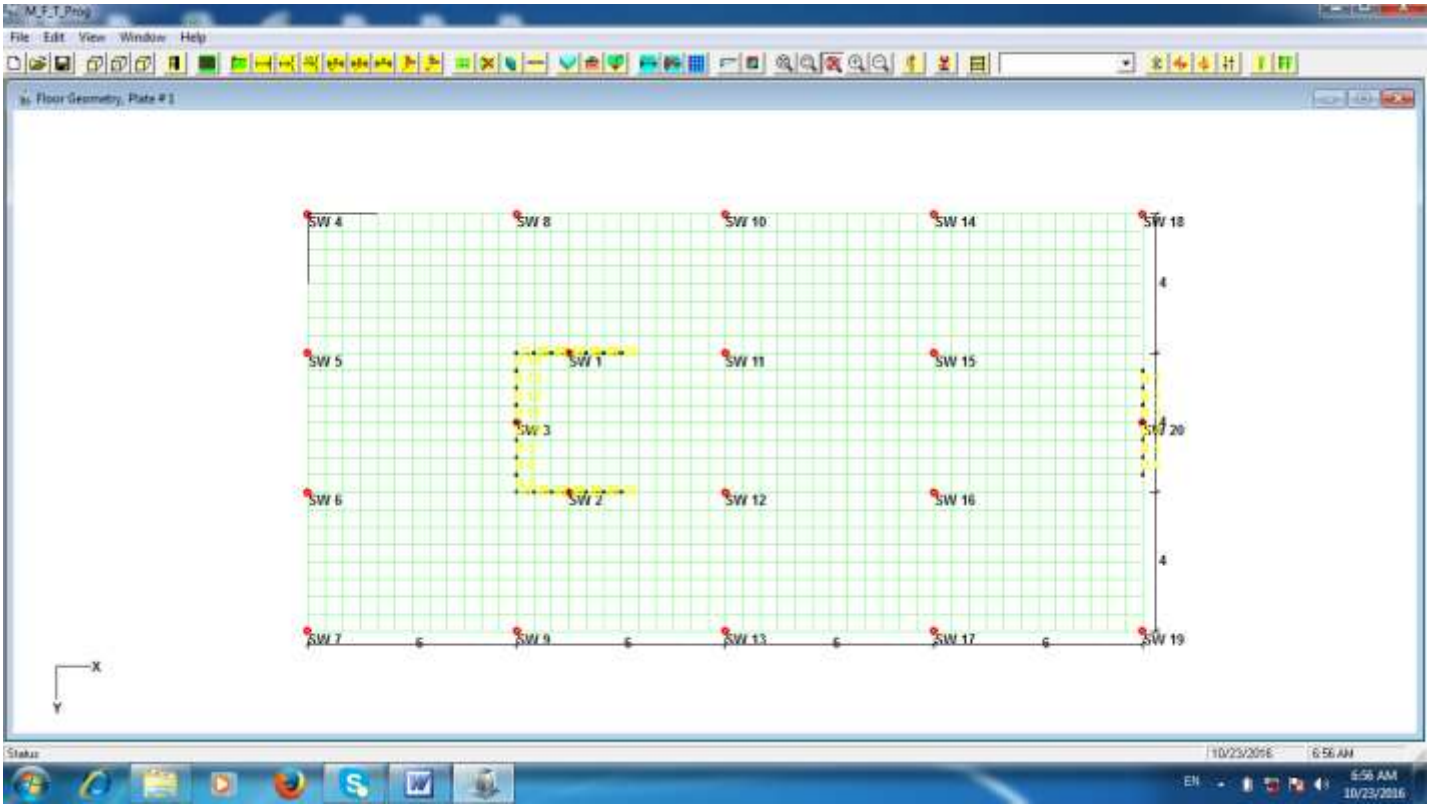

Figure 4.4: The program MFTProgV2 Layout (3D mode)

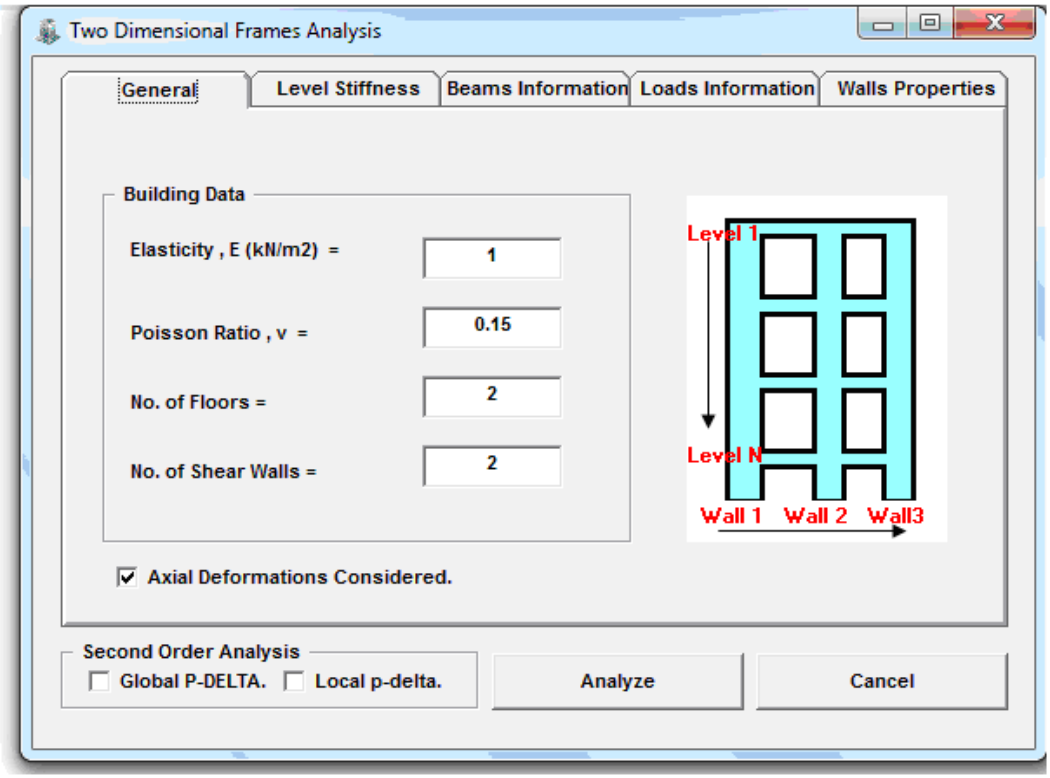

Figure 4.5: The multi-page data input of the two dimensional analyses mode

The Two Dimensional multi-page form includes the following pages:

A) General page used to input the following data: The members Elasticity and Poisson's ratio, Number of floors, Number of shear walls.
B) Level stiffness page. This page contains a flex-grid used to enter the rotational and translational stiffness of the different levels. There are also three radio buttons used for the selection of the different support conditions; fixed bases, pinned bases or other spring rotational and translational stiffness.
C) Beams information page. This page includes a flex-grid used to input the different data of portal frame beams e.g. length, inertia, shear area and U.D. loads, from which the level stiffness and the fixed moments and forces will be calculated and automatically send to the level stiffness and loads information pages.
D) Loads information page, which includes a flex-grid used to enter the level fixed moments and forces and the lateral forces acting at the different levels.
E) Walls properties page, which includes a flex-grid used to enter the different floors heights and the properties of the different walls or columns, inertias and shear areas.

There are two buttons in the bottom of the form one used for analyzing the frame and the other is used to quit the analysis mode. There is a check box used to select the type of the analysis: Linear or P-Delta analyses, global and local.

Pressing the analyze button results in performing the analysis and showing the results page, see the Figure 4.6.

The results page includes a picture box used for plotting the bending moment and the shear force diagrams and the deformed shape of the frame. There are also two flex-grids used to show the different output results in a tabulated form.

The tabulated outputs are the rotations and translations of the different joints and the bending moments and shear forces in the different levels and floors. A global equilibrium check can be ensured by comparing the applied shear with the calculated shear and a local equilibrium check can be insured by checking the summation of the moments at the different levels as shown in Figure 4.7.

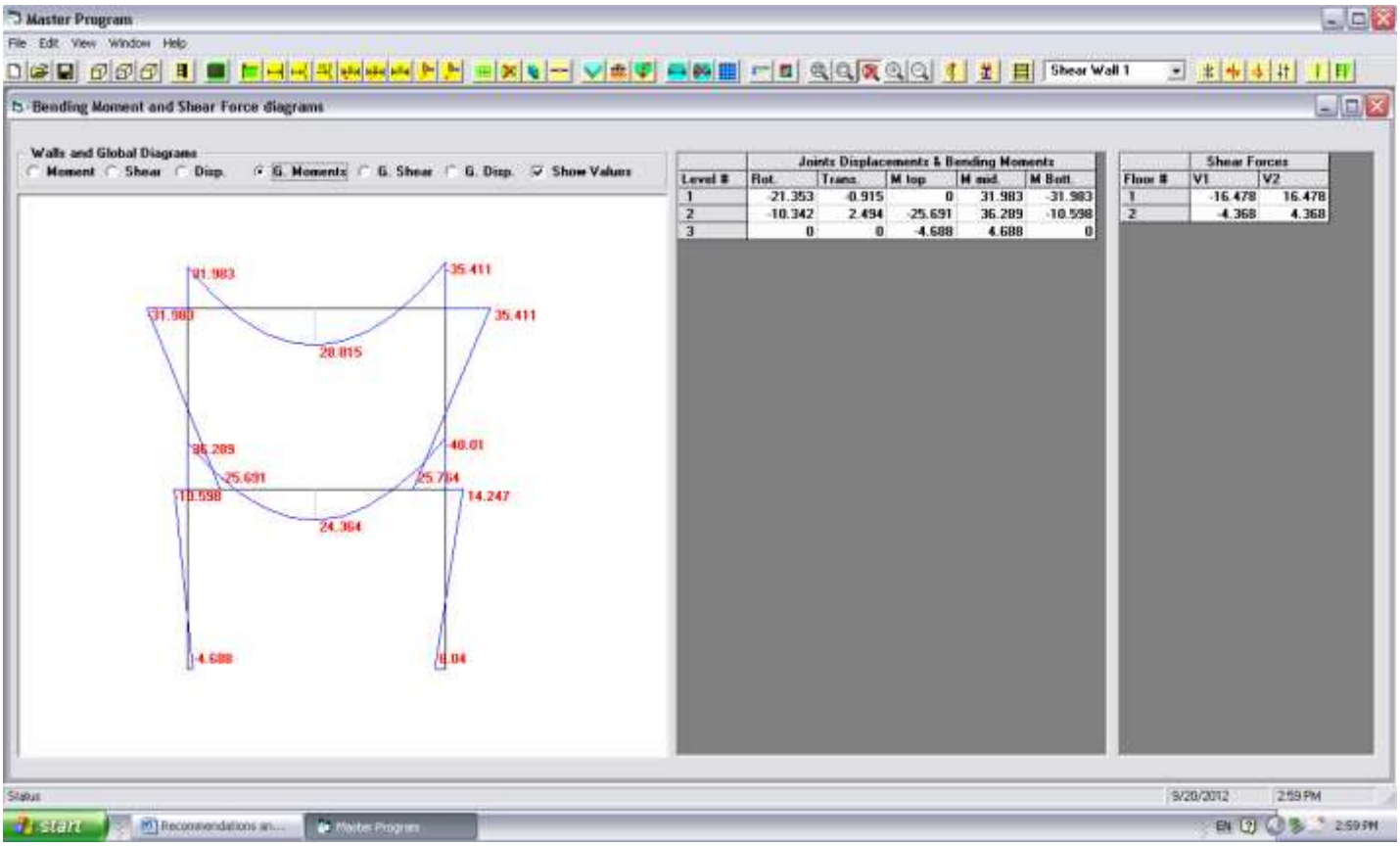

Figure 4.6: The results page of the two dimensional analysis mode

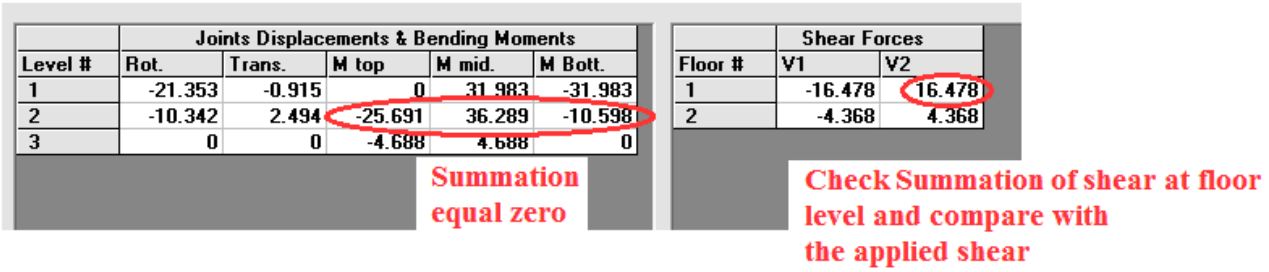

Figure 4.7: Local and global equilibrium checks

4.2.2 The Three Dimensional analysis

Pressing the three dimensional button results in showing the building dimensions form, Figure 4.8. The form includes text boxes for entering the overall building dimensions in both *x* and *y* directions and the number of segments or plates in each direction.

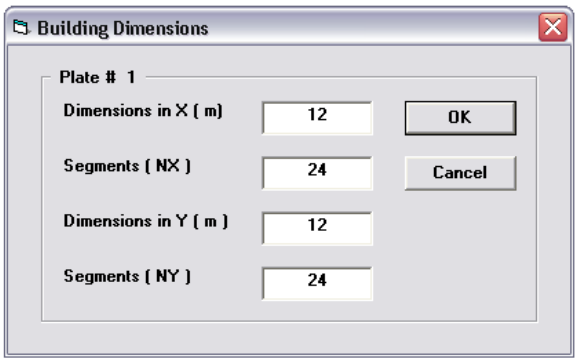

Figure 4.8: The building floor dimensions form

The finite elements constructed in this way can be modified and adjusted for dimensions; also one can add or reduce rows and/or columns of elements. After preparing the floor data, one has the option to add shear walls, beams and columns graphically by selecting the appropriate joints.

The materials and properties of plates, beams and added columns can be entered by using the related buttons and forms.

The plate loads can also be entered. At this stage only uniformly distributed loads can be added.

After finishing entering all the floor information, then one can go to the program menu and select from the file menu the item: "Calculate Level Stiffness…"

By clicking this item, the stiffness of the floor will be calculated and incorporated in the analysis as a floor level stiffness, the fixed end moments are also calculated if there are any applied vertical loads.

The building and material information e.g. number of floors, number of shear walls, Elasticity and Poisson's ratio of shear walls , and number of the different building parts can be entered in one page, Figure 4.9.

The shear walls properties, i.e. widths, depths, inertias shear areas, the location coordinates in the plan and the orientation of the principal axes are all entered in flex-grid available in shear walls information page, Figure 4.10.

The plate number and the floor heights and the global forces and moments in the different levels are entered in one page as shown in Figure 4.11.

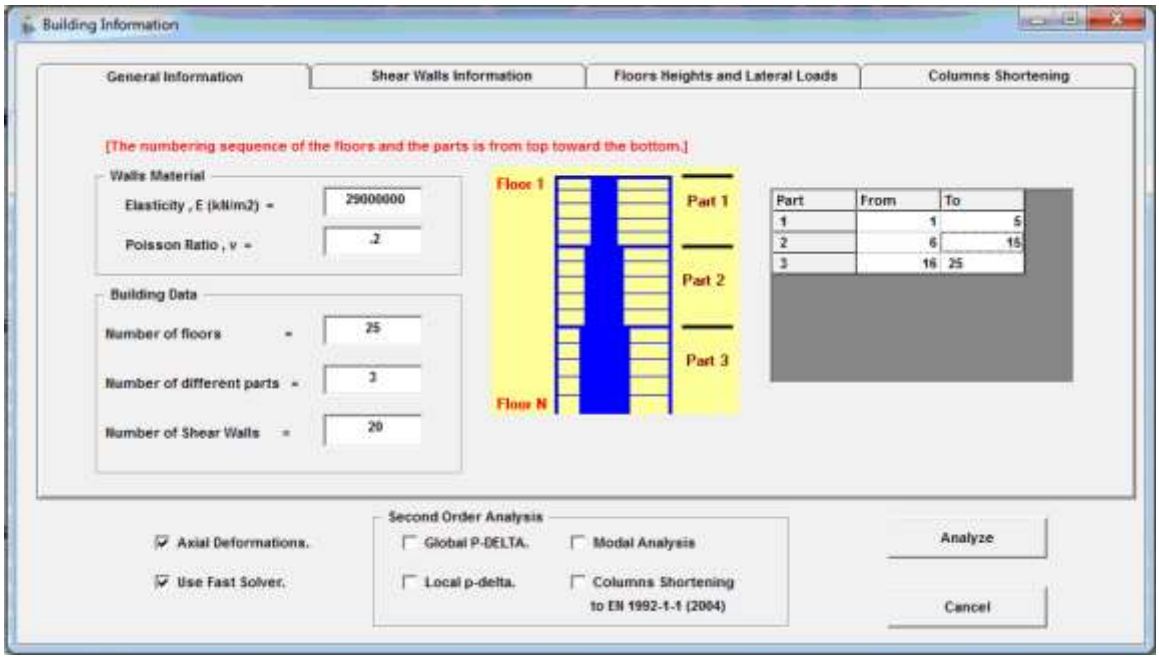

Figure 4.9: Main form of the three dimensional analysis

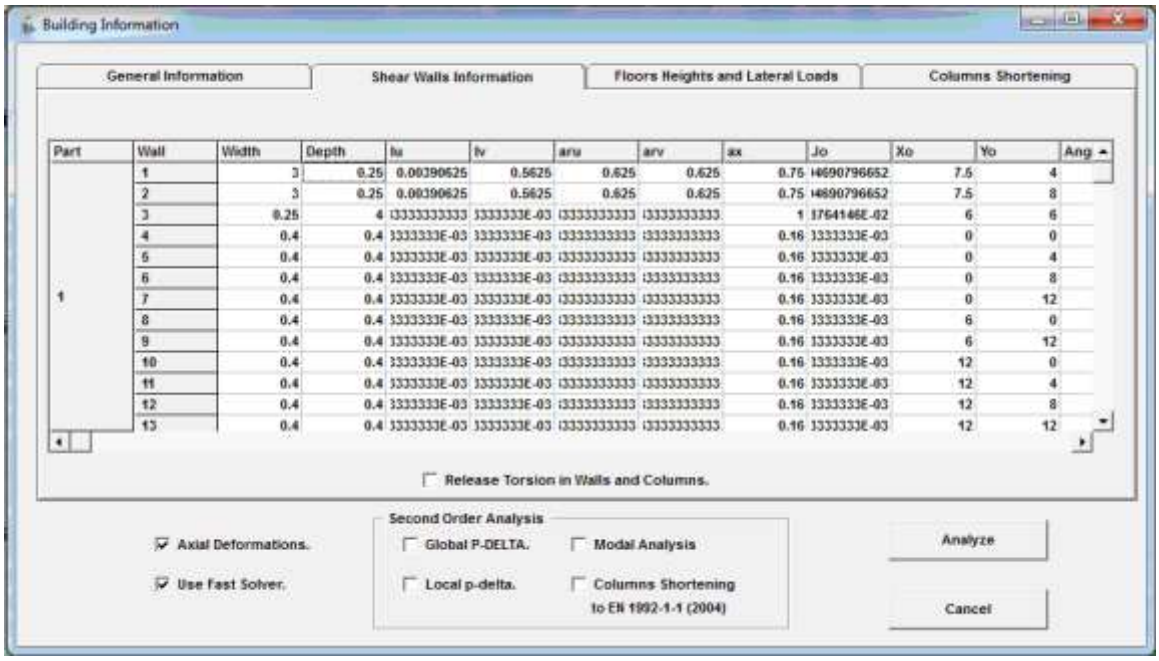

Figure 4.10: Walls and columns properties entering

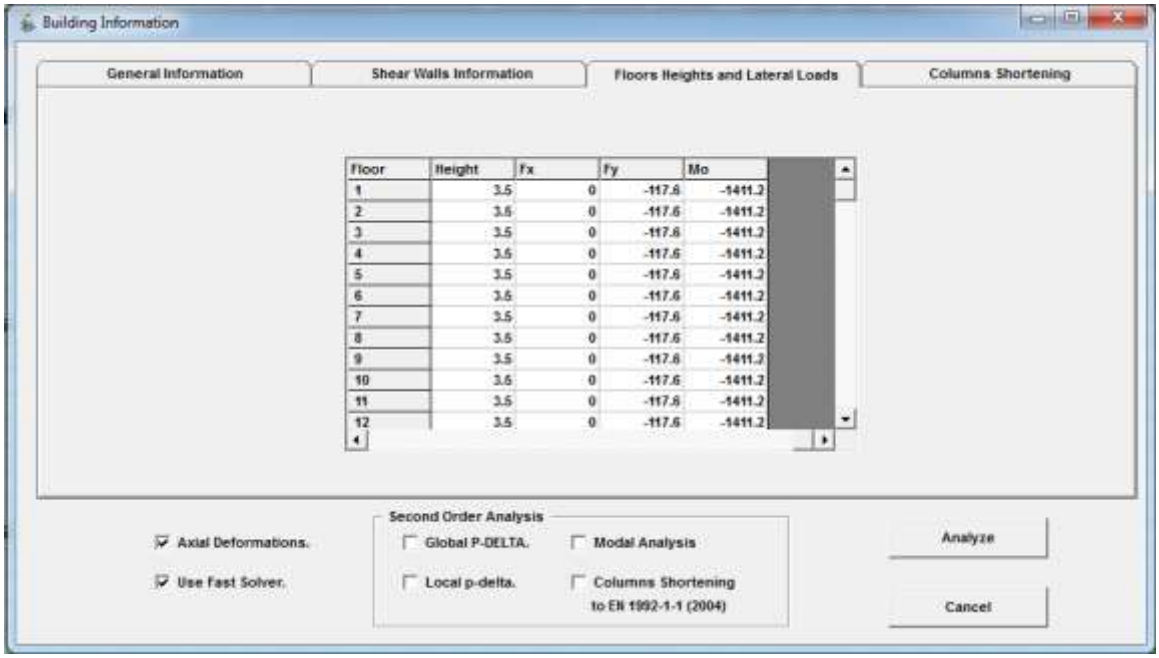

Figure 4.11: Floors heights and lateral loading entering

After finish entering all the required data and pressing the "Analyze" button, the analysis is performed and the output result form appears. This form includes a picture box that presents the different diagrams (e.g. Bending moments, Shear forces, Twist moments, Axial force diagrams), for each selected shear walls. Also a flex-grid is available to tabulate the moments and forces at each level for each shear wall as shown in Figure 4.12. The same flex-grid presents a complete global equilibrium check.

The deformed shape for each shear wall can be shown in the same picture box.

The moments per unit width M_x, M_y and M_{xy} and shear stress Q_x and Q_y contours for each floor can also be calculated and plotted from the resulting rotations and vertical displacements for all shear walls of the concerned floor level, Figures 4.15 and 4.13.

A global perspective deformed shape of the whole building can also be shown, as in Figure 4.13.

Instead of using the finite elements floor of the program, the MFTProgV2 has a feature of importing and calculating floor stiffness from a StaadPro one floor fixed supported model to be incorporated in the analysis, Figure 4.14. This procedure is performed by sending unit displacements to the StaadPro package model in different load conditions. After running the StaadPro model, the support reactions are retrieved in a form of rotational-translational floor stiffness and can be used in the transformation procedure.

Floor	Torsion	Axial	Sum:(Frx)	Sum:(Fry)	Sum:(Mro)	Sum:(Mrx)	Sum:(Mry)	Sum:(Fro)
1	-5.481	441.633						
	-5.481	441.633	0	117.6	1411.2	-30692.4	62208	-5184
2	-6.346	891.141						
	-6.346	891.141	0	235.2	2822.4	-60973.2	124416	-10368
3	-7.753	1337.122						
	-7.753	1337.122	0	352.8	4233.6	-90842.4	186624	-15552
4	-9.53	1780.964						
	-9.53	1780.964	0	470.4	5644.8	-120300	248832	-20736
5	-11.57	2221.284						
	-11.57	2221.284	0	588	7056	-149346	311040	-25920
6	-13.73	2657.932						
	-13.73	2657.932	0	705.6	8467.2	-177980.4	373248	-31104
7	-16.06	3092.737						
	-16.06	3092.737	0	823.2	9878.4	-206203.2	435456	-36288
8	-18.542	3524.965						
	-18.542	3524.965	0	940.8	11289.6	-234014.4	497664	-41472
9	-21.108	3954.293						
	-21.108	3954.293	0	1058.4	12700.8	-261414	559872	-46656
10	-23.712	4380.307						
	-23.712	4380.307	0	1176	14112	-288402	622080	-51840
11	-26.308	4802.589						
	-26.308	4802.589	0	1293.6	15523.2	-314978.4	684288	-57024
12	-28.845	5220.706						
	-28.845	5220.706	0	1411.2	16934.4	-341143.2	746496	-62208
13	-31.267	5634.189						
	-31.267	5634.189	0	1528.8	18345.6	-366896.4	808704	-67392
14	-33.498	6042.627						
	-33.498	6042.627	0	1646.4	19756.8	-392238	870912	-72576
	-35.471	6445.239						

Figure 4.12: Global equilibrium check at the different floors levels

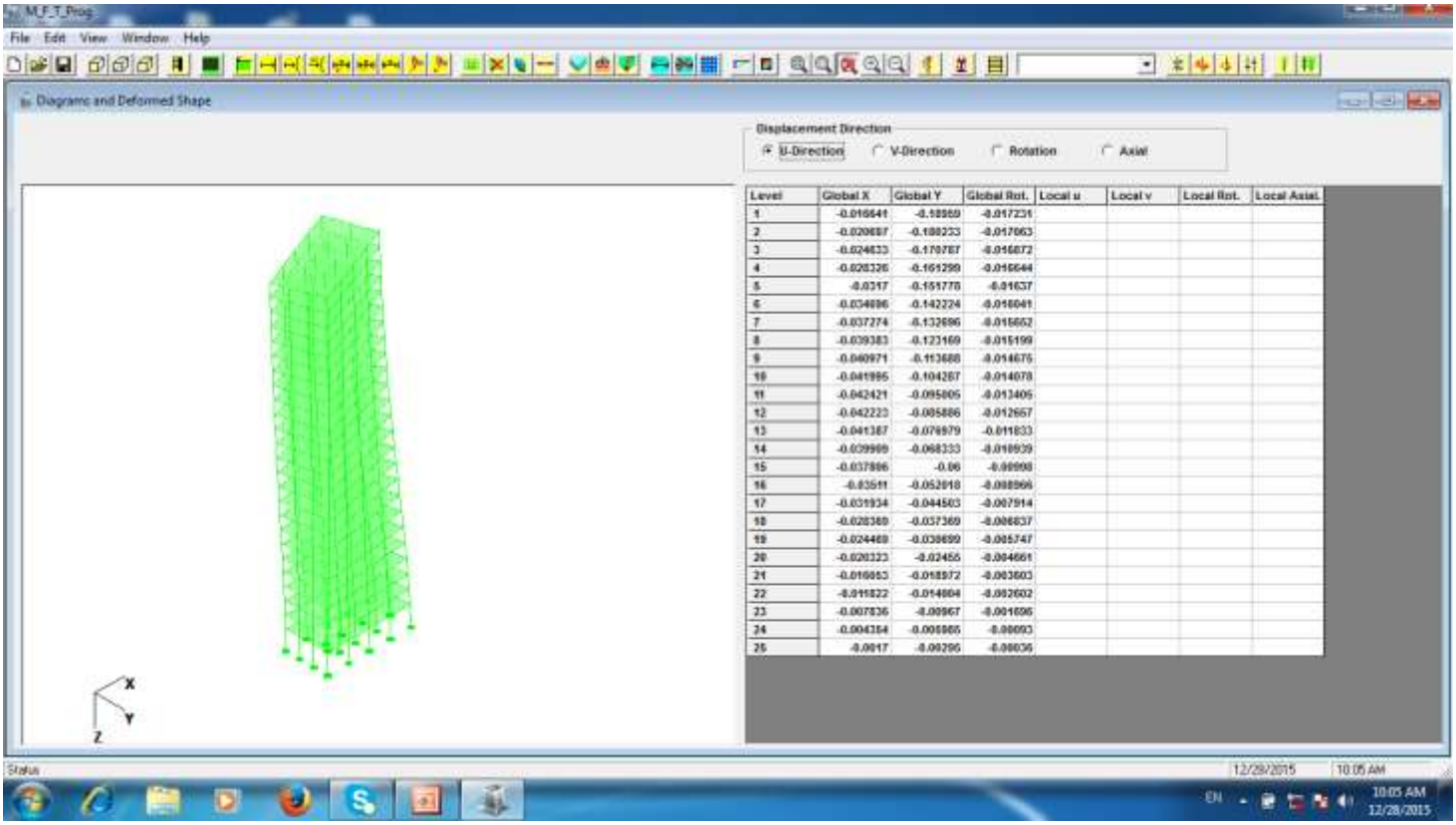

Figure 4.13: Global deformed shape

Figure 4.14: StaadPro Floor stiffness and Fixing Moments form

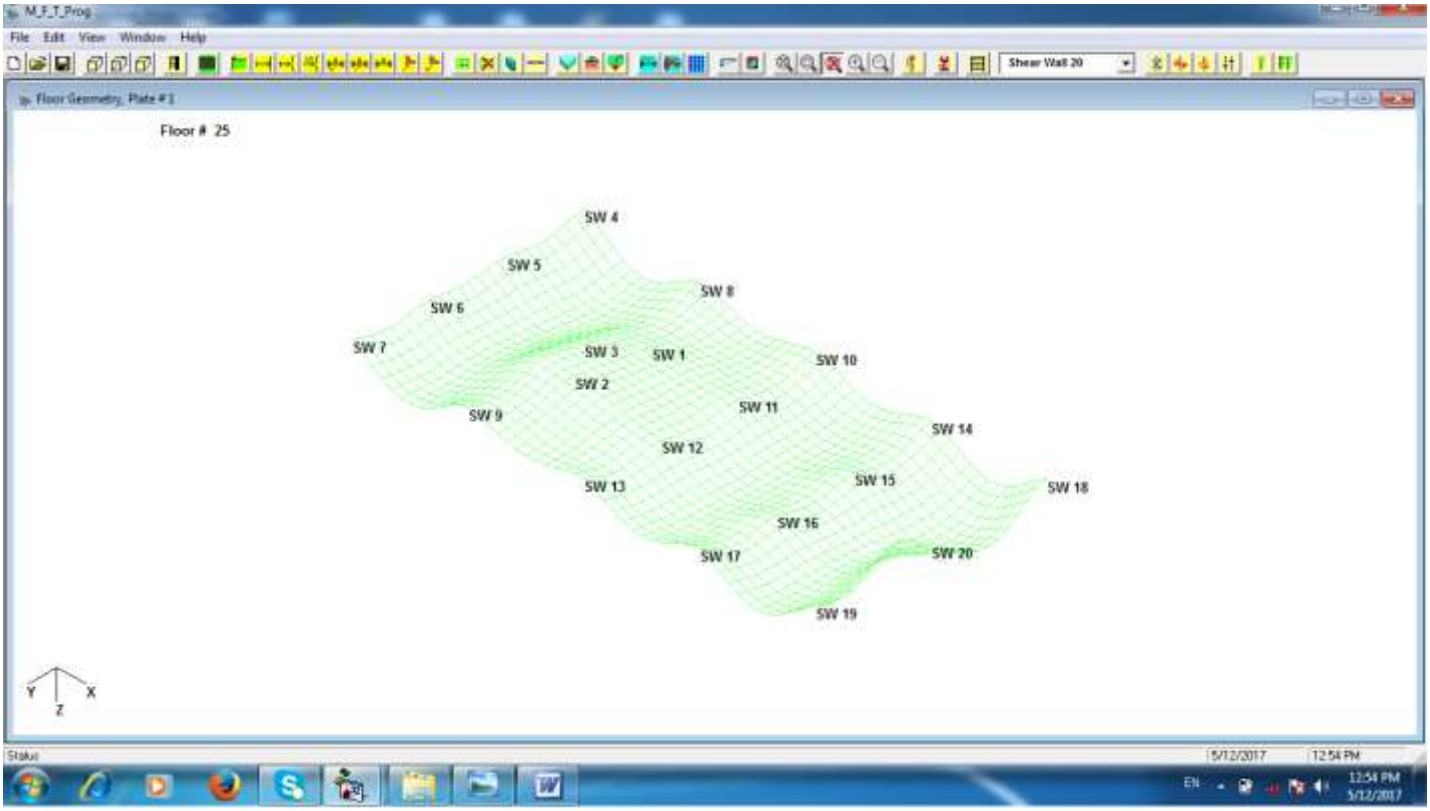

Figure 4.15: Deformed shape of a concerned floor

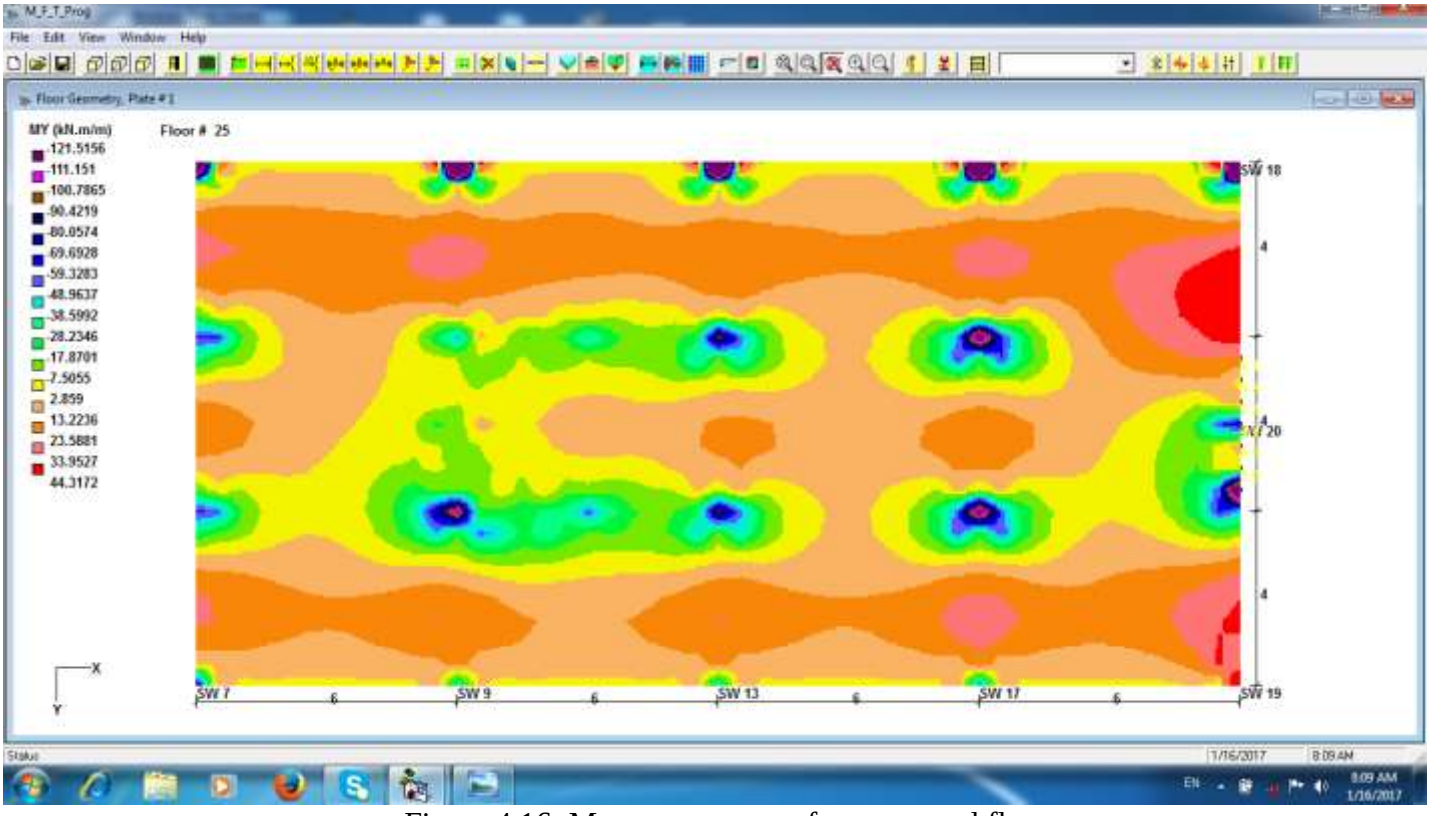

Figure 4.16: Moment contour of a concerned floor

CHAPTER FIVE

Program Applications and Verification of Results

5.1 Introduction

In order to demonstrate the effectiveness of the program, several different two dimensional and three dimensional problems are analyzed. The results obtained are compared with published results and with results obtained using commercial packages: StaaPro2004, StaadProV8i and ETABS.

In the following sections, several examples analyzed using MFTProg are presented. Some examples are chosen from published references and analyzed by using the two dimensional option of the program.

5.2 Numerical Examples

Using MFTProg, two simple portal frames examples were studied. A model of a fifteen floors symmetric building with non-symmetrical lateral loadings was also carried out. The results were compared with those obtained by MTProg (with axial deformations in the vertical members neglected, Ibrahim, 2013), and with those obtained using StaadPro2004 and ETABS.

5.2.1 Two Floor One-bay Portal Frame

The bending moments and support reactions were obtained using the simplified method for a two storey frame under the vertical and horizontal loading shown in the Figure 5.1.

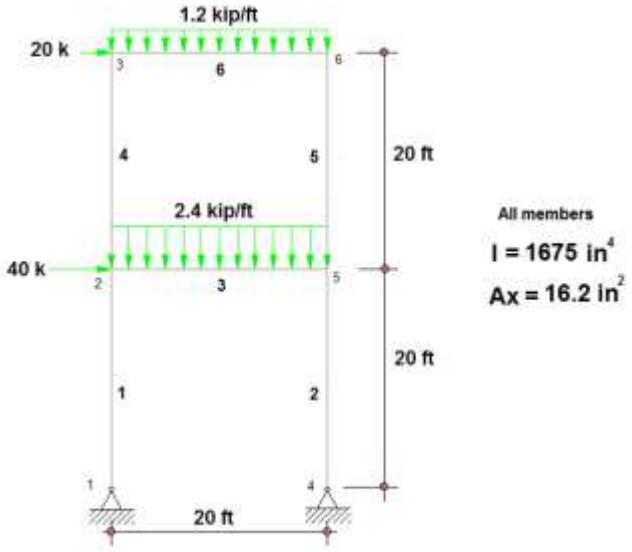

Figure 5.1: One-bay Frame properties and loading

The results obtained are compared with the results from McCormac and Elling (1988) and StaadPro2004 results as shown in Table 5.1.

Table 5.1: Comparison of moments and forces at joints 3, 6 and 4 (2 Floor 1 bay Frame)

Results	M3, kip-ft	M6, kip-ft	H4, kip
Reference	141.90	206.30	31.16
StaadPro2004	145.79 (2.74)	209.03 (1.32)	31.18 (0.06)
MFTProg[1]	145.98 (2.88)	208.84 (1.23)	31.21 (0.16)
MFTProg[2]	142.06 (0.11)	206.06 (-0.12)	31.20 (0.13)

[1] Considering shear deformation. [2] Neglecting shear deformation. (%diff.)

The comparison of the results shows very close agreement.

5.2.2 Two Floor Two-bay Portal Frame

The bending moments were obtained using the simplified method for a two storey frame under the vertical and horizontal loading shown in the Figure 5.2.

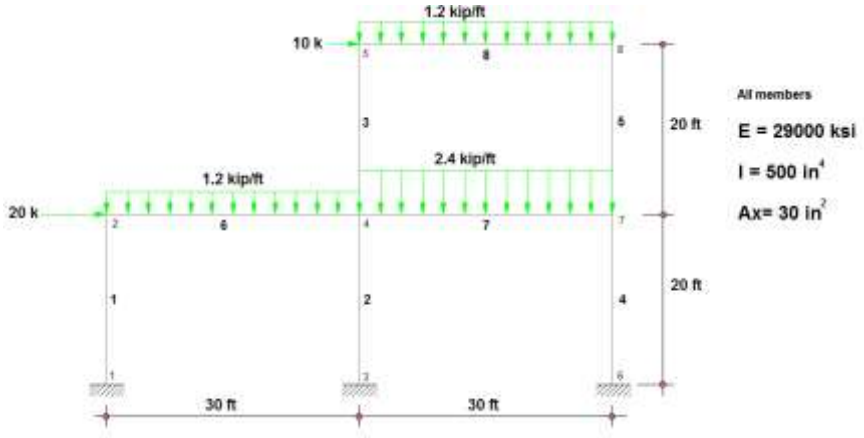

Figure 5.2: Two-bay Frame properties and loading

The bending moments results obtained were compared with the results from McCormac and Elling (1988), and StaadPro2004 as shown in Table 5.2.

Table 5.2: Comparison of moments at joints 1, 3 and 6 (2 Floor 2 bay Frame)

Results	M1, kip-in	M3, kip-in	M6, kip-in
Reference	1147.00	1462.00	1750.00
StaadPro2004	1150.30 (0.29)	1461.85 (-0.01)	1748.63 (-0.08)
MFTProg[1]	1145.71 (-0.11)	1463.50 (0.10)	1750.87 (0.05)
MFTProg[2]	1142.05 (-0.43)	1463.70 (0.12)	1752.24 (0.13)

[1] Considering shear deformation. [2] Neglecting shear deformation. (%diff.)

Comparison of the published results and the results obtained using StaadPro2004 with those obtained by MFTProg, show very close agreement.

5.2.3 Model of a hypothetical fifteen storey building subjected to unsymmetrical lateral loading

The plan shown in Figure 5.3 is for a 12m x 12m floor slab of thickness = 0.25 m. The hypothetical building is composed of 15 floors of floor height = 3.5 m for all floors except the lower floor which is of height = 5.5 m.

All building members are concrete of elasticity, E = 21718500 kN/m^2,

and Poisson's ratio, v = 0.17

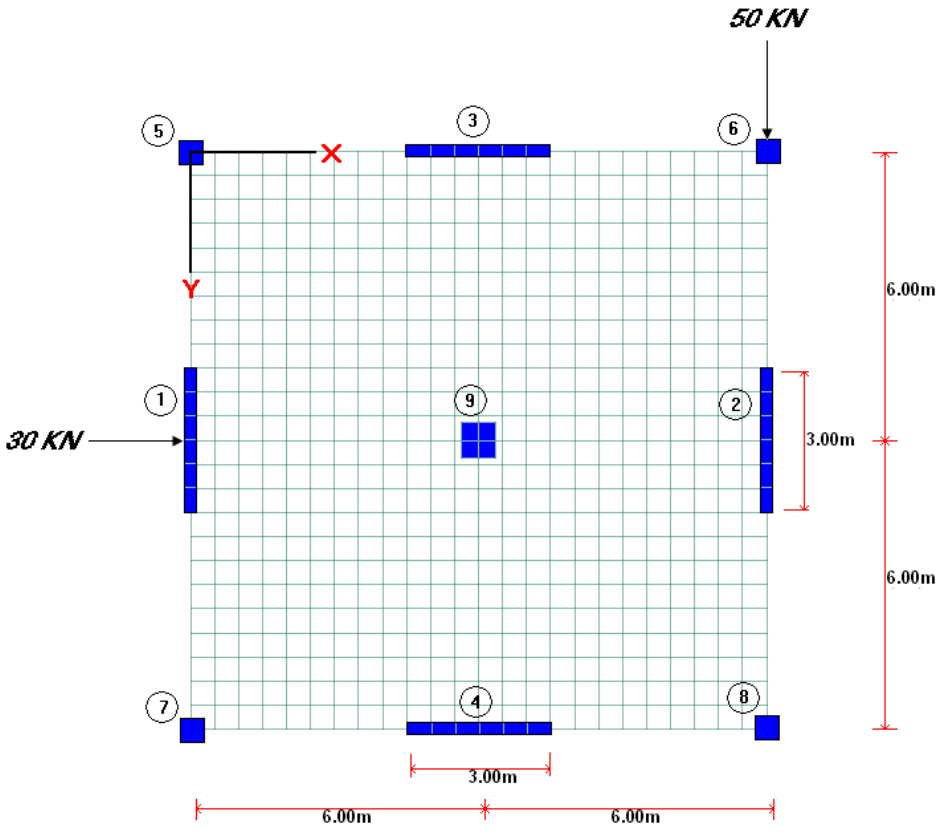

Figure 5.3: 12m x 12m floor plan for 15 Storey, Square Building

The section properties of the vertical elements (in meters) are:

Columns: Corners: 0.60 x 0.60 and Interior: 0.85 x 0.85

Shear walls: The lower 7 floors: 0.30 x 3.00 and The upper 8 floors: 0.25 x 3.00

The building is subjected to the lateral loads shown in Figure 5.3, (30 kN and 50 kN) at all floor levels.

5.2.3.1 Verification of Results

The building has been analyzed by using MFTProg with the axial deformation in the vertical members considered. The accuracy of the results is verified by using MTProg, Ibrahim (2013), and the structural analysis packages StaadPro2004 and ETABS.

The MFTProg displacements, shear forces and bending moment results are shown in Figures 5.4 to 5.14.

Comparison of the top displacements of the origin (Column #5) as a bench mark, obtained using MFTProg and the different packages is shown in Figures 5.15, 5.16 and 5.17 and Table 5.4. Comparison of the maximum shear force and maximum bending moment of shear walls 1 to 4 are shown in Figures 5.18 to 5.25 and Table 5.3.

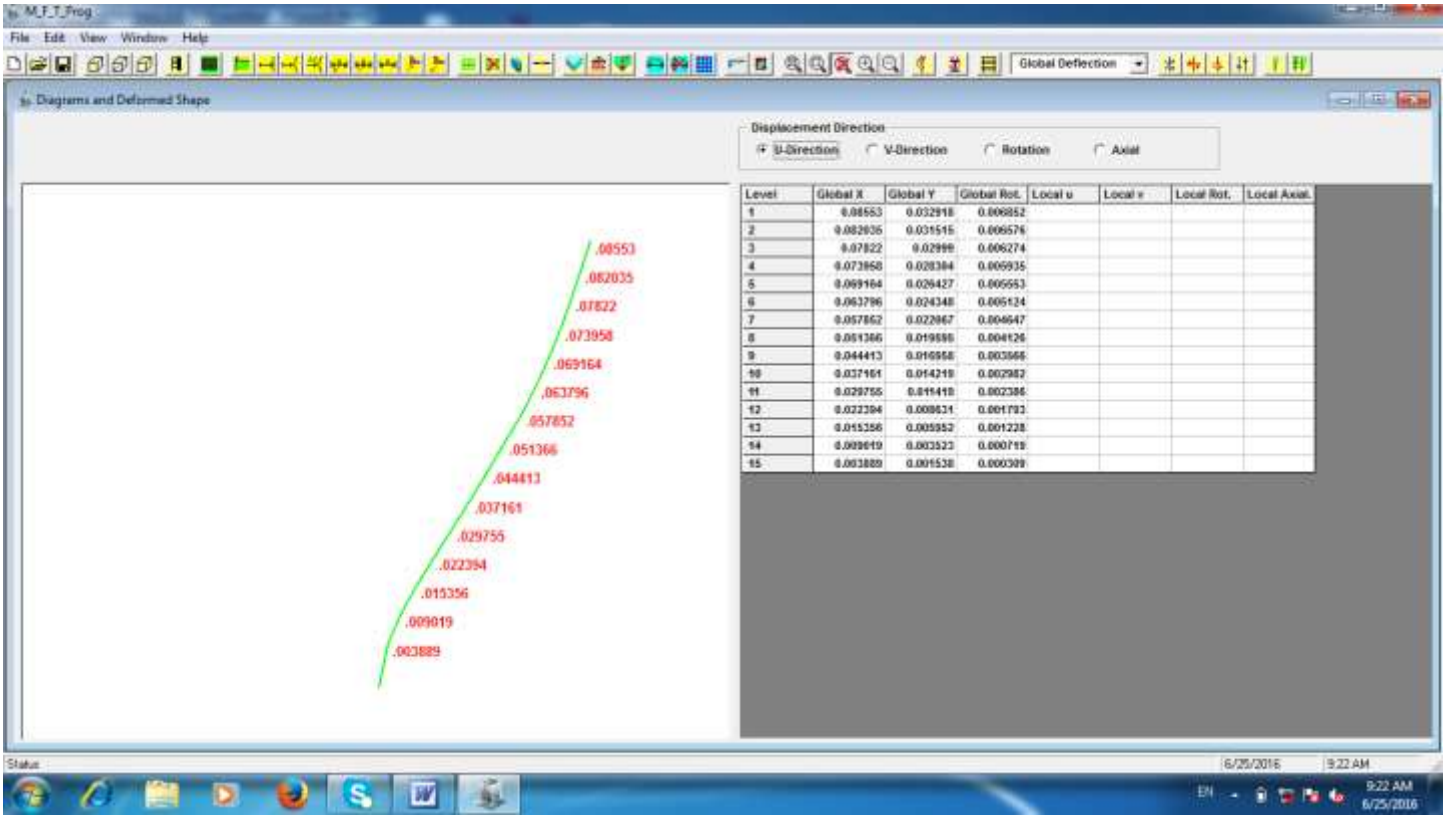

Figure 5.4: Displacements of Column # 5 in *x*-direction.

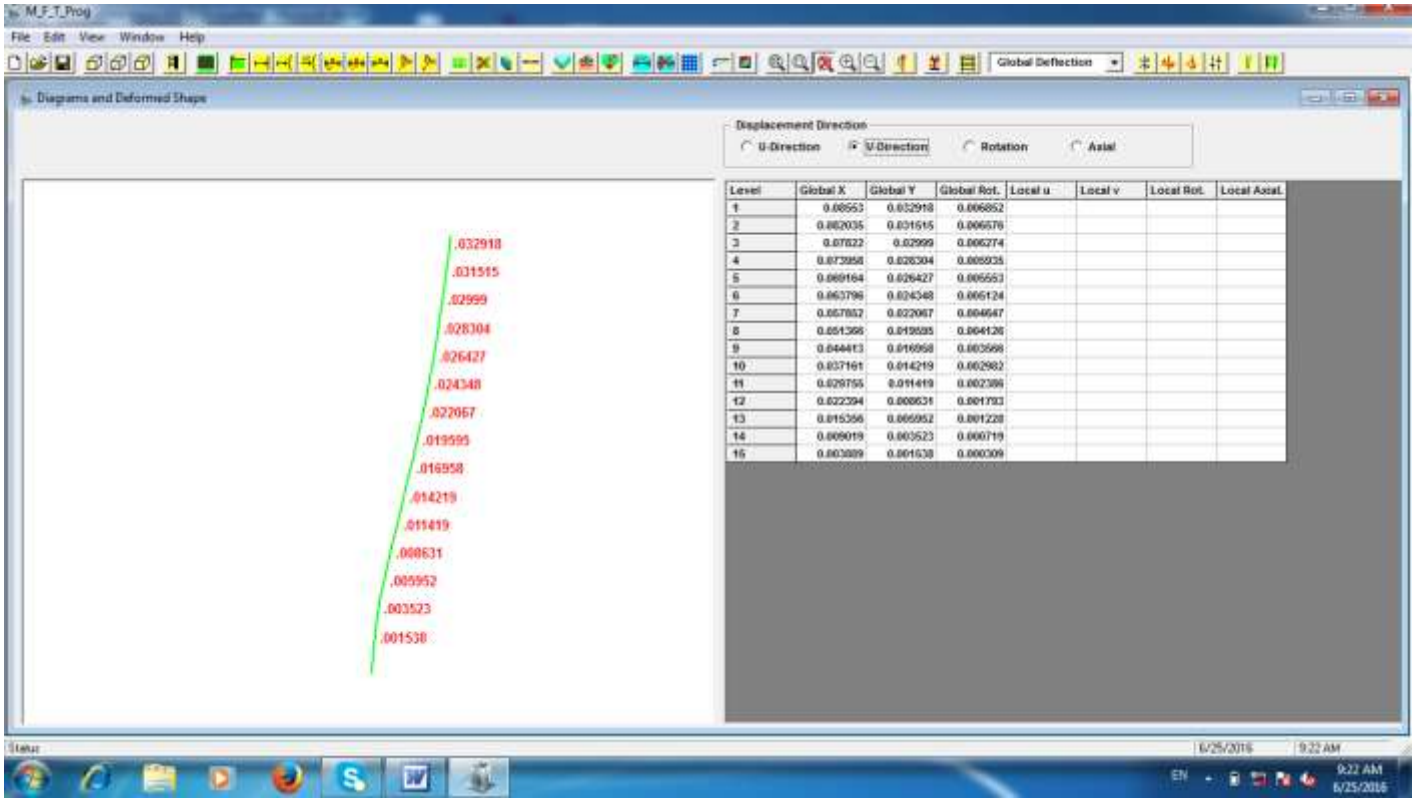

Figure 5.5: Displacements of Column # 5 in *y*-direction.

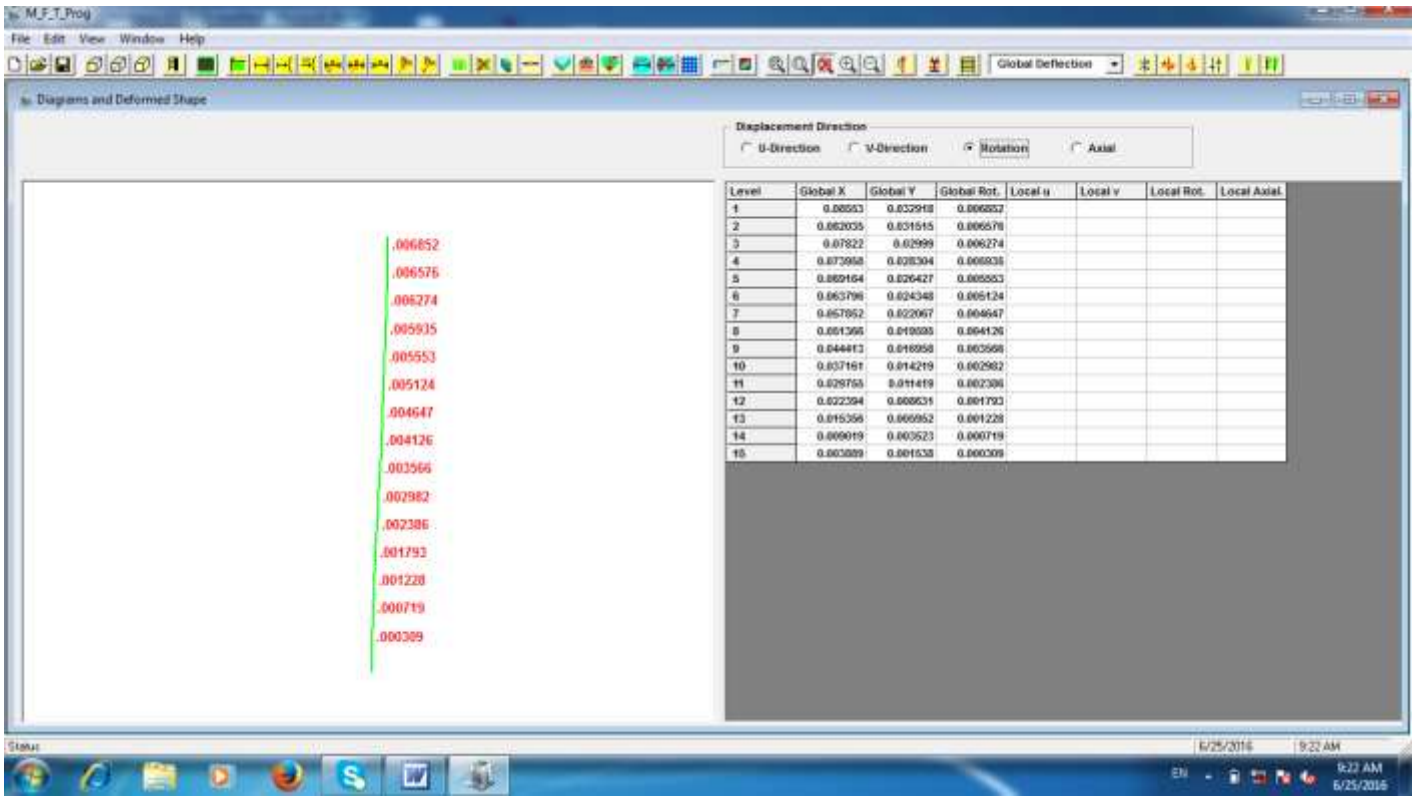

Figure 5.6: Twist rotations of the floor at the different levels.

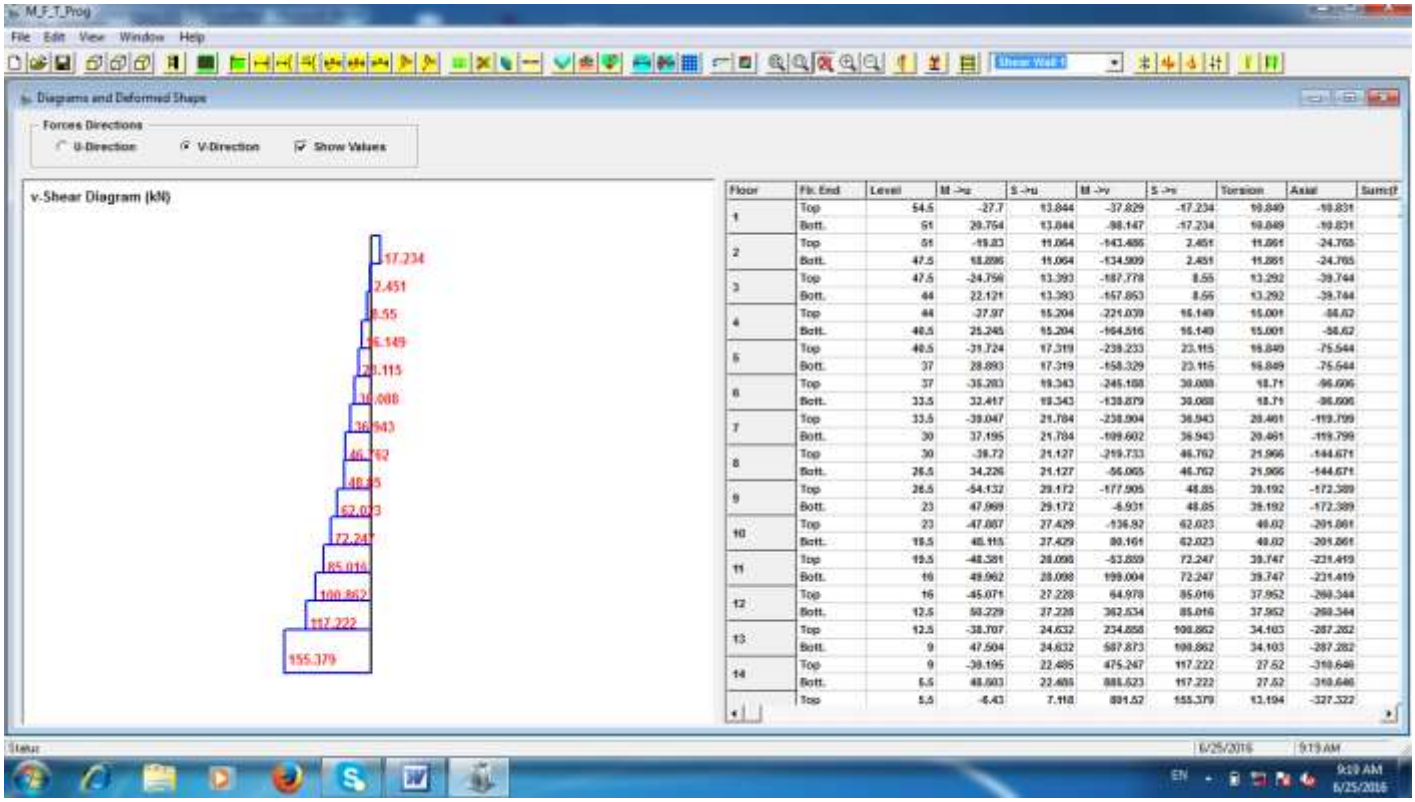

Figure 5.7: MFTProg shear force diagram for shear wall #1

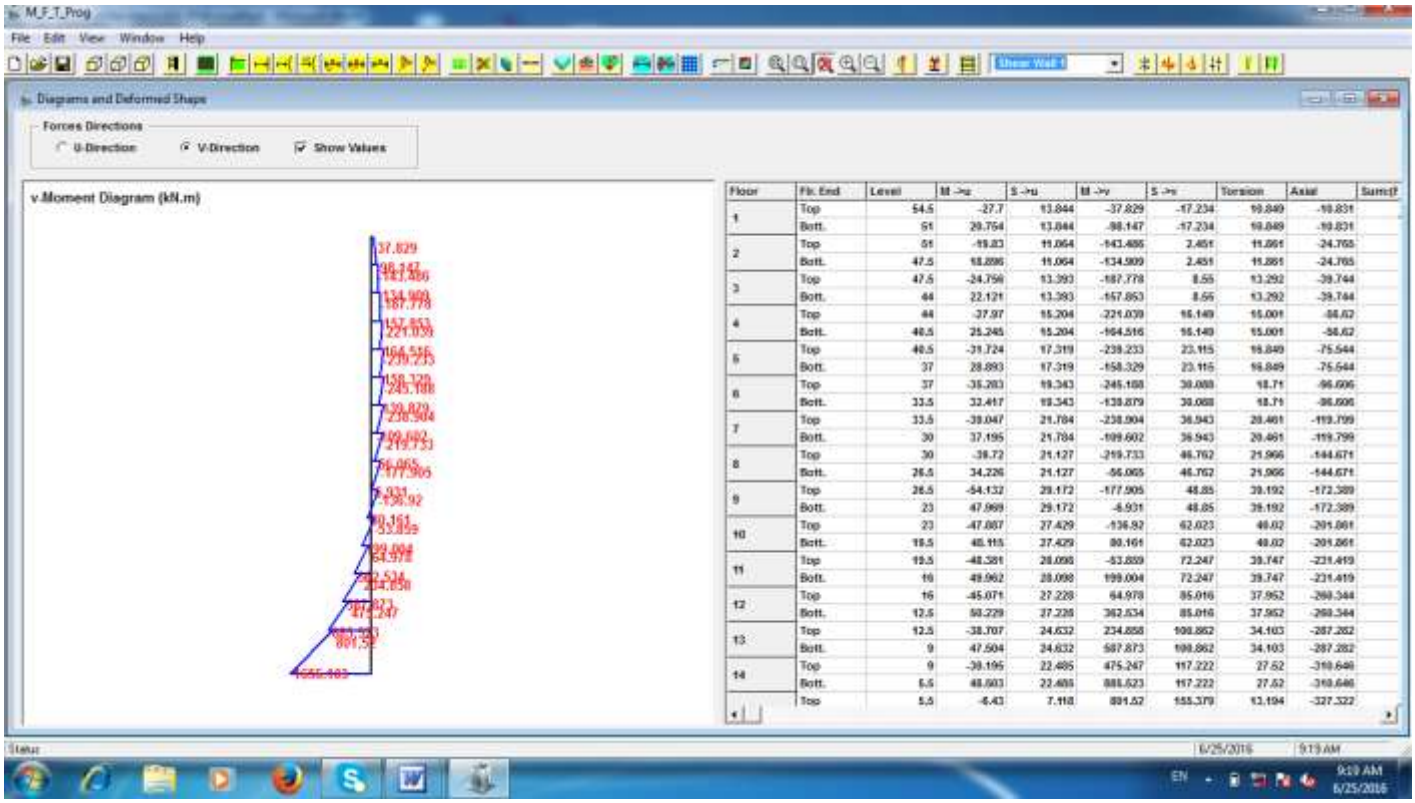

Figure 5.8: MFTProg bending moment diagram for shear wall #1

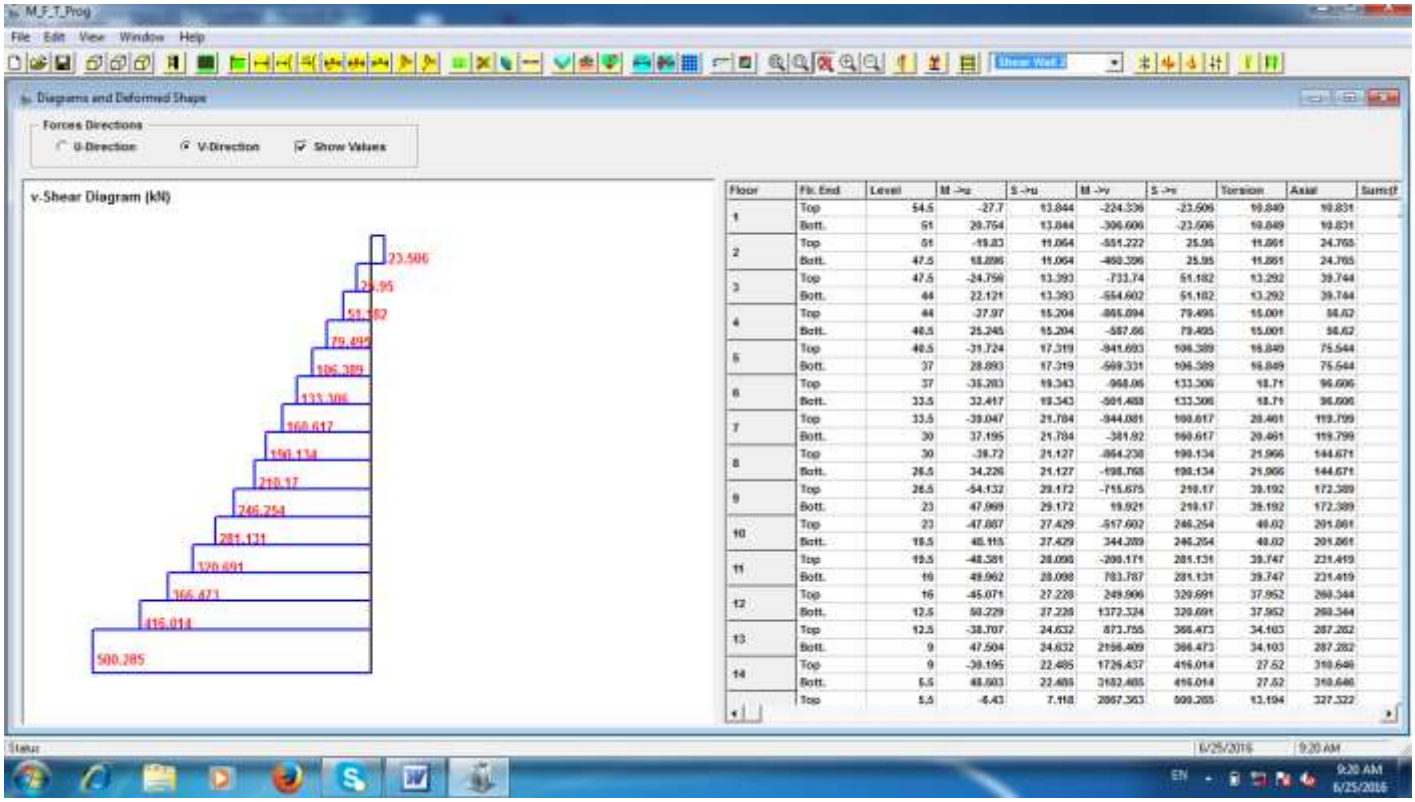

Figure 5.9: MFTProg shear force diagram for shear wall #2

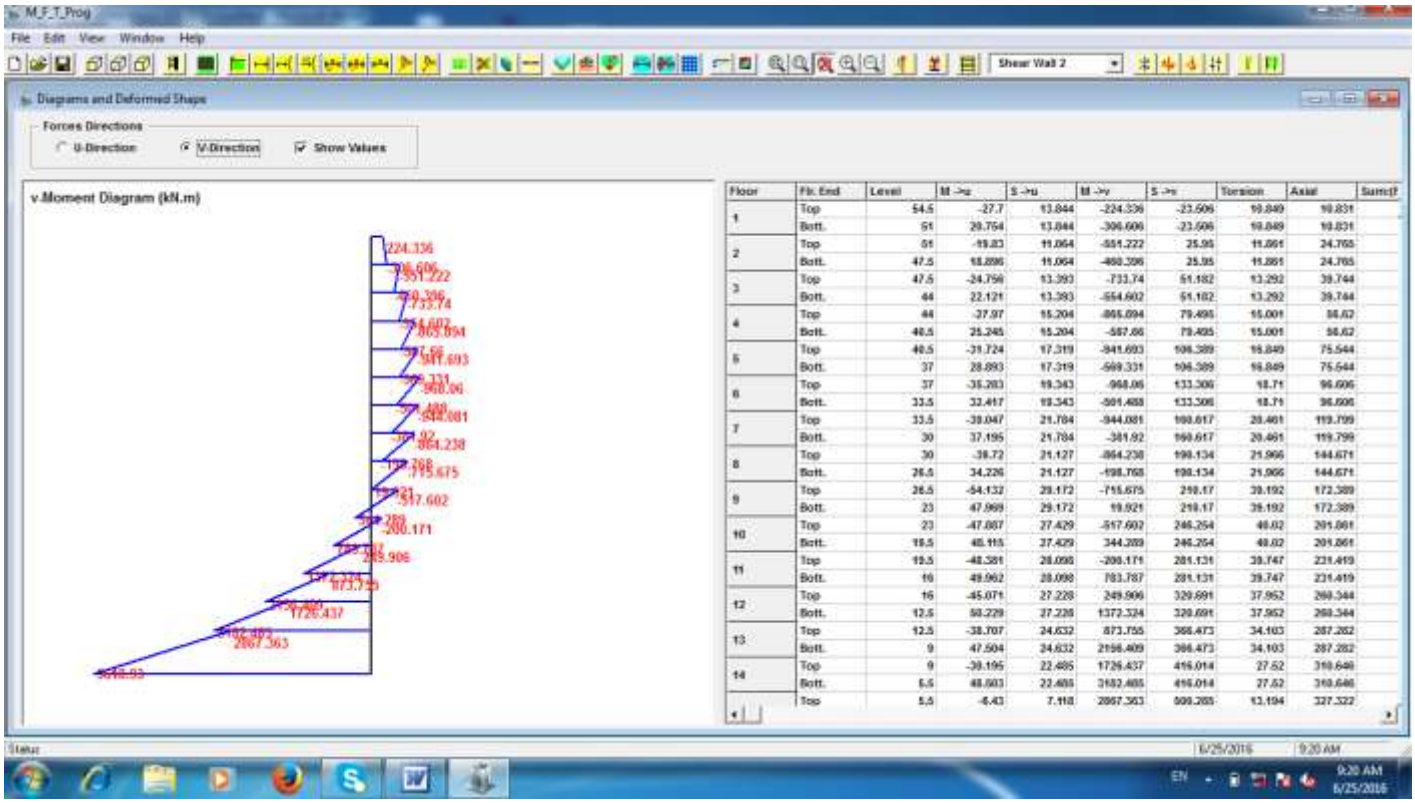

Figure 5.10: MFTProg bending moment diagram for shear wall #2

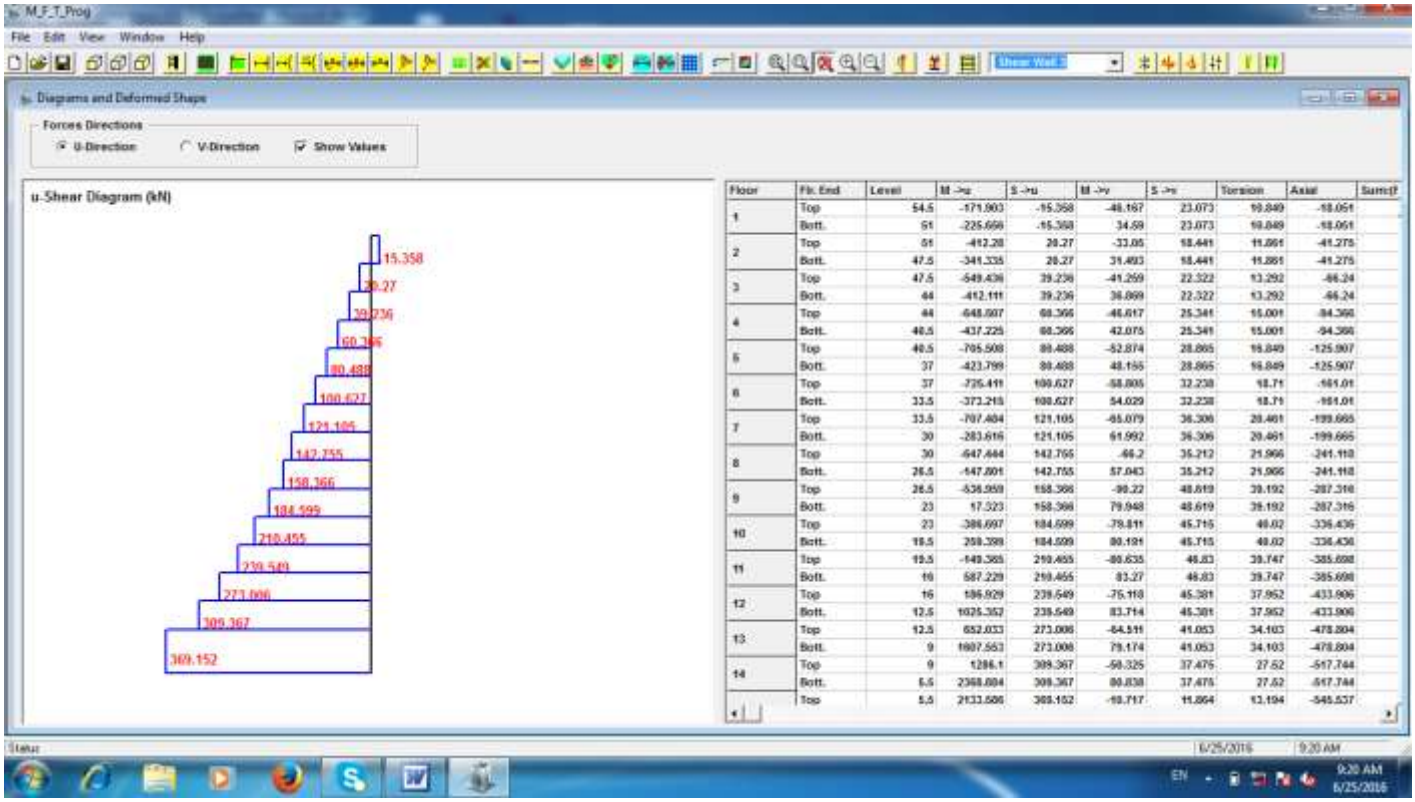

Figure 5.11: MFTProg shear force diagram for shear wall #3

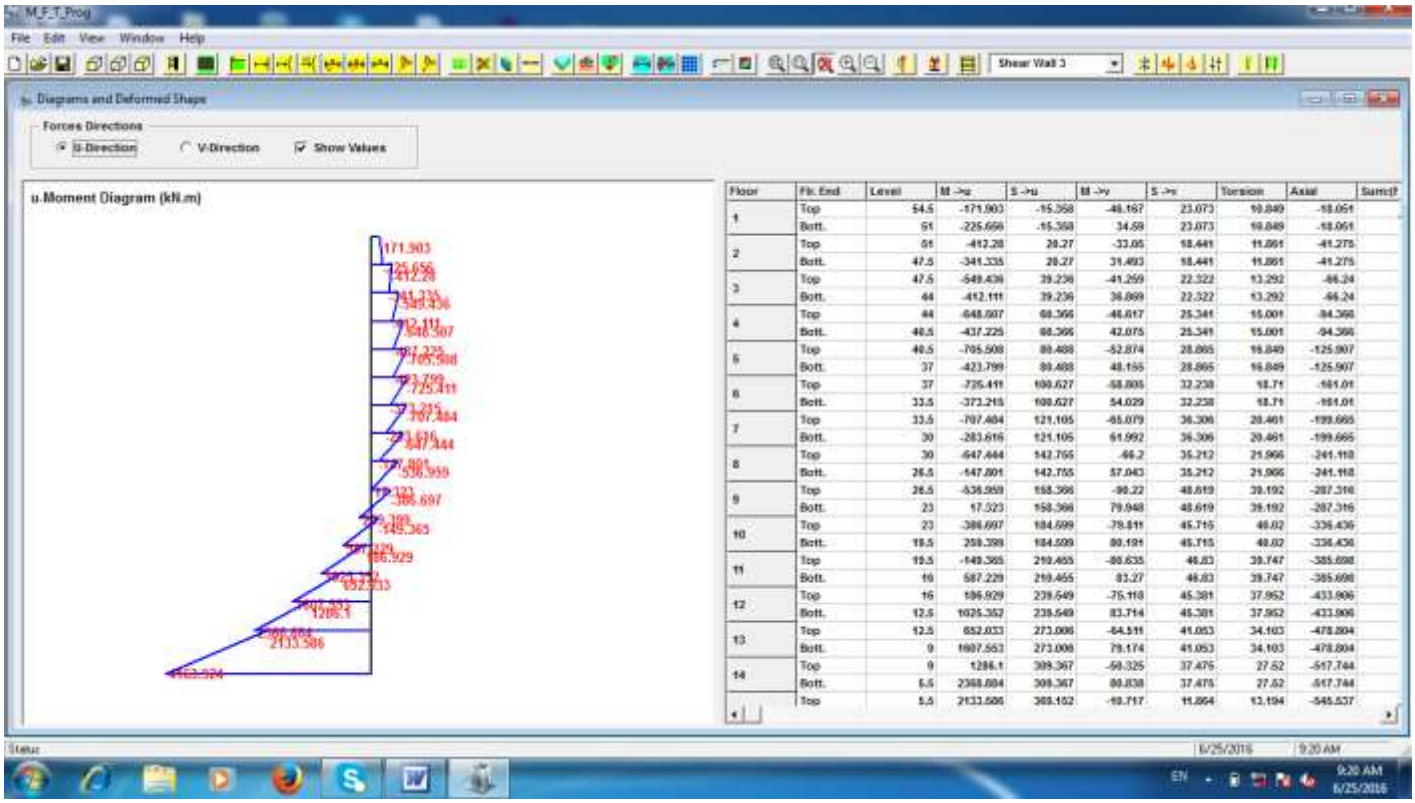

Figure 5.12: MFTProg bending moment diagram for shear wall #3

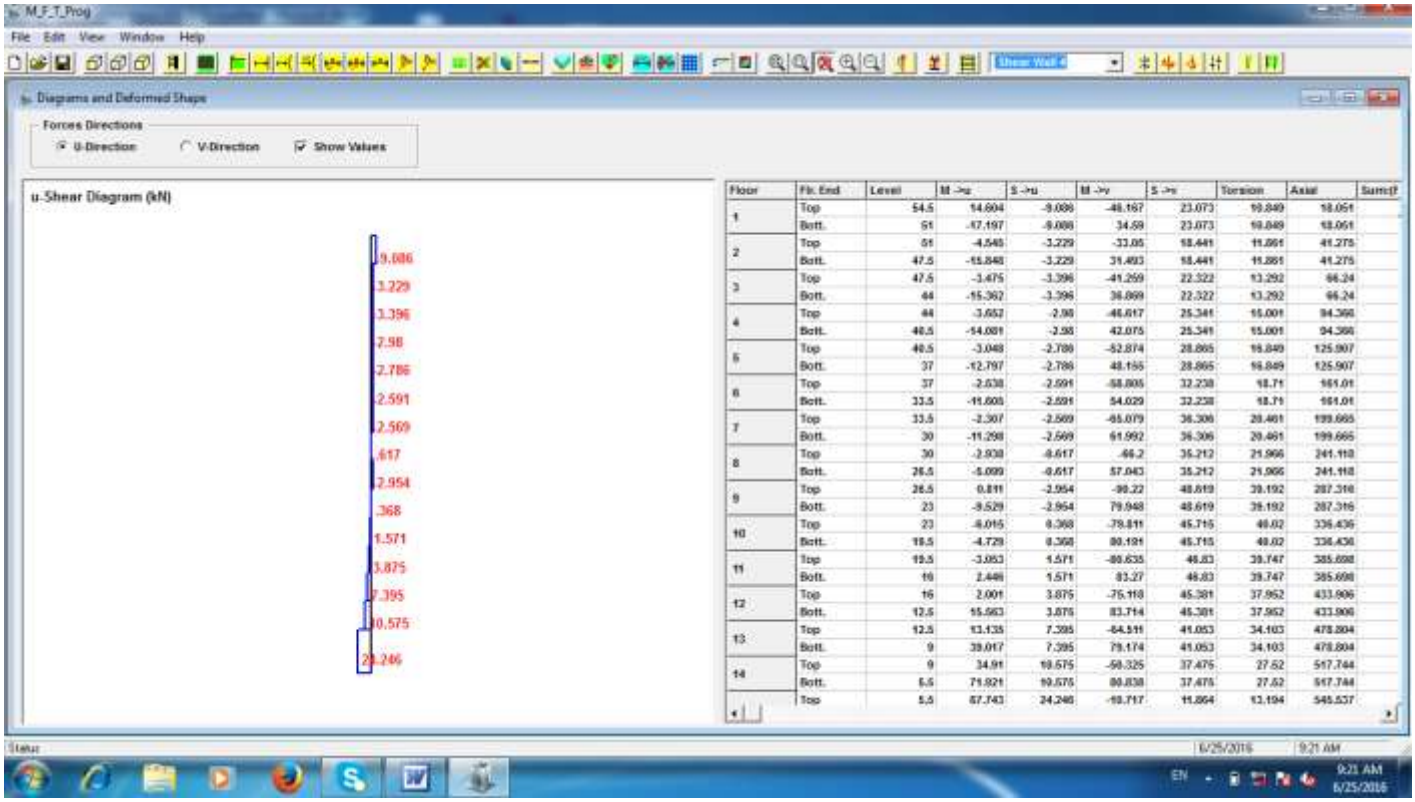

Figure 5.13: MFTProg shear force diagram for shear wall #4

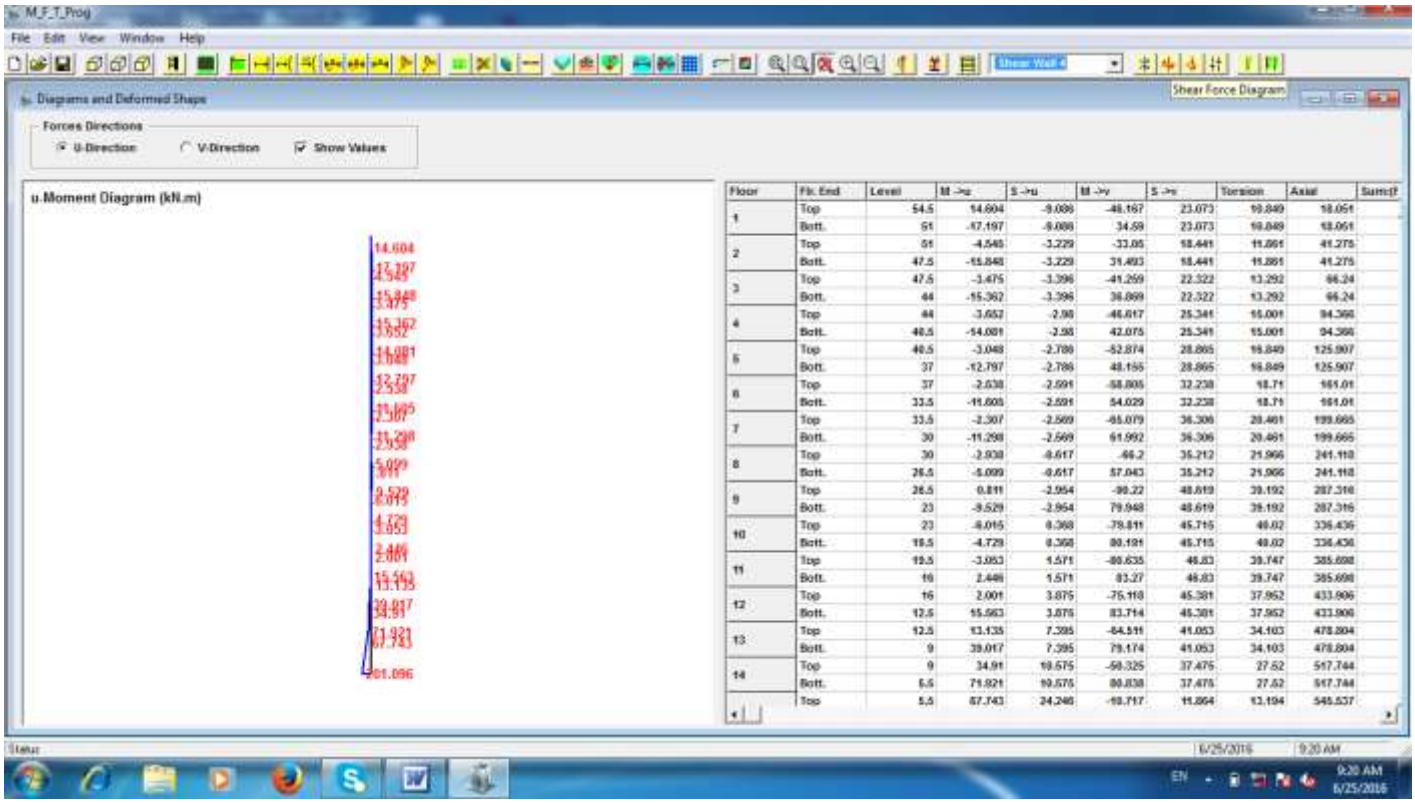

Figure 5.14: MFTProg bending moment diagram for shear wall #4

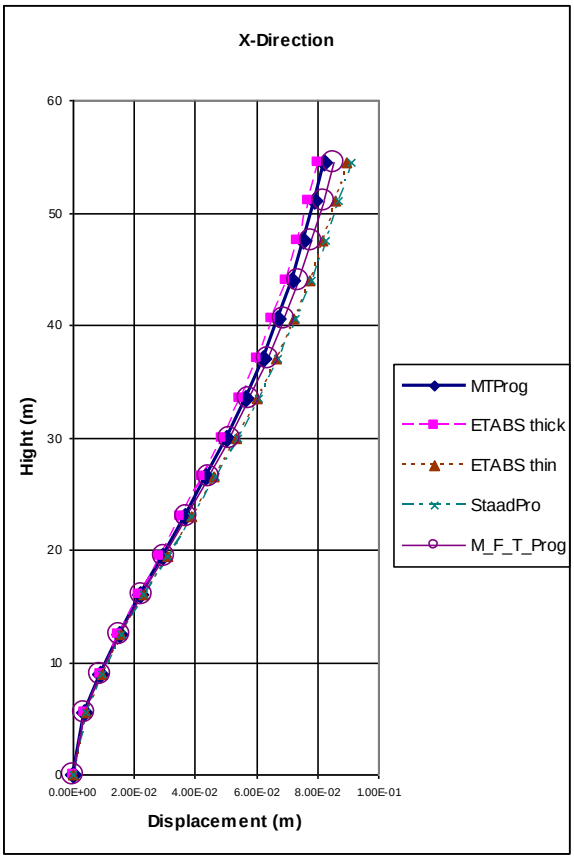

Figure 5.15: Comparisons of displacements of Column #5 in *x*-direction

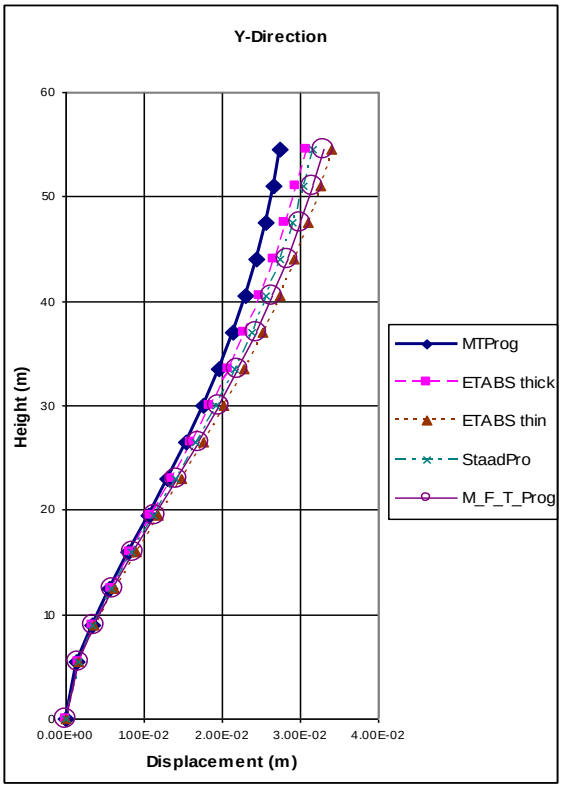

Figure 5.16: Comparisons of displacements of Column #5 in *y*-direction

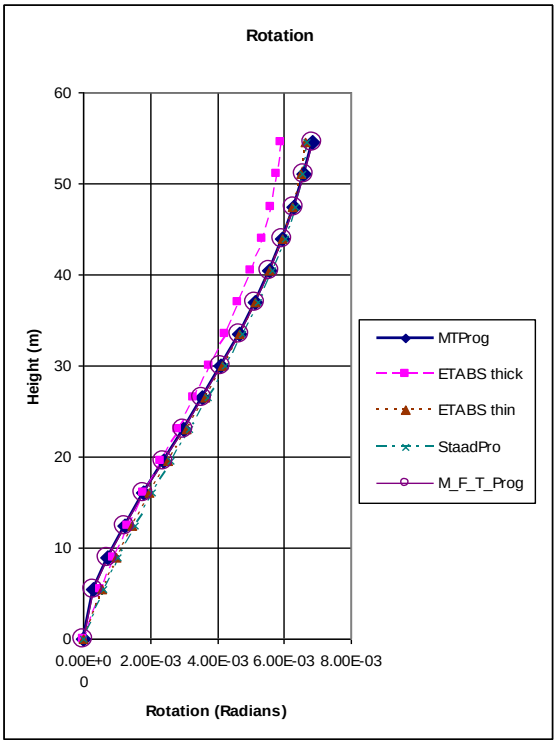

Figure 5.17: Comparisons of twist rotations of the floors in radians

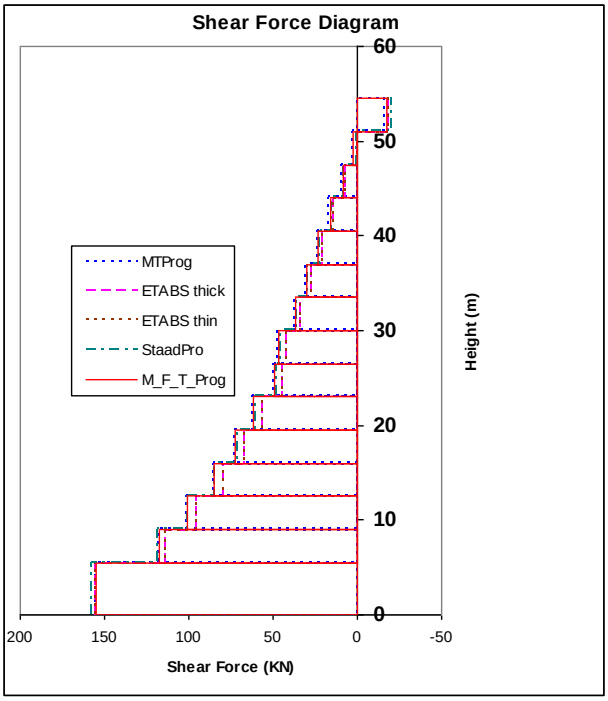

Figure 5.18: Comparisons of S.F.D. for shear wall #1

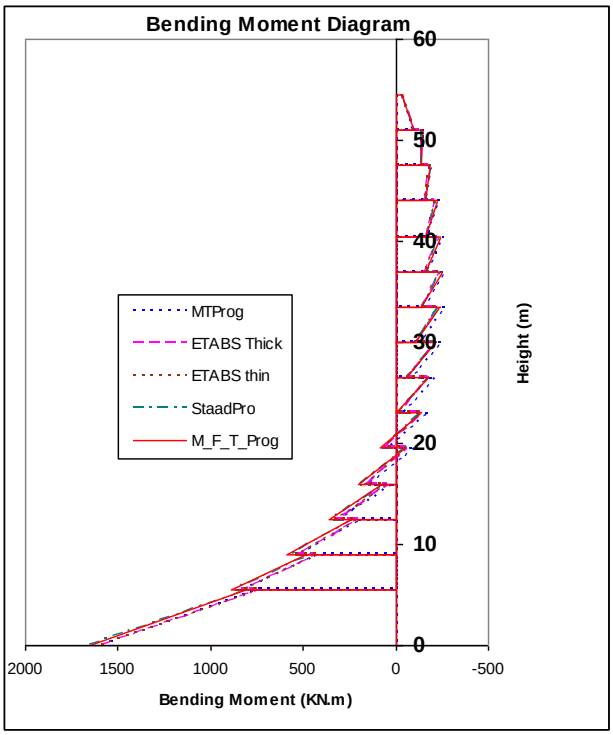

Figure 5.19: Comparisons of B.M.D. for shear wall #1

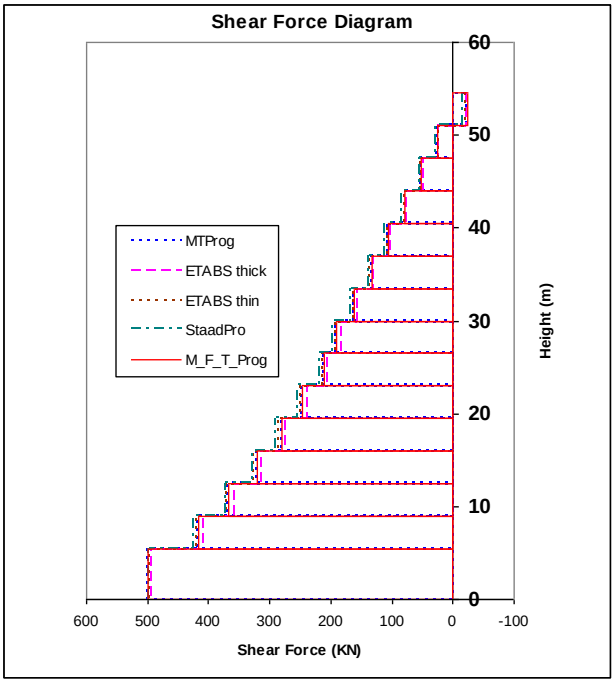

Figure 5.20: Comparisons of S.F.D. for shear wall #2

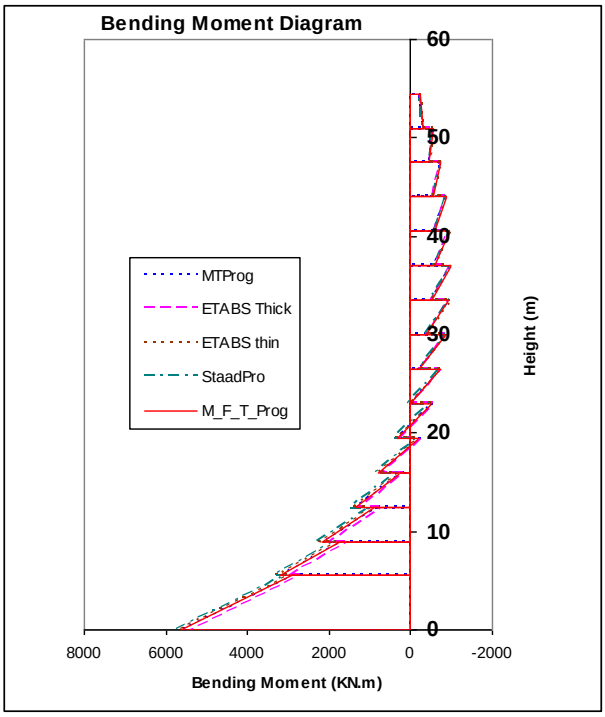

Figure 5.21: Comparisons of B.M.D. for shear wall #2

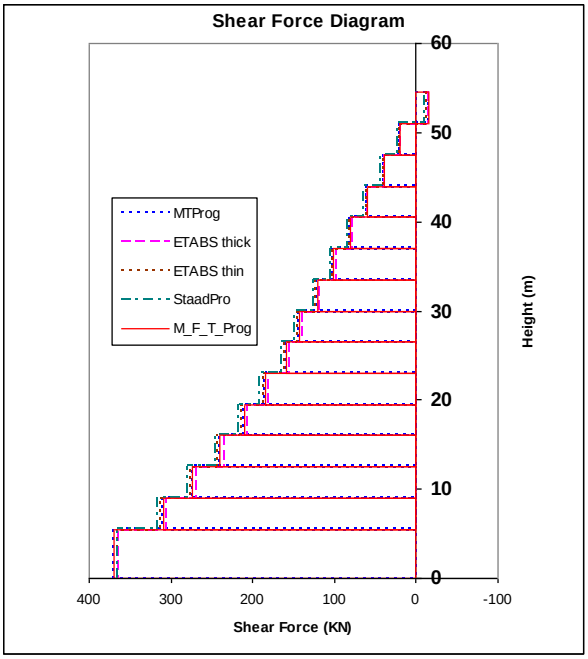

Figure 5.22: Comparisons of S.F.D. for shear wall #3

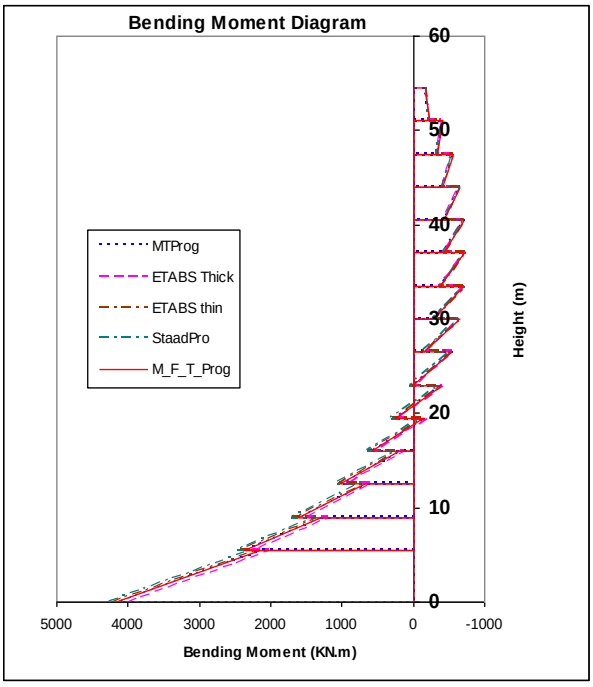

Figure 5.23: Comparisons of B.M.D. for shear wall #3

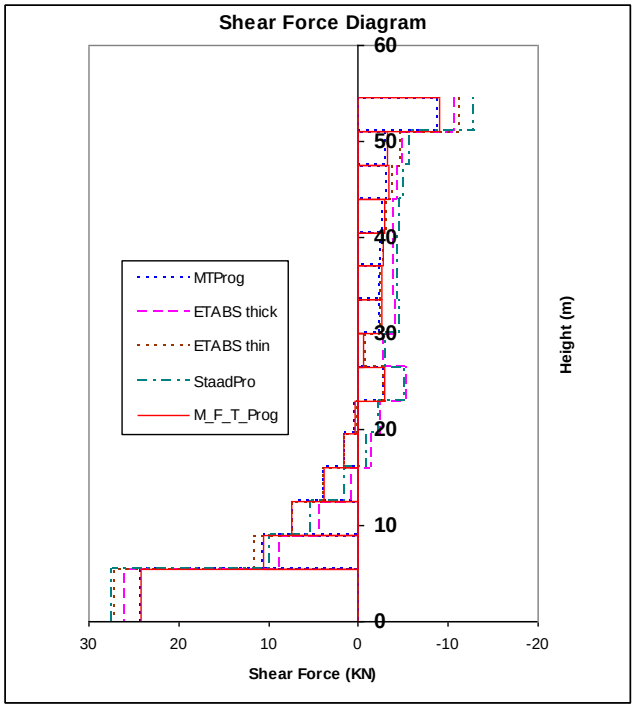

Figure 5.24: Comparisons of S.F.D. for shear wall #4

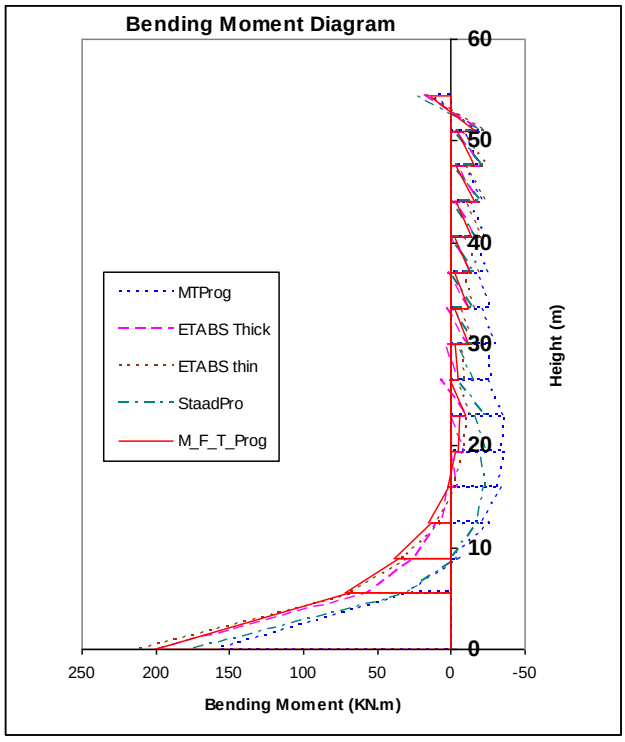

Figure 5.25: Comparisons of B.M.D. for shear wall #4

Table 5.3: Comparisons of the maximum shear force (kN) and bending moment (kN.m)

Wall #	Wall 1				Wall 2			
Package	Shear	% Diff.	Moment	% Diff.	Shear	% Diff.	Moment	% Diff.
MFTProg	155.4	0	1656.1	0	500.3	0	5618.9	0
MTProg[3]	155.4	0.00	1583.7	-4.37	500.3	0.00	5546.6	-1.29
StaadPro2004	157.8	1.54	1651.4	-0.28	497.1	-0.64	5741.2	2.18
ETABS[1]	155.7	0.19	1604.8	-3.10	494.6	-1.14	5424.3	-3.46
ETABS[2]	157.7	1.48	1697.9	2.52	497.2	-0.62	5727.2	1.93

Table 5.3 (continued)

Wall #	Wall 3				Wall 4			
Package	Shear	% Diff.	Moment	% Diff.	Shear	% Diff.	Moment	% Diff.
MFTProg	369.2	0	4163.9	0	24.2	0	201.1	0
MTProg[3]	369.1	-0.03	4120.5	-1.04	24.2	0.00	157.7	-21.58
StaadPro2004	365.6	-0.98	4261	2.33	27.3	12.81	174.5	-13.23
ETABS[1]	364.1	-1.38	4016.9	-3.53	26.1	7.85	200.7	-0.20
ETABS[2]	365.8	-0.92	4240.5	1.84	27.2	12.40	214.6	6.71

[1] Thick Slab. [2] Thin Slab. [3]Ibrahim (2013).

Table 5.4: Displacements of the origin (column 5), in mm and radians

Package	*X*(mm)	% Diff.	*Y*(mm)	% Diff.	Twist(rad)	% Diff.
MFTProg	85.53	0	32.92	0	0.00685	0
MTProg[3]	82.21	-3.88	27.38	-16.83	0.00685	0.00
StaadPro2004	90.86	6.23	31.7	-3.71	0.00669	-2.34
ETABS[1]	80	-6.47	30.7	-6.74	0.00591	-13.72
ETABS[2]	89.7	4.88	33.9	2.98	0.00662	-3.36

In all the comparisons, the differences were found to be very small for large stress values (shear forces and bending moments in shear walls 1, 2 & 3). The largest percentage difference is found in shear wall #4, but this resists very small stresses compared with its section. Appendix G, presents more discussion of the results.

As shown in Figures 5.15 to 5.25, and Tables 5.3 and 5.4, consideration of the axial deformations in the vertical members has affected the bending moments in all shear walls, and also the displacements in *x* and *y* directions.

5.3 Summary:

In this chapter, verification for the program MFTProg has been carried out by solving different two and three dimensional examples, using linear static analysis. The results obtained for the two portal frames were compared with published results and with StaadPro2014 results. The obtained results of the hypothetical square building was compared with results obtained using the commercial computer analysis packages StaadPro2004 and ETABS.

CHAPTER SIX

Cases Study and Analysis of Results

6.1 Introduction

In this chapter two case studies were considered. A case of a 2D frame of 15 floors subjected to vertical and lateral loads, and a case of a 3D asymmetrical 25 floors building subjected to vertical and wind loads. In the 3D problem, the floor stiffness was modeled by using rectangular plate bending finite element incorporated in the program to account for the out of plane stiffness of the level's floor slabs. The degrees of freedom, DOFs, are corresponding to the two rotations about the principal axes and one translation in the vertical direction of the system.

The results obtained were compared with those obtained using StaadPro2004, StaadProV8i, SAP200V16 and ETABS. In StaadPro packages, the second order P-Delta results were obtained from 10 iterations, and in ETABS, the results were obtained from displacements relative tolerance of $1x10^{-3}$ and maximum 10 iterations.

The performed analyses using the proposed transformation methods, for the 2D and 3D models were:

(1) Static analysis considering the axial deformations in the vertical members.

(2) Nonlinear second order P-Delta analysis.

(3) Dynamic analysis considering linear effects.

(4) Dynamic analysis considering the nonlinear second order effects.

(5) Elastic stability and buckling analysis.

6.2 Dynamic Analysis using the transformation method

As shown in chapter three, the dynamic properties of the building, the natural frequencies and the corresponding mode shapes, are obtained from the un-damped free vibrated system using the direct iteration method or the inverse iteration method (Stodola concept). Using these dynamic properties, the dynamic analyses were performed. The dynamic analyses performed for the two buildings were the response spectra method and the time history method.

6.2.1 The vibration Modes

The first natural frequencies and their modes are important in the dynamic analyses. In these two models analyses, the first 6 vibration modes of the 2D building and the first 9 modes of the 3D building were obtained and used in the dynamic analysis. For the 3D model, these are the minimum number of the modes required to capture at least 90 percent of the total building mass in the two directions separately. Although, more than 90% is captured in two modes in the case of the 2D model, 6 modes were considered in the analysis to capture more than 99%, (refer to section 3.17).

6.2.2 Participating Mass Ratios

In the response spectrum analysis, enough number of modes should be included in the calculations as it is a measure of accuracy of the analysis. Most of the design codes of practice require that the computations of the responses should include enough modes to capture at least 90 percent of the total building mass. In the analyses, the number of modes required to capture 90 percent of the total masses are determined for each direction separately.

6.2.3 The top floor lateral displacement

The lateral translation of the building top floor was obtained using the MFT method and compared with the results obtained from the other packages. The lateral displacement is important response affecting the building performance.

6.2.4 The Base Reactions

The base reactions (base shear and overturning moment), were obtained using the MFT method and compared with the results from the other packages. The base reactions are measure of the total effect of the lateral inertial forces acting on the structure.

6.2.5 Response Spectrum Analysis

In response spectrum analysis it is necessary to find out the natural frequencies, the mode shapes and the lumped masses, from which the participation factors are calculated and used with the acceleration period curve (the response spectrum curve) to calculate the responses of the structure for each vibration mode.

The response spectrum used in the proposed analyses was taken from the UBC code, Figure 6.1, with assumed seismic zone of factor Z = 0.075 and soil profile S_E. The corresponding seismic coefficients C_a and C_v were 0.19 and 0.26 respectively.

A damping ratio of 5 % was assumed in the analyses and the SRSS (The square root of the sum of squares) and the CQC (complete quadratic combination) methods were used in combining the individual modal contributions.

The results of the proposed response spectrum analysis of the two 2D and 3D models were compared with those obtained from StaadProVi8, SAP2000V16 and ETABS and are shown in the following sections.

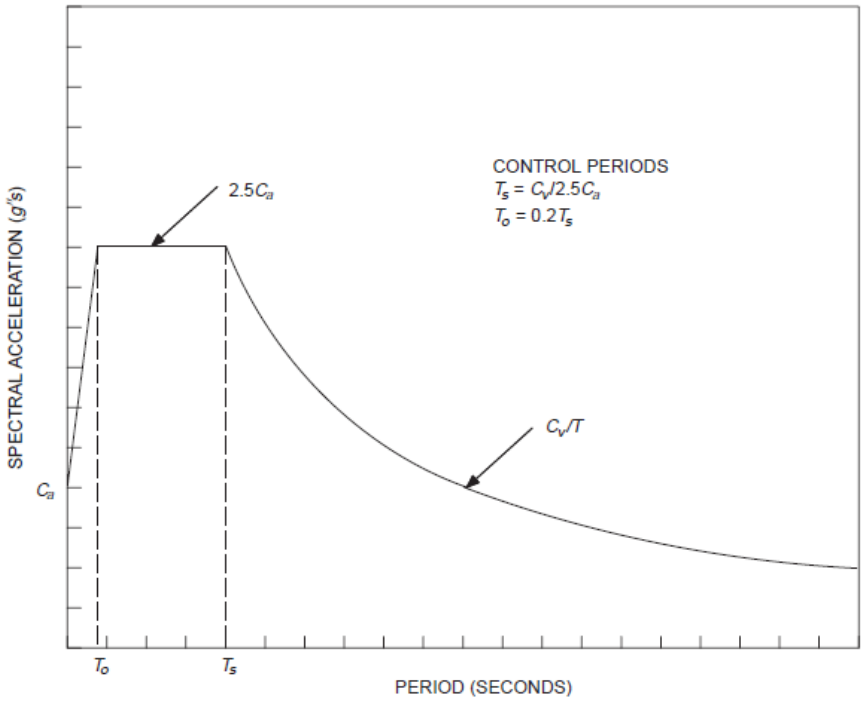

Figure 6.1: UBC-1997 Design Response Spectra

6.2.6 Time History Analysis

The time history analysis was performed for the two models using the proposed method and the obtained results were compared with the results obtained from the different structural packages. The results of the two 2D and 3D models are presented as shown in this section. The same mass and inertia values used in the response spectrum analyses were also used in the time history analyses.

The acceleration-time record of N-S component of El Centro Earthquake, 18 May 1940 shown in Figure 6.2, was directly applied to the base of the building models in *x*-direction for the case of 2D model and in *y*-direction for the case of 3D model. The record of the first 31.2 seconds of the earthquake, having a step-size of 0.02 seconds, was used in the

two analyses. A damping ratio of 5 % was used in the analyses of the 2D and 3D models. The modal superposition method which provides a highly efficient and accurate procedure for performing time-history analysis was used in this study. Closed-form integration of the modal equations was used to compute the response, assuming linear variation of the time functions between the input data time points. The following time history responses were computed and plotted for each model:

1. Lateral displacement at the top floor.
2. Induced total base shear force.
3. Induced total base overturning moment.

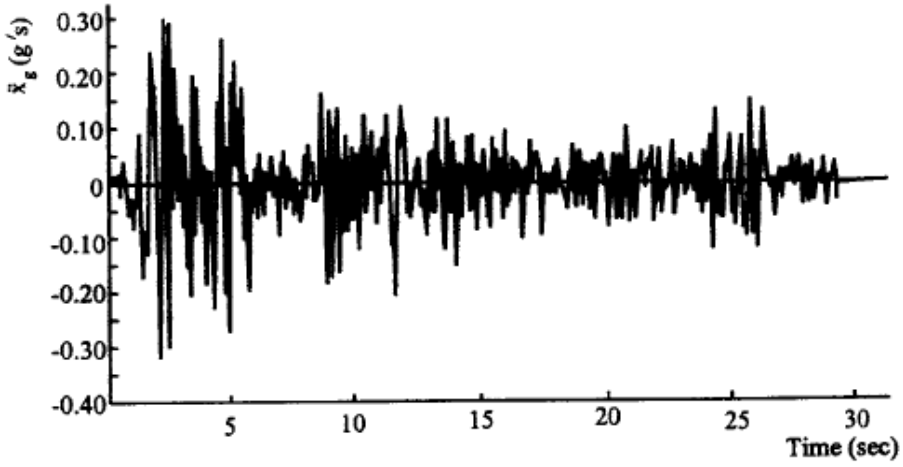

Figure 6.2: N-S component of El Centro Earthquake records, 18 May 1940 (www.vibrationdata.com)

6.3 The fifteen floors 2D building Model

The displacements and bending moments were obtained using the proposed method for a fifteen multi-storey 2D frame under the vertical and horizontal loading shown in Figure 6.3. All building members are concrete of elasticity, $E = 29x10^6$ kN/m^2,
and Poisson's ratio, $\nu = 0.2$

6.3.1 Static Linear and second order Analysis of the 2D building model

Linear and second-order (P-Delta) analyses were carried out, and comparisons of the results with exact results are shown in Tables 6.1 to 6.4.

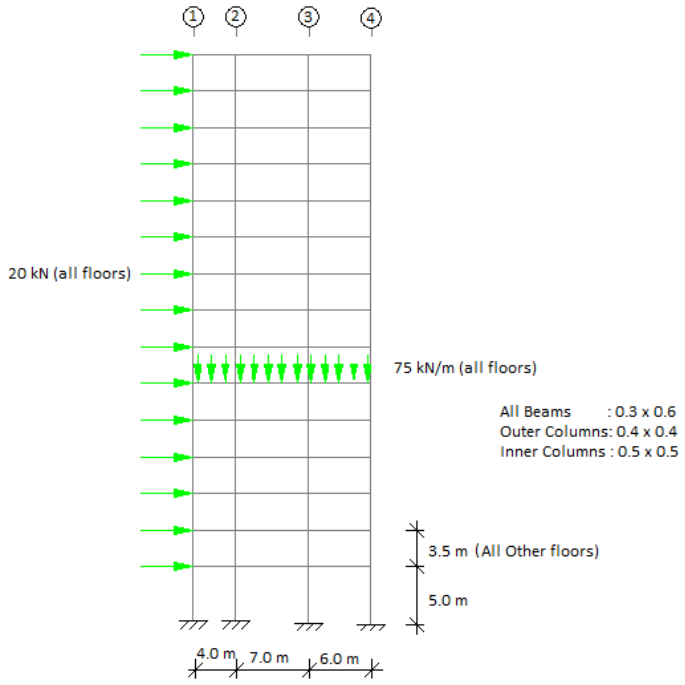

Figure 6.3: Fifteen floors 2D Frame, properties and loading

The displacements and the bending moments results obtained using the proposed method compared with results obtained using StaadPro2004, are shown in Tables 6.1 to 6.4.

Table 6.1: Displacements in the top floor level (mm), (2D Frame), Linear Analysis:

Results	Columns (1)		Columns (2)		Columns (3)		Columns (4)	
	Lateral	Axial	Lateral	Axial	Lateral	Axial	Lateral	Axial
MFTProgV2	88.28	-14.82	88.28	-23.43	88.28	-28.83	88.28	-25.12
StaadPro2004	88.45	-14.81	88.39	-23.44	88.15	-28.84	88.04	-25.11
% Diff.	-0.19	0.07	-0.12	-0.04	0.15	-0.03	0.27	0.04

Table 6.2: Maximum bending moment in the lower floor, (kN.m), (2D Frame), Linear Analysis:

Results	Columns (1)	Columns (2)	Columns (3)	Columns (4)
MFTProgV2	122.26	280.55	307.13	152.87
StaadPro2004	121.76	279.21	307.86	153.89
% Diff.	0.41	0.48	-0.24	-0.66

Table 6.3: Displacements in the top floor level (mm), (2D Frame), P-Delta Analysis:

Results	Columns (1)		Columns (2)		Columns (3)		Columns (4)	
	Lateral	Axial	Lateral	Axial	Lateral	Axial	Lateral	Axial
MFTProgV2 (1)	97.03	-14.59	97.03	-23.41	97.03	-28.85	97.03	-25.34
MFTProgV2 (2)	97.47	-14.58	97.47	-23.42	97.47	-28.86	97.47	-25.34
StaadPro2004	97.19	-14.57	97.13	-23.42	96.89	-28.86	96.78	-25.33
% Diff.(1)	-0.16	0.14	-0.10	-0.04	0.14	-0.03	0.26	0.04

(1) Including only Global P-Delta. (2) Including Global and local P-Deltas.

Table 6.4: Maximum bending moment in the lower floor (kN.m), (2D Frame), P-Delta Analysis:

Results	Columns (1)	Columns (2)	Columns (3)	Columns (4)
MFTProgV2 (1)	143.01	328.30	354.00	172.95
MFTProgV2 (2)	143.16	325.69	350.28	171.13
StaadPro2004	142.51	326.95	354.72	173.99
% Diff.(1)	0.35	0.41	-0.20	-0.60

The comparison of the results shows very close agreement and some times the results are identical, both in the linear and second-order analysis.

As shown in Tables 6.1 to 6.4, the lateral displacements which are calculated including the P-Delta effects are greater than those calculated using ordinary linear analysis. In general, the second order analysis values may be increased with the increase of the vertical loads and/or increase in the building height. Including the local p-delta effects in the analysis, results in extra increase in the lateral displacements.

6.3.2 Buckling Analysis of the 2D building model

The buckling analysis for the 2D building model was carried out, using the incremental method described by Coates et al (1990), the eign solution (Vianello method), described by Clough and Penzien (2003), and the proposed improved Vianello method. Comparisons between the results assuming linear shape, cubic shape and Euler buckling using the stability functions were also studied.

Table 6.5 shows the results of the fundamental buckling factor calculated using the proposed program with the aid of the incremental subroutine of Coates et al. The results are compared with those obtained using StaadPro2014 (Stardyne Advanced Engine), StaadProV8i and ETABS 2013.

Table 6.5: Minimum Buckling factor using the different packages

Buckling Analysis Package	**Minimum buckling factor**
MFTProgV2, Linear Shape	7.9764
MFTProgV2, Cubic Shape	7.1040
MFTProgV2, Euler stability functions	7.0281
StaadPro2014 (Stardyne Advanced Engine)	7.1061
StaadProV8i	7.1016
ETABS2013	7.1360

The buckling analysis was carried out using the eign solution. The Vianello method and the proposed improved Vianello method were carried out for the first six buckling modes, for the linear and the cubic deformed shape functions and the Euler stability functions. The results obtained are compared with those obtained from ETABS2013. The results are shown in Table 6.6 and the buckling mode shapes are shown in Figures 6.4 to 6.9.

Table 6.6: Buckling factors of the first six modes using the different packages

Buckling Analysis	Mode1	Mode2	Mode3	Mode4	Mode5	Mode6
MFTProgV2 (Linear)	7.976	10.569	12.934	15.195	17.612	20.067
MFTProgV2 (Cubic)	7.100	9.982	12.005	13.879	15.829	17.800
MFTProgV2 (Euler)	7.049	9.960	11.955	13.805	15.712	17.675
ETABS2013	7.136	10.037	12.069	13.957	15.931	17.925

In Table 6.5, the MFTProgV2 cubic shape give results that are very close to the results of StaadPro2014 (Stardyne advanced Engine), the percentage difference is -0.03%.
The MFTProgV2 (Euler stability functions) gives the exact solution and shows lesser buckling factor.

The results of the proposed program linear deformed shape show greater values of the buckling factors than the cubic shape values and the results of the cubic shape show greater values than the Euler buckling values. This can be seen in Table 6.6, for all buckling modes. These differences are very small. The explanation of greater buckling load of the linear shape compared with the cubic shape and the cubic shape greater than the Euler exact solution lies in the fact that an assumed deflected shape implies the application of constraints in order to force the column to take up an artificial shape. This, as has been seen, has the effect of stiffening the column with a consequent increase in critical load.

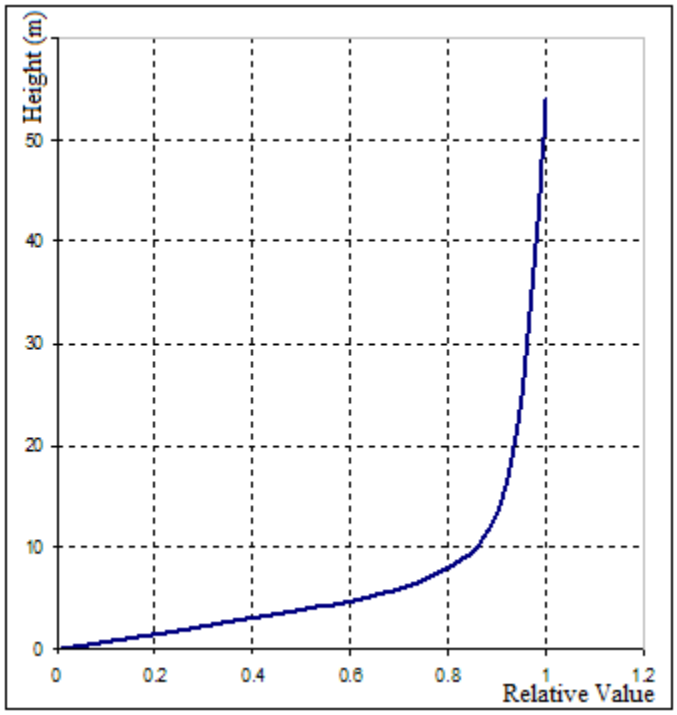

Figure 6.4: MFTProgV2, Buckling mode shape No. 1

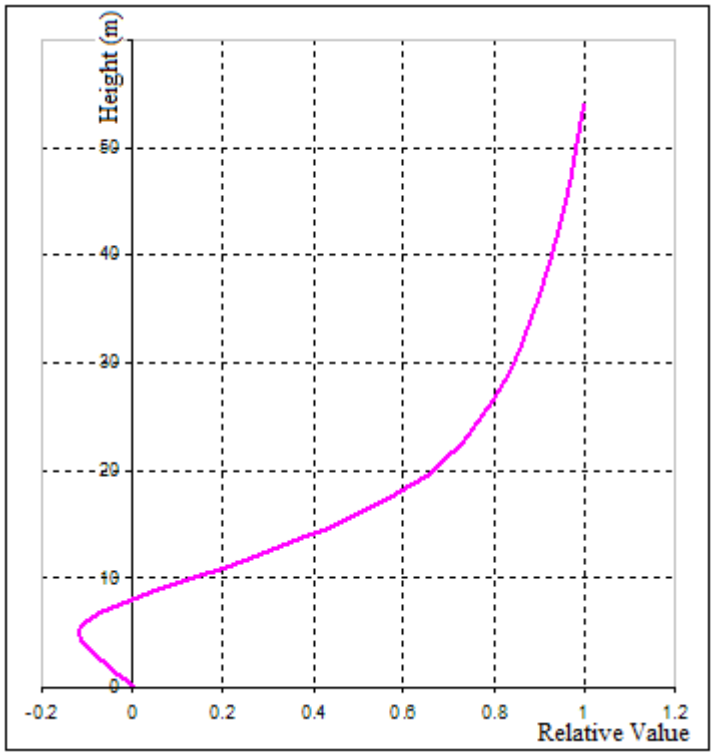

Figure 6.5: MFTProgV2, Buckling mode shape No. 2

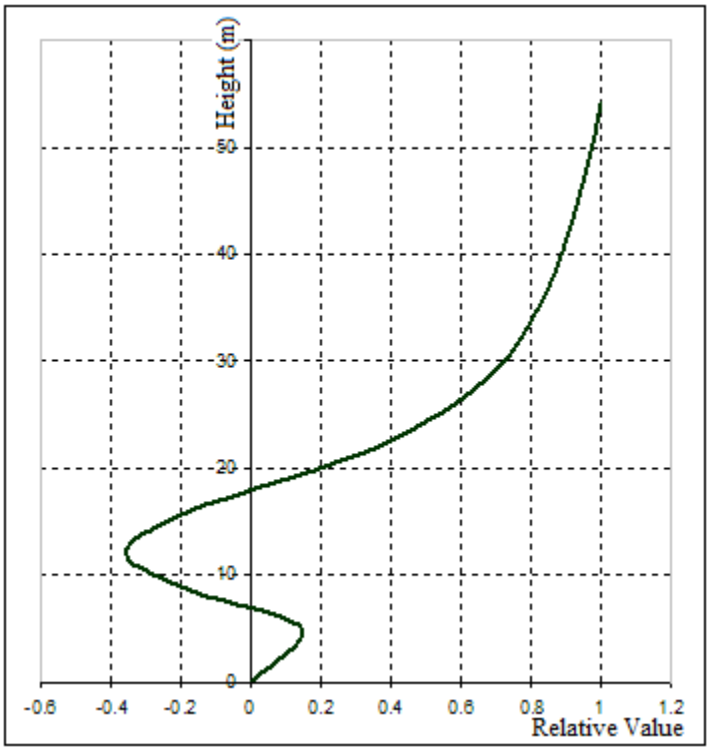

Figure 6.6: MFTProgV2, Buckling mode shape No. 3

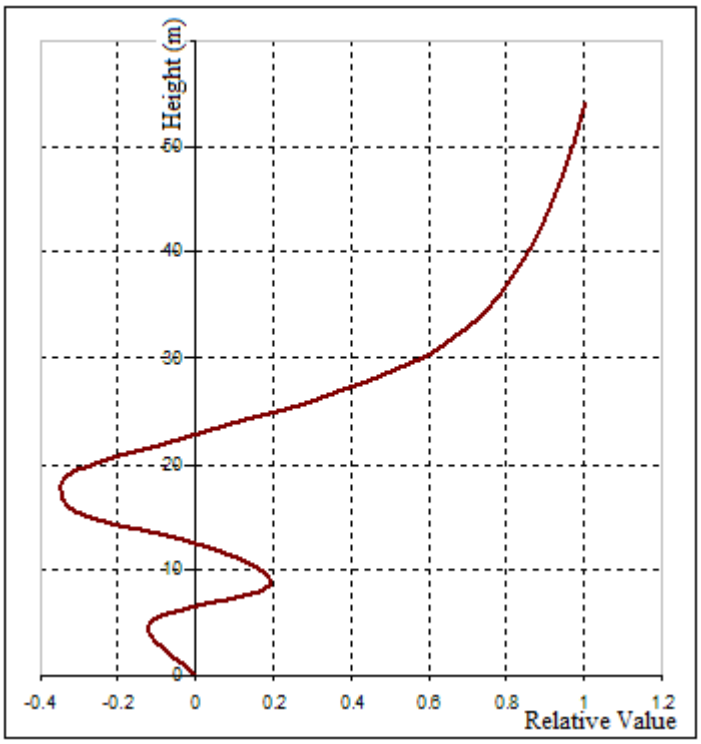

Figure 6.7: MFTProgV2, Buckling mode shape No. 4

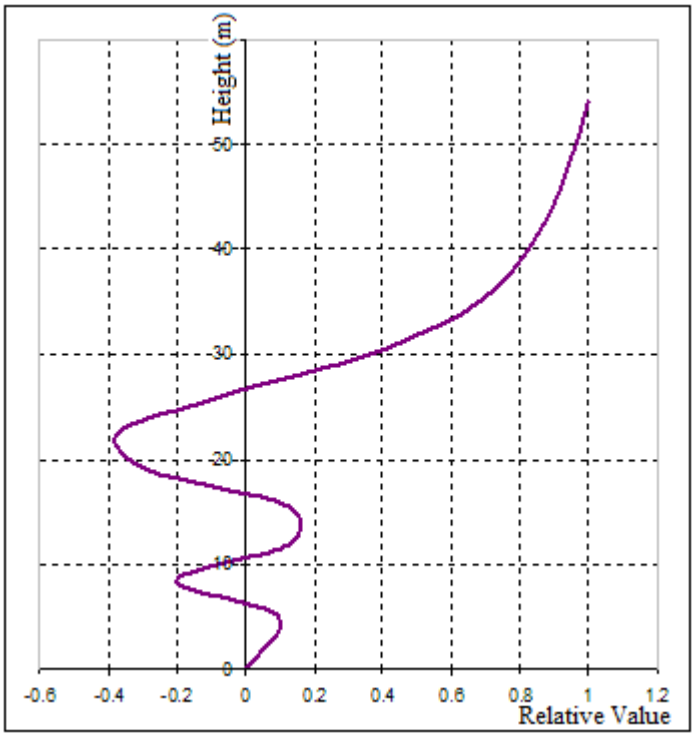

Figure 6.8: MFTProgV2, Buckling mode shape No. 5

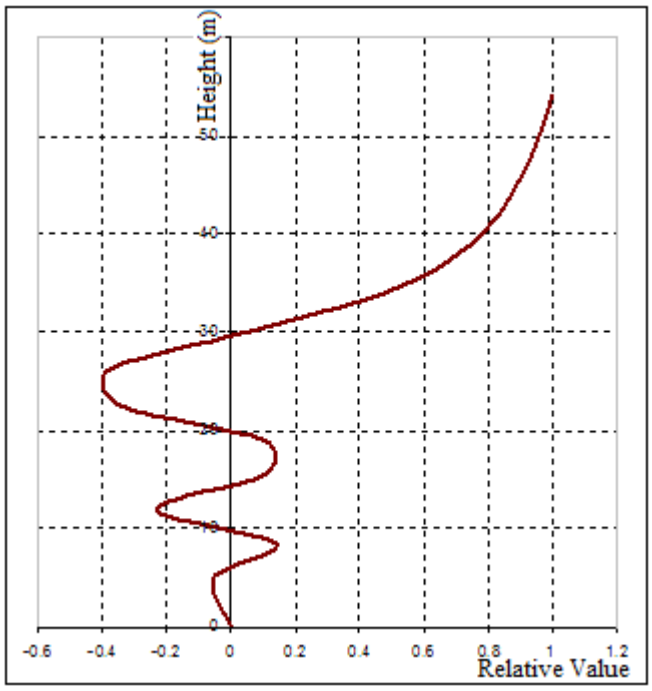

Figure 6.9: MFTProgV2, Buckling mode shape No. 6

6.3.3 Dynamic analysis of the 2D model

The dynamic analysis was performed for the 2D building model, Figure 6.3. The response spectra method was performed first with linear effects and then the method was performed including the P-Delta second order effects. The time history was then performed including the linear and second order effects.

Mass Source

The lumped mass for the 2D model in any floor level was calculated as follows and shown in Table 6.7:

m_{tot} = 75*(4+7+6)/9.80665 = 130.0138 kg

Table 6.7: Floor Masses of the 2D Building (Mass in kg)

Floor	Mass (kg)
1 to 15	130.0138

Table 6.8: Comparisons of the first six Natural frequencies of 2D Building (cycles/second)

Mode	MFTProgV2	StaadPro(%Diff)	ETABS(%Diff)	SAP2000V16(%Diff)
1	0.27	0.27 (0)	0.27 (0)	0.27 (0)
2	0.825	0.825 (0)	0.825 (0)	0.823 (-0.24)
3	1.467	1.468 (0.07)	1.467 (0)	1.466 (-0.07)
4	2.112	2.112 (0)	2.111 (-0.05)	2.109 (-0.14)
5	2.793	2.793 (0)	2.792 (-0.04)	2.789 (-0.14)
6	3.5	3.5 (0)	3.499 (-0.03)	3.461 (-1.11)

Table 6.8, shows the comparison between the natural frequencies using the proposed method and the different analysis packages. The table shows negligible differences and identical results. Some slight deviations in comparing the results with those obtained from SAP2000V16 are noticed.

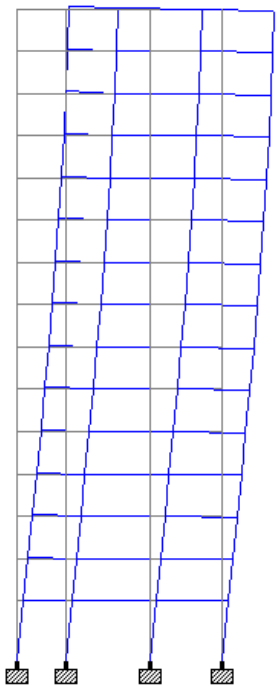

Figure 6.10: First Mode Shape (Linear Analysis)

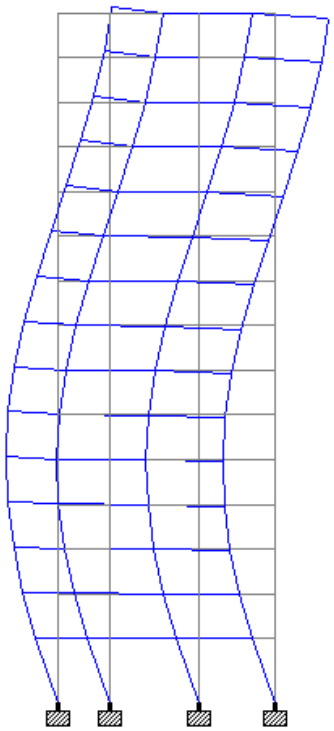

Figure 6.11: Second Mode Shape (Linear Analysis)

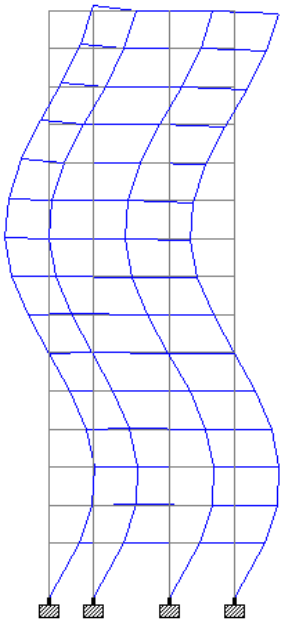

Figure 6.12: Third Mode Shape (Linear Analysis)

Table 6.9: Comparisons of the first three modes shape ordinates (Linear Analysis)

	Mode 1			Mode 2			Mode 3		
Floor	MFTProg V2	StaadPro	ETABS	MFTProg V2	StaadPro	ETABS	MFTProg V2	StaadPro	ETABS
1	1	1	1	1	1	1	1	1	1
2	0.975	0.975	0.975	0.868	0.868	0.868	0.721	0.720	0.720
3	0.942	0.942	0.942	0.675	0.675	0.675	0.289	0.288	0.288
4	0.902	0.902	0.902	0.434	0.433	0.433	-0.204	-0.204	-0.204
5	0.855	0.855	0.855	0.162	0.162	0.162	-0.646	-0.645	-0.645
6	0.801	0.801	0.801	-0.119	-0.119	-0.119	-0.935	-0.934	-0.935
7	0.741	0.740	0.741	-0.388	-0.388	-0.388	-1.006	-1.005	-1.006
8	0.675	0.675	0.675	-0.624	-0.624	-0.624	-0.843	-0.842	-0.842
9	0.604	0.604	0.604	-0.809	-0.809	-0.809	-0.483	-0.483	-0.483
10	0.530	0.530	0.530	-0.929	-0.928	-0.928	-0.009	-0.009	-0.009
11	0.452	0.452	0.452	-0.974	-0.974	-0.974	0.470	0.470	0.470
12	0.372	0.372	0.372	-0.942	-0.942	-0.941	0.845	0.844	0.844
13	0.291	0.291	0.291	-0.835	-0.834	-0.834	1.028	1.028	1.028
14	0.210	0.210	0.210	-0.661	-0.660	-0.660	0.978	0.978	0.978
15	0.127	0.127	0.127	-0.426	-0.426	-0.426	0.695	0.695	0.695

The comparison between the first three mode shapes using MFTProgV2, StaadProV8i and ETABS packages shows almost identical modes shapes as shown in Table 6.9.

6.3.4 Response spectra Analysis for the 2D model

Response spectra analysis was performed for the 2D model. The excited response acceleration was taken from the UBC design code with assumed damping ratio of 5%. The considered modal combination methods used in this analysis were the SRSS and the CQC methods. Comparison of the modal masses participating ratios and their accumulations are shown in Tables 6.10 and 6.11. Comparisons of the lateral displacement at the top floor, the base shear and the base overturning moment for MFTProgV2 and the different packages are shown in Tables 6.14 to 6.17.

Table 6.10: Comparison of the modal masses participating ratios:

Mode	MFTProgV2	StaadProV8i(%Diff)	ETABS(%Diff)	SAP2000V16(%Diff)
1	83.603	83.603 (0)	83.604 (0)	83.559 (-0.05)
2	11.101	11.102 (0.01)	11.101 (0)	11.137 (0.32)
3	2.893	2.893 (0)	2.893 (0)	2.896 (0.1)
4	1.166	1.165 (-0.09)	1.166 (0)	1.168 (0.17)
5	0.55	0.549 (-0.18)	0.55 (0)	0.55 (0)
6	0.291	0.291 (0)	0.291 (0)	0.092 (-68.38)

Table 6.11: Comparison of the accumulated modal masses participating ratios:

Mode	MFTProgV2	StaadProV8i(%Diff)	ETABS(%Diff)	SAP2000V16(%Diff)
1	83.603	83.603 (0)	83.604 (0)	83.559 (-0.05)
2	94.704	94.705 (0)	94.704 (0)	94.696 (-0.01)
3	97.597	97.598 (0)	97.597 (0)	97.592 (-0.01)
4	98.763	98.763 (0)	98.762 (0)	98.759 (0)
5	99.312	99.312 (0)	99.312 (0)	99.309 (0)
6	99.603	99.603 (0)	99.603 (0)	99.401 (-0.2)

The comparisons between modal masses participating ratios using MFTProgV2, StaadProV8i and ETABS packages show almost identical results. Some difference between the results of SAP2000V16 and the other packages is noticed.

The response spectra acceleration obtained using the UBC curve was calculated and is shown in Table 6.12. The modal cross-correlation coefficients used in the CQC combination method were calculated and are shown in Table 6.13.

Table 6.12: MFTProgV2 Response acceleration using the UBC response spectra curve

Mode	Natural frequency Hz	Period (seconds)	Response Acceleration m/s^2
1	0.270	3.704	0.691
2	0.825	1.212	2.106
3	1.467	0.681	3.877
4	2.112	0.474	4.658
5	2.793	0.358	4.658
6	3.500	0.286	4.658

Table 6.13: Modal Cross-correlation Coefficients

Mode	1	2	3	4	5	6
1	1	0.0062	0.0020	0.0011	0.0007	0.0005
2	0.0062	1	0.0273	0.0094	0.0050	0.0032
3	0.0020	0.0273	1	0.0683	0.0217	0.0112
4	0.0011	0.0094	0.0683	1	0.1117	0.0358
5	0.0007	0.0050	0.0217	0.1117	1	0.1623
6	0.0005	0.0032	0.0112	0.0358	0.1623	1

I- Lateral Displacement at the top floor of the 2D building model

Tables 6.14 and 6.15, show the lateral displacement response at the top floor of the building model due to the UBC design code acceleration response curve, obtained by response spectra analysis in *x*-direction using MFTProgV2 method and the other packages.

Table 6.14: Comparison of the lateral displacement response at the top floor (m), Proposal 1

Response	MFTProgV2	StaadProV8i(%Diff)	ETABS(%Diff)	SAP2000V16(%Diff)
ALL SRSS	0.320198	0.320157 (-0.01)	0.320213 (0)	0.3202 (0)
ALL CQC	0.319952	0.320115 (0.05)	0.319967 (0)	0.31987 (-0.03)

Table 6.15: Comparison of the lateral displacement response at the top floor (m), Proposal 2

Response	MFTProgV2	StaadProV8i(%Diff)	ETABS (%Diff)	SAP2000V16(%Diff)
ALL SRSS	0.33953	0.320157 (-5.71)	0.320213 (-5.69)	0.3202 (-5.69)
ALL CQC	0.33989	0.320115 (-5.82)	0.319967 (-5.86)	0.31987 (-5.89)

Proposal 1 used the displacements responses calculated from the acceleration response ($S_d = S_a/\omega^2$), and the participation factor of the mode, while Proposal 2 used the displacement obtained from a full frame analysis using the equivalent static forces obtained from the acceleration responses.

According to Ghali et al. (2009), the equivalent static forces should be applied on the structure to calculate the displacements, internal forces, or reactions (as required) for the concerned mode (Proposal 2).

In Table 6.14, the lateral displacement results obtained by performing response spectrum analysis are presented for proposal 1. The table gives the total lateral displacement at the top floor of the building structures. For the SRSS, the closest result to the MFTProgV2 result is obtained from SAP2000V16 which is of 0.0006 % difference, and for the CQC, the closest results is obtained from ETABS which is of 0.0047 % difference.

And in Table 6.15, the lateral displacement results obtained by performing response spectrum analysis are presented for proposal 2. The table gives the total lateral displacement at the top floor of the building structures. For the SRSS, the closest result to MFTProgV2 result is obtained from ETABS and SAP2000V16 which is of -5.69 % difference, and for the CQC, the closest results is obtained from StaadProV8i which is of -5.82 % difference. MFTProgV2 proposal 1 gives closer results than proposal 2.

II- Resultant Shear Force at the Base of the 2D building model

Table 6.16, shows the resultant shear force response at the base of the building due to the UBC design code acceleration response curve, obtained by response spectra analysis in *x*-direction using MFTProgV2 and the other packages.

Table 6.16: Comparisons of the Response Spectrum Base Shear force:

Mode	MFTProgV2	StaadProV8i(%Diff)	ETABS(%Diff)	SAP2000V16(%Diff)
1	1122.43	1127.73 (0.47)	1127.26 (0.43)	-
2	455.32	456.18 (0.19)	455.93 (0.13)	-
3	211.09	218.78 (3.64)	218.71 (3.61)	-
4	105.89	105.85 (-0.04)	105.88 (-0.01)	-
5	49.93	49.91 (-0.04)	49.93 (0)	-
6	26.43	26.42 (-0.04)	26.43 (0)	-
ALL SRSS	1235.37	1241.83 (0.52)	1241.3 (0.48)	1240.624 (0.43)
ALL CQC	1243.25	1246.26 (0.24)	1249.31 (0.49)	1248.417 (0.42)

In Table 6.16, the base shear results obtained by performing response spectrum analysis are presented. The table gives the total shear forces at the base of the building structures. For the SRSS, the closest result to MFTProgV2 result is obtained from SAP2000V16 which is of 0.43 % difference, and for the CQC, the closest results is obtained from StaadProV8i which is of 0.24 % difference.

III- Resultant overturning moment at the Base of the 2D building model

Table 6.17, shows the resultant overturning moment response at the base of the building due to the UBC design code acceleration response curve, obtained by response spectra analysis in *x*-direction using MFTProgV2 and the other packages.

Table 6.17: Comparisons of the Response Spectrum Base Overturning Moment:

Mode	MFTProgV2	StaadProV8i(%Diff)	ETABS(%Diff)	SAP2000V16(%Diff)
1	40737.25	40748.97 (0.03)	40732.05 (-0.01)	-
2	-3390.03	-3390.4 (0.01)	-3389.47 (-0.02)	-
3	1205.56	1205.35 (-0.02)	1205.365 (-0.02)	-
4	-472.95	-472.99 (0.01)	-473.038 (0.02)	-
5	158.36	158.32 (-0.03)	158.449 (0.06)	-
6	-92.71	-92.76 (0.05)	-92.774 (0.07)	-
ALL SRSS	40898.98	40910.68 (0.03)	40893.75 (-0.01)	41047.3189 (0.36)
ALL CQC	40876.52	40888.2 (0.03)	40871.29 (-0.01)	41025.7514 (0.37)

In Table 6.17, the base overturning moment results obtained by performing response spectrum analysis are presented. The table gives the total overturning moment at the base of the building structures. For the SRSS, the closest results to MFTProgV2 is obtained from ETABS which is of -0.01 % difference, and for the CQC, the closest results is obtained from ETABS which is of -0.01 % difference.

For the base overturning moment in all packages, the CQC results are less than the SRSS results due to the effect of the reverse response, i.e. some responses in the different modes have different signs as shown in Table 6.17.

6.3.5 P-Delta response spectra analysis

The P-Delta second order analysis was incorporated in the dynamic analysis using the direct iteration method and the inverse iteration method (Stodola concept), and using the cubic-displacement shape. As for the linear dynamic analysis, the first six natural frequencies together with the corresponding mode shapes were computed.

Table 6.18: Comparisons of the first six P-Delta natural frequencies (cycle/second):

Mode	MFTProgV2	StaadProV8i(%Diff)	ETABS(%Diff)
1	0.255	0.255 (0)	0.255 (0)
2	0.791	0.791 (0)	0.791 (0)
3	1.415	1.416 (0.07)	1.415 (0)
4	2.043	2.044 (0.05)	2.043 (0)
5	2.710	2.710 (0)	2.709 (-0.04)
6	3.404	3.404 (0)	3.404 (0)

From Table 6.18, the comparison between the natural frequencies using the proposed method and the different analysis packages shows negligible differences and mostly identical results.

Table 6.19: Comparisons of percentage P-Delta modal Mass Participating ratios:

Mode	MFTProgV2	StaadProV8i(%Diff)	ETABS(%Diff)
1	84.332	84.330 (0)	84.329 (0)
2	10.752	10.770 (0.17)	10.773 (0.2)
3	2.725	2.710 (-0.55)	2.713 (-0.44)
4	1.064	1.070 (0.56)	1.069 (0.47)
5	0.499	0.500 (0.2)	0.498 (-0.2)
6	0.259	0.260 (0.39)	0.262 (1.16)

Table 6.20: Comparison of percentage accumulated P-Delta modal Mass Participating ratios:

Mode	MFTProgV2(%Diff)	StaadProV8i(%Diff)	ETABS(%Diff)
1	84.332	84.333 (0)	84.329 (0)
2	95.084	95.105 (0.02)	95.102 (0.02)
3	97.809	97.816 (0.01)	97.814 (0.01)
4	98.873	98.885 (0.01)	98.883 (0.01)
5	99.372	99.382 (0.01)	99.381 (0.01)
6	99.631	99.644 (0.01)	99.643 (0.01)

Comparisons of percentage modal Mass Participating ratios and their accumulations show good agreement between MFTProgV2 and the other packages, as can be seen from Tables 6.19 and 6.20.

I- Lateral Displacement at the top floor of the 2D building model

Tables 6.21 and 6.22, show the lateral displacement response at the top floor of the building model due to the UBC design code acceleration response curve, obtained by response spectra analysis in *x*-direction using MFTProgV2 and the other packages, for proposals 1 and 2 respectively.

Table 6.21: Comparison of the P-Delta lateral displacement response at the top floor (m), MFTProgV2 Proposal 1

Response	MFTProgV2	StaadProV8i(%Diff)	ETABS(%Diff)
ALL SRSS	0.335827	0.335779 (-0.01)	0.335823 (0)
ALL CQC	0.335586	0.335739 (0.05)	0.335581 (0)

Table 6.22: Comparison of the P-Delta lateral displacement response at the top floor (m), MFTProgV2 Proposal 2

Response	MFTProgV2	StaadProV8i(%Diff)	ETABS(%Diff)
ALL SRSS	0.35664	0.335779 (-5.85)	0.335823 (-5.84)
ALL CQC	0.35705	0.335739 (-5.97)	0.335581 (-6.01)

Proposal 1 used the displacements responses calculated from the acceleration response ($S_d = S_a/\omega^2$), and the participation factor of the mode, while Proposal 2 used the displacement obtained from a full frame analysis using the equivalent static forces obtained from the acceleration responses.

Table 6.21 gives the total lateral displacement at the top floor of the building structures, proposal 1. For the SRSS, the closest results to MFTProgV2 result is obtained from ETABS which is of -0.00119 % difference, and for the CQC, the closest results is obtained from ETABS which is of -0.00149 % difference. Table 6.22 gives the total lateral displacement at the top floor of the building structures, proposal 2. For the SRSS, the closest results to MFTProgV2 result is obtained from ETABS which is of -5.84 % difference, and for the CQC, the closest results is obtained from StaadProV8i which is of -5.97 % difference.

MFTProgV2 proposal 1 gives closer results to the different packages than proposal 2.

II- Resultant Shear Force at the Base of the 2D building model

Table 6.23, shows the resultant shear force response at the base of the building due to the UBC design code acceleration response curve, obtained by response spectra analysis in *x*-direction using MFTProgV2 and the other packages.

Table 6.23: Comparison of Response Spectrum P-Delta Base Shear Reactions (kN):

Mode	MFTProgV2	StaadProV8i(%Diff)	ETABS(%Diff)
1	1073.43	1073.86 (0.04)	1073.57 (0.01)
2	425.12	426.05 (0.22)	425.95 (0.2)
3	198.29	197.36 (-0.47)	197.39 (-0.45)
4	96.67	97.06 (0.4)	97.13 (0.48)
5	45.29	45.17 (-0.26)	45.22 (-0.15)
6	23.51	23.79 (1.19)	23.82 (1.32)
ALL SRSS	1176.54	1177.15 (0.05)	1176.86 (0.03)
ALL CQC	1183.59	1180.98 (-0.22)	1183.91 (0.03)

Table 6.23 gives the total shear forces at the base of the building structures. For the SRSS, the closest results to MFTProgV2 result is obtained from ETABS which is of 0.03 % difference, and for the CQC, the closest result is obtained from ETABS which is of 0.03 % difference.

III- Resultant overturning moment at the Base of the 2D building model

Table 6.24, shows the resultant overturning moment response at the base of the building due to the UBC design code acceleration response curve, obtained by response spectra analysis in *x*-direction using MFTProgV2 and the other packages.

Table 6.24: Comparison of Response Spectrum P-Delta Base overturning moment:

Mode	MFTProgV2	StaadProV8i(%Diff)	ETABS(%Diff)
1	38585.55	38600.94 (0.04)	38591.43 (0.02)
2	-3666.84	-3656.84 (-0.27)	-3654.23 (-0.34)
3	1166.4	1141.68 (-2.12)	1142.244 (-2.07)
4	-500.53	-494.63 (-1.18)	-494.515 (-1.2)
5	156.68	153.27 (-2.18)	153.502 (-2.03)
6	-99.1	-94.63 (-4.51)	-94.622 (-4.52)
ALL SRSS	38780.61	38794.14 (0.03)	38784.45 (0.01)
ALL CQC	38756.73	38770.4 (0.04)	38760.7 (0.01)

Table 6.24 gives the total overturning moment at the base of the building structures. For the SRSS, the closest result to the MFTProgV2 is obtained from ETABS which is of 0.01 % difference, and for the CQC, the closest results is obtained from ETABS which is of 0.01 % difference.

6.3.6 Time History Analysis for the 2D model

Time history analysis was performed for the 2D model. The natural frequencies and the corresponding mode shapes calculated in the previous section and used in the response spectra method were used together with the El Centro earthquake time history acceleration records assumed applied at the base of the building. The assumed damping ratio is 5%. Comparisons of the lateral displacement at the top floor level, the base shear and the base overturning moment for the proposed method and the different packages are shown in the following sections.

I- Lateral Displacement at the top floor of the 2D building model

Figures 6.13 to 6.16, give the graphs for the lateral displacement history at the top floor of the building model due to El Centro earthquake, obtained by time history analysis in *x*-direction using MFTProgV2 and the other packages. The minimum and the maximum responses are shown in Table 6.25.

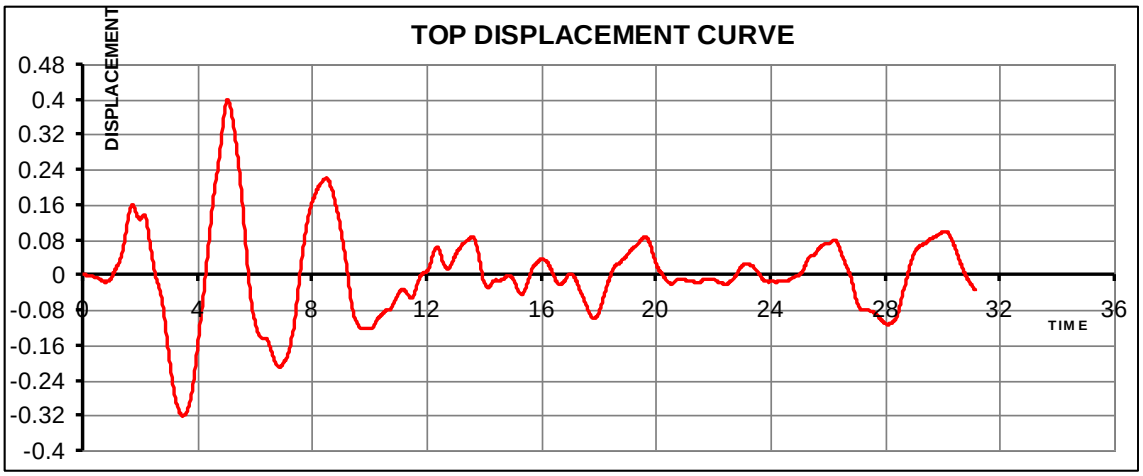

Figure 6.13: History of displacement in *x*-direction at the top floor level using MFTProgV2

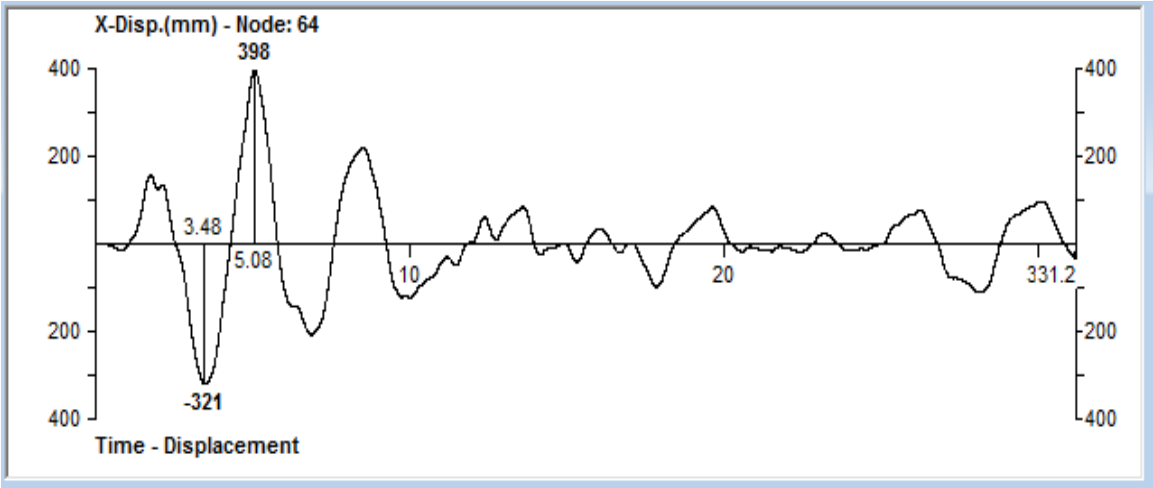

Figure 6.14: History of displacement in *x*-direction at the top floor level using the StaadPro2004

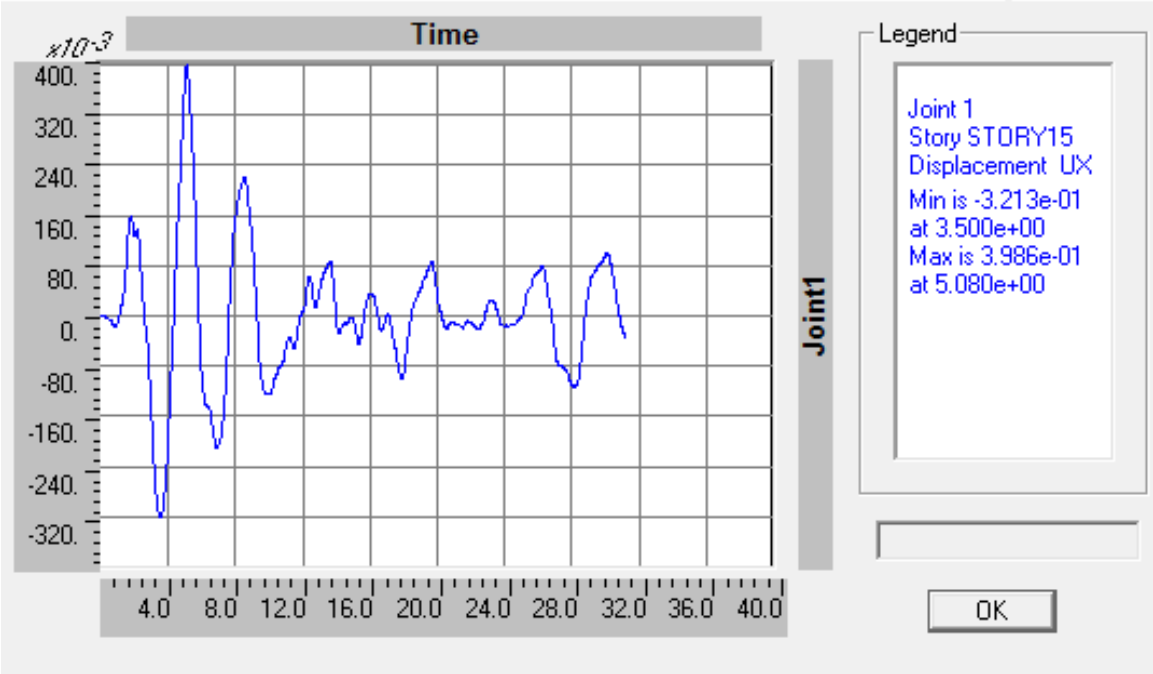

Figure 6.15: History of displacement in *x*-direction at the top floor level using ETABS

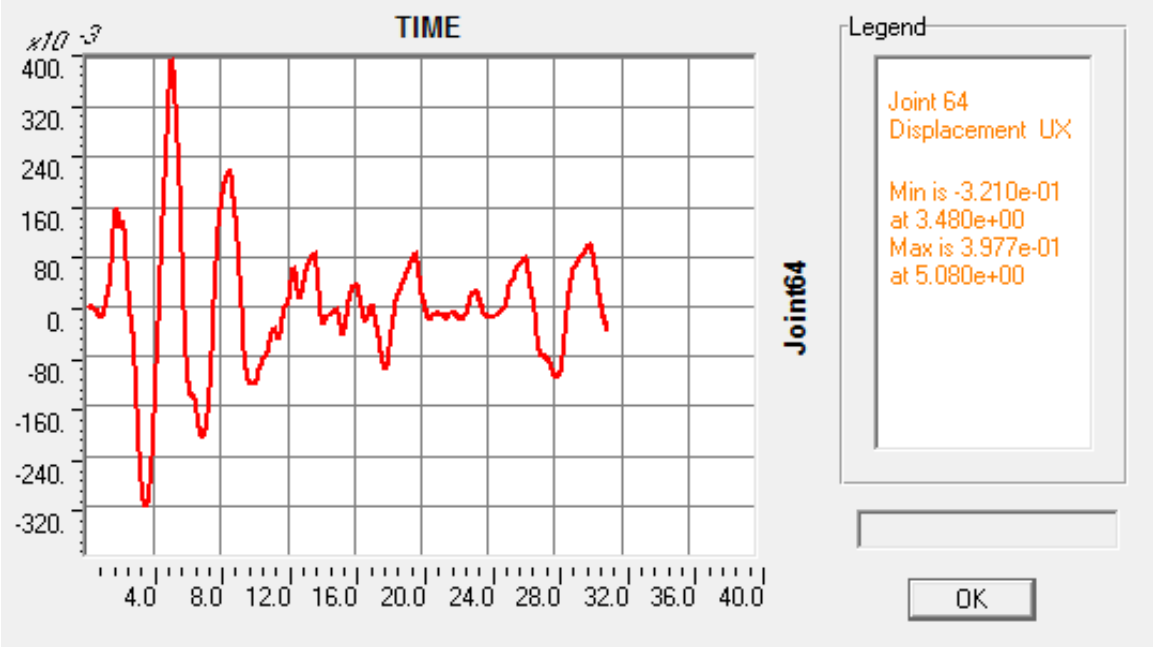

Figure 6.16: History of displacement in *x*-direction at the top floor level using SAP2000V16

Table 6.25: Minimum and maximum displacements at the top floor (mm):

Response	MFTProgV2	StaadProV8i(%Diff)	SAP2000V16(%Diff)	ETABS(%Diff)
Minimum	-321.26	-321 (-0.08)	-321 (-0.08)	-321.3 (0.01)
At time	3.5	3.49	4.8	3.5
Maximum	398.5	399 (0.13)	397.7 (-0.2)	398.6 (0.03)
At time	5.08	5.08	5.08	5.08

The diagrams shown in Figures 6.13 to 6.16 are similar and show very good agreement. Table 6.25 gives the maximum and minimum response values together with the corresponding time. For the minimum response, the closest result to MFTProgV2 is obtained from ETABS which is of 0.01 % difference, and for the maximum response, the closest result is obtained also from ETABS which is of 0.03 % difference.

II- Resultant Shear Force at the Base of the 2D building model

Figures 6.17 to 6.19 give the graphs for the resultant shear force history at the base of the building obtained by time history analysis in *x*-direction using MFTProgV2 and the other packages. The minimum and the maximum responses are shown in Table 6.26.

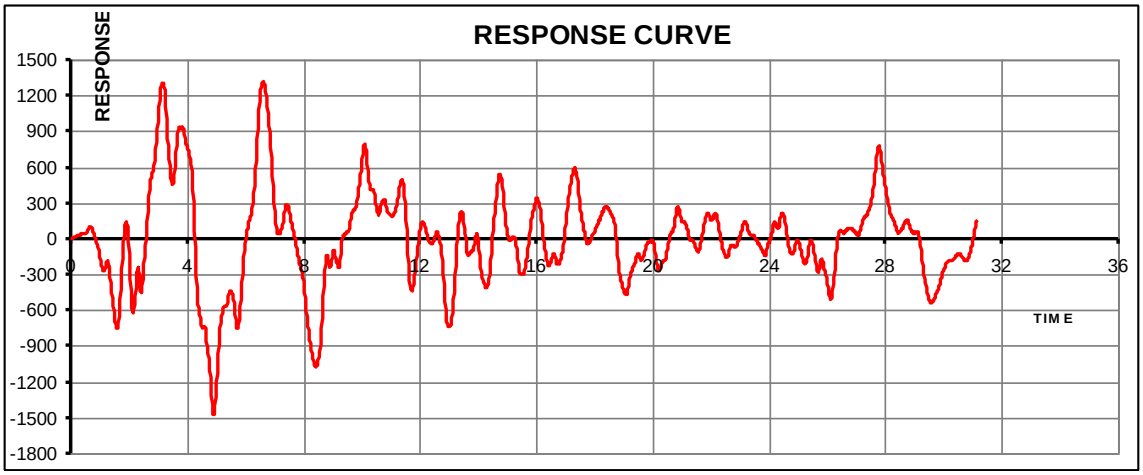

Figure 6.17: History of base Shear in *x*-direction using MFTProgV2

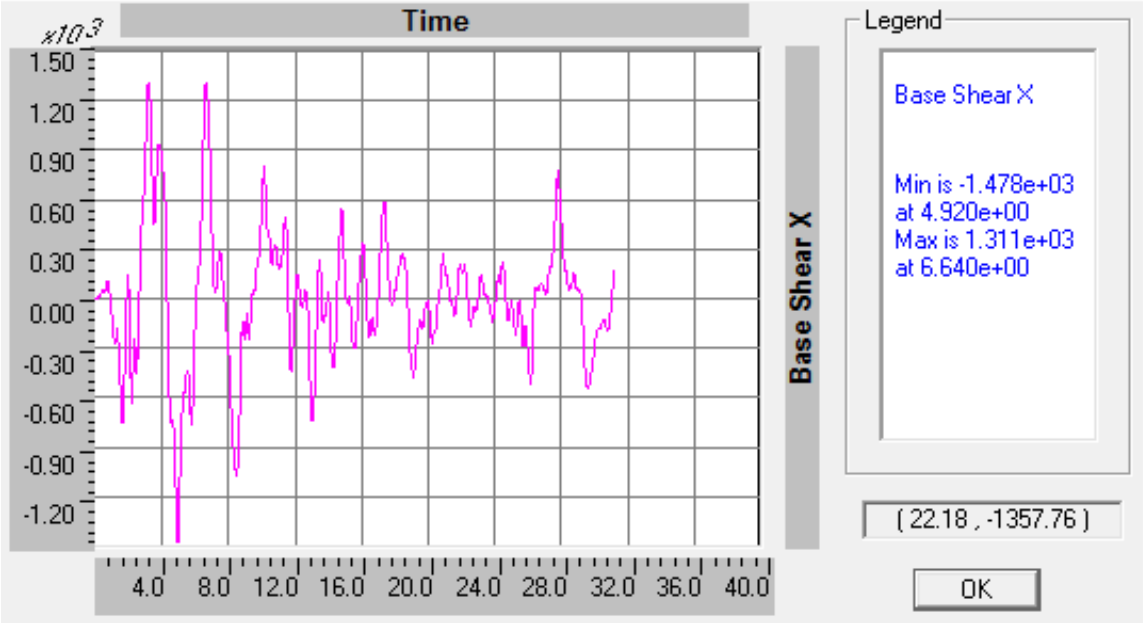

Figure 6.18: History of base Shear in *x*-direction using ETABS

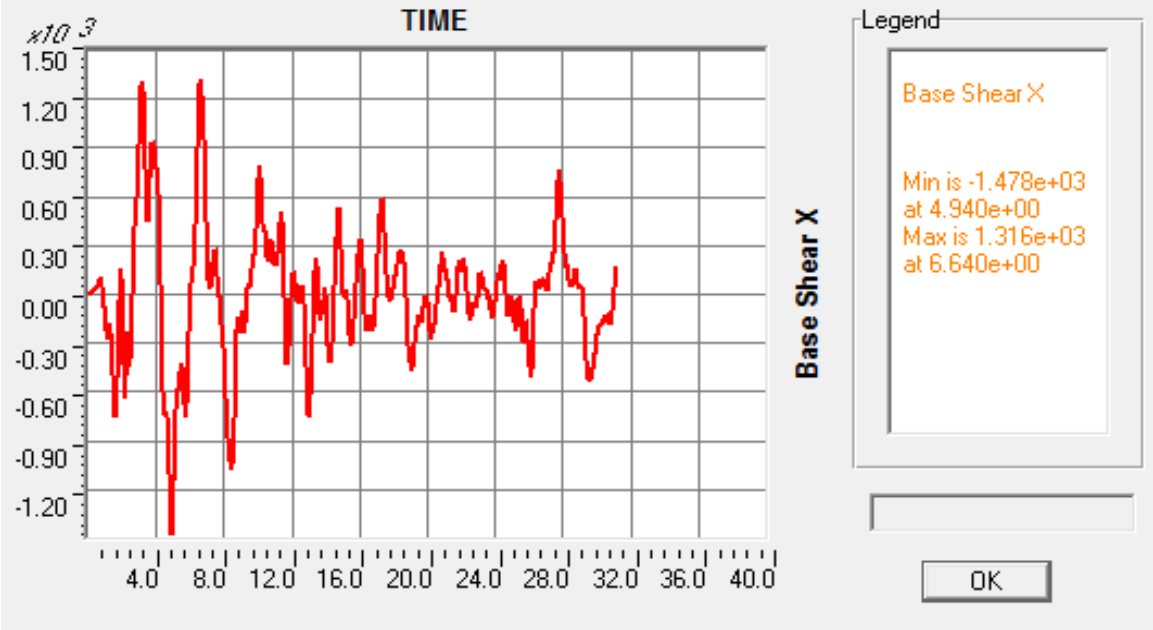

Figure 6.19: History of base Shear in *x*-direction using SAP2000V16

Table 6.26: Minimum and maximum base shear (kN):

Response	MFTProgV2	StaadProV8i(*)	SAP2000V16	ETABS
Minimum	-1477.73	-1481.713 (0.27)	-1478 (0.02)	-1478 (0.02)
At time	4.92	4.927778	4.94	4.92
Maximum	1310.39	N.A.	1316 (0.43)	1311 (0.05)
At time	6.64	N.A.	6.64	6.64

(*): Obtained from output results.

The diagrams in Figures 6.17 to 6.19 are similar and show very good agreement. Table 6.26 gives the maximum and minimum total shear forces at the base of the building structure with the corresponding time. For the minimum response, the closest results to MFTProgV2 result is obtained from ETABS and SAP2000V16 which is of 0.02 % difference, and for the maximum response, the closest result is obtained from ETABS which is of 0.05 % difference.

III- Resultant overturning moment at the Base of the 2D building model

Figures 6.20 to 6.22 give the graphs for the resultant overturning moment history at the base of the building obtained by time history analysis in *x*-direction using the proposed method and the other packages. The minimum and the maximum responses are shown in Table 6.27

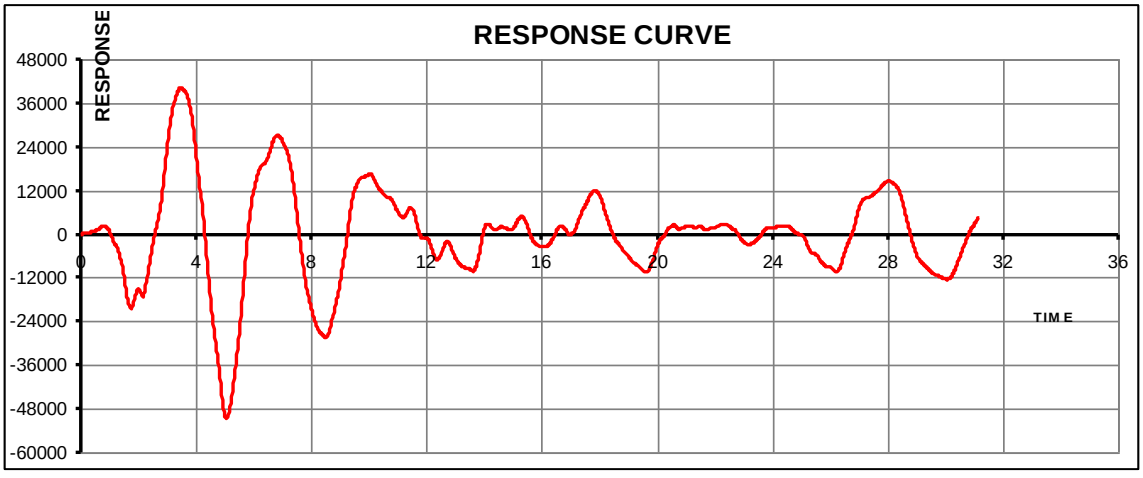

Figure 6.20: History of Base overturning moment about *y*-direction using MFTProgV2

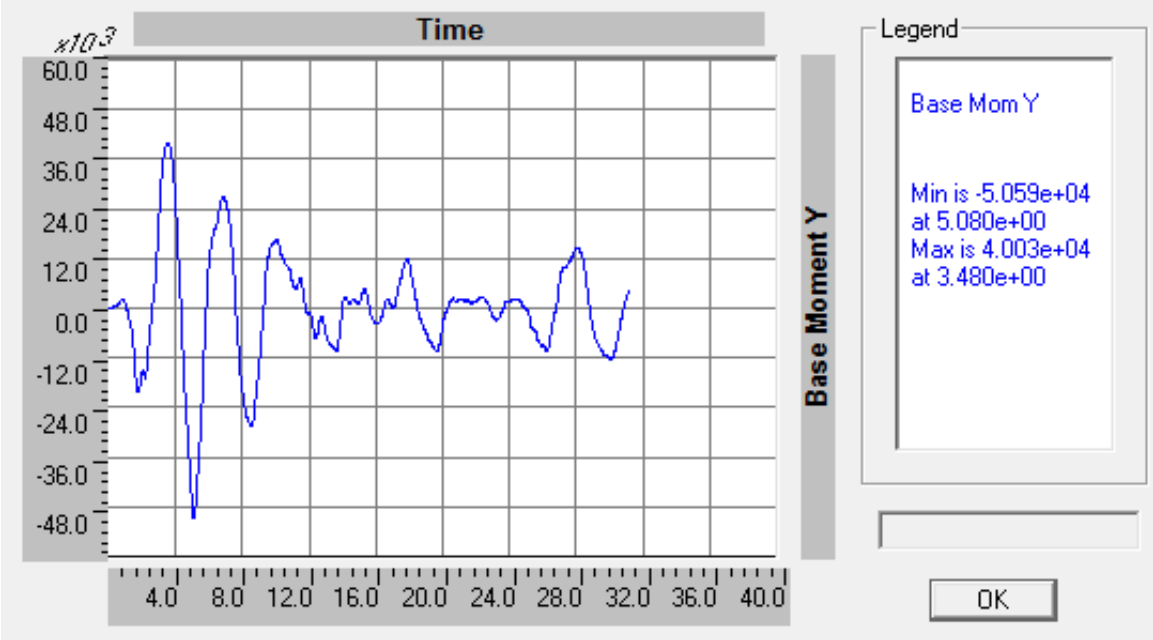

Figure 6.21: History of base overturning moment about *y*-direction using ETABS

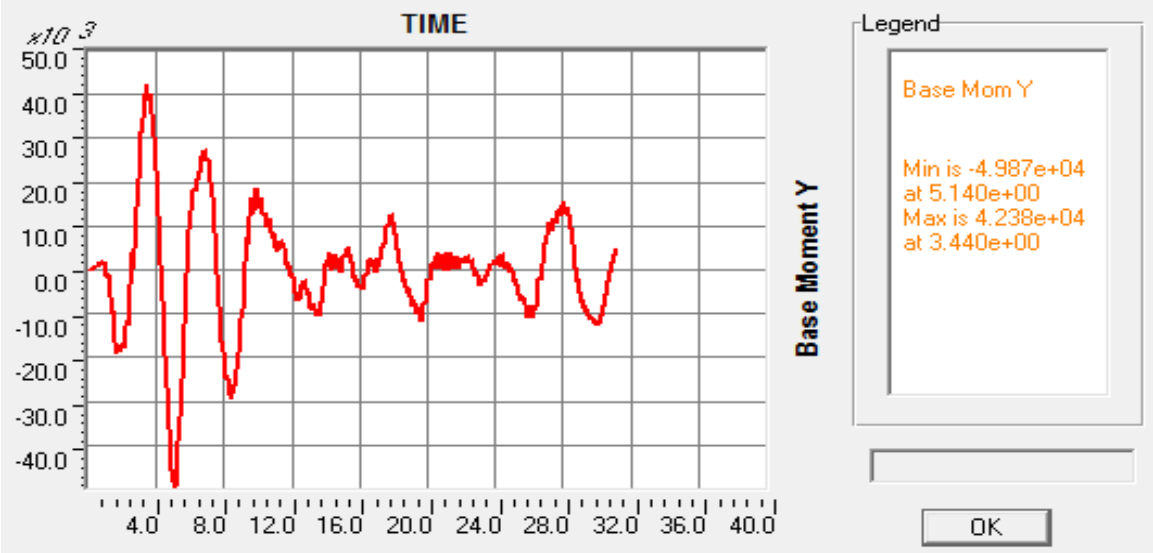

Figure 6.22: History of base overturning moment about *y*-direction using SAP2000V16

Table 6.27: Minimum and maximum base overturning moment (kN.m):

Response	MFTProgV2	ETABS(%Diff)	SAP2000V16(%Diff)
Minimum	-50587	-50590 (0.01)	-49870 (-1.42)
At time	5.08	5.08	5.14
Maximum	40026.94	40030 (0.01)	42380 (5.88)
At time	3.48	3.48	3.44

The diagrams in Figures 6.20 to 6.22 are similar and show very good agreement. Table 6.27 gives the maximum and minimum response values together with the corresponding time. For the minimum response, the closest result to MFTProgV2 result is obtained from ETABS which is of 0.01 % difference, and for the maximum response, the closest result is obtained from ETABS which is of 0.01 % difference.

6.3.7 P-Delta Time History Analysis

P-Delta second order time history analysis was incorporated in the dynamic time history analysis using the direct iteration method and the inverse iteration method (Stodola concept), and using the cubic-displacement shape. As for the linear dynamic analysis, the first six natural frequencies together with the corresponding mode shapes were computed and used in the analysis.

I- Lateral Displacement at the top floor of the 2D building model

Figures 6.23 to 6.25 give the graphs for the lateral displacement at the top floor of the building model obtained by time history analysis in *x*-direction using the proposed method and the other packages. The minimum and the maximum responses are shown in Table 6.28.

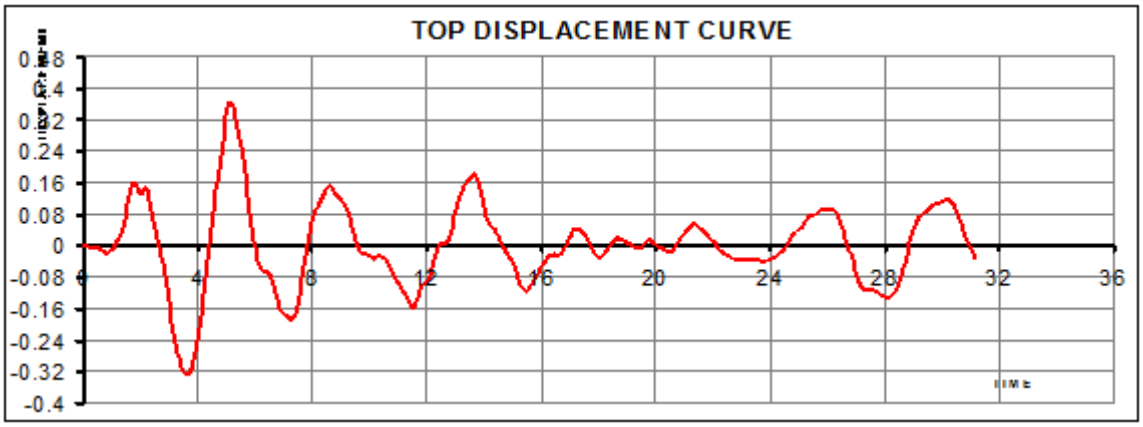

Figure 6.23: History of P-Delta displacement in x-dir. at the top level using MFTProgV2

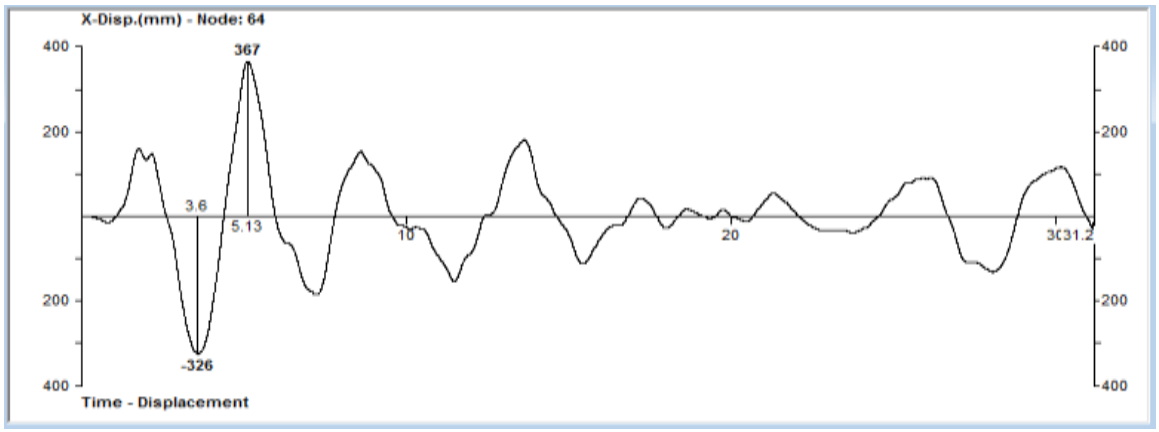

Figure 6.24: History of P-Delta displacement in *x*-direction at the top floor level using StaadProV8i

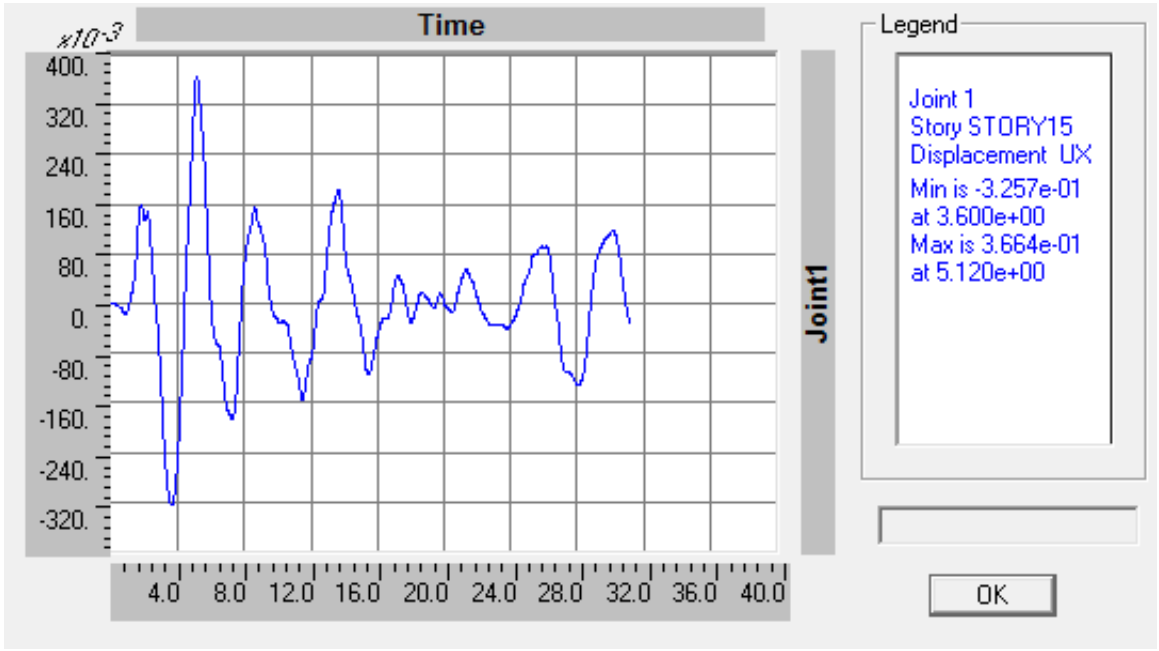

Figure 6.25: History of P-Delta displacement in *x*-direction at the top floor level using ETABS

Table 6.28: Minimum and maximum P-Delta displacements at the top floor (mm):

Response	MFTProgV2	StaadProV8i(%Diff)	ETABS(%Diff)
Minimum	-325.6	-326 (0.12)	-325.7 (0.03)
At time	3.6	3.6	3.6
Maximum	366.272	366 (-0.07)	366.4 (0.03)
At time	5.12	5.13	5.12

The diagrams in Figures 6.23 to 6.25 are similar and show very good agreement. Table 6.28 gives the maximum and minimum response values together with the corresponding time. For the minimum response, the closest result to MFTProgV2 result is obtained from ETABS which is of 0.03 % difference, and for the maximum response, the closest result is obtained from ETABS which is of 0.03 % difference.

II- Resultant Shear Force at the Base of the 2D building model

Figures 6.26 and 6.27 give the graphs for the resultant shear force history at the base of the building obtained by time history analysis in *x*-direction using MFTProgV2 and the other packages. The minimum and the maximum responses are shown in Table 6.29.

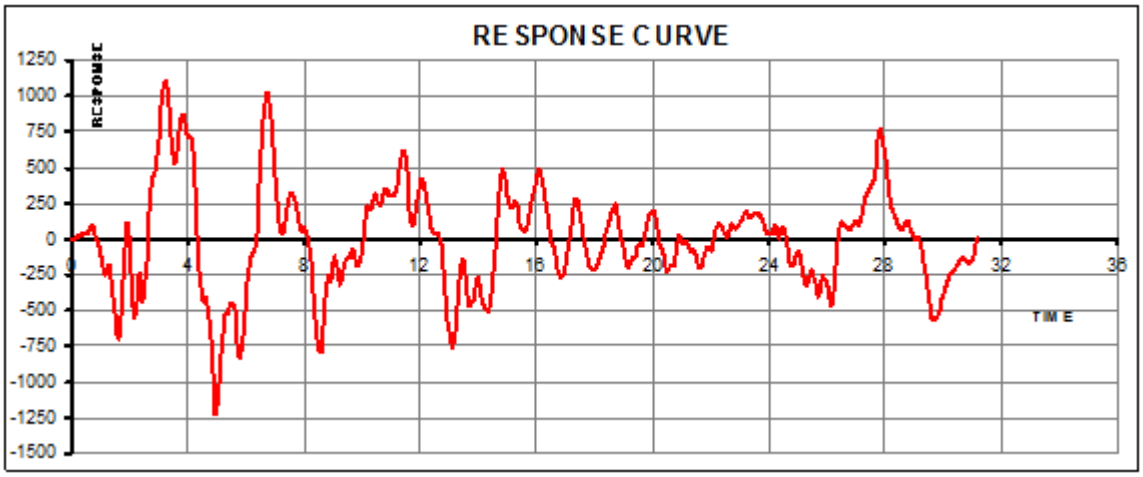

Figure 6.26: History of P-Delta base Shear in *x*-direction using MFTProgV2

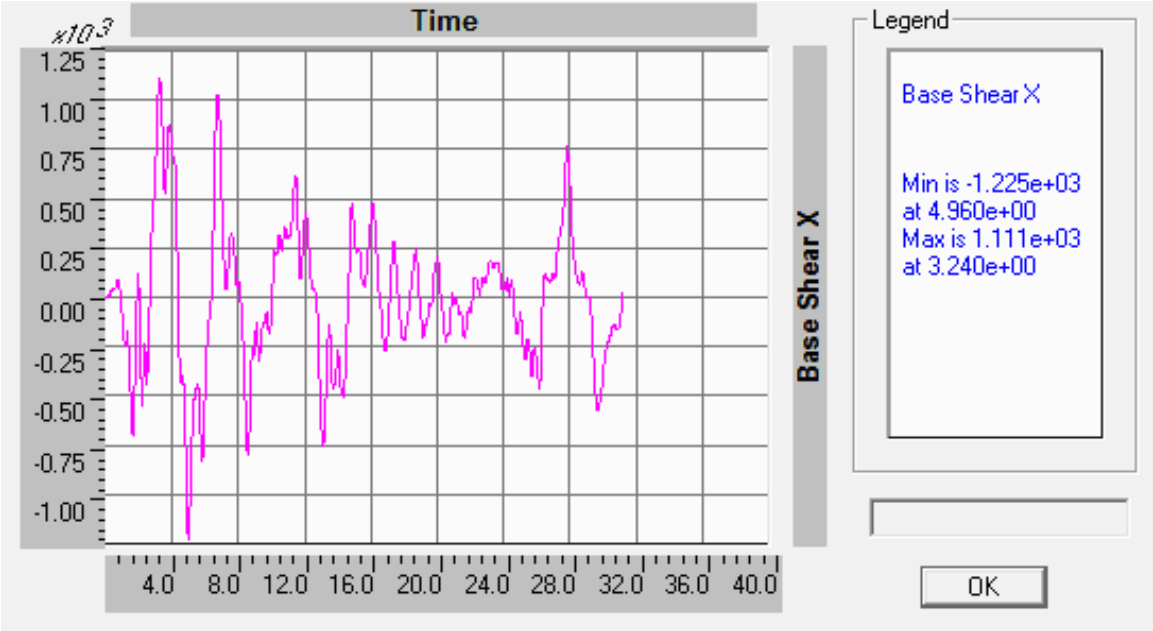

Figure 6.27: History of P-Delta base Shear in *x*-direction using ETABS

Table 6.29: Minimum and maximum P-Delta Base Shear (kN):

Response	MFTProgV2	StaadProV8i(%Diff)	ETABS(%Diff)
Minimum	-1223.9	-1215.244 (-0.71)	-1225 (0.09)
At time	4.96	4.945834	4.96
Maximum	1110.844	N.A.	1111 (0.01)
At time	3.24	N.A.	3.24

The diagrams in Figures 6.26 and 6.27 are similar and show very good agreement. Table 6.29 gives the maximum and minimum total shear forces at the base of the building structure with the corresponding time. For the minimum response, the closest result to MFTProgV2 is obtained from ETABS which is of 0.09 % difference, and for the maximum response, the closest result is obtained from ETABS which is of 0.01 % difference.

III- Resultant overturning moment at the Base of the 2D building model

Figures 6.28 and 6.29 give the graphs for the resultant overturning moment history at the base of the building obtained by time history analysis in *x*-direction using MFTProgV2 and the other packages. The minimum and the maximum responses are shown in Table 6.30.

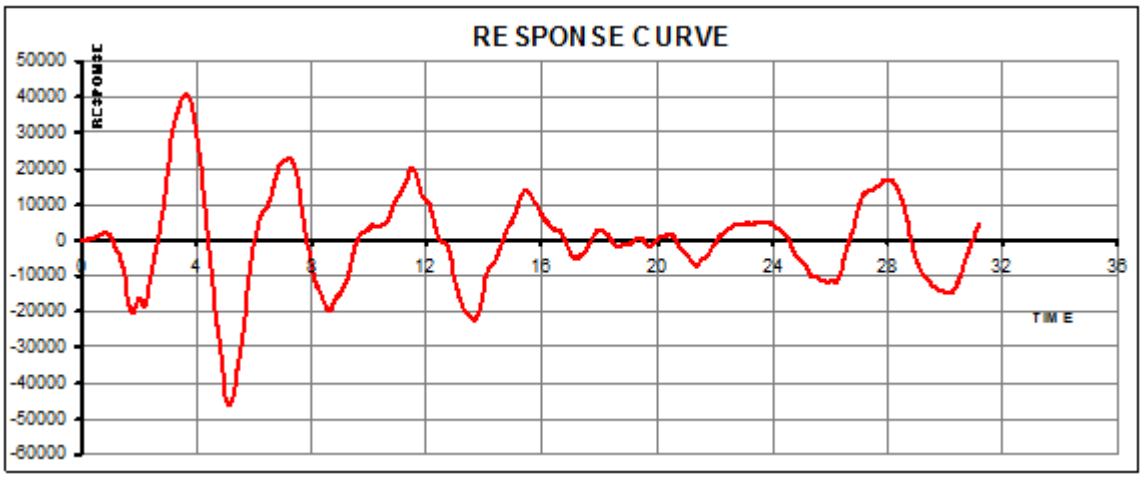

Figure 6.28: History of P-Delta base overturning moment about *y*-direction using MFTProgV2

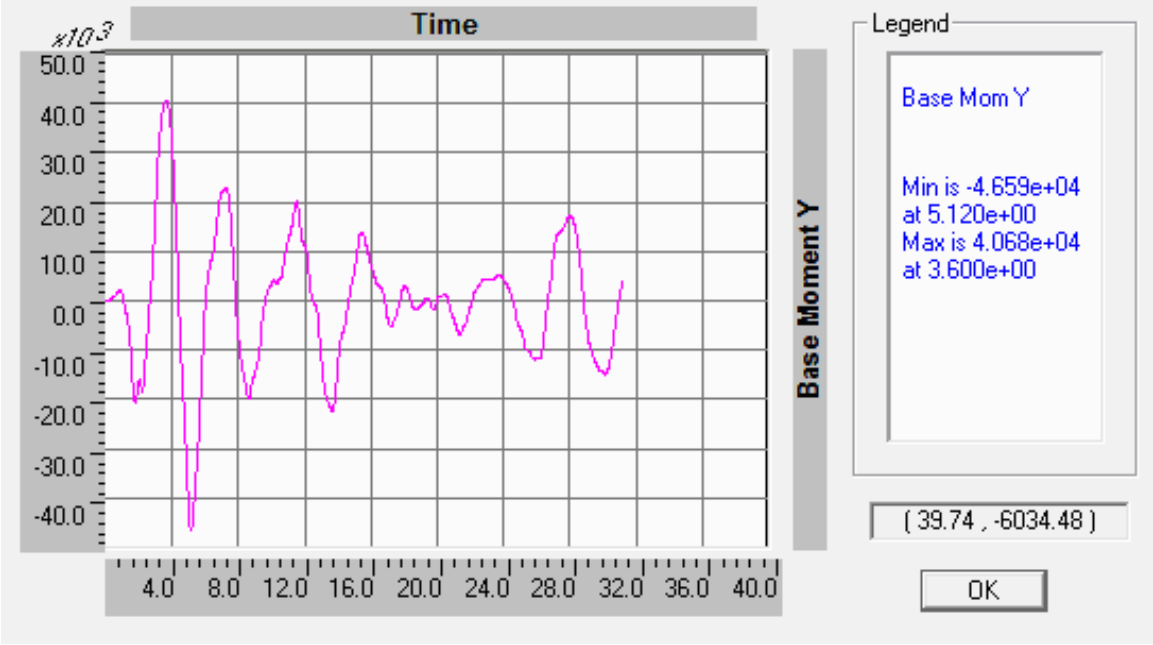

Figure 6.29: History of P-Delta base overturning moment about *y*-direction using ETABS

Table 6.30: Minimum and maximum P-Delta base overturning moment (kN.m):

Response	MFTProgV2	StaadProV8i(%Diff)	ETABS(%Diff)
Minimum	-46412.4	N.A.	-46590 (0.38)
At time	5.12	N.A.	5.12
Maximum	40579.84	N.A.	40680 (0.25)
At time	3.6	N.A.	3.6

The diagrams in Figures 6.28 and 6.29 are similar and show very good agreement. Table 6.30 gives the maximum and minimum response values together with the corresponding time. For the minimum response, the closest result to MFTProgV2 result is obtained from ETABS which is of 0.38 % difference, and for the maximum response, the closest result is obtained from ETABS which is of 0.25 % difference.

6.4 The twenty five floors 3D building Model

The building plan area, shown in Figure 6.30 is: 24 m x 12 m. The floor slab is of thickness = 0.2 m. The building is composed of 25 floors of floor height = 3.5 m for all floors except the lower floor which is of height = 5.5 m.

All building members are concrete of elasticity, E = $29x10^6$ kN/m^2,

and Poisson's ratio, v = 0.2

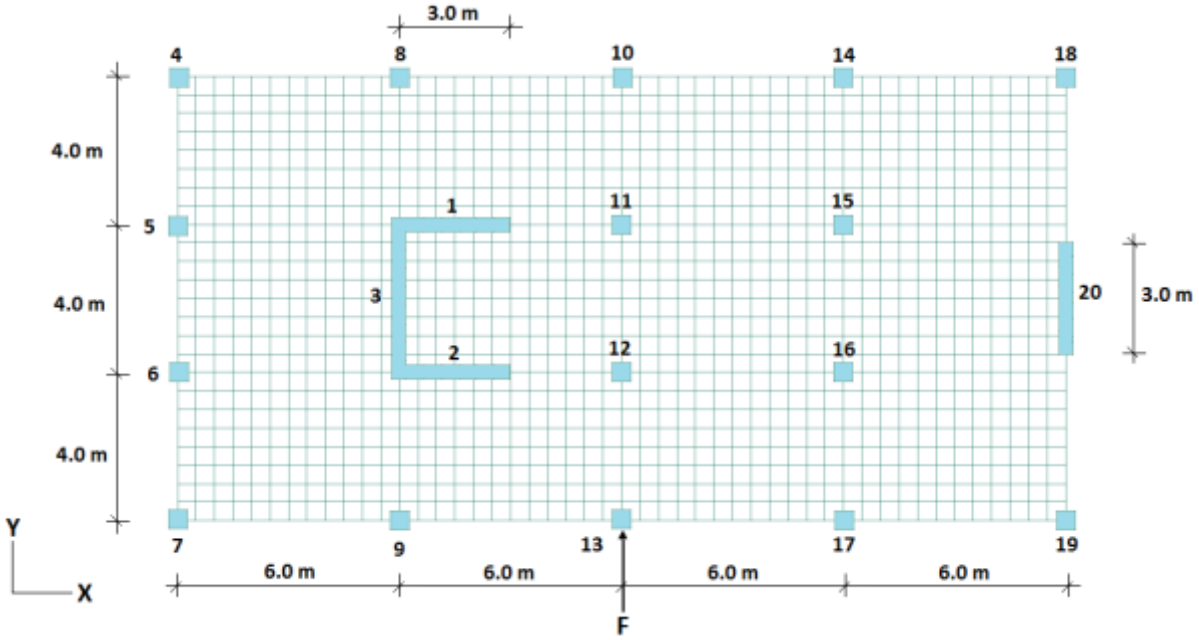

Figure 6.30: 24 m x 12 m floor plan for 25 Storey Building

The section properties of the vertical elements (in meters) are:

All Columns: 0.60 m x 0.60 m for the 10 lower floors, 0.50 m x 0.50 m for the 10 middle floors, and 0.40 m x 0.40 m for the 5 upper floors

The Shear walls are of lengths 3.0 m (walls 1, 2 and 20), and 4.0 m (wall 3), and thicknesses are: 0.30 m for the 10 lower floors and 0.25 m for the 15 upper floors.

The building is subjected to vertical area load of 18 kN/m^2 at all floors, and to lateral loads (F, in *Y*-direction and in the location shown in Figure 6.30, at column 13), of 151.2 kN at the lower floor level, and 117.6 kN at all other floors levels.

The slab was modeled by finite plate elements presented by Ghali and Neville (1978), of meshes size 0.5 m x 0.5 m. The columns and walls were modeled by frame members. The

edge shear wall and the U-shaped core were connected at the floor levels with torsion released rigid beams represent the rigid parts of the walls, Akis (2004).

6.4.1 Static Linear and second order Analysis of the 3D building model

Linear and second-order (P-Delta) analyses were carried out, and comparisons of the obtained results with exact results from different packages, ETABS and StaadPro2004, based on FEM, are shown in Tables 6.31 to 6.33 and Figures 6.31 to 6.41.

Analysis using ETABS, were performed for two options. The first option was based on thin-plate (Kirchhoff) formulation, which neglects the transverse shearing deformations, and the second option used thick-plate (Mindline/Reissner) formulation which includes the effects of transverse shearing deformations, (CSI Analysis Reference Manual).

Comparison of displacements in *Y*-direction and the twist rotation of the floors at the building center (Column 10), obtained using MFTProg and the different packages is shown in Table 6.31 and Figures 6.31 to 6.33. Comparisons of the bending moments and shear forces of the U-shaped core (assembly of walls 1, 2 and 3) and the edge shear wall (wall 20) are shown in Tables 6.32 and 6.33, and Figures 6.34 and 6.41.

Comparisons of the moment My contour in the bottom floor using MFTProg and StaadPro2014 for both linear and second order P-Delta analyses are also plotted in Figures 6.42 to 6.45.

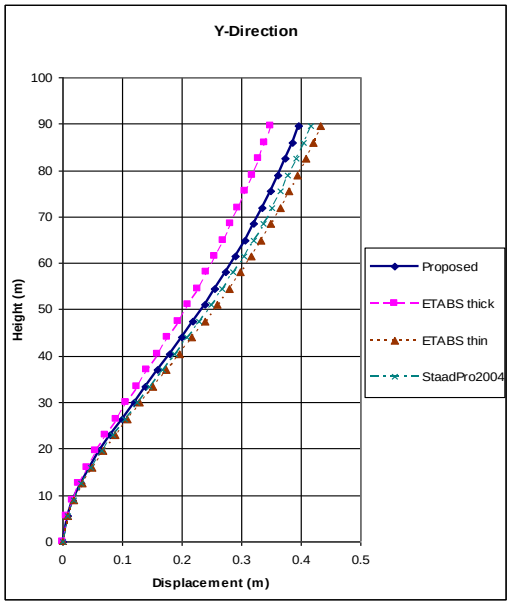

Figure 6.31: P-Delta Analysis, Displacements in *y*-direction

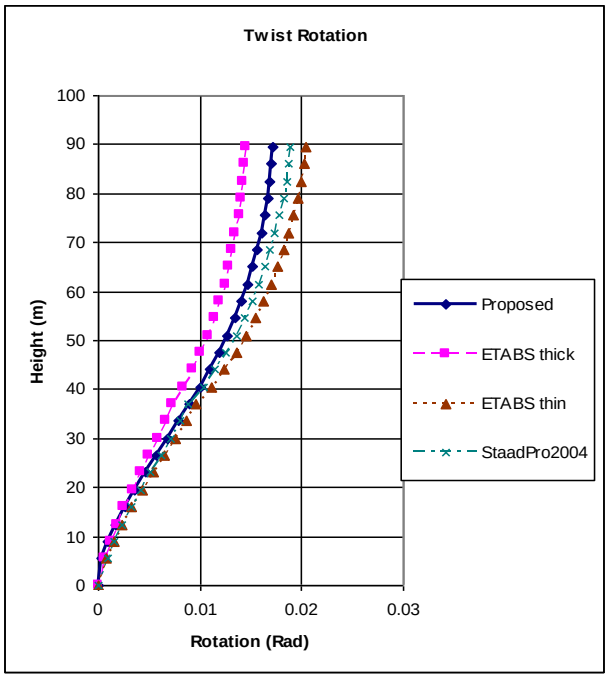

Figure 6.32: P-Delta Analysis, Rotations in radians

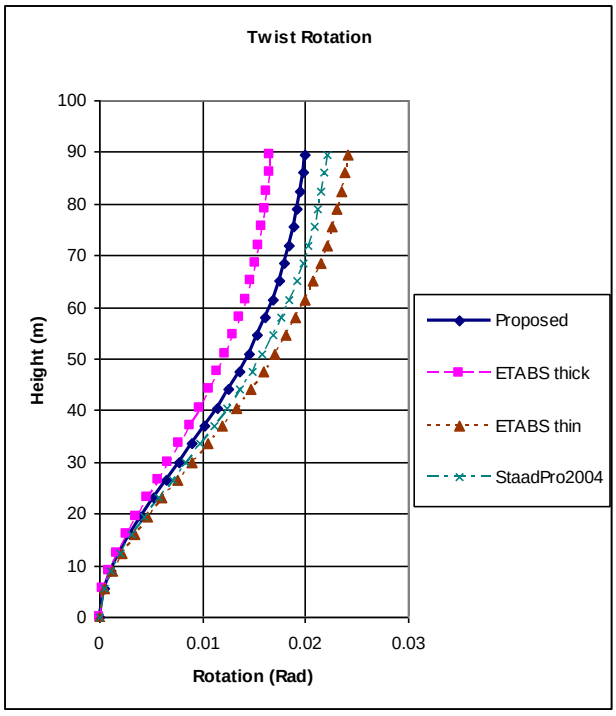

Figure 6.33: P-Delta Analysis, Rotations in radians (torsion released)

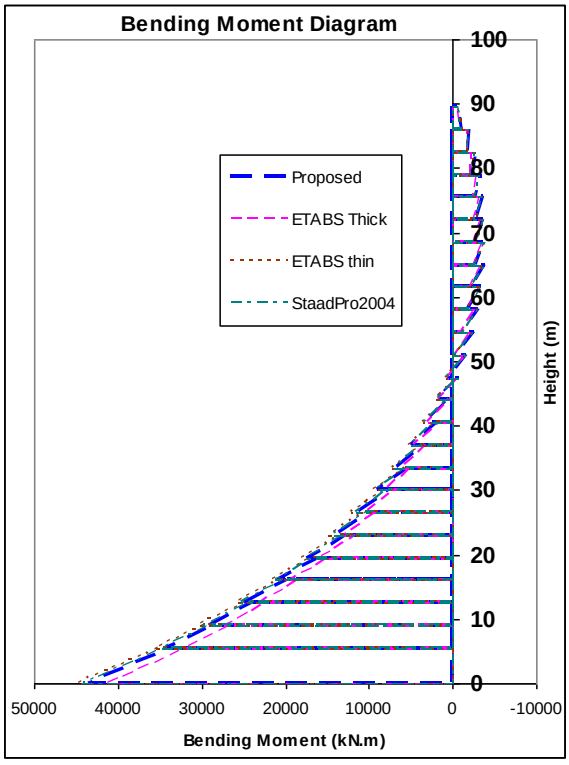

Figure 6.34: Linear Analysis, B.M.D. for U-Shaped Core

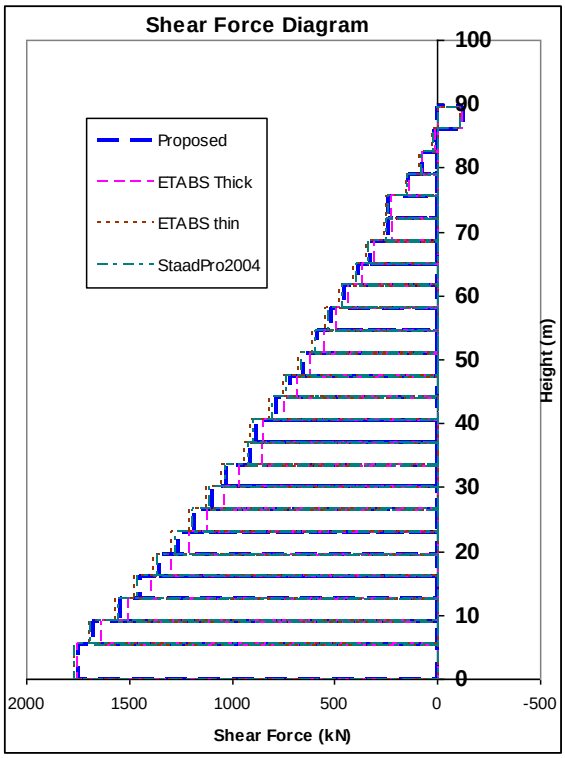

Figure 6.35: Linear Analysis, S.F.D. for U-Shaped Core

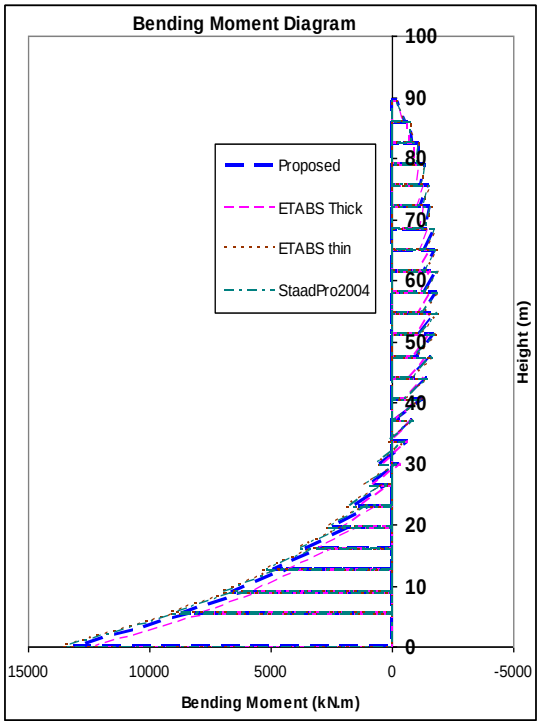

Figure 6.36: Linear Analysis, B.M.D. for edge shear wall

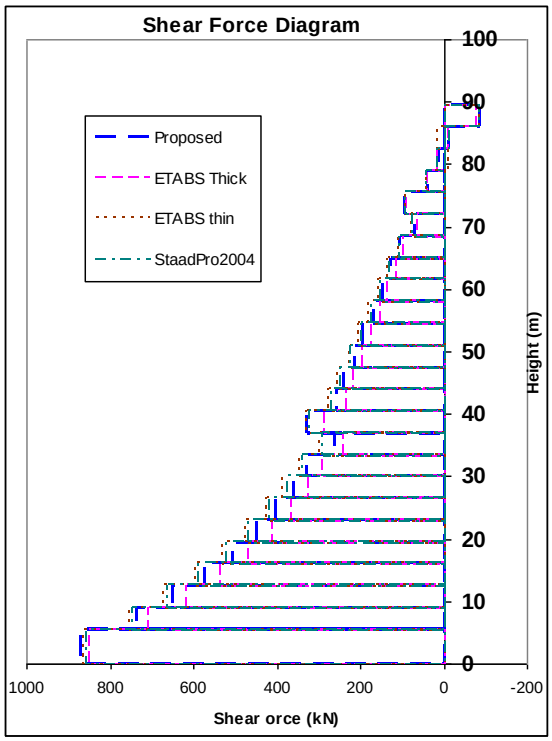

Figure 6.37: Linear Analysis, S.F.D. for edge shear wall

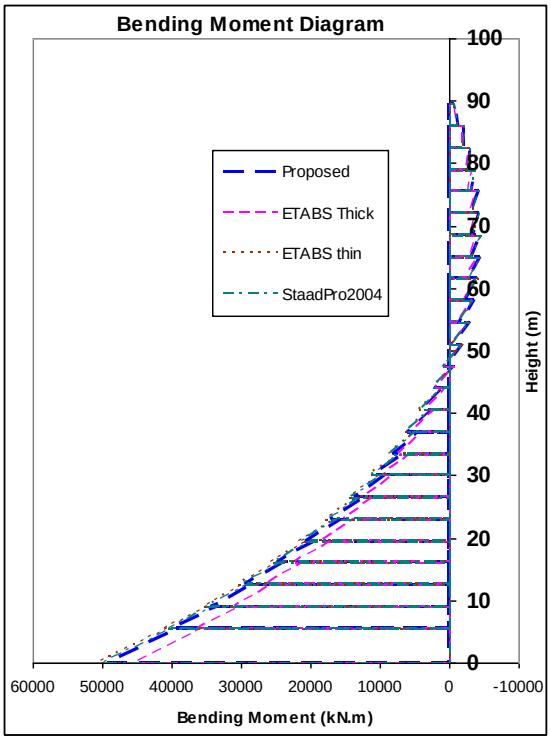

Figure 6.38: P-Delta Analysis, B.M.D. for U-Shaped Core

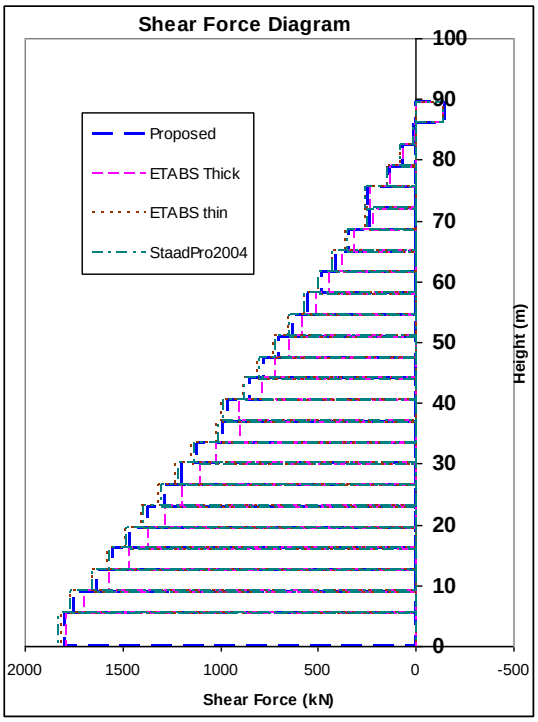

Figure 6.39: P-Delta Analysis, S.F.D. for U-Shaped Core

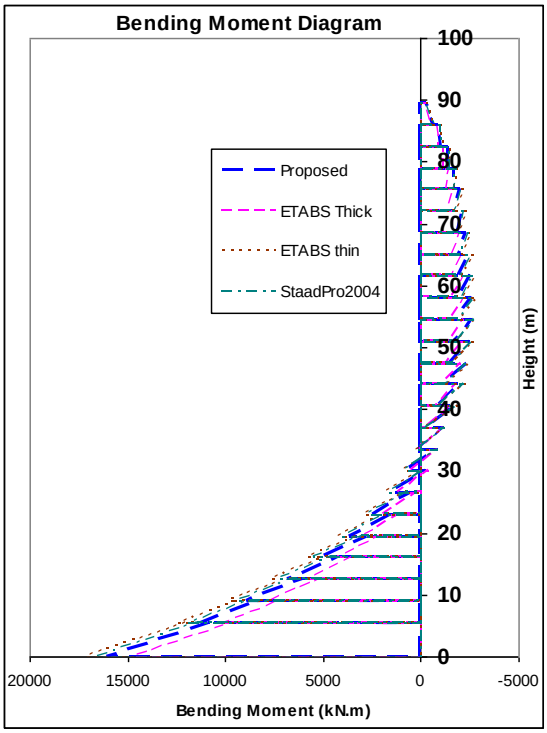

Figure 6.40: P-Delta Analysis, B.M.D. for edge shear wall

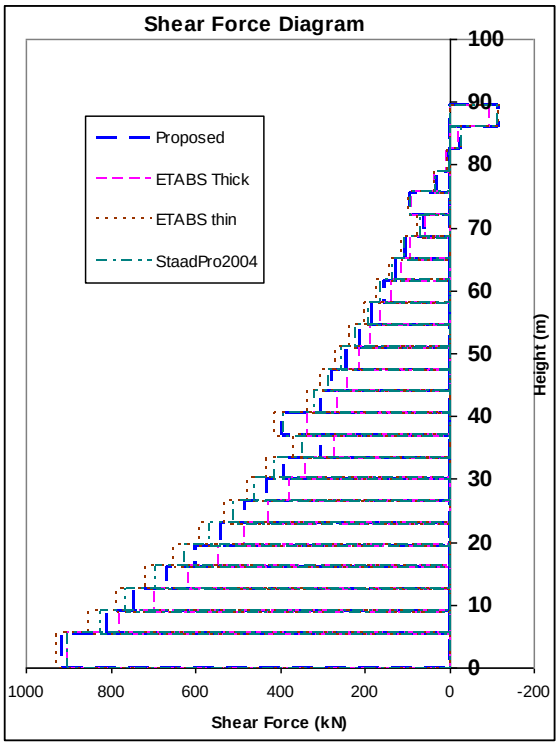

Figure 6.41: P-Delta Analysis, S.F.D. for edge shear wall

Table 6.31: Displacements and rotation in the top floor level (mm, rad), (3D Frame):

Package	Linear			Second order (P-Delta)		
Trans. & Rot.	Y-Dir	Axial	Twist	Y-Dir	Axial	Twist
MFTProg	319.60	36.21	0.0120	396.36	37.73	0.0172
StaadPro2004	331.20	36.04	0.0130	415.61	37.60	0.0189
%Diff.	-3.50	0.47	-7.69	-4.63	0.35	-8.99

Table 6.32: Maximum bending moment in U-Shaped Core (kN.m), (3D Frame):

Package	Linear	Second order
MFTProg	43505.86	49183.91
StaadPro2004	44108.82	50071.03
%Diff.	-1.37	-1.77

Table 6.33: Maximum bending moment in Edge Shear Wall (kN.m), (3D Frame):

Package	Linear	Second order
MFTProg	13130.94	15985.60
StaadPro2004	13431.23	16541.75
%Diff.	-2.24	-3.36

In all the comparisons of the displacements and the bending moments, for both linear and second order analysis, the differences are found to be very small.

The differences in the models displacements are proportional to the building height. ETABS (thick-plate) model has more rigid floor and less displacements and twist rotations than the other exact models, Figures 6.31 and 6.32. The assumption of the rigid diaphragm in MFTProg is further resisting and reducing the twist rotations in the lower levels of the building compared with StaadPro2004 and ETABS (thin-plate) models, Figure 6.32. This is due to the fact that, the torsion stiffness of the vertical members in the lower levels are very large compared with that in the upper levels, and the twist rotations in the vertical members are constrained to follow the rigid diaphragms twist rotations. This effect may be illustrated by comparing the results of the models with all the vertical members released for torsion, Figure 6.33. In this case the differences in the models twist rotations are almost proportional to the building height.

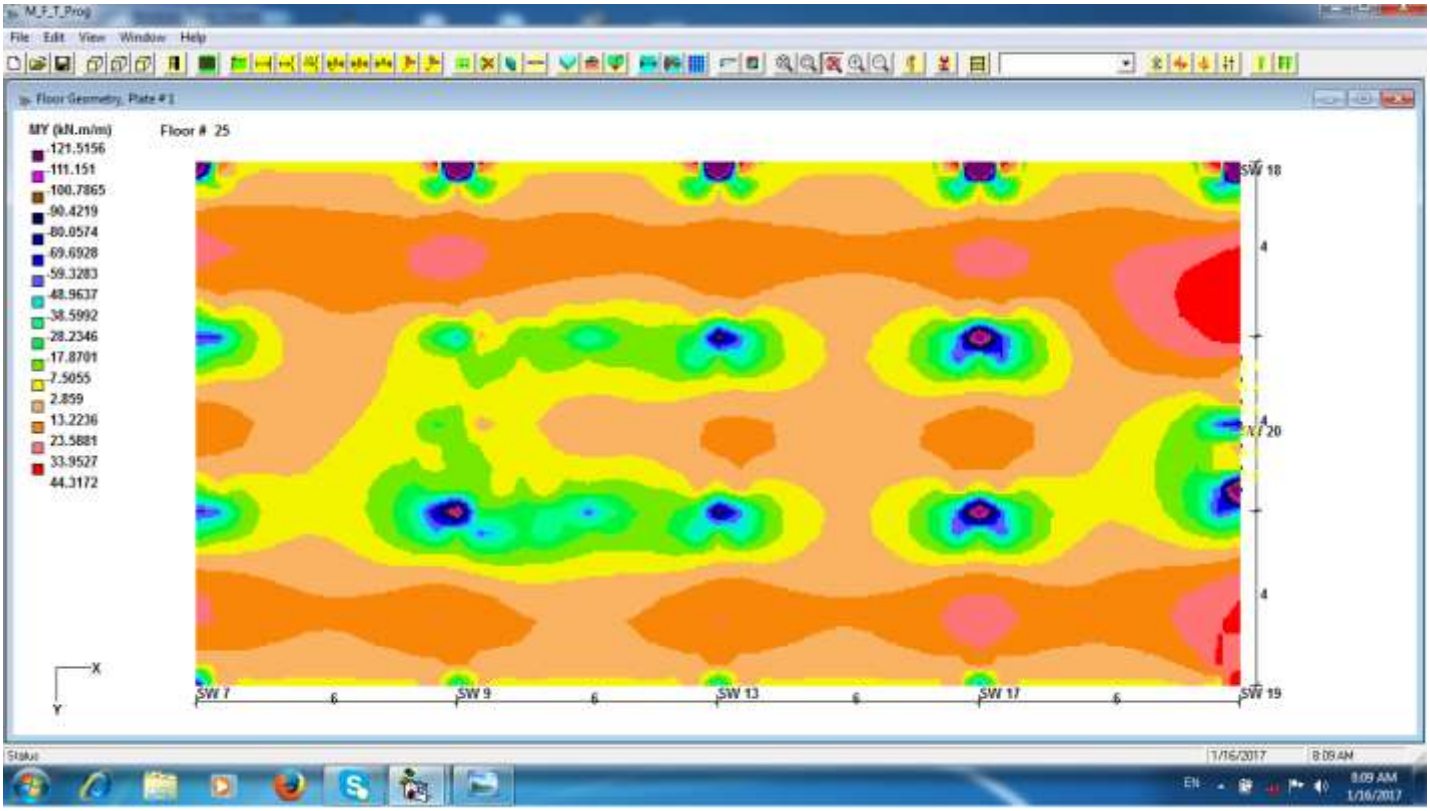

Figure 6.42: MFTProg moment M_y contour in kN.m/m for bottom floor slab

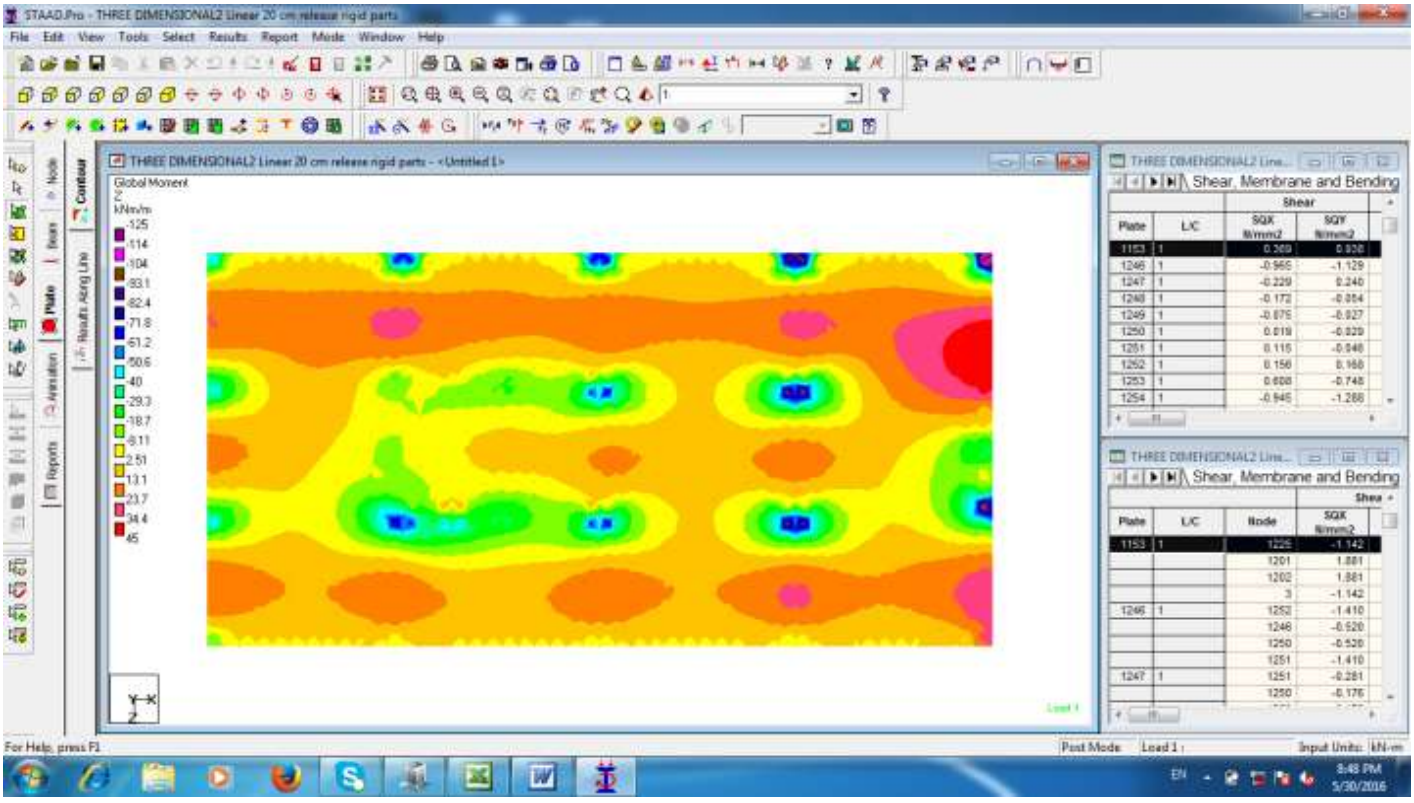

Figure 6.43: StaadPro moment M_y contour in kN.m/m for bottom floor slab

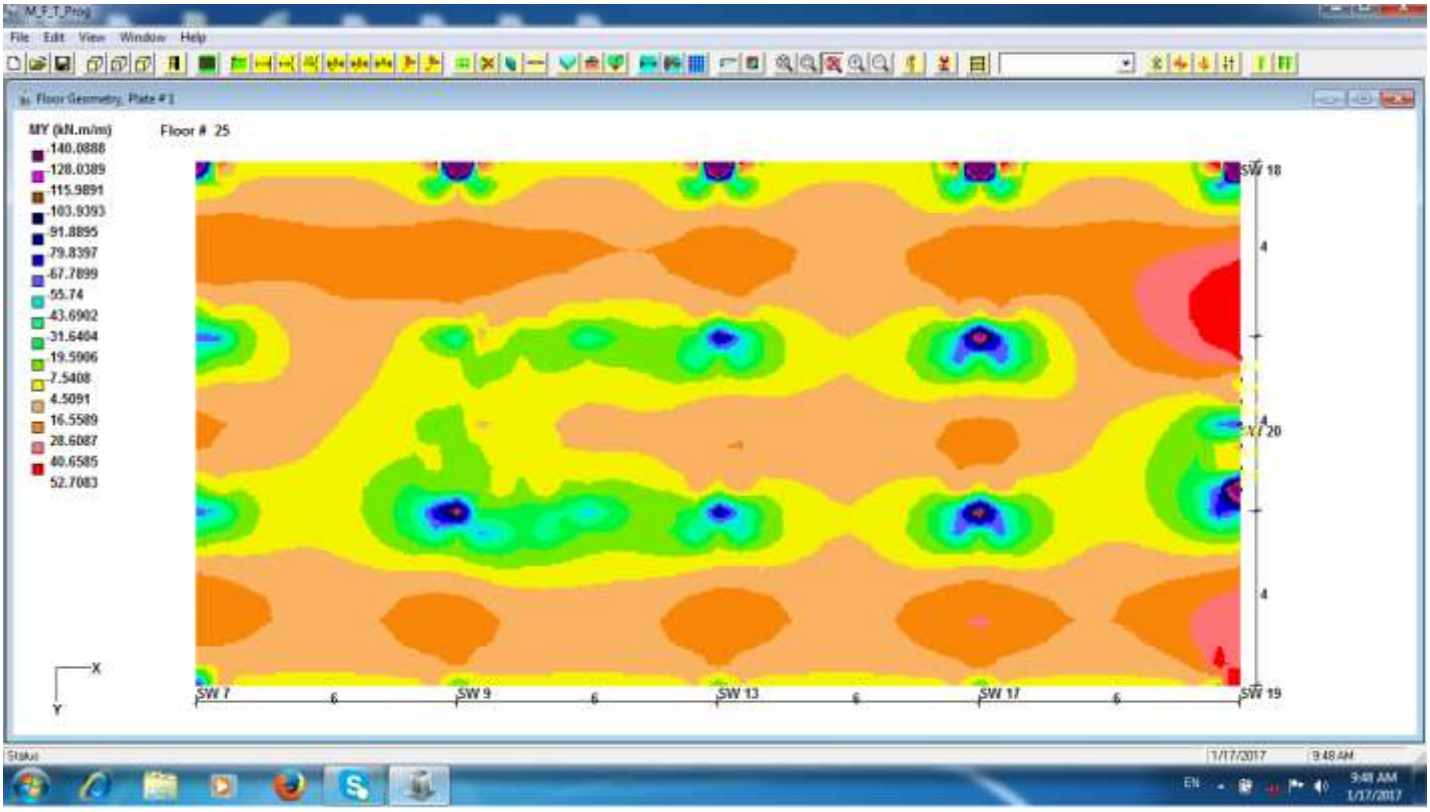

Figure 6.44: MFTProg P-Delta analysis moment M_y contour in kN.m/m for bottom floor slab

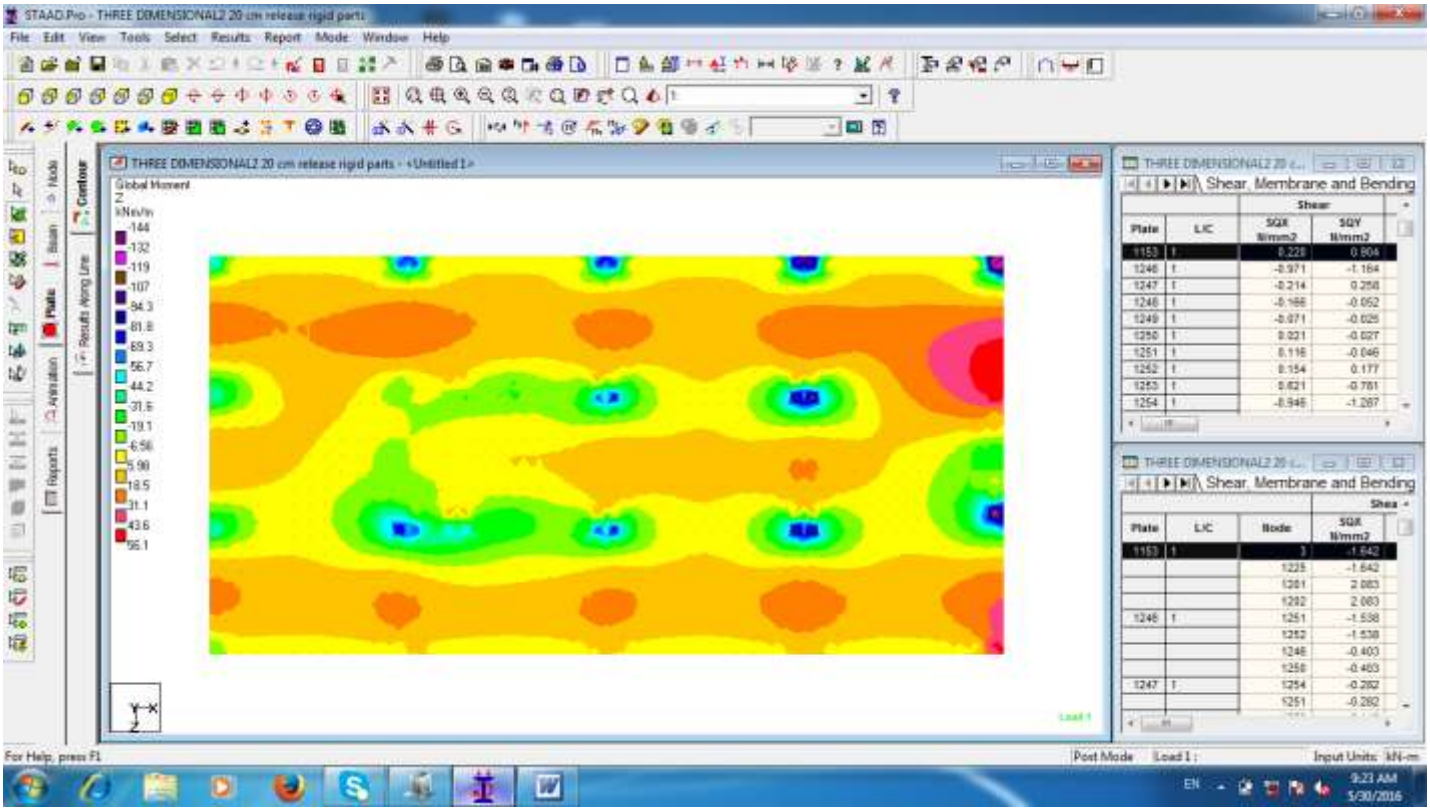

Figure 6.45: StaadPro P-Delta analysis moment M_y contour in kN.m/m for bottom floor slab

6.4.1.1 Effect of Finite Element Formulation Accuracy

The differences in the results of the different programs models may be due to the following factors:

1- The differences in the finite element formulation accuracy of the different programs, which affect the floor rotational-translational stiffness, and accordingly the building deformations and stresses.

2- The small deformations in the floor slab of the exact models due to the induced in-plane stresses, compared with the non-deformable rigid diaphragm of the proposed model. These deformations proofed to be negligible, as the differences in the twist rotations of the different models were not much affected by releasing the torsional stiffness of the vertical members, (Figures 6.32 and 6.33).

In order to examine the effects of the finite element formulation accuracy on the results of the different models, a special subroutine was created and implemented in the developed program. The subroutine was designed to calculate the floor rotational-translational stiffness from StaadPro one floor model. Therefore it enabled MFTProg to use the Finite elements formulation of StaadPro program. By using this subroutine, the floor stiffness of StaadPro was borrowed and used in the proposed method instead of the embedded one.

The subroutine has been created using the capabilities of OpenStaad, the Application Programming Interface (API), of StaadPro package, and executed by constructing a one floor StaadPro model supported by fully enforced supports in the locations of the columns and walls. A unit rotation or translation was exerted in each support in the directions of the different DOFs, and the corresponding reactions in all supports were retrieved and arranged systematically to construct the rotational-translational stiffness of the floor. Comparison of the results of the proposed model including the borrowed floor, with the results obtained using StaadPro2004 exact model, show zero or very small differences, as shown in Tables 6.34 to 6.36. Comparisons of the moment My contour in the bottom floor using MFTProg with borrowed StaadPro floor and Full StaadPro2014 model for both linear and second order P-Delta analyses are also plotted in Figures 6.46 to 6.49.

Table 6.34: Displacements and rotation in the top floor level (mm, rad), (3D Frame), (Borrowed StaadPro Floor):

Package	Linear			Second order (P-Delta)		
Trans. & Rot.	Y-Dir	Axial	Twist	Y-Dir	Axial	Twist
MFTProg	331.02	36.04	0.0130	415.09	37.60	0.0189
StaadPro2004	331.20	36.04	0.0130	415.61	37.60	0.0189
%Diff.	-0.05	0.00	0.00	-0.13	0.00	0.00

Table 6.35: Maximum bending moment in U-Shaped Core (kN.m), (3D Frame), (Borrowed StaadPro Floor):

Package	Linear	Second order
MFTProg	44106.59	50074.39
StaadPro2004	44108.82	50071.03
%Diff.	-0.01	0.01

Table 6.36: Maximum bending moment in Edge Shear Wall (kN.m), (3D Frame), (Borrowed StaadPro Floor):

Package	Linear	Second order
MFTProg	13467.59	16571.60
StaadPro2004	13431.23	16541.75
%Diff.	0.27	0.18

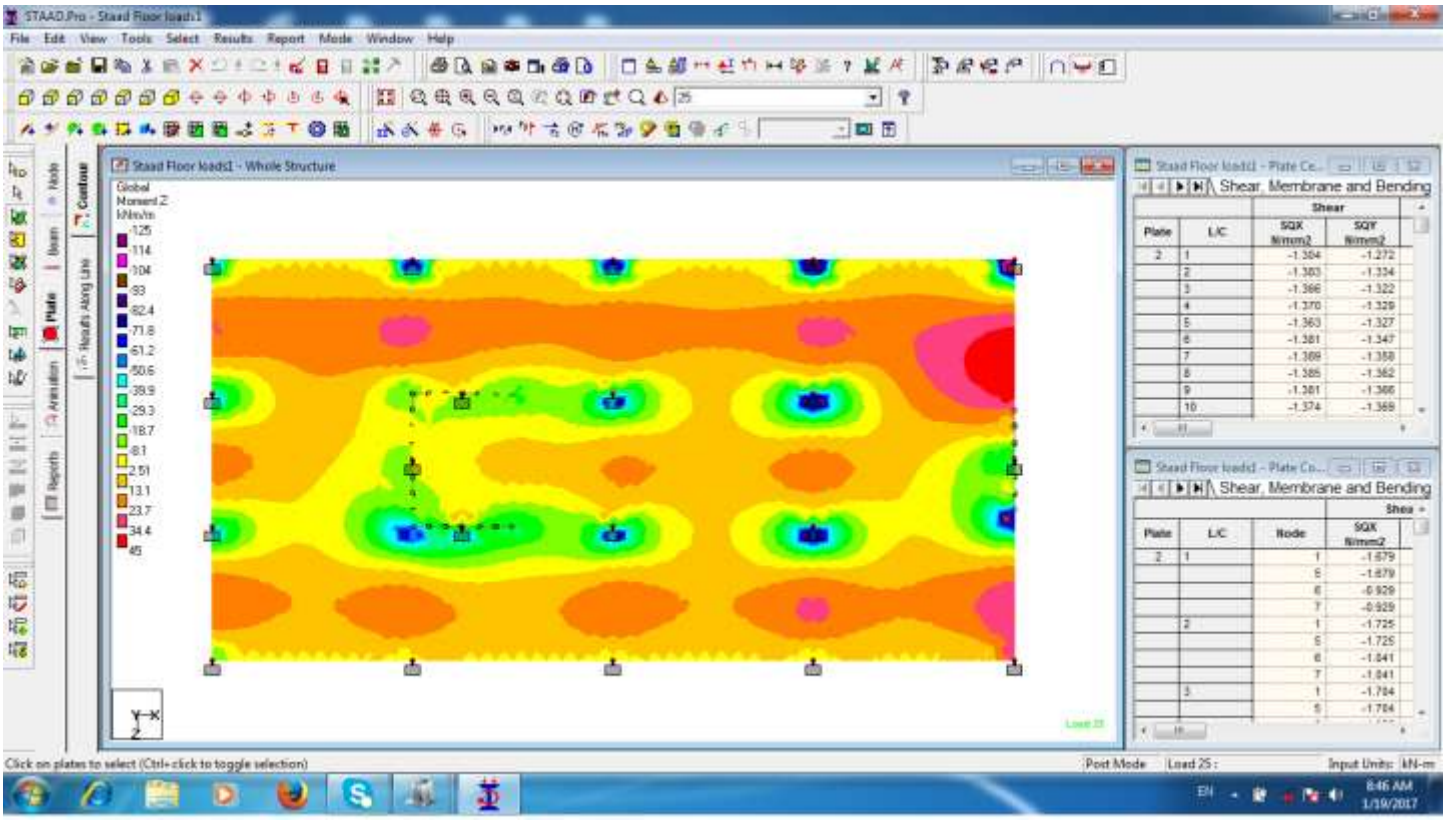

Figure 6.46: MFTProg+StaadPro one floor model moment M_y contour for bottom floor slab

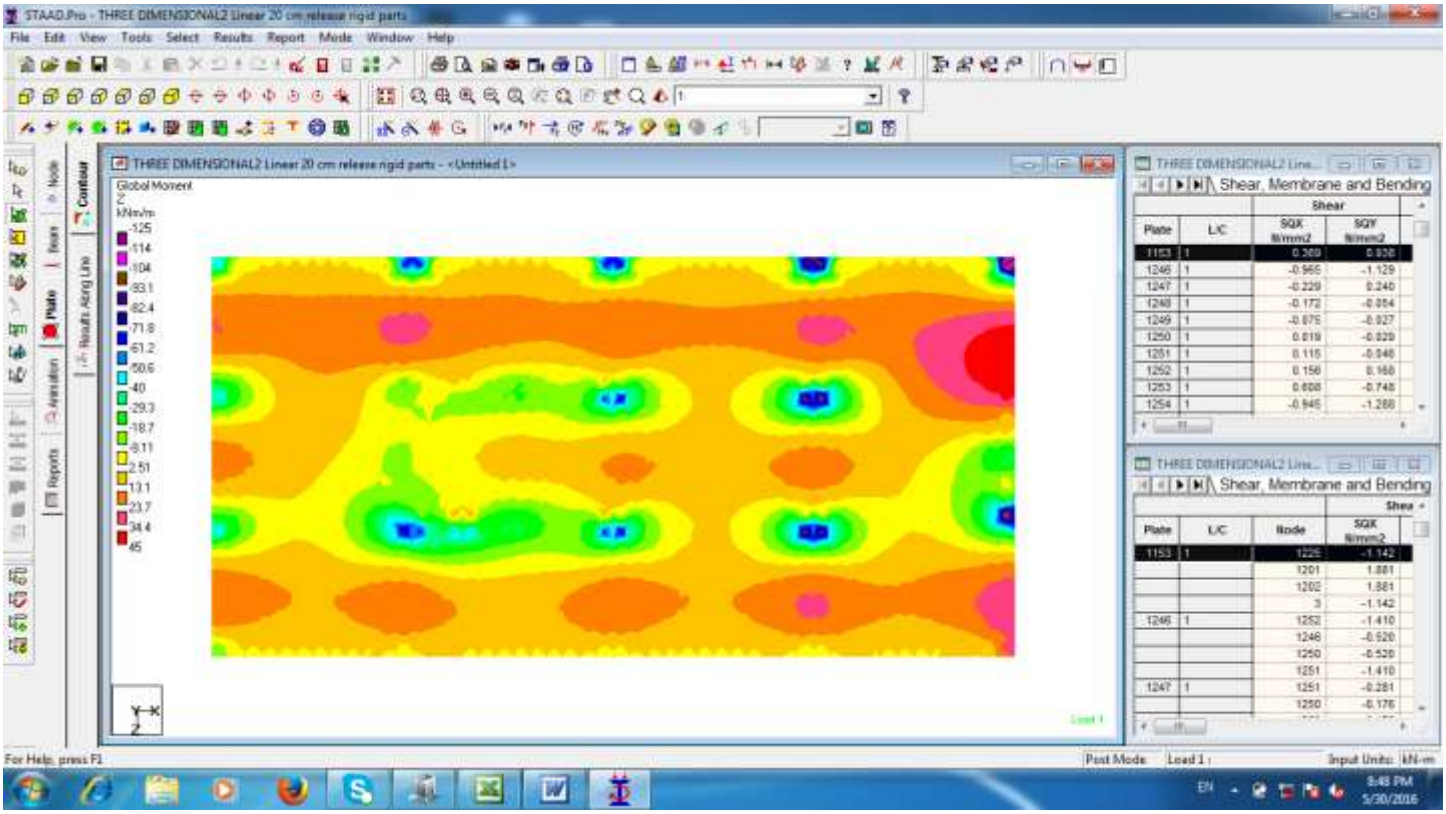

Figure 6.47: StaadPro (Full model) moment M_y contour for bottom floor slab

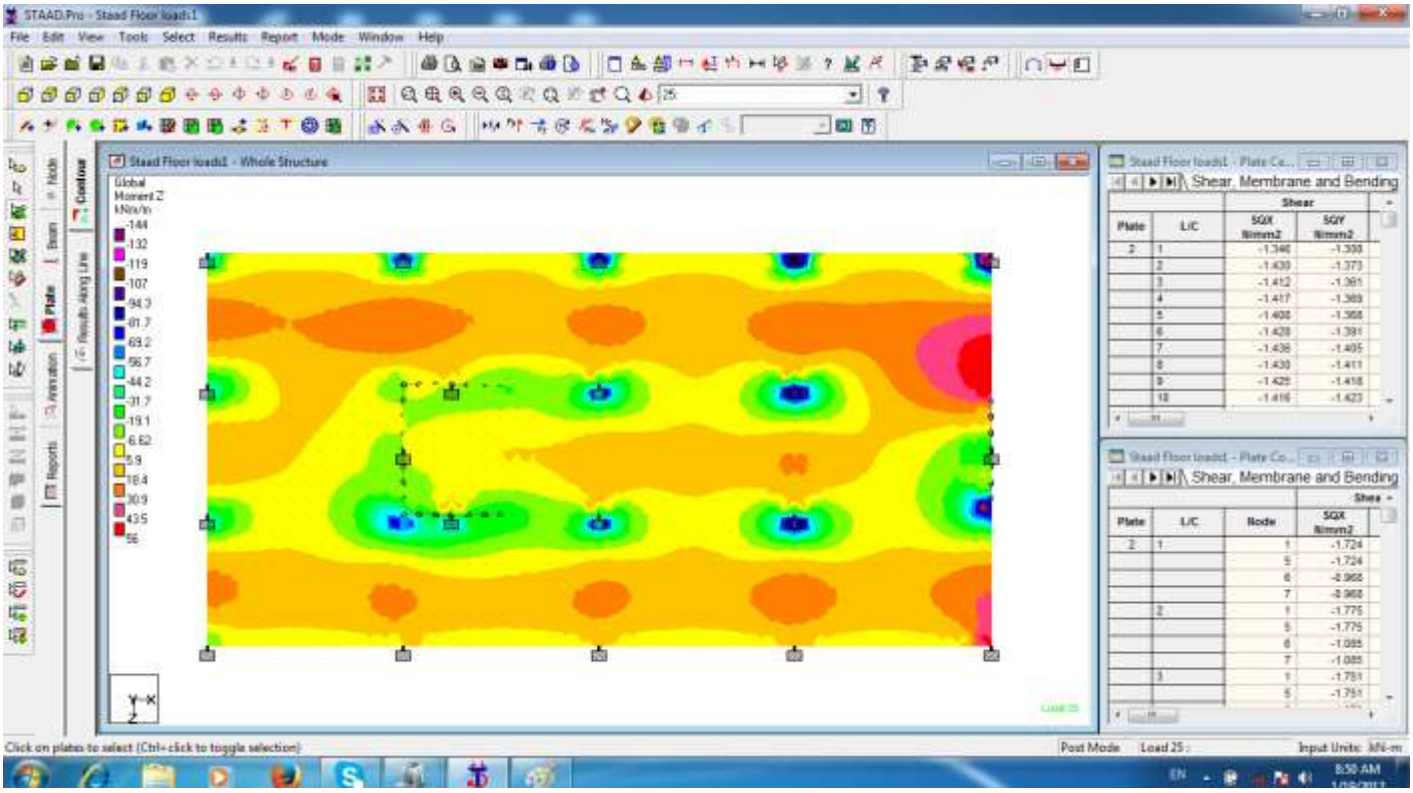

Figure 6.48: MFTProg + StaadPro one floor model P-Delta analysis moment M_y for bottom slab

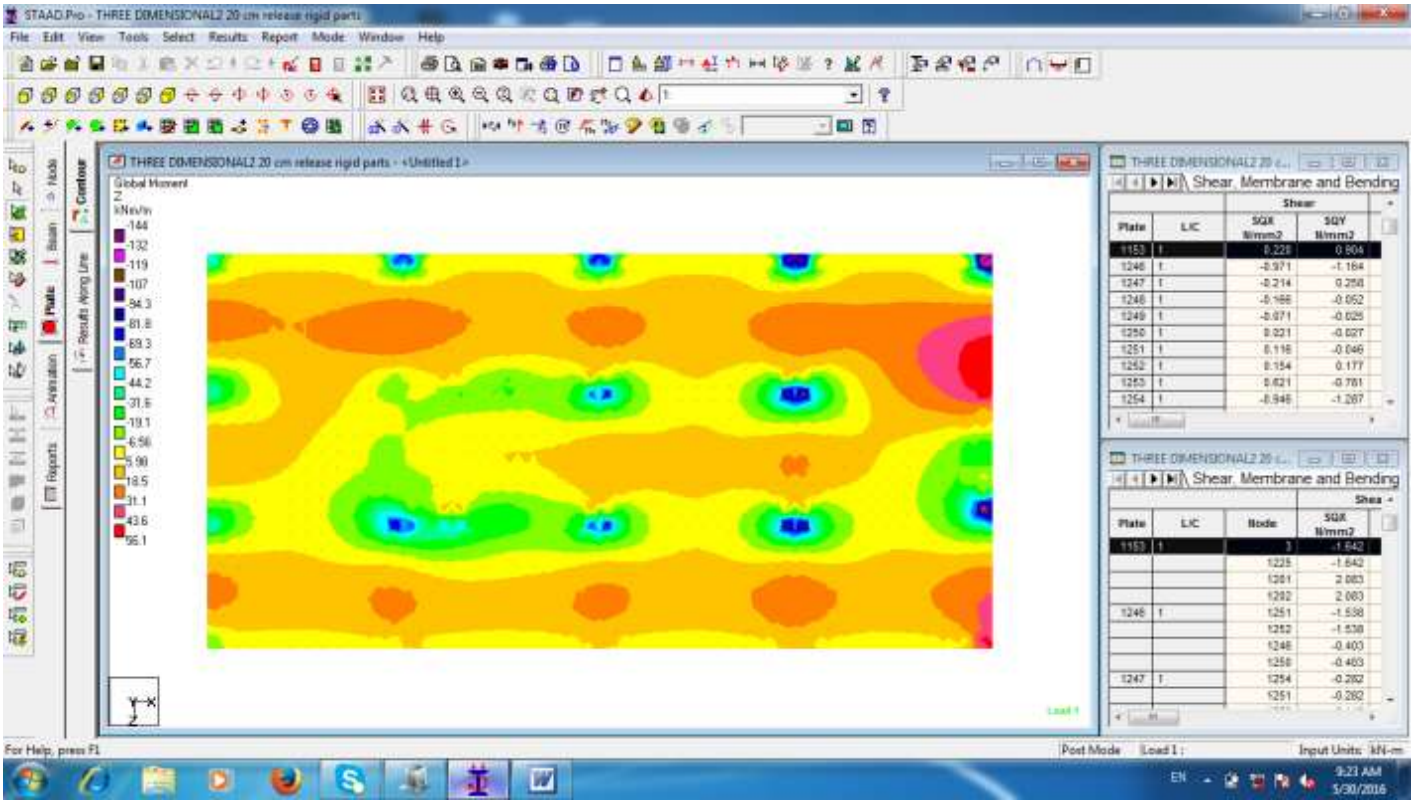

Figure 6.49: StaadPro (Full model) P-Delta analysis moment M_y contour for bottom slab

6.4.1.2 Comparison of Numbers of Unknowns

The floor slab idealized by 48 x 24 finite elements with 20 vertical members (columns and walls) shown in Figure 6.30, was used to compare the proposed method with the conventional matrix methods of analysis. The total number of unknowns for a building with same floor and of total N floors is:

(a) Conventional matrix methods (6 DOFs/joint):

$S1 = [(49 \times 25 \times N + 20) \times 6]$

(b) Proposed Method:

The unknowns in the proposed method are composed of two parts:

1-Coupled unknowns for one floor with 3 DOFs/joint, solved simultaneously and used to obtain the floors level stiffness.

2-Two Rotations plus one axial translation for each column/wall at all levels including the supports level. The unknowns solved separately, each (20x3) unknowns per each level.

$S2 = [49 \times 25 \times 3] + [20 \times 3] \,.\, (N+1)$

Note: coupled unknowns are in square brackets [ ].

For N= 150 floors: $S1$= 1,102,620 Coupled unknowns and, $S2$ = 12,735 unknowns (partially coupled), Ratio = $S1/S2$ = 86 times.

6.4.1.3 Analysis of a hypothetical 150 floors Building using MFTProg

To evaluate the program running time, the floor, Figure 6.30, was used in a 150 floors hypothetical building, but with slab thickness of 0.25 m, and all floors height = 3.0 m.

The building members are of elasticity, E = 40×10^6 kN/m^2 and Poisson's ratio, v = 0.2

The section properties of the vertical elements are:

All Columns: 1.00 m x 1.00 m

All shear walls are of thicknesses 0.5 m.

The building is subjected to lateral loads (F = 1.0 kN).

The problem was solved for elastic linear analysis using MFTProg. The elapsed running time was 83 seconds only. The displacement and twist rotation of the floors at the location of column#10, the bending moment and the shear force diagrams for the U-Shaped core and the edge shear wall are shown in Figures 6.50 to 6.56 and Tables 6.37 to 6.39. The global deformed shape of the building is shown in Figure 6.57.

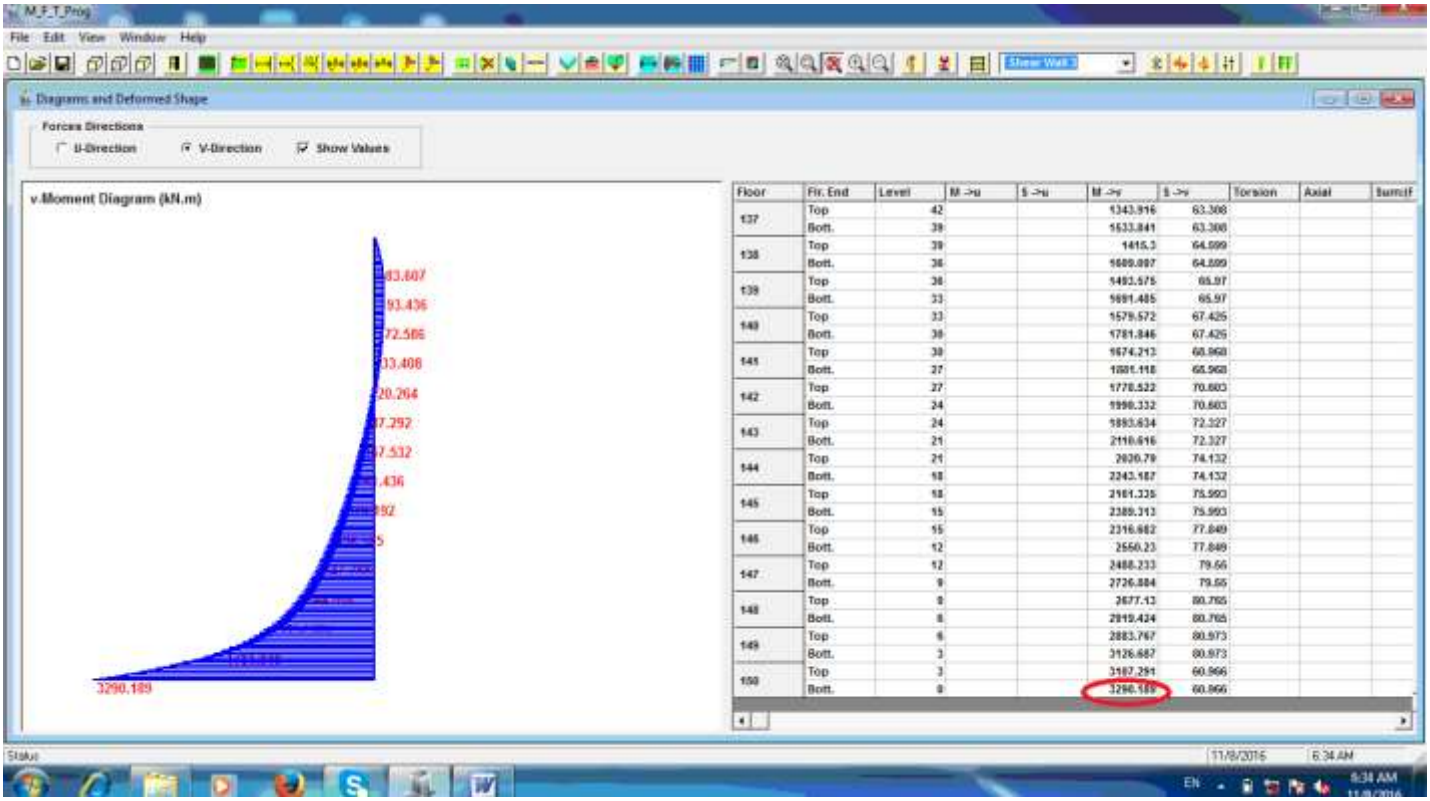

Figure 6.50: 150 Floors Building, Bending Moment Diagram for U-Shaped Core (kN.m).

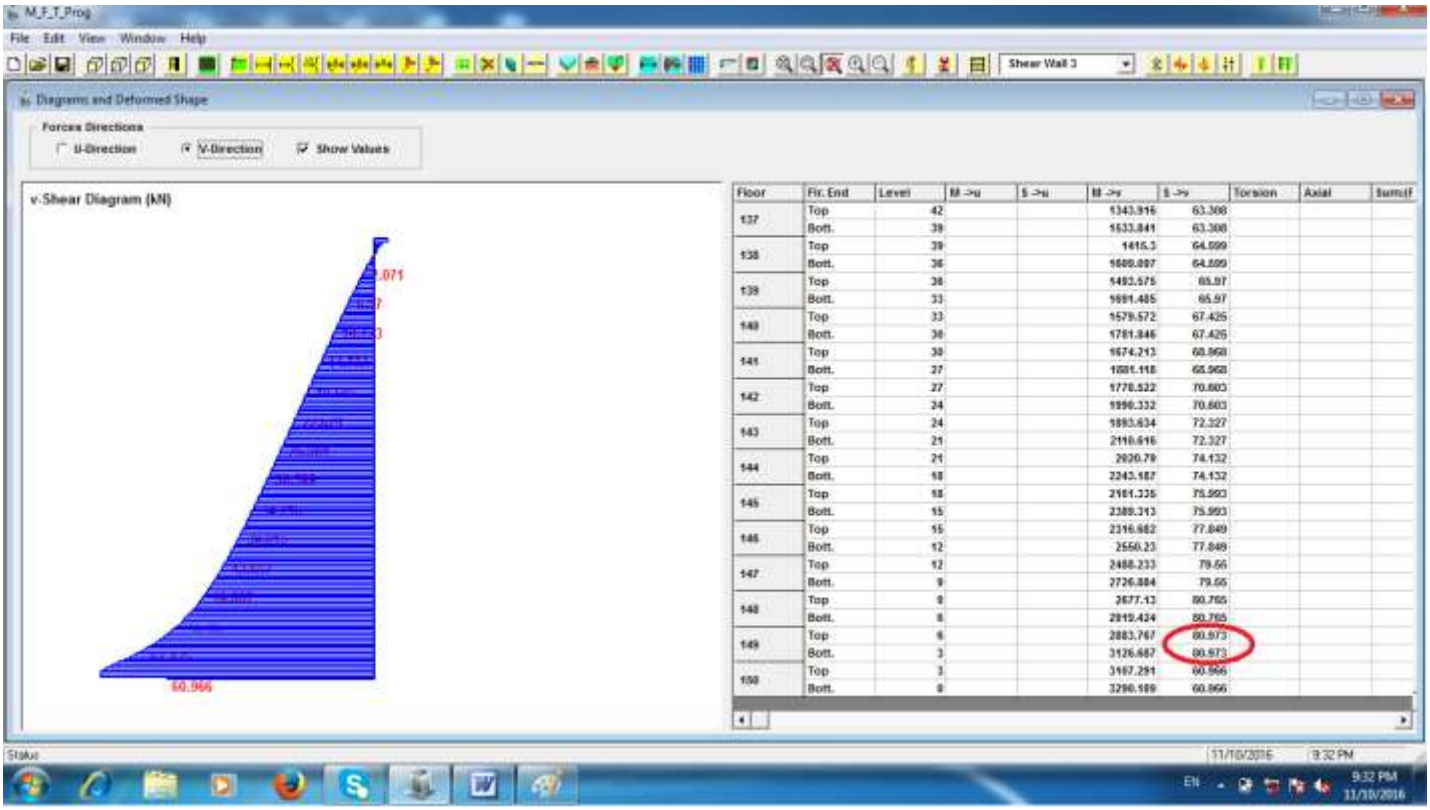

Figure 6.51: 150 Floors Building, Shear Force Diagram for U-Shaped Core (kN).

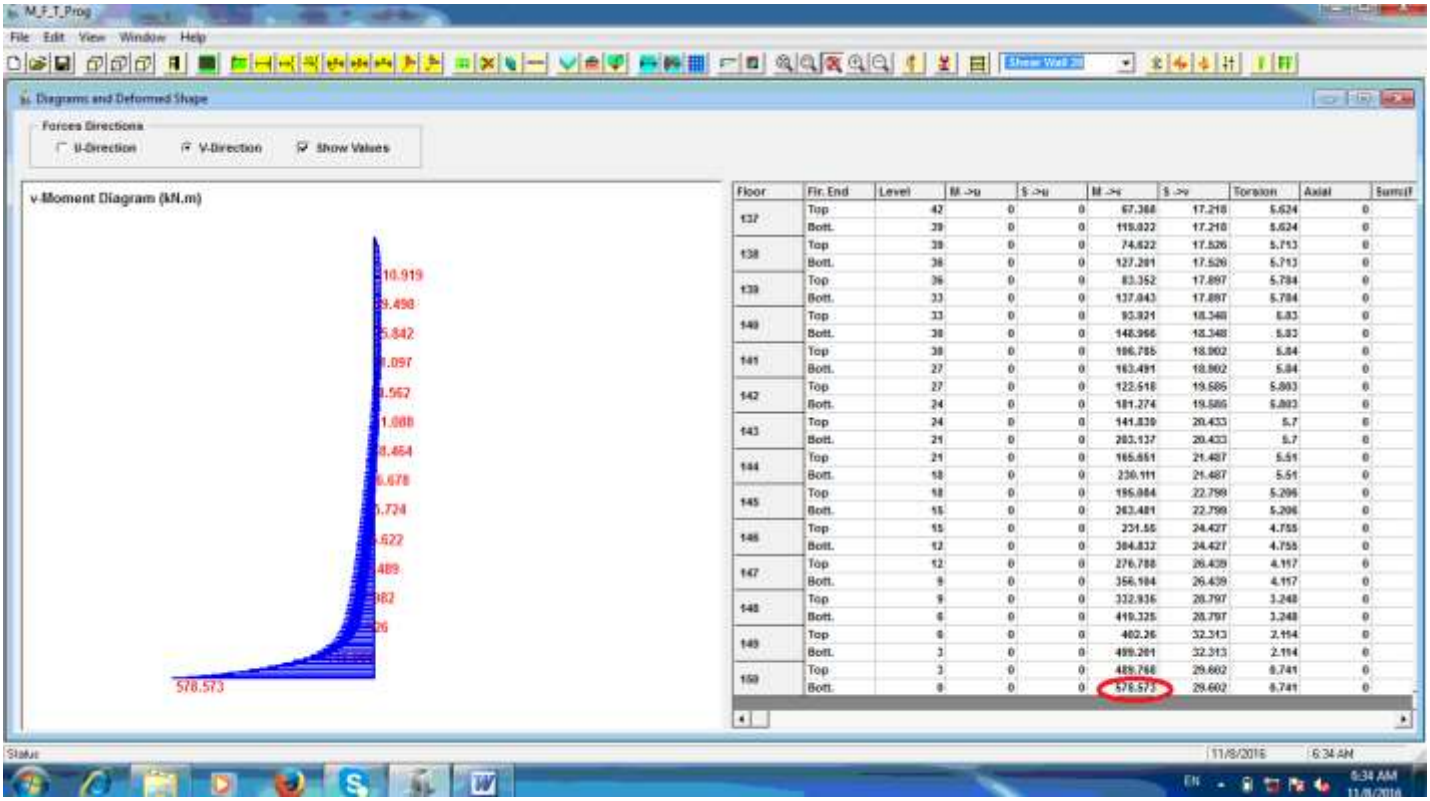

Figure 6.52: 150 Floors Building, Bending Moment Diagram for Edge shear wall (kN.m).

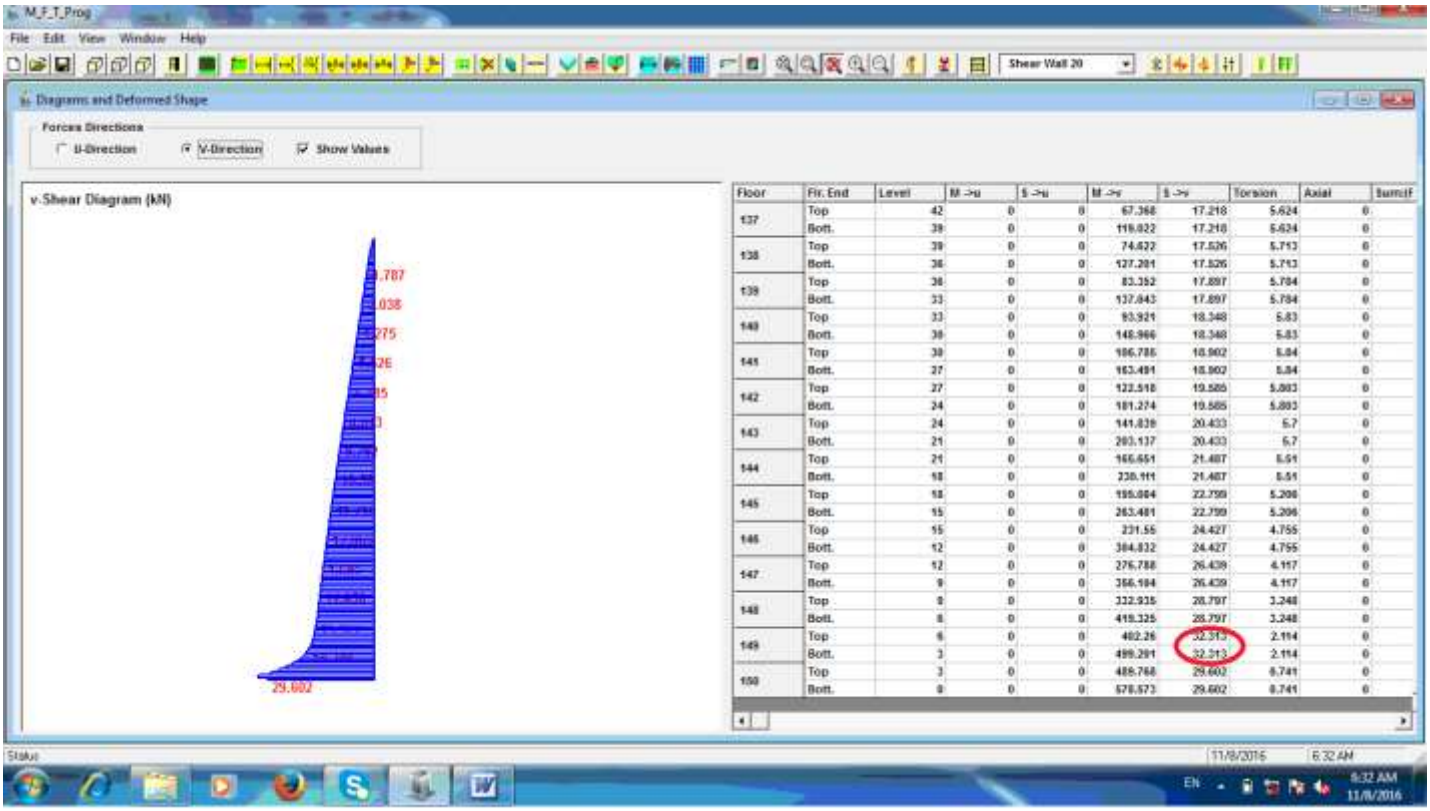

Figure 6.53: 150 Floors Building, Shear Force Diagram for Edge shear wall (kN).

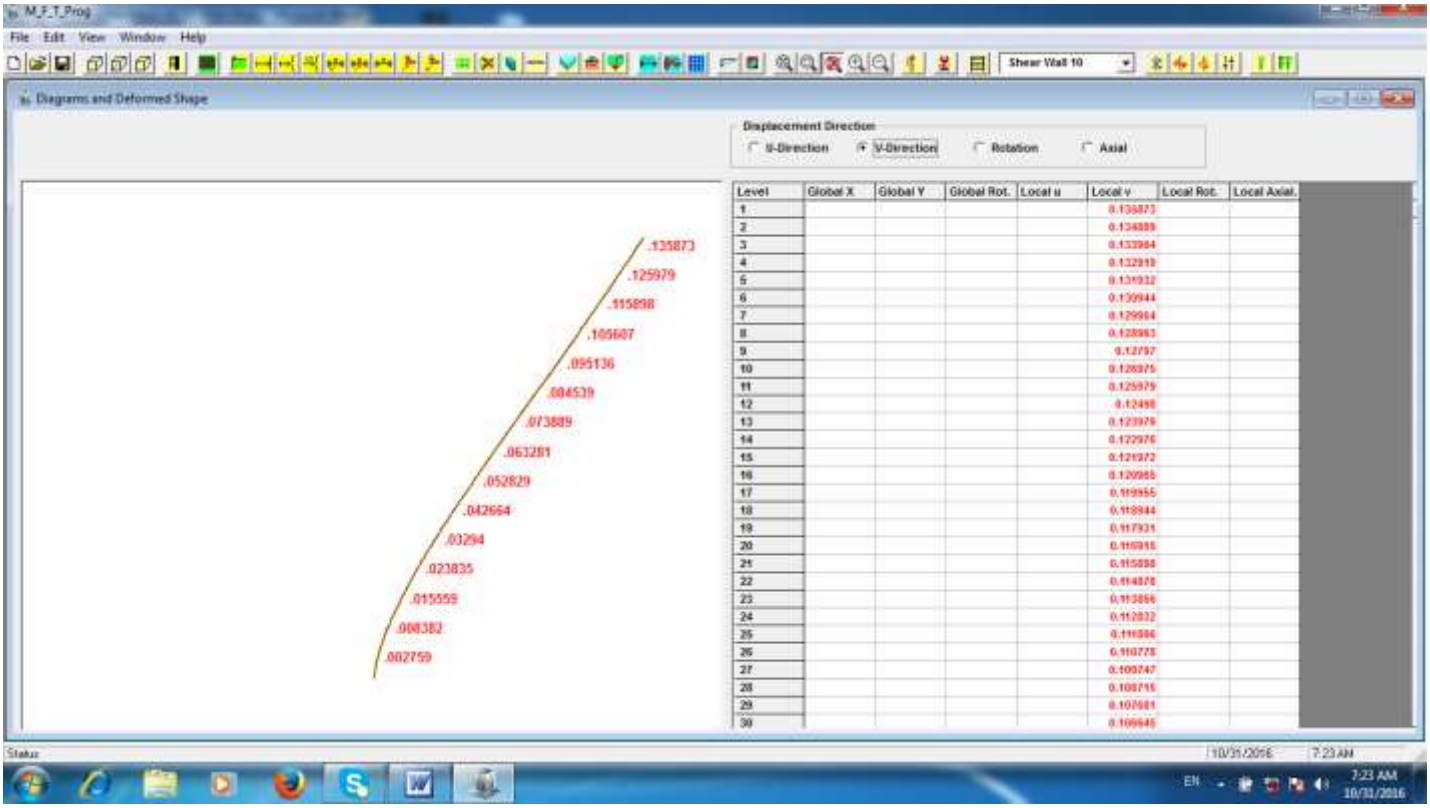

Figure 6.54: 150 Floors Building, Displacements in *y*-direction (m).

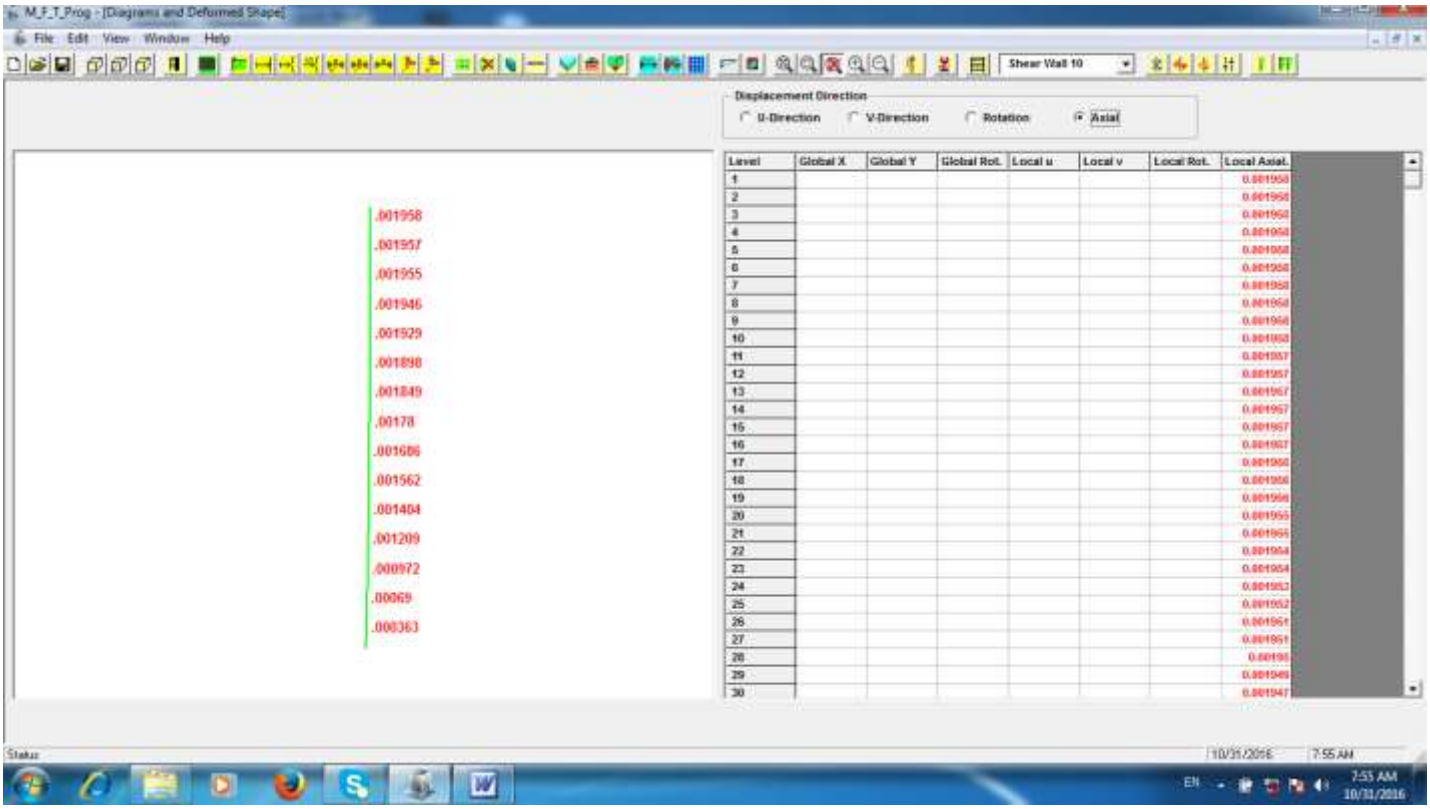

Figure 6.55: 150 Floors Building, Axial Displacements in column #10 (m).

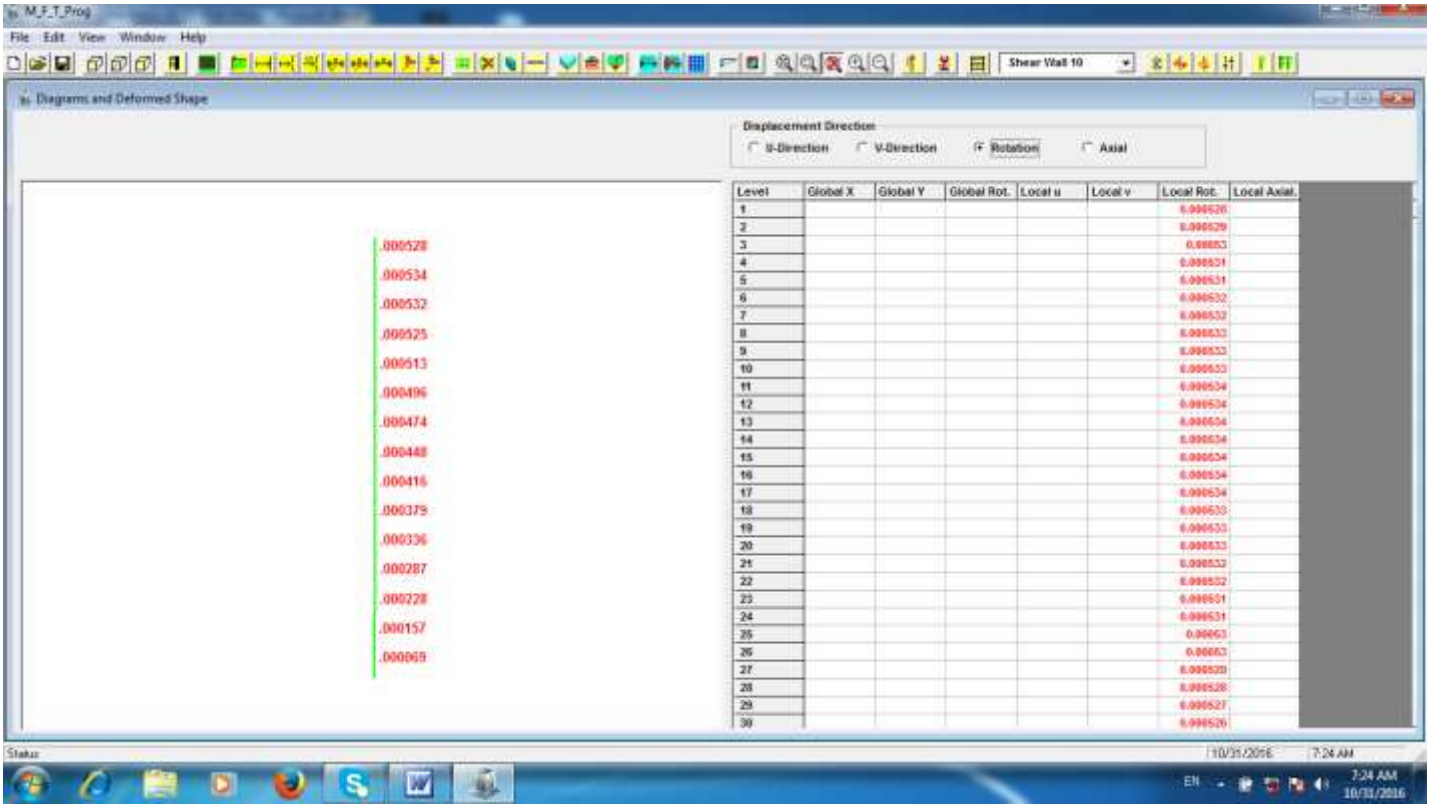

Figure 6.56: 150 Floors Building, Floors Twist Rotations in radians.

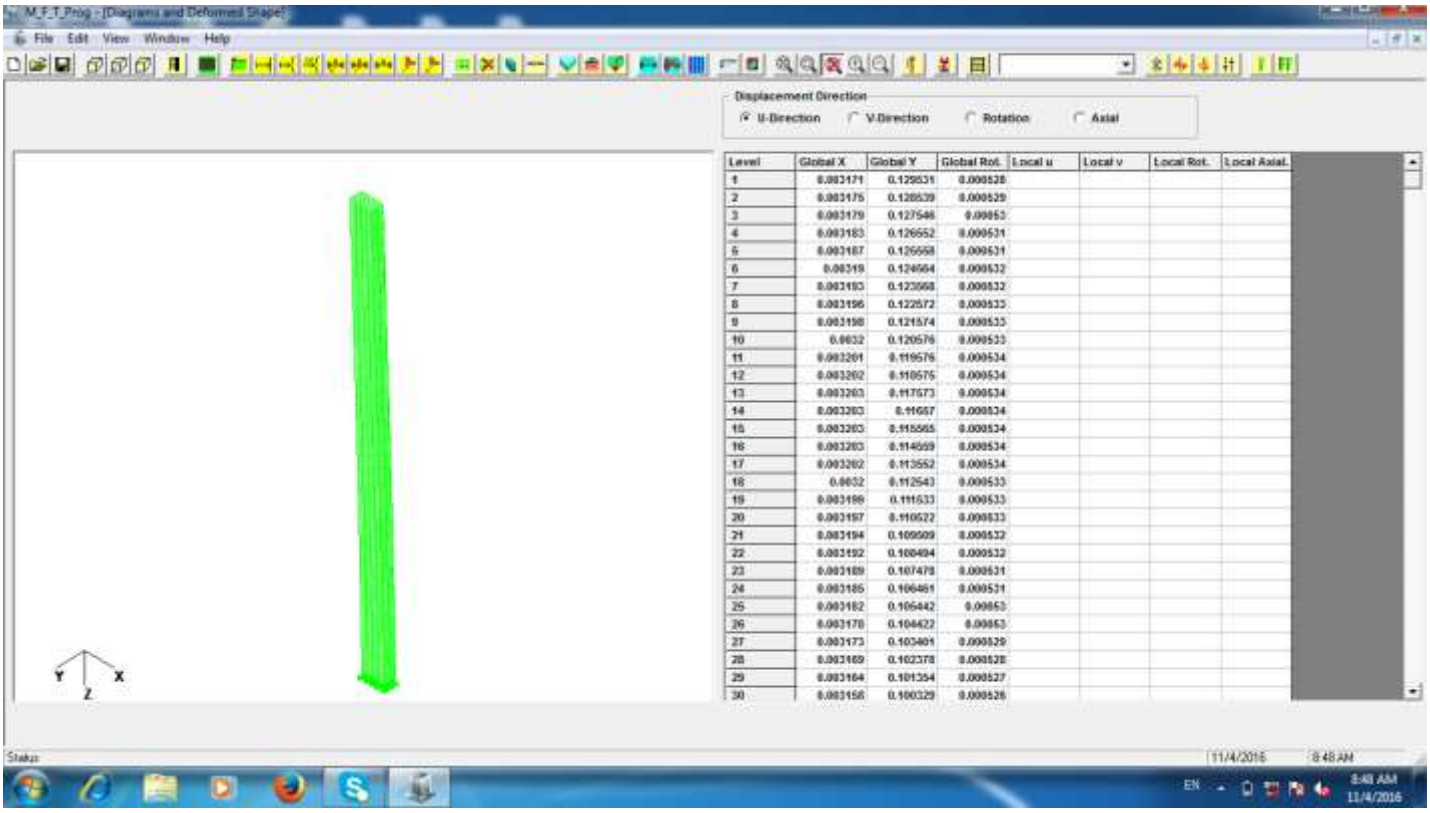

Figure 6.57: Perspective view for the deformed shape of the 150 Floors Building.

Table 6.37: Displacements and rotation in the top floor level (mm, rad), (150 Floor model):

Package	Y-Dir	Axial (col.#10)	Twist
MFTProg	135.873	1.958	0.000528

Table 6.38: Maximum bending moment (kN.m) and Shear Force (kN), in U-Shaped Core, (150 Floor model):

Package	Shear	Moment
MFTProg	80.973(*)	3290.189

(*) Maximum value: at level 149.

Table 6.39: Maximum bending moment (kN.m) and Shear Force (kN), in Edge Shear Wall, (150 Floor model):

Package	Shear	Moment
MFTProg	32.313(*)	578.573

(*) Maximum value: at level 149.

6.4.1.4 Running time and numbers of unknowns for N numbers of floors

The same floor, Figure 6.30, was analyzed for different assumed numbers of floors. The elapsed running time and the comparison of the numbers of unknowns are shown in Figures 6.58 and 6.59 respectively, and in Tables 6.40 and 6.41.

Table 6.40: Elapsed running time in seconds using MFTProg

No. of Floors	Running time (sec.)
150	82.9
300	119.7
600	193.4
900	267.4
1000	292.1

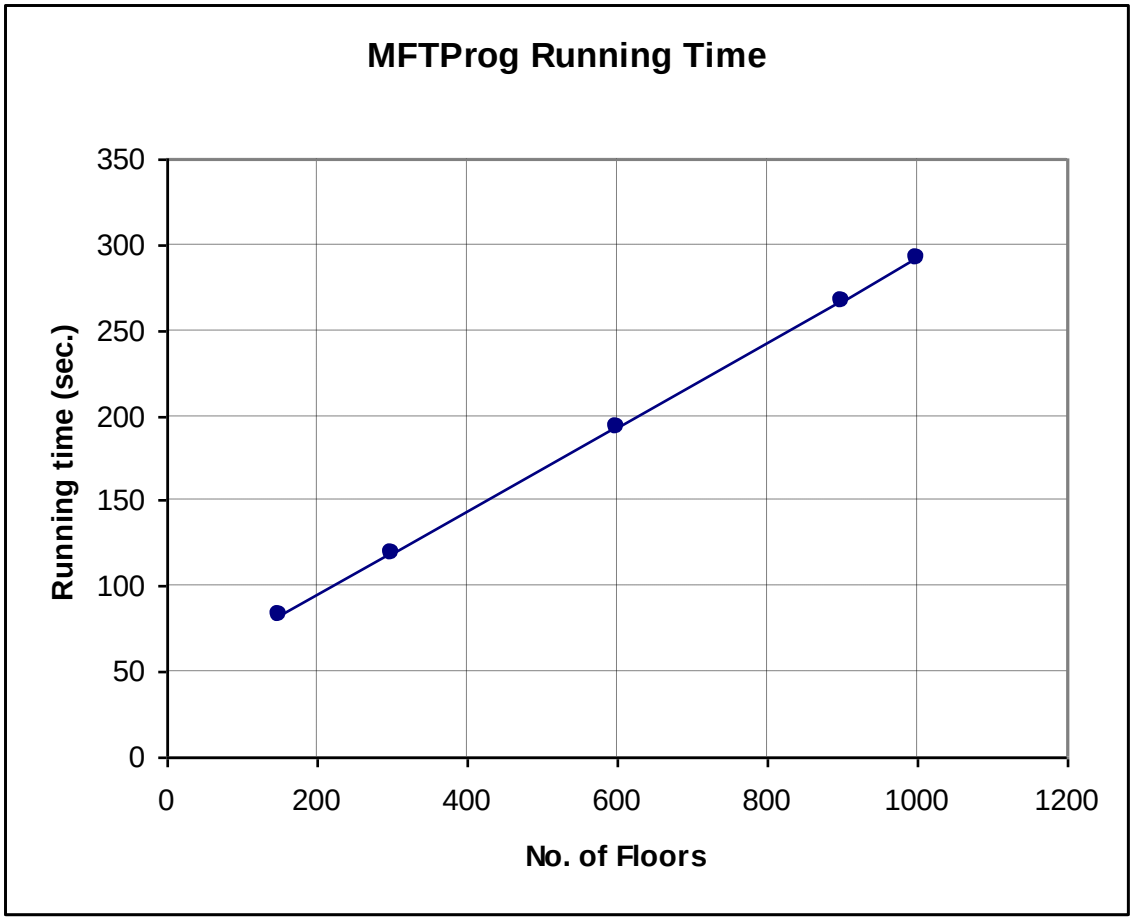

Figure 6.58: Elapsed running time in seconds using MFTProg

Table 6.41: Comparison of numbers of unknowns

No. of Floors	Conventional (S1)	MFTProg (S2)	Ratio= S1/S2
150	1,102,620	12,735	86.6
300	2,205,120	21,735	101.5
600	4,410,120	39,735	111.0
900	6,615,120	57,735	114.6
1000	7,350,120	63,735	115.3

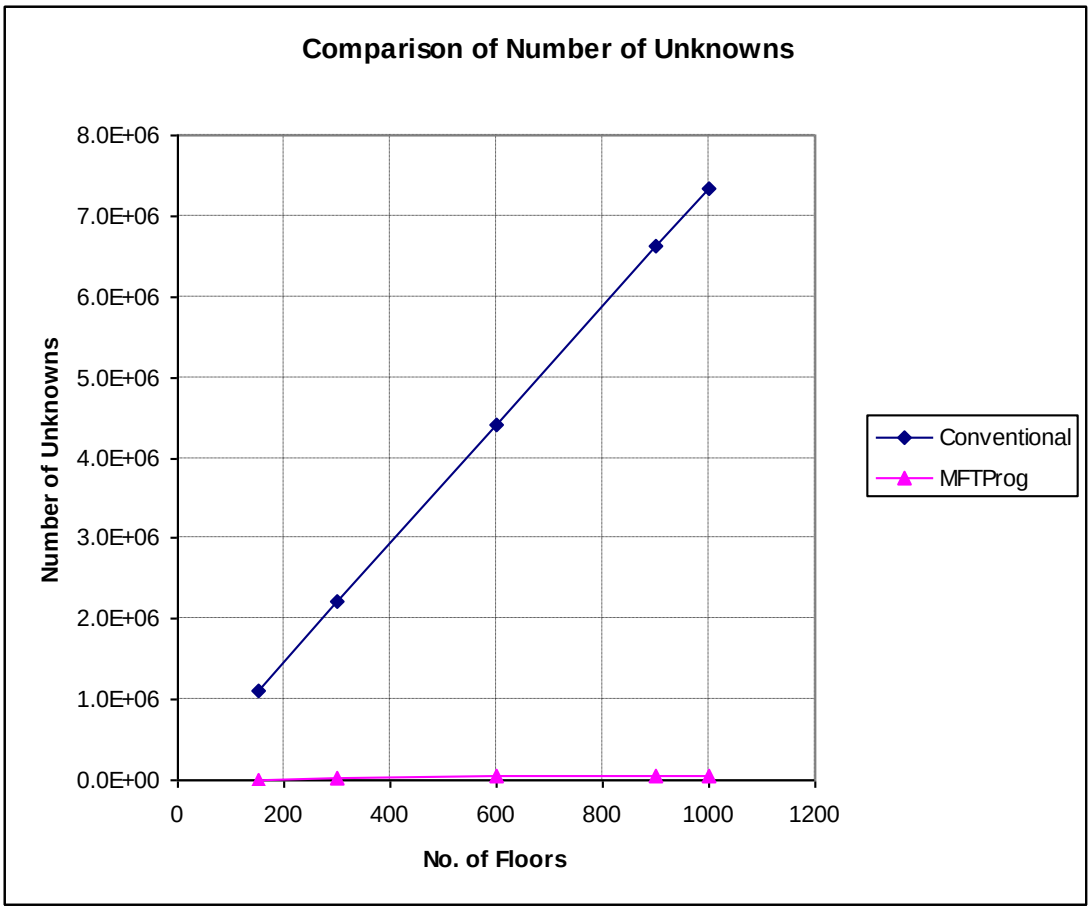

Figure 6.59: Comparisons of the numbers of unknowns

From the above presentation, it is clearly seen that the analysis of super tall buildings can be easily performed and with very low cost by using MFTProg.

These comparisons have been carried out by using computer: Dell Inspiron, Intel(R) Core™i3-2350M CPU @ 2.30 GHz, 4.00 GB of RAM.

6.4.2 Buckling Analysis of the 3D building model

The buckling analysis for the 3D building model was carried out, using the proposed bisection method and by using the eign solution (Vianello method). Comparisons between the results assuming linear shape, cubic shape and Euler buckling with stability functions were also studied.

Table 6.42 shows the results of the fundamental buckling factor calculated using MFTProgV2 with the proposed bisection subroutine. The results are compared with those obtained using StaadProV8i and ETABS 2013.

Table 6.42: Minimum Buckling factor using the different packages

Buckling Analysis Package	**Minimum buckling factor**
MFTProgV2, Linear Shape	4.181
MFTProgV2, Cubic Shape	4.165
MFTProgV2, Euler stability functions	4.157
StaadProV8i	4.152
ETABS2013 (thin)	3.983
ETABS2013 (thick)	4.731

The analysis was also carried out using the eign solution. The Vianello method was carried out for the first six buckling modes for the linear shape function. The results obtained were compared with those obtained from ETABS2013 thin and thick plate. The results are shown in Table 6.43, and the buckling mode shapes are shown in Figure 6.60.

Table 6.43: Buckling factors of the first six modes using the different packages

Buckling Analysis	Mode1	Mode2	Mode3	Mode4	Mode5	Mode6
MFTProgV2 (Linear)	4.373	5.167	8.184	9.883	9.945	13.832
ETABS2013 (thin)	3.983	4.832	7.724	9.129	9.375	12.943
ETABS2013 (thick)	4.731	5.815	8.739	9.991	10.673	14.060

In Table 6.42, the MFTProgV2 Euler buckling analysis give very close result to the result of StaadProV8i, the percentage difference is 0.11%.

The MFTProgV2 (Euler stability functions) is exact solution and gives less buckling factor compared to the cubic and the linear shapes buckling values.

In Table 6.42, the results of MFTProgV2 linear deformed shape show greater values of the buckling factors than the cubic shape values and the results of the cubic shape show greater values than the Euler buckling values. The reason for these cases was already explained in the 2D model case. In Table 6.43, the buckling factors for all modes of MFTProgV2 (Linear), fall in-between the values of ETABS (thin) and ETABS (thick) and show good agreement.

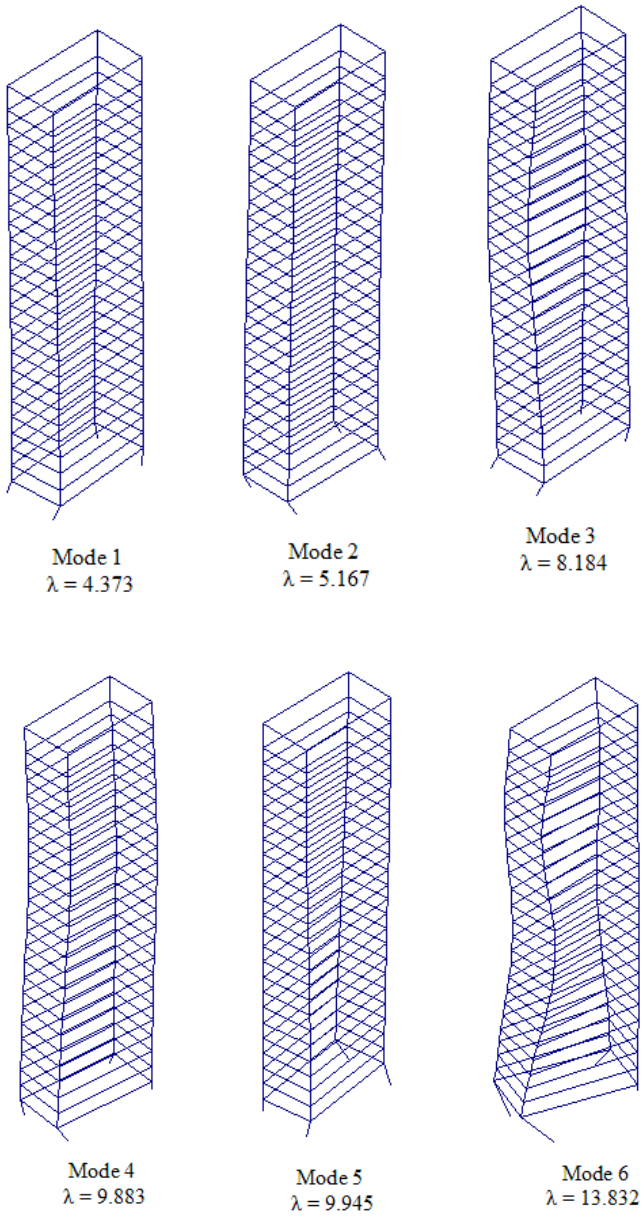

Figure 6.60: Buckling modes 1 to 6

The following cross check for the proposed bisection subroutine was carried out:

The calculated buckling factor found for the cubic shape was (4.165), which is greater than 1. Because the starting buckling factor is 1, this is means that the load factor is increased until the correct buckling factor is reached. The total load was multiplied by 10 to keep the applied load greater than the building buckling load. By running MFTProgV2 for the new applied loads, the load factor starts with 1.0 and then decreases until the correct buckling factor is reached. The calculated new buckling factor obtained was (0.41656) which is match with the value (4.165/10), and proves the efficiency of the proposed subroutine.

6.4.3 Dynamic analysis for the 3D model

The dynamic analysis was performed for the 3D model. The response spectra method was performed first with linear effects and then the spectra was also performed including the P-Delta second order effects. The time history was then performed including the linear and also the second order effects.

The lumped mass and the mass polar inertia for the 3D model in any floor level were calculated as follows:

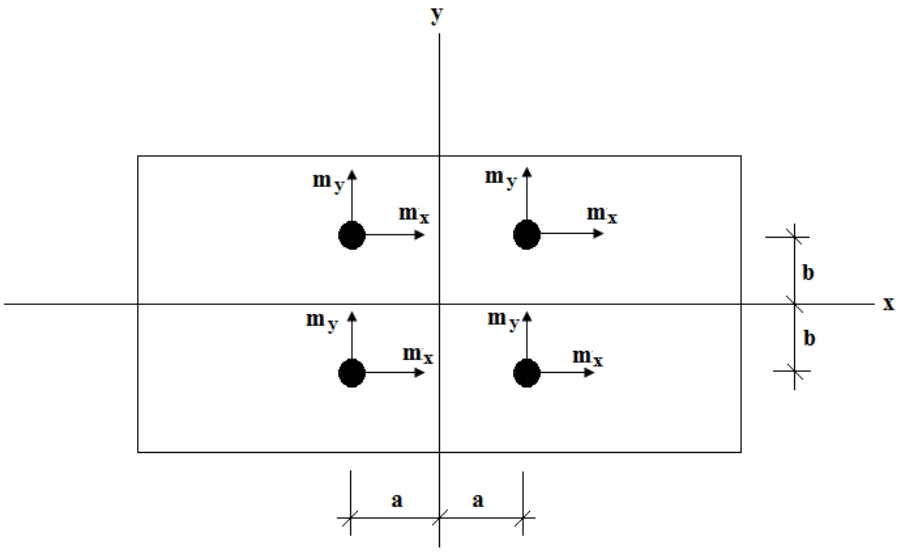

Figure 6.61: Mass polar inertia for 4 lumped masses, (Proposal 1)

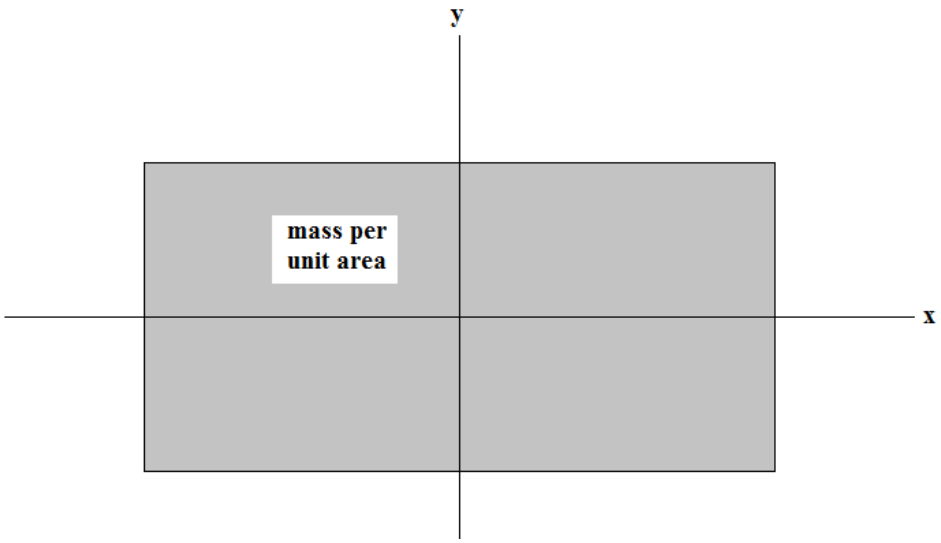

Figure 6.62: Mass polar inertia for uniformly distributed mass, (Proposal 2)

In the three dimensional model, the total mass in any floor was calculated for the two proposals shown in Figures 6.61 and 6.62, as follows:

$mx_{tot} = my_{tot} = 18*12*24/9.80665 = 528.62$ kg

The lumped masses in the *x* and *y* directions and the polar inertia for the 4 lumped masses in Proposal 1, were calculated as follows:

For, a = b = 5.5 m:

The lumped masses in the *x* and *y* directions were:

$mx_{lumped} = my_{lumped} = 18*12*24/4/9.80665 = 132.155$ kg

and the polar inertia was:

$m_{ro} = 18*(12*24/4)*5.5^2*8/9.80665 = 31981.56$ kg.m^2

The polar inertia for the uniform mass in Proposal 2, was calculated as follows:

$m_{ro} = 18*(12*24^3/12+24*12^3/12)/9.80665$

$= 31717.25$ kg.m^2

The lumped masses in Proposal 1, is an approximation used in some packages to simplify and accelerate the eign solution. The relative percentage difference between the two proposals is:

= (31981.56-31717.25)/31717.25*100

= 0.83 %

The masses and moments of inertias for all floors of the two illustrated proposals of the 3D building model are shown in Table 6.44.

Table 6.44: Floor Masses and Moments of Inertia of the 3D Building (Mass in kg and Moment of Inertia in $kg.m^2$)

Floor	Mass, mx_{tot} (kg)	Mass, my_{tot} (kg)	Inertia m_{ro} (4 lumped masses)($kg.m^2$)	Inertia m_{ro} (distributed) ($kg.m^2$)
1 to 25	528.62	528.62	31981.56	31717.25

Table 6.45: Comparisons of the first nine Natural frequencies of 3D Building (cycles/second)

Mode	StaadProV8i[1](%Diff)	MFTProgV2[1] (%Diff)	MFTProgV2[2]	ETABS(thin)[2] (%Diff)	ETABS(thick)[2] (%Diff)
1	0.141 (0)	0.141 (0)	0.141	0.136 (-3.55)	0.149 (5.67)
2	0.151 (0.67)	0.15 (0)	0.150	0.145 (-3.33)	0.159 (6)
3	0.213 (0.95)	0.21 (-0.47)	0.211	0.206 (-2.37)	0.218 (3.32)
4	0.494 (2.49)	0.481 (-0.21)	0.482	0.468 (-2.9)	0.505 (4.77)
5	0.532 (3.3)	0.515 (0)	0.515	0.503 (-2.33)	0.541 (5.05)
6	0.828 (3.5)	0.798 (-0.25)	0.800	0.789 (-1.38)	0.822 (2.75)
7	1.033 (3.3)	0.998 (-0.2)	1.000	0.979 (-2.1)	1.031 (3.1)
8	1.112 (4.02)	1.069 (0)	1.069	1.052 (-1.59)	1.106 (3.46)
9	1.785 (4.32)	1.708 (-0.18)	1.711	1.683 (-1.64)	1.743 (1.87)

The superscripts 1 and 2 refer to Proposal 1 and Proposal 2 respectively.

As shown in table 6.45, the difference is very small and therefore, the two proposed cases were assumed identical. In all the comparisons StaadPro2004 and StaadProV8i packages used proposal 1 and all the other packages include MFTProgV2 are using the Proposal 2. The comparisons between the natural frequencies obtained using MFTProgV2[2] and the different analysis packages, show good agreement.

6.4.4 Response spectra Analysis for the 3D model

The response spectra analysis was performed for the 3D model. As for the 2D model, the excited response acceleration was taken from the UBC design code with assumed damping ratio of 5%. The considered modal combination methods used in this analysis were the SRSS and the CQC methods. Comparisons of the lateral displacement, the base

shear and the base overturning moment for MFTProgV2 and the different packages are shown in Tables 6.50 to 6.53.

Table 6.46: Comparison of the modal masses participating ratios in *x*-direction:

Mode	MFTProgV2	StaadProV8i(%Diff)	ETABS(thin) (%Diff)	ETABS(thick) (%Diff)
1	0	0	0	0
2	73.147	73.48 (0.46)	72.864 (-0.39)	73.488 (0.47)
3	0	0	0	0
4	0	0	0	0
5	12.983	13.13 (1.13)	13.105 (0.94)	12.845 (-1.06)
6	0	0	0	0
7	0	0	0	0
8	5.405	5.28 (-2.31)	5.463 (1.07)	5.292 (-2.09)
9	0	0	0	0

Table 6.47: Comparison of the accumulated modal masses participating ratios in *x*-direction:

Mode	MFTProgV2	StaadProV8i(%Diff)	ETABS(thin) (%Diff)	ETABS(thick) (%Diff)
1	0	0	0	0
2	73.147	73.477 (0.45)	72.864 (-0.39)	73.488 (0.47)
3	73.147	73.477 (0.45)	72.864 (-0.39)	73.488 (0.47)
4	73.147	73.477 (0.45)	72.864 (-0.39)	73.488 (0.47)
5	86.13	86.609 (0.56)	85.969 (-0.19)	86.334 (0.24)
6	86.13	86.609 (0.56)	85.969 (-0.19)	86.334 (0.24)
7	86.13	86.609 (0.56)	85.969 (-0.19)	86.334 (0.24)
8	91.535	91.891 (0.39)	91.432 (-0.11)	91.626 (0.1)
9	91.535	91.891 (0.39)	91.432 (-0.11)	91.626 (0.1)

Table 6.48: Comparison of the modal masses participating ratios in *y*-direction:

Mode	MFTProgV2	StaadProV8i(%Diff)	ETABS(thin) (%Diff)	ETABS(thick) (%Diff)
1	48.499	49.21 (1.47)	47.754 (-1.54)	48.675 (0.36)
2	0	0	0	0
3	22.148	21.74 (-1.84)	22.679 (2.4)	22.081 (-0.3)
4	8.095	8.22 (1.54)	8.048 (-0.58)	8.045 (-0.62)
5	0	0	0	0
6	6.994	7.01 (0.23)	7.115 (1.73)	7.052 (0.83)
7	3.062	3.05 (-0.39)	3.087 (0.82)	2.982 (-2.61)
8	0	0	0	0
9	2.231	2.09 (-6.32)	2.097 (-6.01)	1.935 (-13.27)

Table 6.49: Comparison of the accumulated modal masses participating ratios in *y*-direction:

Mode	MFTProgV2	StaadProV8i(%Diff)	ETABS(thin) (%Diff)	ETABS(thick) (%Diff)
1	48.499	49.212 (1.47)	47.754 (-1.54)	48.675 (0.36)
2	48.499	49.212 (1.47)	47.754 (-1.54)	48.675 (0.36)
3	70.646	70.952 (0.43)	70.433 (-0.3)	70.756 (0.16)
4	78.742	79.167 (0.54)	78.481 (-0.33)	78.801 (0.07)
5	78.742	79.167 (0.54)	78.481 (-0.33)	78.801 (0.07)
6	85.736	86.18 (0.52)	85.596 (-0.16)	85.853 (0.14)
7	88.799	89.228 (0.48)	88.682 (-0.13)	88.835 (0.04)
8	88.799	89.228 (0.48)	88.682 (-0.13)	88.835 (0.04)
9	91.029	91.321 (0.32)	90.78 (-0.27)	90.77 (-0.28)

The comparisons between the modal masse participating ratios and their accumulations in the *x* and *y* directions using the proposed method, StaadProV8i and ETABS thin and thick plates show a very small differences, as shown in Tables.

I- Lateral Displacement at the top floor of the 3D building model

Tables 6.50 and 6.51 show the lateral displacement response at the top floor of the building model due to the UBC design code acceleration response curve, obtained by response spectra analysis in *y*-direction using MFTProgV2 and the other packages for proposal 1 and 2 respectively.

Table 6.50: Comparison of the lateral displacement response at the top floor (m), Proposal 1

Response	MFTProg V2	StaadProV8i (%Diff)	ETABS(thin) (%Diff)	ETABS(thick) (%Diff)	SAP2000 (thin) (%Diff)	SAP2000 (thick) (%Diff)
ALL SRSS	0.46146	0.463041 (0.34)	0.474174 (2.76)	0.436886 (-5.33)	0.46662 (1.12)	0.43056 (-6.7)
ALL CQC	0.468434	0.470168 (0.37)	0.481418 (2.77)	0.445146 (-4.97)	0.47289 (0.95)	0.43792 (-6.51)

Table 6.51: Comparison of the lateral displacement response at the top floor (m), Proposal 2

Response	MFTProg V2	StaadProV8i (%Diff)	ETABS(thin) (%Diff)	ETABS(thick) (%Diff)	SAP2000 (thin) (%Diff)	SAP2000 (thick) (%Diff)
ALL SRSS	0.44462	0.463041 (4.14)	0.474174 (6.65)	0.436886 (-1.74)	0.46662 (4.95)	0.43056 (-3.16)
ALL CQC	0.45571	0.470168 (3.17)	0.481418 (5.64)	0.445146 (-2.32)	0.47289 (3.77)	0.43792 (-3.9)

Proposal 1 used the displacements responses calculated from the acceleration response ($S_d = S_a/\omega^2$), and the participation factor of the mode, while Proposal 2 used the displacement obtained from a full frame analysis using the equivalent static forces obtained from the acceleration responses.

Table 6.50 gives the total lateral displacement at the top floor of the building structures, proposal 1. For the SRSS, the closest results to MFTProgV2 result is obtained from StaadProV8i which is of 0.34 % difference, and for the CQC, the closest result is also obtained from StaadProV8i which is of 0.37 % difference.

Table 6.51 gives the total lateral displacement at the top floor of the building structures, proposal 2. For the SRSS, the closest result to MFTProgV2 result is obtained from ETABS (thick) which is of -1.74 % difference, and for the CQC, the closest result is also obtained from ETABS (thick) which is of -2.32 % difference.

MFTProgV2 proposal 1 gives closer results to the different packages than proposal 2.

II- Resultant Shear Force at the Base of the 3D building model

Table 6.52, shows the resultant shear force response at the base of the building due to the UBC design code acceleration response curve, obtained by response spectra analysis in *y*-direction using the proposed method and the other packages.

Table 6.52: Comparisons of the Response Spectrum Base Shear force (kN):

Mode	MFTProg V2	StaadProV 8i(%Diff)	ETABS (thin) (%Diff)	ETABS (thick) (%Diff)	SAP2000 (thin) (%Diff)	SAP2000 (thick) (%Diff)
1	2305.62	2333.19 (1.2)	2191.59 (-4.95)	2454.66 (6.46)	-	-
2	0	0	0	0	-	-
3	1572.23	1564.77 (-0.47)	1580.22 (0.51)	1622.56 (3.2)	-	-
4	1314.65	1370.1 (4.22)	1280.28 (-2.61)	1367.77 (4.04)	-	-
5	0	0	0	0	-	-
6	1884.42	1958.62 (3.94)	1897.17 (0.68)	1951.38 (3.55)	-	-
7	1032.11	1067.59 (3.44)	1020.79 (-1.1)	1041.16 (0.88)	-	-
8	0	0	0	0	-	-
9	1286.22	1267.96 (-1.42)	1213.97 (-5.62)	1150.01 (-10.59)	-	-
ALL SRSS	3973.26	4043.87 (1.78)	3879.98 (-2.35)	4091.85 (2.98)	3871.973 (-2.55)	4092.598 (3.00)
ALL CQC	4168.21	4228.81 (1.45)	4073.39 (-2.27)	4298.29 (3.12)	4140.134 (-0.67)	4346.12 (4.27)

Table 6.52 gives the total shear forces at the base of the building structure in *y*-direction. For the SRSS, the closest result to MFTProgV2 is obtained from StaadProV8i which is of 1.78 % difference, and for the CQC, the closest result is obtained from SAP2000V16 (thin) which is of -0.67 % difference.

III- Resultant overturning moment at the Base of the 3D building model

Table 6.53, shows the resultant overturning moment response at the base of the building due to the UBC design code acceleration response curve, obtained by response spectra analysis in *y*-direction using the proposed method and the other packages.

Table 6.53: Comparisons of the Response Spectrum Base Overturning Moment (kN.m):

Mode	MFTProgV2	StaadProV8i(%Diff)	ETABS (thin) (%Diff)	ETABS (thick) (%Diff)	SAP2000 (thin) (%Diff)	SAP2000 (thick) (%Diff)
1	-145366.59	-146700.9 (0.92)	-138438 (-4.77)	-154679 (6.41)	-	-
2	0	0	0	0	-	-
3	-102515.18	-102117.5 (-0.39)	-103282 (0.75)	-106080 (3.48)	-	-
4	-9221.24	-9097.35 (-1.34)	-9143.45 (-0.84)	-8846.03 (-4.07)	-	-
5	0	0	0	0	-	-
6	-22382.84	-21819.11 (-2.52)	-22445 (0.28)	-22616.1 (1.04)	-	-
7	-12626.8	-13035.05 (3.23)	-12716.9 (0.71)	-12760.3 (1.06)	-	-
8	0	0	0	0	-	-
9	-8686.49	-8260.81 (-4.9)	-7851.48 (-9.61)	-6884.64 (-20.74)	-	-
ALL SRSS	180171.37	180958.9 (0.44)	175051.4 (-2.84)	189680.1 (5.28)	160393.43 (-10.98)	173203.79 (-3.87)
ALL CQC	185357.62	185888.57 (0.29)	179882.5 (-2.95)	195681.3 (5.57)	164315.07 (-11.35)	178126.49 (-3.9)

Table 6.53 gives the total overturning moment at the base of the building structure about *x*-axis. For the SRSS, the closest result to MFTProgV2 result is obtained from StaadProV8i which is of 0.44 % difference, and for the CQC, the closest result is obtained from StaadProV8i which is of 0.29 % difference.

6.4.5 P-Delta response spectra analysis

The P-Delta second order analysis was incorporated in the dynamic analysis using the direct iteration method and the inverse iteration method (Stodola concept), and using the cubic-displacement shape. As for the linear dynamic analysis, the natural first nine natural frequencies together with the corresponding mode shapes were computed.

Table 6.54: Comparisons of the first nine P-Delta natural frequencies (cycle/second):

Mode	StaadProV8i[1] (%Diff)	MFTProgV2[1] (%Diff)	MFTProgV2[2]	ETABS(thin)[2] (%Diff)	ETABS(thick)[2] (%Diff)
1	0.124 (0)	0.124 (0)	0.124	0.118 (-4.84)	0.133 (7.26)
2	0.136 (0.74)	0.135 (0)	0.135	0.129 (-4.44)	0.145 (7.41)
3	0.202 (1)	0.199 (-0.5)	0.200	0.195 (-2.5)	0.206 (3)
4	0.466 (2.64)	0.453 (-0.22)	0.454	0.438 (-3.52)	0.477 (5.07)
5	0.507 (3.47)	0.49 (0)	0.490	0.476 (-2.86)	0.516 (5.31)
6	0.812 (3.7)	0.782 (-0.13)	0.783	0.771 (-1.53)	0.803 (2.55)
7	0.996 (3.43)	0.961 (-0.21)	0.963	0.941 (-2.28)	0.994 (3.22)
8	1.08 (4.25)	1.036 (0)	1.036	1.016 (-1.93)	1.072 (3.47)
9	1.745 (4.62)	1.665 (-0.18)	1.668	1.637 (-1.86)	1.697 (1.74)

The superscripts 1 and 2 refer to Proposal 1 and Proposal 2 respectively.

As shown in Table 6.54, the comparison between the natural frequencies using MFTProgV2 and the different analysis packages shows good agreement.

Table 6.55: Comparison of the P-Delta modal masses participating ratios in *x*-direction:

Mode	MFTProgV2	StaadProV8i(%Diff)	ETABS(thin) (%Diff)	ETABS(thick) (%Diff)
1	0	0	0	0
2	73.313	73.65 (0.46)	73.025 (-0.39)	73.656 (0.47)
3	0	0	0	0
4	0	0	0	0
5	12.802	12.96 (1.23)	12.925 (0.96)	12.673 (-1.01)
6	0	0	0	0
7	0	0	0	0
8	5.398	5.26 (-2.56)	5.458 (1.11)	5.28 (-2.19)
9	0	0	0	0

Table 6.56: Comparison of the accumulated P-Delta modal masses participating ratios in *x*-direction:

Mode	MFTProgV2	StaadProV8i(%Diff)	ETABS(thin) (%Diff)	ETABS(thick) (%Diff)
1	0	0	0	0
2	73.313	73.647 (0.46)	73.025 (-0.39)	73.656 (0.47)
3	73.313	73.647 (0.46)	73.025 (-0.39)	73.656 (0.47)
4	73.313	73.647 (0.46)	73.025 (-0.39)	73.656 (0.47)
5	86.116	86.611 (0.57)	85.95 (-0.19)	86.328 (0.25)
6	86.116	86.611 (0.57)	85.95 (-0.19)	86.328 (0.25)
7	86.116	86.611 (0.57)	85.95 (-0.19)	86.328 (0.25)
8	91.513	91.875 (0.4)	91.408 (-0.11)	91.608 (0.1)
9	91.513	91.875 (0.4)	91.408 (-0.11)	91.608 (0.1)

Table 6.57: Comparison of the P-Delta modal masses participating ratios in *y*-direction:

Mode	MFTProgV2	StaadProV8i(%Diff)	ETABS(thin) (%Diff)	ETABS(thick) (%Diff)
1	47.881	48.63 (1.56)	46.719 (-2.43)	47.473 (-0.85)
2	0	0	0	0
3	22.784	22.34 (-1.95)	23.733 (4.17)	23.312 (2.32)
4	7.979	8.12 (1.77)	7.917 (-0.78)	7.91 (-0.86)
5	0	0	0	0
6	7.04	7.04 (0)	7.173 (1.89)	7.118 (1.11)
7	3.082	3.07 (-0.39)	3.105 (0.75)	2.991 (-2.95)
8	0	0	0	0
9	2.016	1.86 (-7.74)	1.954 (-3.08)	1.813 (-10.07)

Table 6.58: Comparison of the accumulated P-Delta modal masses participating ratios in *y*-direction:

Mode	MFTProgV2	StaadProV8i(%Diff)	ETABS(thin) (%Diff)	ETABS(thick) (%Diff)
1	47.881	48.633 (1.57)	46.719 (-2.43)	47.473 (-0.85)
2	47.881	48.633 (1.57)	46.719 (-2.43)	47.473 (-0.85)
3	70.666	70.972 (0.43)	70.452 (-0.3)	70.785 (0.17)
4	78.645	79.091 (0.57)	78.369 (-0.35)	78.695 (0.06)
5	78.645	79.091 (0.57)	78.369 (-0.35)	78.695 (0.06)
6	85.685	86.135 (0.53)	85.542 (-0.17)	85.813 (0.15)
7	88.767	89.204 (0.49)	88.647 (-0.14)	88.804 (0.04)
8	88.767	89.204 (0.49)	88.647 (-0.14)	88.804 (0.04)
9	90.783	91.064 (0.31)	90.601 (-0.2)	90.616 (-0.18)

The comparisons between the modal mass participating ratios and their accumulations in the *x* and *y* directions using MFTProgV2, StaadProV8i and ETABS thin and thick plates show very small differences, as shown in Tables 6.55 to 6.58.

I- Lateral Displacement at the top floor of the 3D building model

Tables 6.59 and 6.60, show the lateral displacement response at the top floor of the building model due to the UBC design code acceleration response curve, obtained by response spectra analysis in *y*-direction using MFTProgV2 and the other packages for proposals 1 and 2 respectively.

Table 6.59: Comparison of the P-Delta lateral displacement response at the top floor (m), Proposal 1

Response	MFTProgV2	StaadProV8i(%Diff)	ETABS(thin) (%Diff)	ETABS(thick) (%Diff)
ALL SRSS	0.510297	0.512864 (0.5)	0.527419 (3.36)	0.474082 (-7.1)
ALL CQC	0.515622	0.518369 (0.53)	0.532894 (3.35)	0.480804 (-6.75)

Table 6.60: Comparison of the P-Delta lateral displacement response at the top floor (m), Proposal 2

Response	MFTProgV2	StaadProV8i(%Diff)	ETABS(thin) (%Diff)	ETABS(thick) (%Diff)
ALL SRSS	0.49683	0.512864 (3.23)	0.527419 (6.16)	0.474082 (-4.58)
ALL CQC	0.50595	0.518369 (2.45)	0.532894 (5.33)	0.480804 (-4.97)

Proposal 1 used the displacements responses calculated from the acceleration response ($S_d = S_a/\omega^2$), and the participation factor of the mode, while Proposal 2 used the displacement obtained from a full frame analysis using the equivalent static forces obtained from the acceleration responses.

Table 6.59 gives the total lateral displacement at the top floor of the building structure for proposal 1. For the SRSS, the closest results to MFTProgV2 result is obtained from StaadProV8i which is of 0.50 % difference, and for the CQC, the closest result is obtained from StaadProV8i which is of 0.53 % difference.

Table 6.60 gives the total lateral displacement at the top floor of the building structure for proposal 2. For the SRSS, the closest result to MFTProgV2 is obtained from StaadProV8i which is of 3.23 % difference, and for the CQC, the closest result is obtained from StaadProV8i which is of 2.45 % difference.

MFTProgV2 proposal 1 gives closer results to the different packages than proposal 2.

II- Resultant Shear Force at the Base of the 3D building model

Table 6.61, shows the resultant shear force response at the base of the building due to the UBC design code acceleration response curve, obtained by response spectra analysis in *y*-direction using MFTProgV2 and the other packages.

Table 6.61.: Comparisons of the Response Spectrum P-Delta Base Shear force (kN):

Mode	MFTProgV2	StaadProV8i(%Diff)	ETABS(thin) (%Diff)	ETABS(thick) (%Diff)
1	2005.87	2030.48 (1.23)	1860.32 (-7.26)	2130.75 (6.23)
2	0	0	0	0
3	1533.88	1523.34 (-0.69)	1559.43 (1.67)	1625.35 (5.96)
4	1234.13	1287.42 (4.32)	1183.01 (-4.14)	1280.35 (3.75)
5	0	0	0	0
6	1868.76	1933.81 (3.48)	1873.58 (0.26)	1935.15 (3.55)
7	1005.49	1030.98 (2.54)	991.11 (-1.43)	1002.33 (-0.31)
8	0	0	0	0
9	1160.49	1107.51 (-4.57)	1107.15 (-4.6)	1057.38 (-8.89)
ALL SRSS	3708.017	3758.99 (1.37)	3607.01 (-2.72)	3832.58 (3.36)
ALL CQC	3892.608	3936.16 (1.12)	3791.92 (-2.59)	4024.72 (3.39)

Table 6.61 gives the total shear forces at the base of the building structure in *y*-direction. For the SRSS, the closest result to MFTProgV2 result is obtained from StaadProV8i which is of 1.37 % difference, and for the CQC, the closest result is obtained from StaadProV8i which is of 1.12 % difference.

III- Resultant overturning moment at the Base of the 3D building model

Table 6.62, shows the resultant overturning moment response at the base of the building due to the UBC design code acceleration response curve, obtained by response spectra analysis in *y*-direction using MFTProgV2 and the other packages.

Table 6.62: Comparisons of the Response Spectrum P-Delta Base Overturning Moment:

Mode	MFTProgV2	StaadProV8i(%Diff)	ETABS(thin) (%Diff)	ETABS(thick) (%Diff)
1	126256.2	127431.8 (0.93)	117317 (-7.08)	134041 (6.17)
2	0	0	0	0
3	100202.5	99637.42 (-0.56)	102035 (1.83)	106332 (6.12)
4	8114.251	8042.87 (-0.88)	7886.82 (-2.8)	7688.28 (-5.25)
5	0	0	0	0
6	22219.54	21529.95 (-3.1)	22205.3 (-0.06)	22448.3 (1.03)
7	12864.73	13152.42 (2.24)	12925.8 (0.47)	12812.3 (-0.41)
8	0	0	0	0
9	7775.739	7106.545 (-8.61)	7166.84 (-7.83)	6317.45 (-18.75)
ALL SRSS	163605.25	164067.6 (0.28)	157949.6 (-3.46)	173322.3 (5.94)
ALL CQC	167270.83	167570.2 (0.18)	161333.1 (-3.55)	177753 (6.27)

Table 6.62 gives the total overturning moment (in kN.m), at the base of the building structure about *x*-axis. For the SRSS, the closest result to MFTProgV2 result is obtained from StaadProV8i which is of 0.28 % difference, and for the CQC, the closest result is also obtained from StaadProV8i which is of 0.18 % difference.

6.4.6 Time History Analysis for the 3D model

Time history analysis was performed for the 3D model. The natural frequencies and the corresponding mode shapes calculated in the previous section and used in the response spectra method were used with the El Centro earthquake time history acceleration records assumed applied at the base of the building. The assumed damping ratio is 5%. Comparisons of the lateral displacement at the top floor level, the base shear and the base overturning moment for MFTProgV2 and the different packages are presented.

I- Lateral Displacement at the top floor of the 3D building model

Figures 6.63 to 6.68 give the graphs for the lateral displacement history at the top floor of the building model due to El Centro earthquake, obtained by time history analysis in *y*-direction using MFTProgV2 and the other packages. The minimum and the maximum responses are shown in Table 6.63.

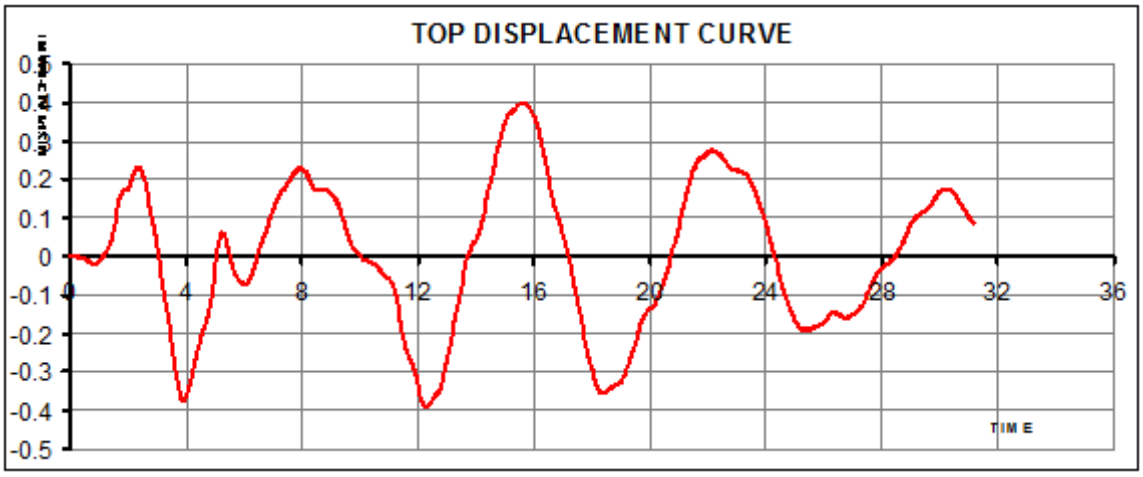

Figure 6.63: History of displacement in *y*-direction at the top floor level using MFTProgV2

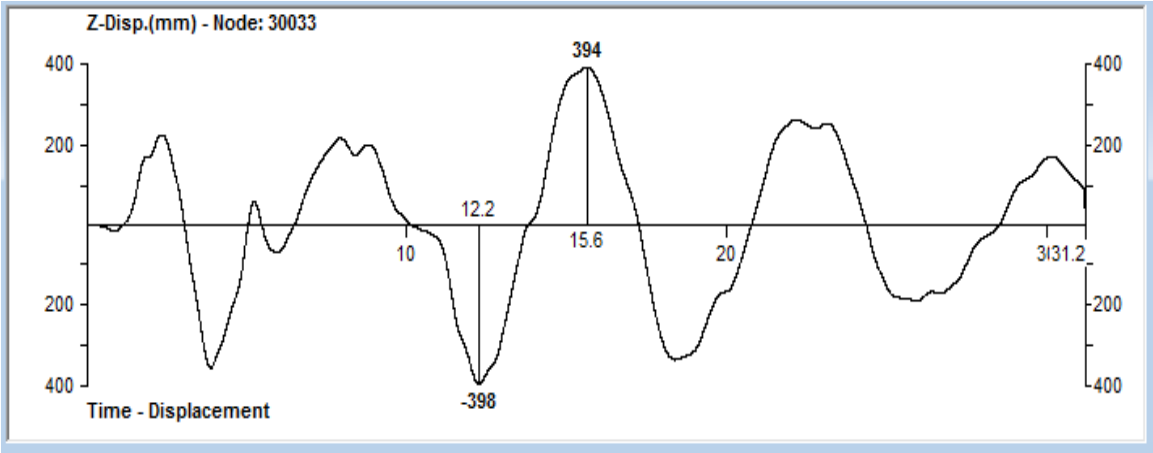

Figure 6.64: History of displacement in *y*-direction at the top floor level using StaadProV8i

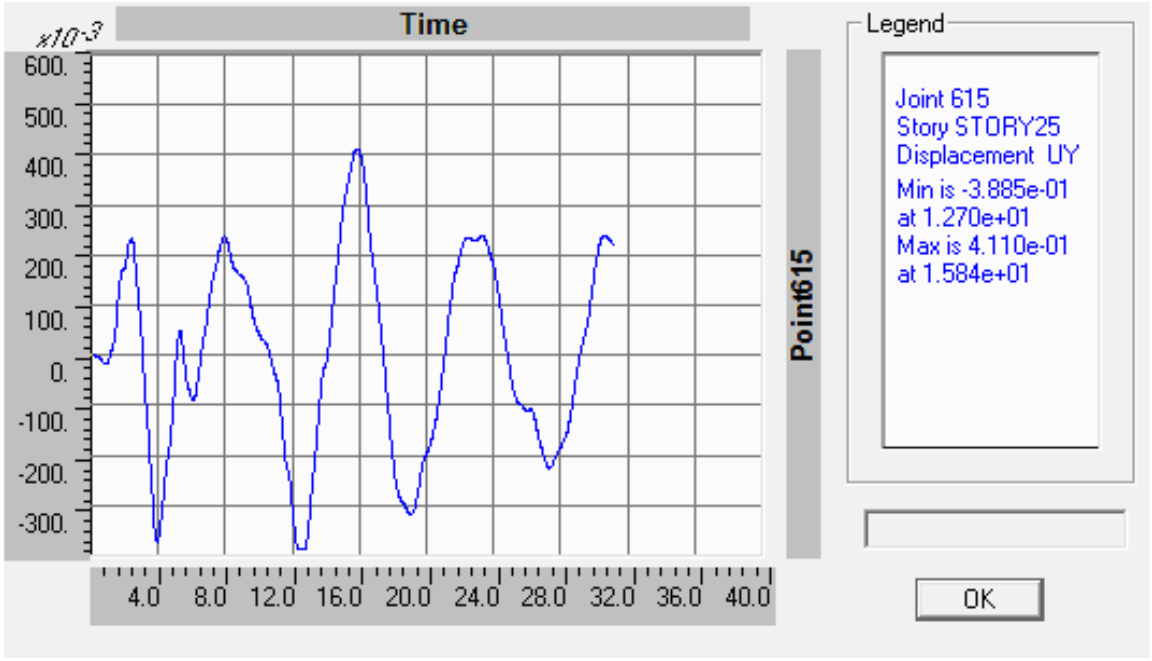

Figure 6.65: History of displacement in *y*-direction at the top floor level using ETABS (thin plate)

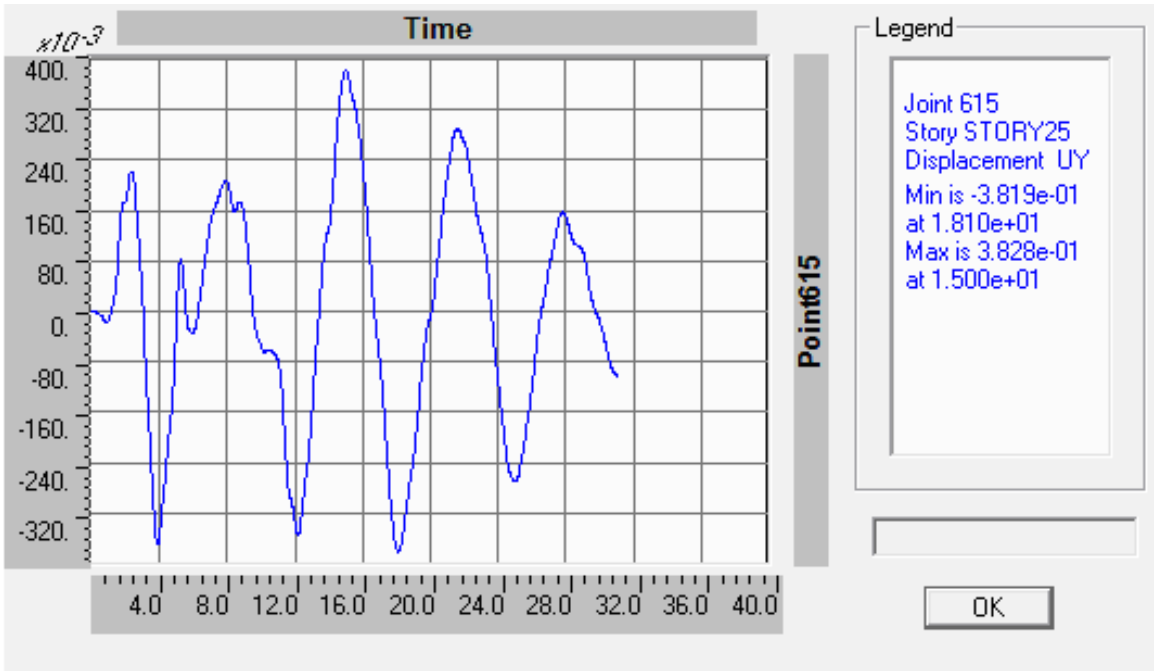

Figure 6.66: History of displacement in *y*-direction at the top floor level using ETABS (thick plate)

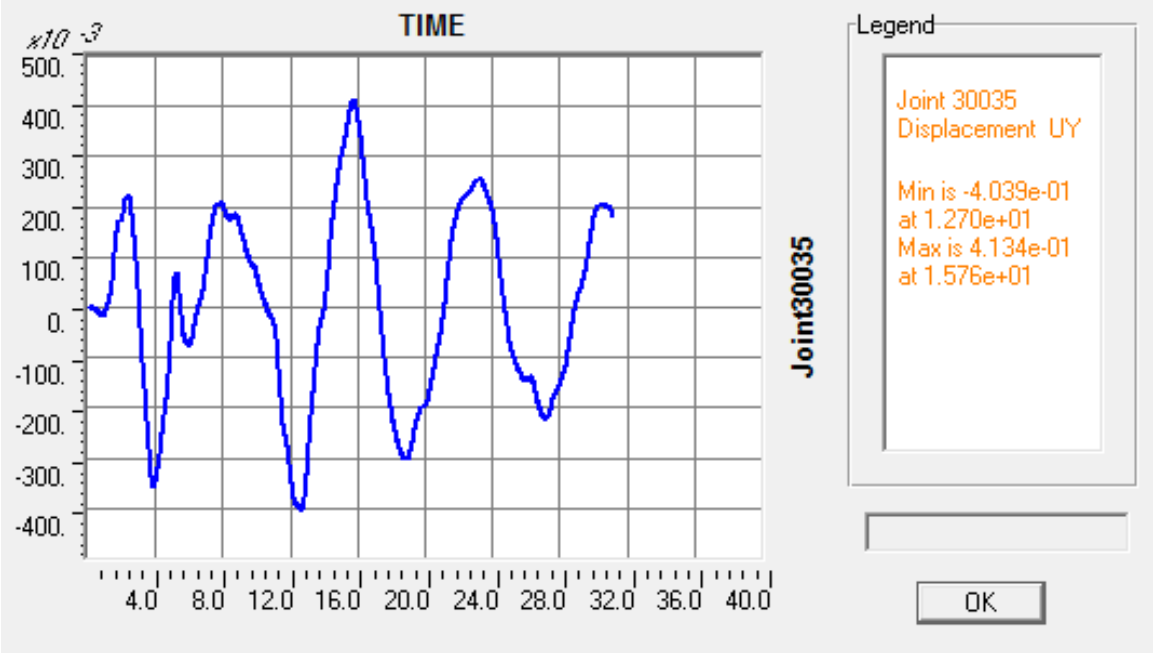

Figure 6.67: History of displacement in *y*-direction at the top floor level using SAP2000V16 (thin plate)

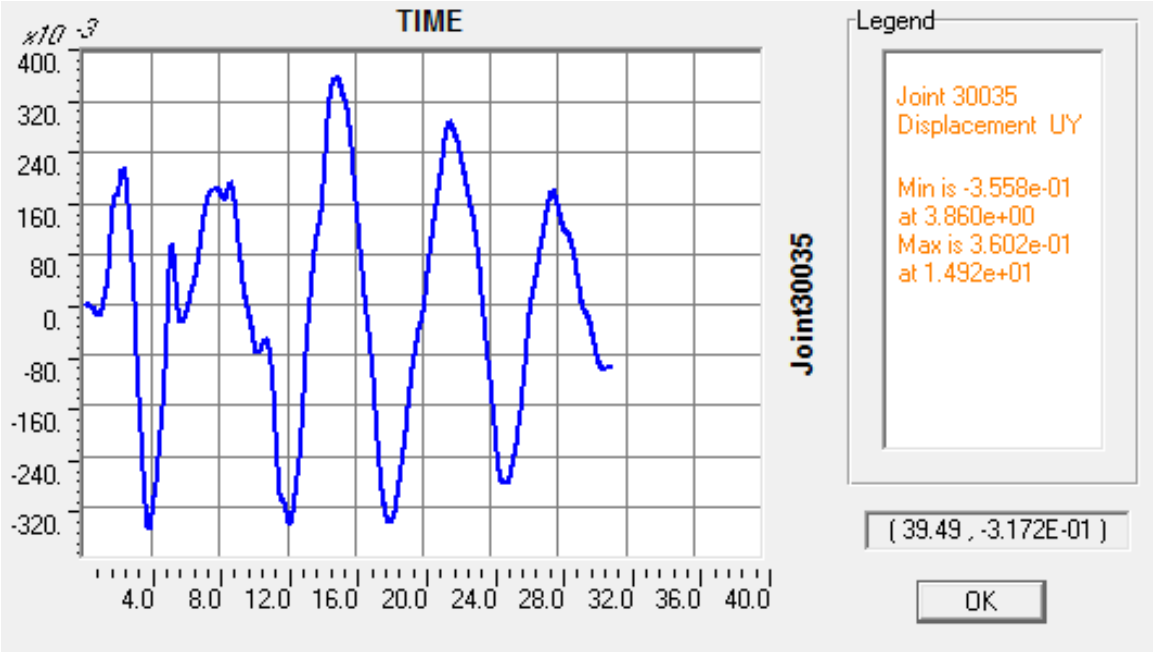

Figure 6.68: History of displacement in *y*-direction at the top floor level using SAP2000V16 (thick plate).

Table 6.63: Minimum and maximum displacements at the top floor (mm):

Response	MFTProgV2	StaadProV8i (%Diff)	ETABS(thin) (%Diff)	ETABS(thick) (%Diff)	SAP(thin) (%Diff)	SAP(thick) (%Diff)
Minimum	-390.3	-398 (1.97)	-388.5 (-0.46)	-381.9 (-2.15)	-403.9 (3.48)	-355.8 (-8.84)
At time	12.3	12.2	12.7	18.1	12.7	3.86
Maximum	399.3	394 (-1.33)	411 (2.93)	382.8 (-4.13)	413.4 (3.53)	360.2 (-9.79)
At time	15.64	15.6	15.84	15	15.76	1.492

The diagrams shown in Figures 6.63 to 6.68 are similar and show very good agreement. Table 6.63 gives the maximum and minimum response values together with the corresponding time. For the minimum response, the closest result to MFTProgV2 result is obtained from ETABS (thin) which is of -0.46 % difference, and for the maximum response, the closest result is obtained from StaadProV8i which is of -1.33 % difference.

II- Resultant Shear Force at the Base of the 3D building model

Figures 6.69 to 6.73 give the graphs for the resultant shear force history in kN at the base of the building obtained by time history analysis in *y*-direction using MFTProgV2 and the other packages. The minimum and the maximum responses are shown in Table 6.64.

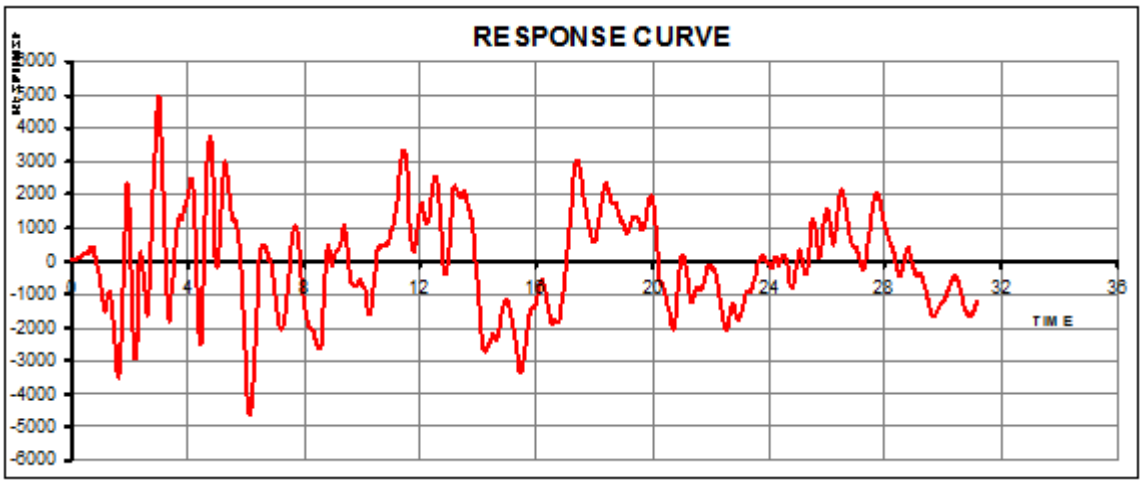

Figure 6.69: History of base Shear in *y*-direction using MFTProgV2

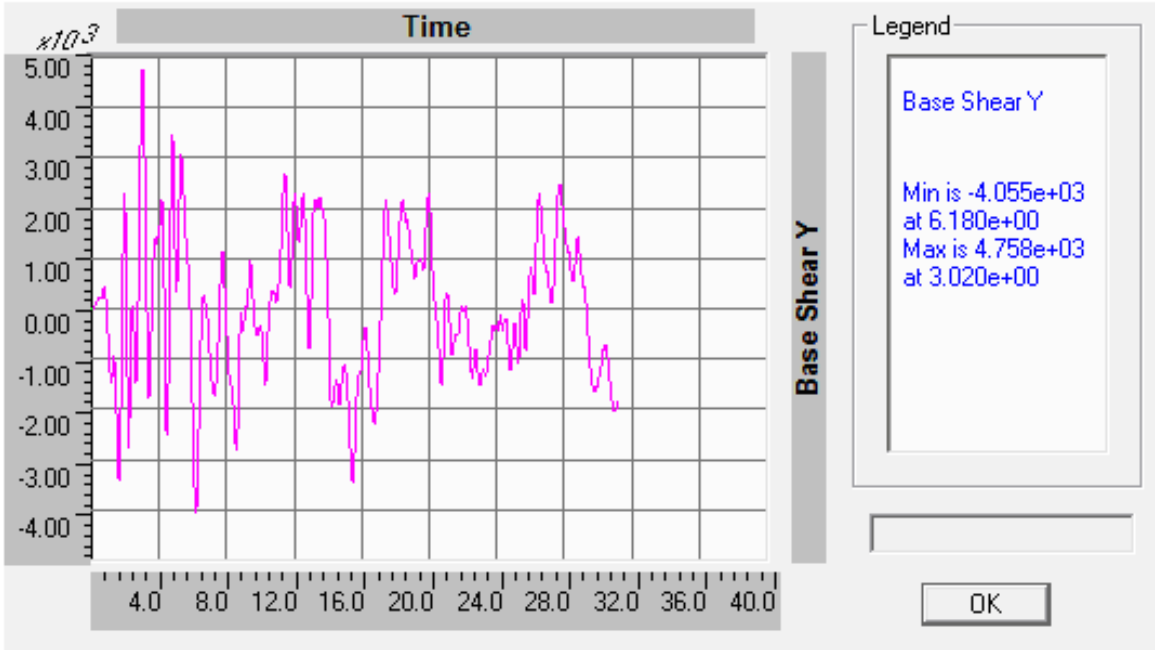

Figure 6.70: History of base Shear in *y*-direction using ETABS (thin plate)

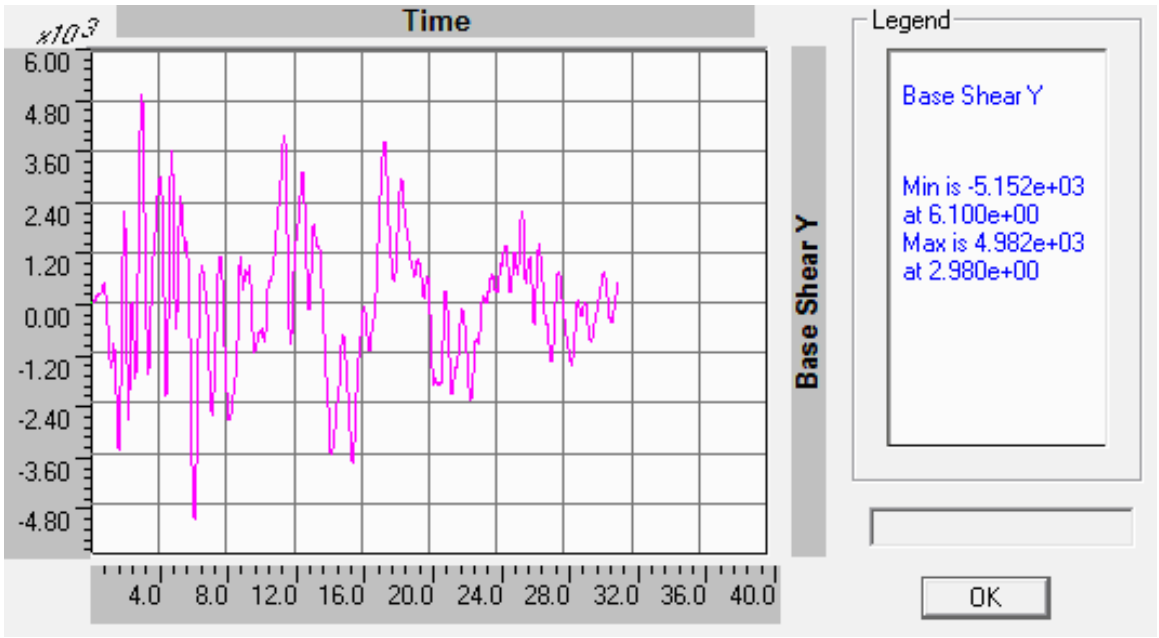

Figure 6.71: History of base Shear in *y*-direction using ETABS (thick plate)

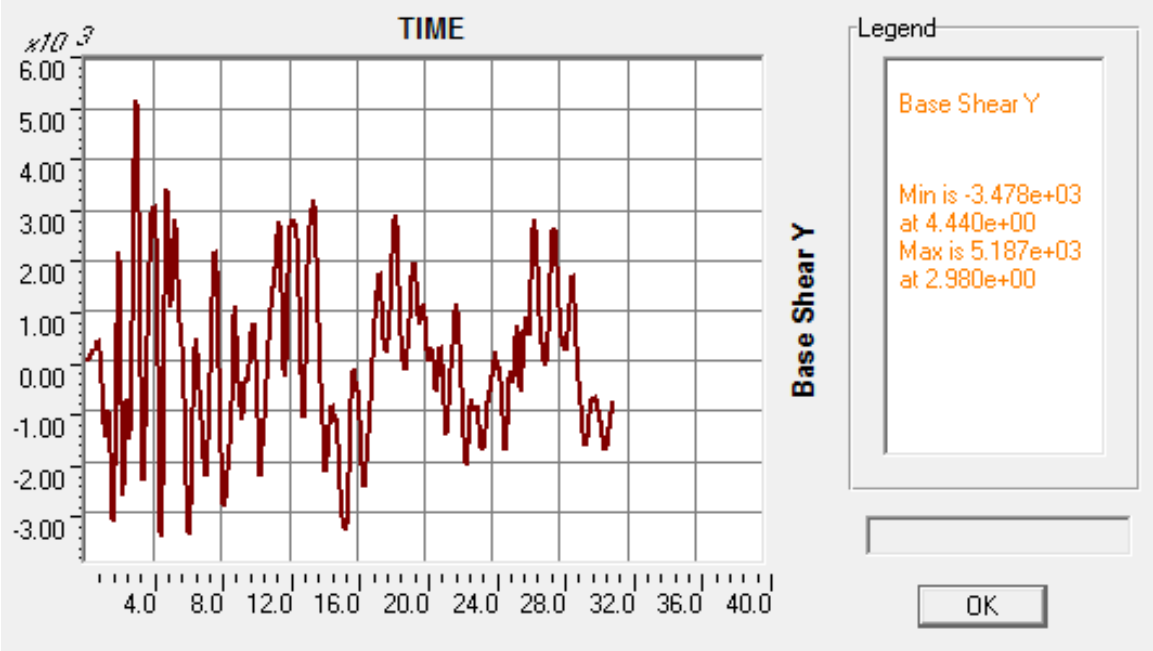

Figure 6.72: History of base Shear in *y*-direction using SAP2000V16 (thin plate)

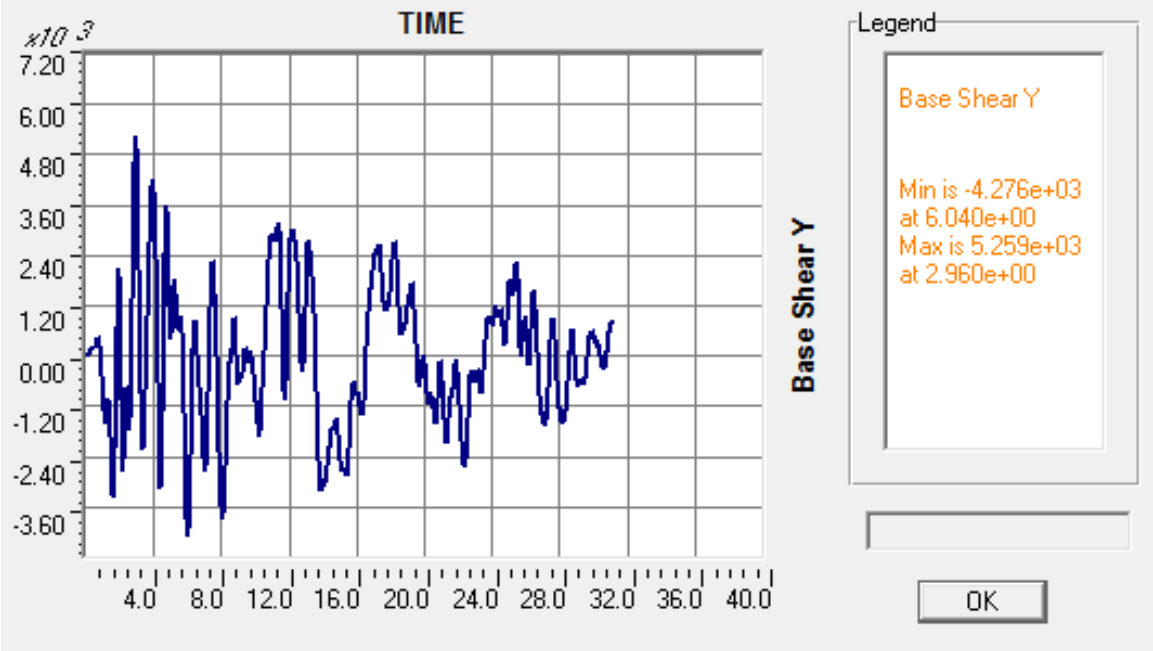

Figure 6.73: History of base Shear in *y*-direction using SAP2000V16 (thick plate)

Table 6.64: Minimum and maximum base shear (kN):

Response	MFTProgV2	StaadProV8i(%Diff)	ETABS(thin) (%Diff)	ETABS(thick) (%Diff)	SAP(thin) (%Diff)	SAP(thick) (%Diff)
Minimum	-4640	N.A	-4055 (-12.61)	-5152 (11.03)	-3478 (-25.04)	-4276 (-7.84)
At time	6.14	N.A	6.18	6.1	4.44	6.04
Maximum	4931.9	5190.859 (5.25)	4758 (-3.53)	4982 (1.02)	5187 (5.17)	5259 (6.63)
At time	3	2.951389	3.02	2.98	2.98	2.96

The diagrams shown in Figures 6.69 to 6.73 are similar and show very good agreement. Table 6.64 gives the maximum and minimum total shear forces at the base of the building structure with the corresponding time. For the minimum response, the closest result to MFTProgV2 result is obtained from SAP2000V16 (thick) which is of -7.84 % difference, and for the maximum response, the closest result is obtained from ETABS (thick) which is of 1.02 % difference.

III- Resultant overturning moment at the Base of the 3D building model

Figures 6.74 to 6.78 give the graphs for the resultant overturning moment history in kN.m at the base of the building about *x*-axis obtained by time history analysis in *y*-direction using MFTProgV2 and the other packages. The minimum and the maximum responses are shown in Table 6.65.

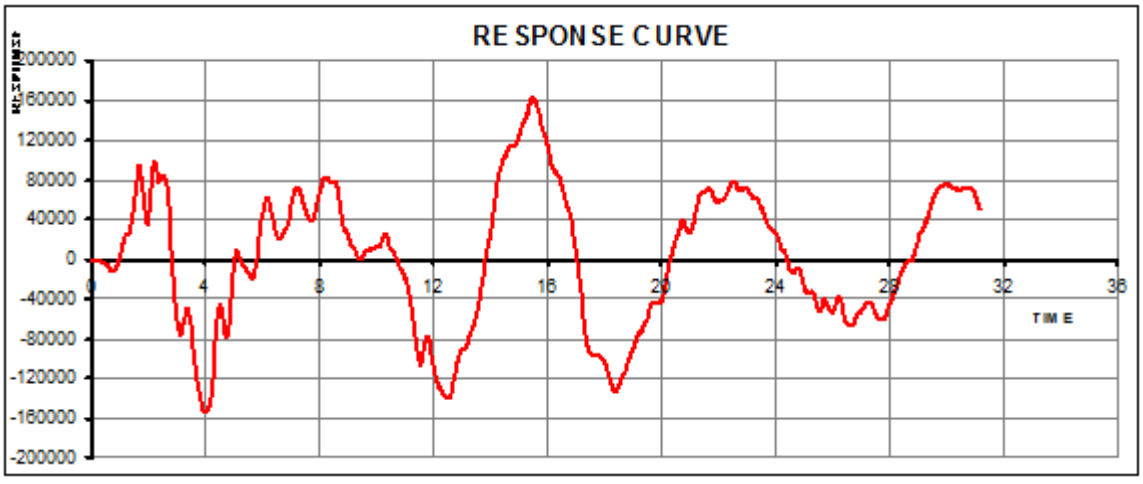

Figure 6.74: History of base overturning moment about *x*-direction using MFTProgV2

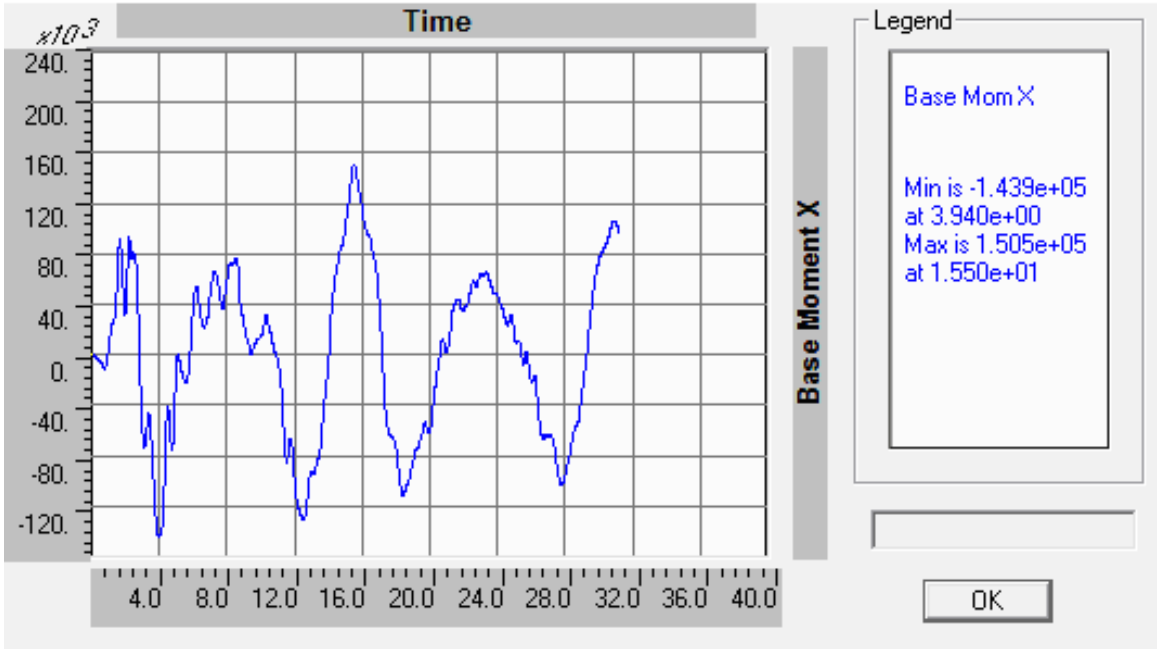

Figure 6.75: History of base overturning moment about *x*-direction using ETABS (thin plate)

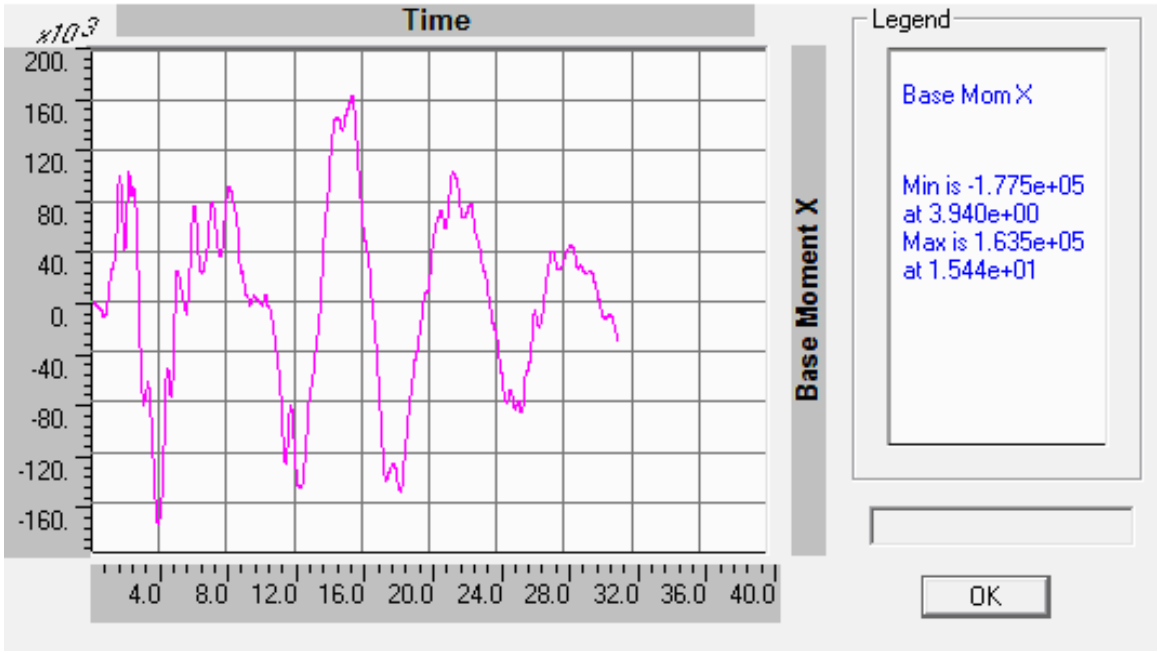

Figure 6.76: History of base overturning moment about *x*-direction using ETABS (thick plate)

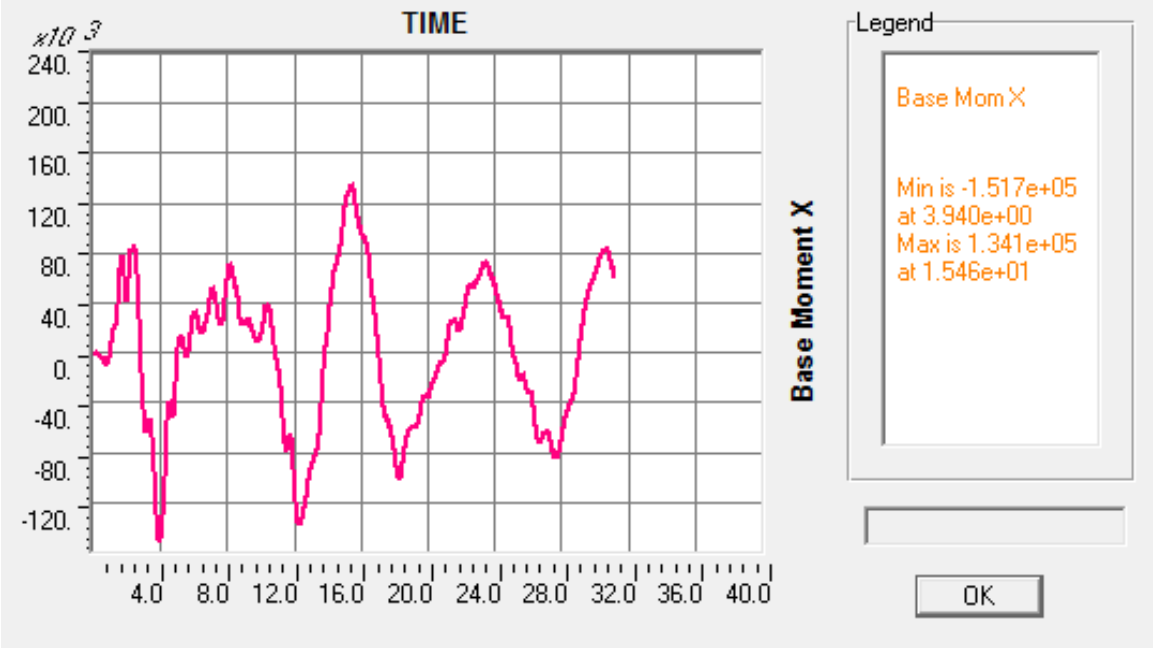

Figure 6.77: History of base overturning moment about *x*-direction using SAP2000V16 (thin plate)

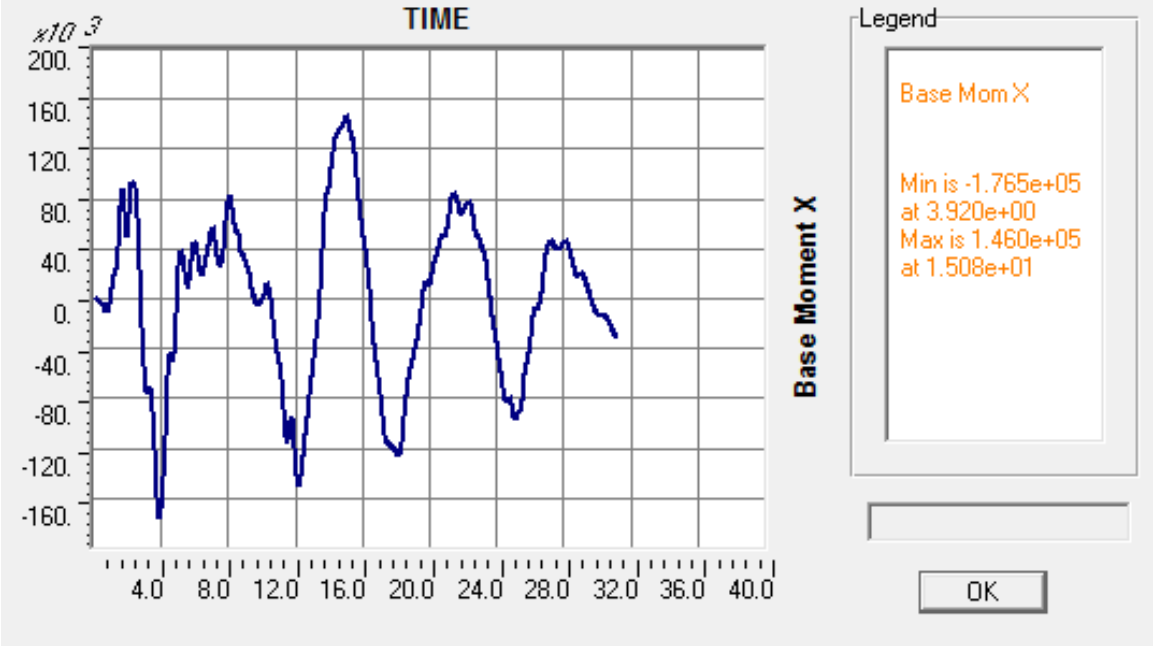

Figure 6.78: History of base overturning moment about *x*-direction using SAP2000V16 (thick plate)

Table 6.65: Minimum and maximum base overturning moment (kN.m):

Response	MFTProgV2	StaadProV8i (%Diff)	ETABS(thin) (%Diff)	ETABS(thick) (%Diff)	SAP(thin) (%Diff)	SAP(thick) (%Diff)
Minimum	-154288.9	N.A.	-143900 (-6.73)	-177500 (15.04)	-151700 (-1.68)	-176500 (14.4)
At time	3.96	N.A.	3.94	3.94	3.94	3.92
Maximum	162225.3	N.A.	150500 (-7.23)	163500 (0.79)	134100 (-17.34)	146000 (-10)
At time	15.48	N.A.	15.5	15.44	15.46	15.08

The diagrams shown in Figures 6.74 to 6.78 are similar and show very good agreement. Table 6.65 gives the maximum and minimum response values together with the corresponding time. For the minimum response, the closest result to MFTProgV2 result is obtained from SAP2000V16(thin) which is of -1.68 % difference, and for the maximum response, the closest result is obtained from ETABS (thick) which is of 0.79 % difference.

6.4.7 P-Delta time history analysis for the 3D model

The P-Delta second order analysis for the 3D model was incorporated in the dynamic time history analysis using the direct iteration method and the inverse iteration method (Stodola concept) and using the cubic-displacement shape. As for the linear dynamic analysis, the first nine natural frequencies together with the corresponding mode shapes were computed and used in the analysis.

I- Lateral Displacement at the top floor of the 3D building model

Figures 6.79 to 6.82 give the graphs for the lateral displacement at the top floor of the building model obtained by time history analysis in *y*-direction using MFTProgV2 and the other packages. The minimum and the maximum responses are shown in Table 6.66.

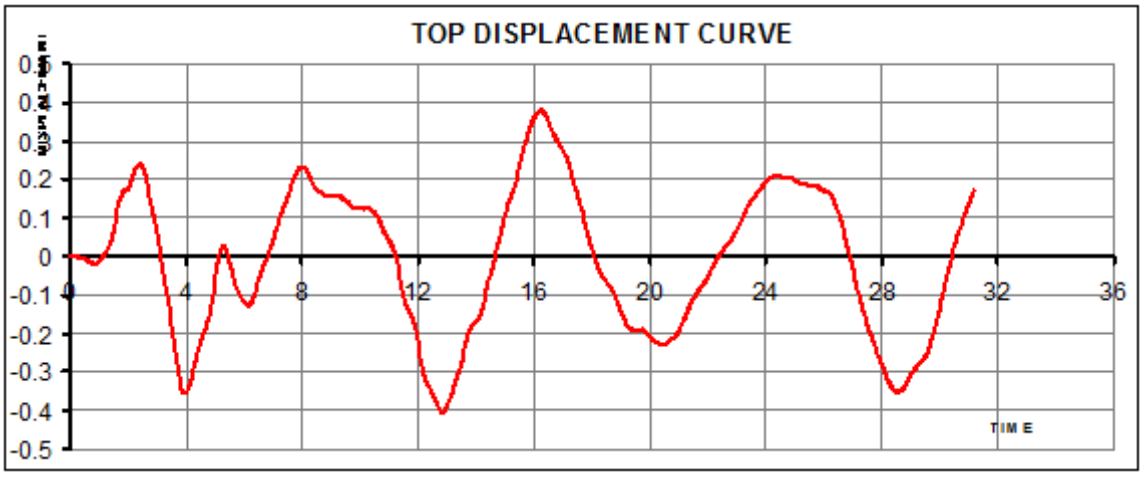

Figure 6.79: History of P-Delta displacement in *y*-direction at the top floor level using MFTProgV2

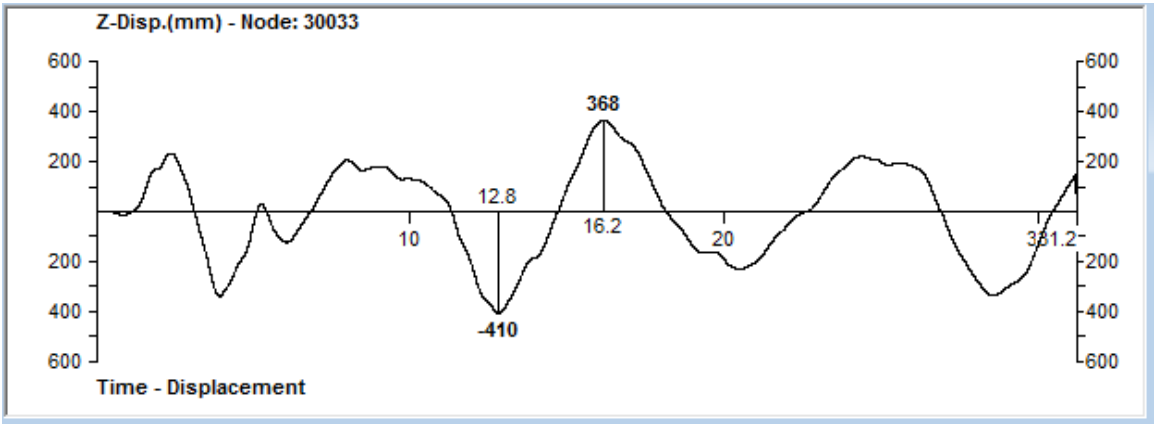

Figure 6.80: History of P-Delta displacement in *y*-direction at the top floor level using StaadProV8i

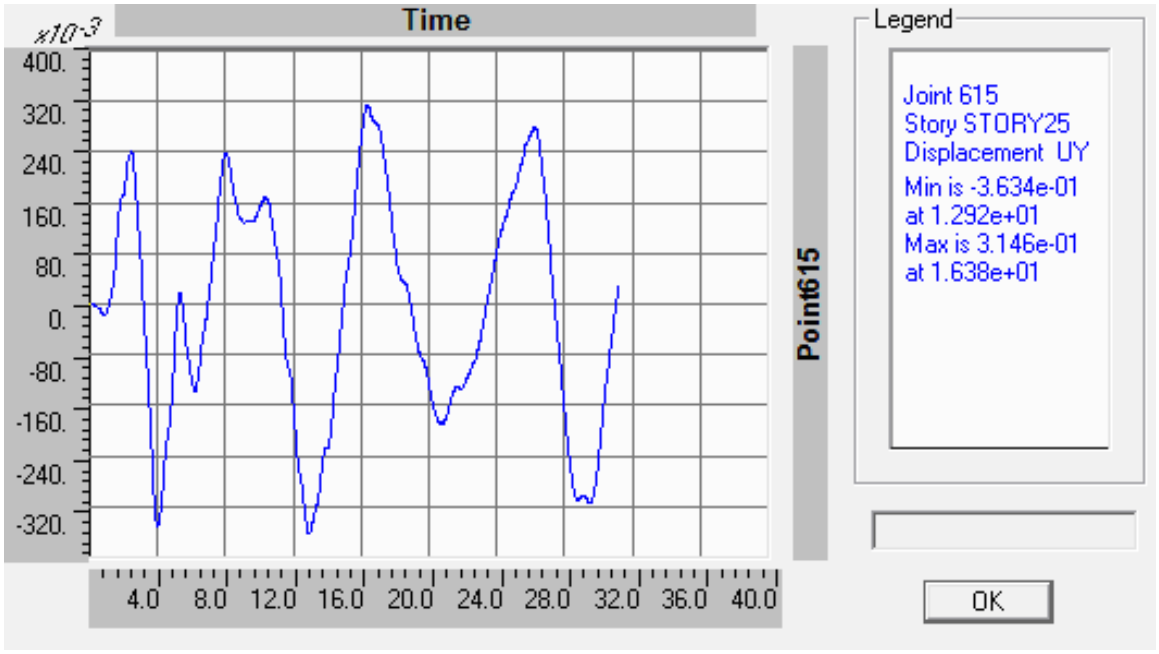

Figure 6.81: History of P-Delta displacement in *y*-direction at the top floor level using ETABS (thin plate)

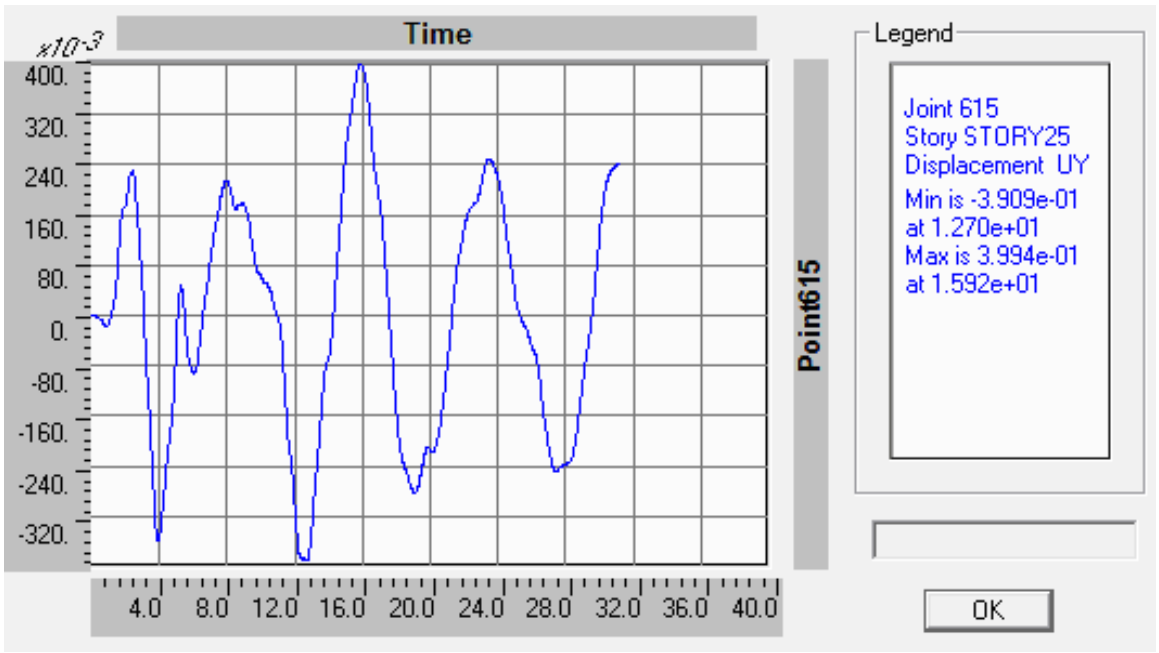

Figure 6.82: History of P-Delta displacement in *y*-direction at the top floor level using ETABS (thick plate)

Table 6.66: Minimum and maximum P-Delta displacements at the top floor (mm):

Response	MFTProgV2	StaadProV8i (%Diff)	ETABS(thin) (%Diff)	ETABS(thick) (%Diff)
Minimum	-404.6	-410 (1.33)	-363.4 (-10.18)	-390.9 (-3.39)
At time	12.84	12.8	12.92	12.7
Maximum	380.411	368 (-3.26)	314.6 (-17.3)	399.4 (4.99)
At time	16.26	16.2	16.38	15.92

The diagrams shown in Figures 6.79 to 6.82 are similar and show very good agreement. Table 6.66 gives the maximum and minimum response values together with the corresponding time. For the minimum response, the closest result to MFTProgV2 result is obtained from StaadProV8i which is of 1.33 % difference, and for the maximum response, the closest result is also obtained from StaadProV8i which is of -3.26 % difference.

II- Resultant Shear Force at the Base of the 3D building model

Figures 6.83 to 6.85 give the graphs for the resultant shear force history in kN at the base of the building obtained by time history analysis in *y*-direction using MFTProgV2 and the other packages. The minimum and the maximum responses are shown in Table 6.67.

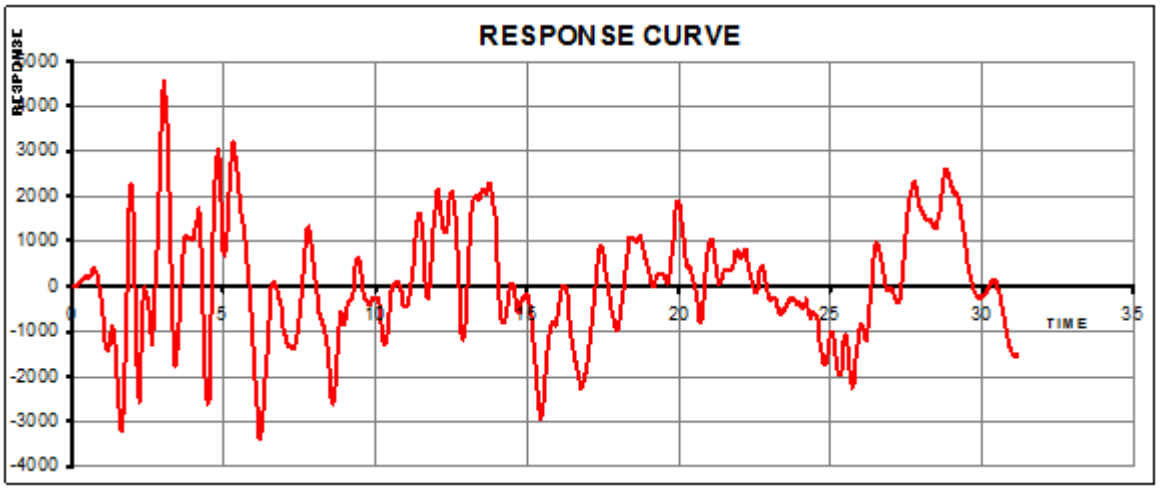

Figure 6.83: History of P-Delta base Shear history in *y*-direction using MFTProgV2

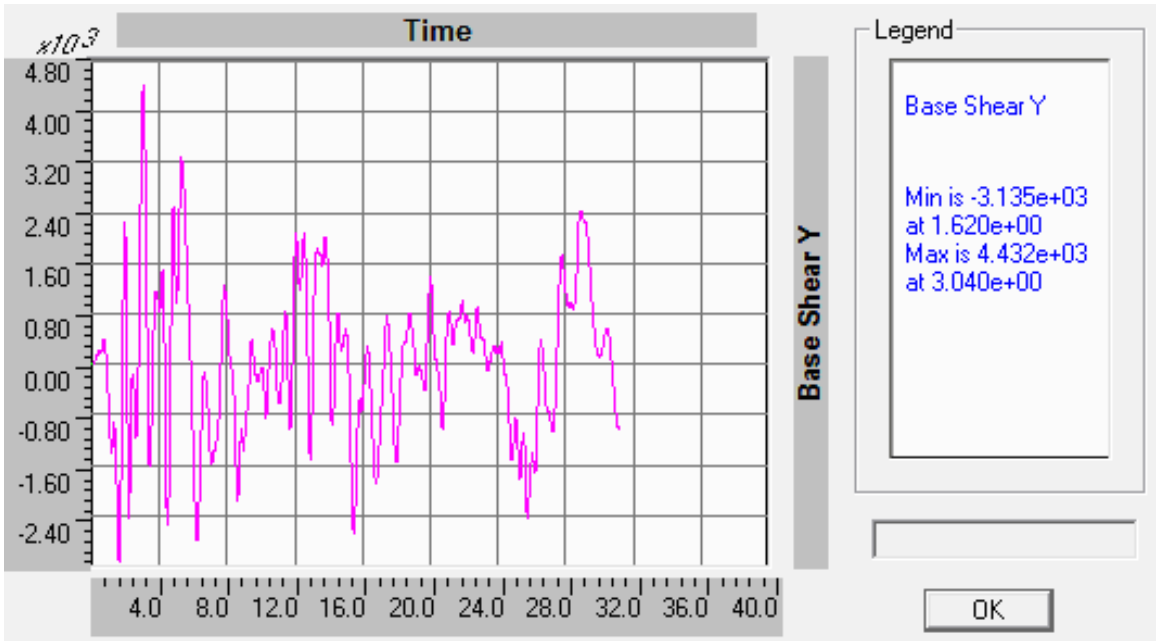

Figure 6.84: History of P-Delta base Shear in *y*-direction using ETABS (thin plate)

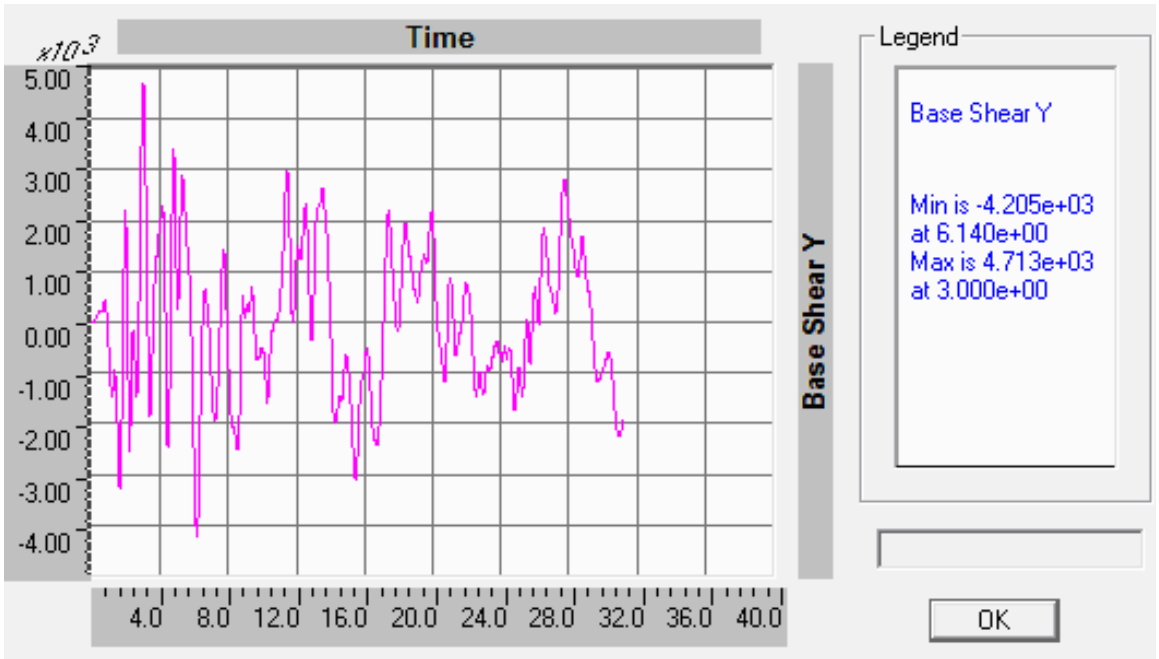

Figure 6.85: History of P-Delta base Shear in *y*-direction using ETABS (thick plate)

Table 6.67: Minimum and maximum P-Delta base shear (kN):

Response	MFTProgV2	StaadProV8i (%Diff)	ETABS(thin) (%Diff)	ETABS(thick) (%Diff)
Minimum	-3398.81	N.A.	-3135 (-7.76)	-4205 (23.72)
At time	6.2	N.A.	1.62	6.14
Maximum	4547.363	4888.243 (7.5)	4432 (-2.54)	4713 (3.64)
At time	3.02	2.973611	3.04	3

The diagrams shown in Figures 6.83 to 6.85 are similar and show very good agreement. Table 6.67 gives the maximum and minimum total shear forces at the base of the building structure with the corresponding time. For the minimum response, the closest result to MFTProgV2 result is obtained from ETABS (thin) which is of -7.76 % difference, and for the maximum response, the closest result is also obtained from ETABS (thin) which is of -2.54 % difference.

III- Resultant overturning moment at the Base of the 3D building model

Figures 6.86 to 6.88 give the graphs for the resultant overturning moment history in kN.m at the base of the building about *x*-axis obtained by time history analysis in *y*-direction using MFTProgV2 and the other packages. The minimum and the maximum responses are shown in Table 6.68.

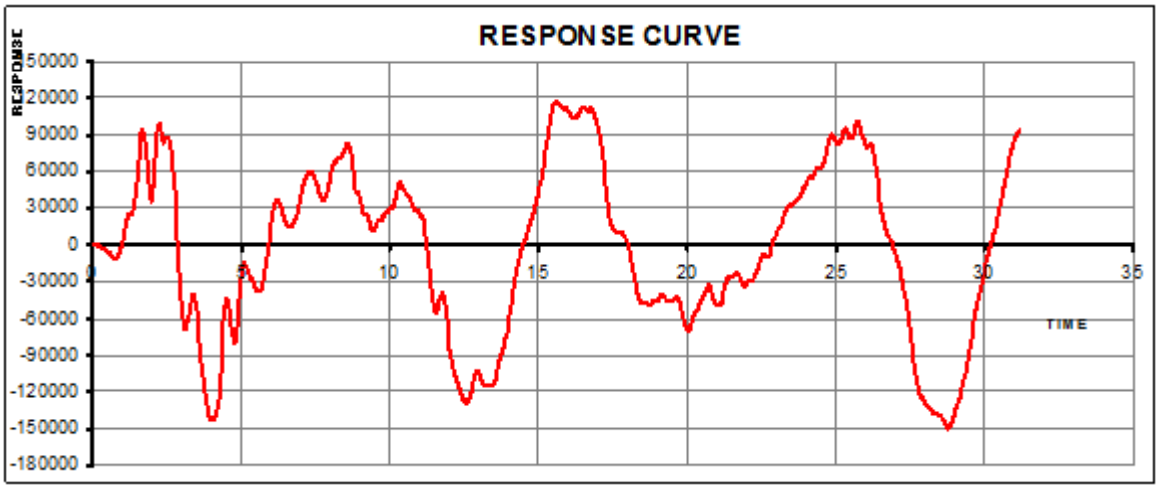

Figure 6.86: History of P-Delta base overturning moment about *x*-direction using MFTProgV2

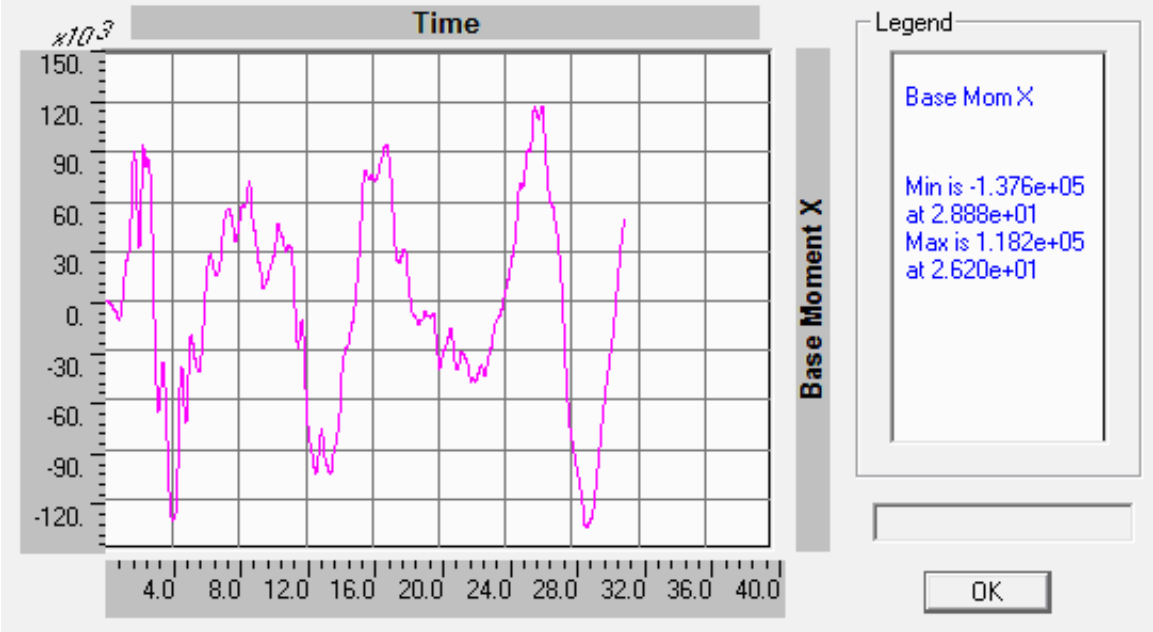

Figure 6.87: History of P-Delta base overturning moment about *x*-direction using ETABS (thin plate)

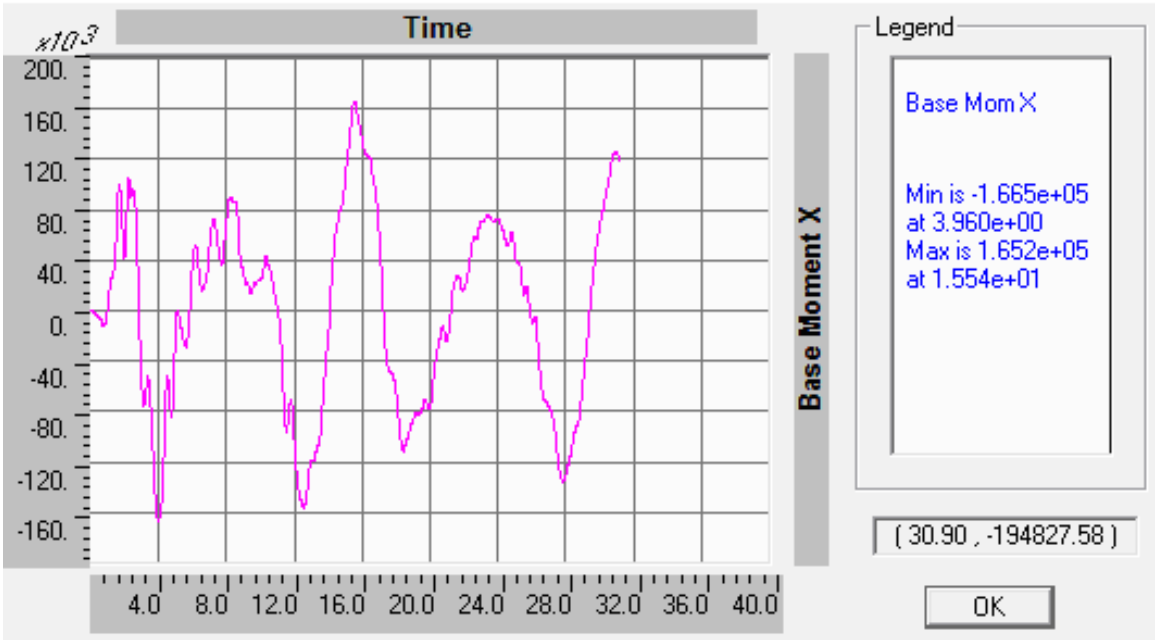

Figure 6.88: History of P-Delta base overturning moment about *x*-direction using ETABS (thick plate)

Table 6.68: Minimum and maximum P-Delta base overturning moment (kN.m):

Response	MFTProgV2	StaadProV8i (%Diff)	ETABS(thin) (%Diff)	ETABS(thick) (%Diff)
Minimum	-149895	N.A.	-137600 (-8.2)	-166500 (11.08)
At time	28.78	N.A.	28.88	3.96
Maximum	117620.2	N.A.	118200 (0.49)	165200 (40.45)
At time	15.6	N.A.	26.2	15.54

The diagrams shown in Figures 6.86 to 6.88 are similar and show very good agreement. Table 6.68 gives the maximum and minimum response values together with the corresponding time. For the minimum response, the closest result to MFTProgV2 result is obtained from ETABS (thin) which is of -8.2 % difference, and for the maximum response, the closest result is also obtained from ETABS (thin) which is of 0.49 % difference.

CHAPTER SEVEN

Conclusions and Recommendations

7.1 General Conclusions

1. A comprehensive review and study of the linear and nonlinear, static and dynamic, and stability analyses of tall buildings have been carried out. The study clearly shows the need for and importance of simplifying these complicated analyses methods.

2. Based on the moment transformation method (MT), the moment-force transformation method (MFT) has been developed to incorporate the axial deformations in the vertical members so as to be used in the analysis of super-tall buildings such as the tube and outrigger structures.

3. The moment-force transformation method (MFT) has been further developed to solve instability problems, nonlinear static, and linear and nonlinear dynamic analysis of tall buildings using the response spectra and the time-history analysis methods.

4. The computer program MFTProg has been developed and used in the static linear 2D and 3D analysis of tall buildings neglecting and/or including the axial deformations in the vertical members.

5. The computer program MFTProgV2 has been developed and used in the buckling analysis and the static and dynamic, linear and nonlinear 2D and 3D analysis of tall buildings.

6. The developed programs allow the use of different plates to represent slabs of different shapes or thicknesses in one model.

7. The accuracy of the results obtained using the developed programs were verified by comparison with results from known finite elements solvers.

8. The saving in computer storage and computing time provided by the proposed programs allow rapid re-analysis of the building to be accomplished in the preliminary analysis and design stages, and in the cases of repeated analysis types such as in the buckling and vibration problems.

9. The ease in data preparation and interpretation of final results, compared with finite element packages, is one of the main advantages of the method.

10. The simplicity in programming the method is an added advantage.

7.2 Results Conclusion

1- The maximum differences in the results obtained using MFTProg to analyze a two floor one-bay portal frame subjected to both vertical and horizontal loads compared with the published results were found to be -0.12 % for the bending moments and 0.13 % for the horizontal support reaction (neglecting shear deformations).

2- The maximum difference in the obtained moments results using MFTProg in the analysis of a two floor two-bay portal frame with setback subjected to both vertical and horizontal loads compared with the published results was found to be -0.11 % (considering shear deformations).

3- A fifteen floors multistory square building including four shear walls and subjected to unsymmetrical lateral loads was analyzed using MFTProg. The closest differences in the maximum shear forces and the bending moments and the displacements and rotations measured in the upper left corner of the building plan compared with the results obtained using the structural analysis packages ETABS and STAADPro2004, were as follows:

4.88 % for displacement in *x*-direction.

2.98 % for displacement in *y*-direction.

-2.34 % floor twist rotation.

The percentage difference of 7.85 % in the shear force was noticed in shear wall #4 with a difference of -0.2 % in bending moment. Shear wall #4 resists very small values of stresses compared with its section.

The differences in results of the other walls were:

0.19 % and -0.28 % for shear force and bending moment respectively, in shear wall #1.

-0.62 % and 1.93 % for shear force and bending moment respectively, in shear wall #2.

-0.92 % and 1.84 % for shear force and bending moment respectively, in shear wall #3.

4- As case study 1, the analysis of a 2D frame of 15 floors Building model subjected to vertical and lateral loads was carried out. The results obtained using MFTProgV2 were compared with those obtained using StaadPro2004, StaadProV8i, SAP200V16 and ETABS, for different analysis types as follows:

A-Static Linear and second order Analysis

In Static Linear and second order Analysis of the building model the maximum differences in the results with exact results were as follows:

0.27 % for lateral displacement at the top floor level in linear analysis.

0.07 % for axial displacement at the top floor level in linear analysis.

-0.66 % for maximum bending moment in the lower level of the columns in linear analysis.

0.26 % for lateral displacement at the top floor level in P-Delta analysis.

0.14 % for axial displacement at the top floor level in P-Delta analysis.

-0.60 % for maximum bending moment in the lower level of the columns in P-Delta analysis.

B-Buckling Analysis of the building model

The MFTProgV2 cubic shape results show very close critical buckling result compared to the values of StaadPro2014 (Stardyne advanced Engine), with a percentage difference of -0.03%.

C-Dynamic analysis of the building model

In a linear and second order dynamic analysis of the model, comparison between the natural frequencies, the mode shapes and the mass participation ratios show almost identical results.

D-Response Spectra Linear Analysis:

The lateral displacement results obtained by performing response spectrum analysis were calculated. For the SRSS method, very close results were obtained by the proposed method and SAP2000V16 with a maximum of 0.0006 % difference. For the CQC method, very close results were obtained from the proposed method and ETABS with a maximum of 0.0047 % difference.

The base shear results obtained by performing response spectrum analysis were calculated. For the SRSS method, the closest results to the proposed method results were obtained from SAP2000V16 with a maximum of 0.43 % difference, and for the CQC method, the closest results to the proposed method were obtained from StaadProV8i with 0.24 % maximum difference.

The base overturning moment results obtained by performing response spectrum analysis were calculated. For the SRSS method, the closest results to the proposed method results were obtained from ETABS with -0.01 % maximum difference, and for the CQC method,

the closest results to the proposed method results were obtained from ETABS which is of -0.01 % difference.

E-Response Spectra P-Delta Analysis

The lateral displacement results obtained by performing response spectrum P-Delta analysis were calculated. For the SRSS method, the closest results to the proposed method results were obtained from ETABS with a maximum of -0.00119 % difference, and for the CQC method, the closest results to the proposed method were obtained from ETABS with -0.00149 % maximum difference.

The base shear results obtained by performing response spectrum P-Delta analysis were calculated. For the SRSS method, the closest results to the proposed method results were obtained from ETABS with a maximum of 0.03 % difference, and for the CQC method, the closest results to the proposed method results were obtained from ETABS with 0.03% maximum difference.

For the SRSS method, the closest results for the base overturning moment results obtained by performing response spectrum P-Delta analysis to the proposed method results were obtained from ETABS with 0.01 % maximum difference, and for the CQC method, the closest results to the proposed method results were obtained from ETABS with 0.01 % maximum difference.

F-Time History Linear Analysis

The top floor lateral displacement results obtained by performing the time history analysis using the proposed method were calculated and compared with the results obtained from different analysis packages. The results variation curves were similar and show very close agreement. For the minimum response, the closest results to the proposed method results were obtained from ETABS with 0.01 % maximum difference, and for the maximum response, the closest results to the proposed method results were obtained also from ETABS with a maximum of 0.03 % difference.

The base shear results obtained by performing the time history analysis were calculated. The results variation curves were similar and show a very close agreement. For the minimum response, the closest results to the proposed method results were obtained from ETABS and SAP2000V16 with a maximum of 0.02 % difference, and for the maximum

response, the closest results to the proposed method results were obtained from ETABS with 0.05 % maximum difference.

The base overturning moment results obtained by performing the time history analysis were calculated. The results variation curves were similar and show a very close agreement. For the minimum response, the closest results to the proposed method were obtained from ETABS with a maximum of 0.01 % difference, and for the maximum response, the closest results to the proposed method results were obtained from ETABS with 0.01 % maximum difference.

G-Time History P-Delta Analysis

The top floor lateral displacement results obtained by performing the time history P-Delta analysis using the proposed method were calculated and compared with the results obtained from different analysis packages. The results variation curves were similar and show very close agreement. For the minimum response, the closest results to the proposed method results were obtained from ETABS with 0.03 % maximum difference, and for the maximum response, the closest results to the proposed method results were obtained also from ETABS with a maximum of 0.03 % difference.

The base shear results obtained by performing the time history P-Delta analysis were calculated. The results variation curves were similar and show a very close agreement. For the minimum response, the closest results to the proposed method results were obtained from ETABS with a maximum of 0.09 % difference, and for the maximum response, the closest results to the proposed method results were obtained from ETABS with 0.01 % maximum difference.

The base overturning moment results obtained by performing the time history P-Delta analysis were calculated. The results variation curves were similar and show a very close agreement. For the minimum response, the closest results to the proposed method were obtained from ETABS with a maximum of 0.38 % difference, and for the maximum response, the closest results to the proposed method results were obtained from ETABS with 0.25 % maximum difference.

5- As case study 2, the analysis of a 3D frame of 25 floors Building model subjected to vertical and wind loads was carried out. The results obtained using MFTProgV2 were

compared with those obtained using StaadPro2004, StaadProV8i, SAP200V16 and ETABS, for different analysis types as follows:

A-Static Linear and second order Analysis

In Static Linear and second order Analysis of the building model the maximum differences in the results with exact results in the building center (column#10), were as follows:

-3.5 % for lateral displacement in *y*-direction in linear analysis.

0.47 % for axial deformation in linear analysis.

-7.69 % floor twist rotation, in linear analysis.

-4.63 % for lateral displacement in *y*-direction in P-Delta analysis.

0.35% for axial deformation in P-Delta analysis.

-8.99 % floor twist rotation in P-Delta analysis.

-1.37 % for maximum bending moment in U-Shaped Core, in linear analysis.

-1.77 % for maximum bending moment in U-Shaped Core, in P-Delta analysis.

-2.24 % for maximum bending moment in Edge Shear Wall, in linear analysis.

-3.36 % for maximum bending moment in Edge Shear Wall, in P-Delta analysis.

In additional discussion of the results, an alternative analysis has been carried out using a borrowed StaadPro Floor stiffness. The analysis yields the following results:

Displacements and rotation in the top floor level in the building center (column #10):

-0.05 % for lateral displacement in *y*-direction in linear analysis.

0.00 % for axial deformation in linear analysis.

0.00 % floor twist rotation, in linear analysis.

-0.13 % for lateral displacement in *y*-direction in P-Delta analysis.

0.00 % for axial deformation in P-Delta analysis.

-0.00 % floor twist rotation in P-Delta analysis.

-0.01 % for maximum bending moment in U-Shaped Core, in linear analysis.

0.01 % for maximum bending moment in U-Shaped Core, in P-Delta analysis.

0.27 % for maximum bending moment in Edge Shear Wall, in linear analysis.

0.18 % for maximum bending moment in Edge Shear Wall, in P-Delta analysis.

The elapsed running time by MFTProg used in solving a 150 floor model was 83 seconds only. Comparison between the number of unknowns using MFTProg and the

conventional matrix methods for the 150 floors model showed that there were 1,102,620 coupled unknowns in the case of conventional matrix methods compared to 12,735 partially coupled unknowns when using MFTProg which is a ratio of 86 times.

B-Buckling Analysis of the building model

The MFTProgV2 Euler functions results show very close critical buckling result compared to the value of StaadProV8i, with a percentage difference of 0.11%.

C-Dynamic analysis of the building model

In a linear and second order dynamic analysis of the model, comparison between the natural frequencies and the mass participation ratios in the two directions show very close agreement.

D-Response Spectra Linear Analysis:

The lateral displacement results obtained by performing response spectrum analysis were calculated. For the SRSS method, very close results were obtained by the proposed method and StaadProV8i with a maximum of 0.34 % difference. For the CQC method, very close results were obtained from the proposed method and StaadProV8i with a maximum of 0.37 % difference.

The base shear results obtained by performing response spectrum analysis were calculated. For the SRSS method, the closest results to the proposed method results were obtained from StaadProV8i with a maximum of 1.78 % difference, and for the CQC method, the closest results to the proposed method were obtained from SAP2000V16 with -0.67 % maximum difference.

The base overturning moment results obtained by performing response spectrum analysis were calculated. For the SRSS method, the closest results to the proposed method results were obtained from StaadProV8i with 0.44 % maximum difference, and for the CQC method, the closest results to the proposed method results were obtained from StaadProV8i which is of 0.29 % difference.

E-Response Spectra P-Delta Analysis

The lateral displacement results obtained by performing response spectrum P-Delta analysis were calculated. For the SRSS method, the closest results to the proposed method results were obtained from StaadProV8i with a maximum of 0.50 % difference,

and for the CQC method, the closest results to the proposed method were obtained from StaadProV8i with 0.53 % maximum difference.

The base shear results obtained by performing response spectrum P-Delta analysis were calculated. For the SRSS method, the closest results to the proposed method results were obtained from StaadProV8i with a maximum of 1.37 % difference, and for the CQC method, the closest results to the proposed method results were obtained from StaadProV8i with 1.12 % maximum difference.

For the SRSS method, the closest results for the base overturning moment results obtained by performing response spectrum P-Delta analysis to the proposed method results were obtained from StaadProV8i with 0.28 % maximum difference, and for the CQC method, the closest results to the proposed method results were obtained from StaadProV8i with 0.18 % maximum difference.

F-Time History Linear Analysis

The top floor lateral displacement results obtained by performing the time history analysis using the proposed method were calculated and compared with the results obtained from different analysis packages. The results variation curves were similar and show very close agreement. For the minimum response, the closest results to the proposed method results were obtained from ETABS (thin) with -0.46 % maximum difference, and for the maximum response, the closest results to the proposed method results were obtained also from StaadProV8i with a maximum of -1.33 % difference.

The base shear results obtained by performing the time history analysis were calculated. The results variation curves were similar and show a very close agreement. For the minimum response, the closest results to the proposed method results were obtained from SAP2000V16 (thick) with a maximum of -7.84 % difference, and for the maximum response, the closest results to the proposed method results were obtained from ETABS (thick) with 1.02 % maximum difference.

The base overturning moment results obtained by performing the time history analysis were calculated. The results variation curves were similar and show a very close agreement. For the minimum response, the closest results to the proposed method were obtained from SAP2000V16 (thin) with a maximum of -1.68 % difference, and for the

maximum response, the closest results to the proposed method results were obtained from ETABS (thick) with 0.79 % maximum difference.

G-Time History P-Delta Analysis

The top floor lateral displacement results obtained by performing the time history P-Delta analysis using the proposed method were calculated and compared with the results obtained from different analysis packages. The results variation curves were similar and show very close agreement. For the minimum response, the closest results to the proposed method results were obtained from StaadProV8i with 1.33 % maximum difference, and for the maximum response, the closest results to the proposed method results were obtained also from StaadProV8i with a maximum of -3.26 % difference.

The base shear results obtained by performing the time history P-Delta analysis were calculated. The results variation curves were similar and show a very close agreement. For the minimum response, the closest results to the proposed method results were obtained from ETABS (thin) with a maximum of -7.76 % difference, and for the maximum response, the closest results to the proposed method results were obtained from ETABS (thin) with -2.54 % maximum difference.

The base overturning moment results obtained by performing the time history P-Delta analysis were calculated. The results variation curves were similar and show a very close agreement. For the minimum response, the closest results to the proposed method were obtained from ETABS (thin) with a maximum of -8.2 % difference, and for the maximum response, the closest results to the proposed method results were also obtained from ETABS (thin) with 0.49 % maximum difference.

7.3 Recommendations Drawn from Results Obtained

It is recommended to use the nonlinear version of the moment-force transformation method in the static and dynamic, linear and nonlinear analysis of tall buildings together with the buckling analysis for the following:

1. Static and dynamic, linear and nonlinear analyses of super-tall buildings in which the axial deformation of the vertical members is dominant and should be considered.
2. Static and dynamic, linear and nonlinear analyses of ordinary portal frames and shear wall-frame interaction problem.

3. Static and dynamic, linear and nonlinear 2D analysis of shear walls with openings, by considering the beams stiffness including also the infinite stiffness of the rigid parts of the walls.

4. Static and dynamic, linear and nonlinear three dimensional analyses of buildings with vertical members irregularly arranged and oriented in the building plan and with different sections in the different levels and with different floor heights.

5. Elastic instability analysis of 2D and 3D tall buildings.

7.4 Recommendations for Future Research

For future research it is recommended to:

1- Develop method to take into account elastic-plastic analysis incorporating both elastic instability and plastic yielding in members.

2- Further develop the program to incorporate the elastic-plastic responses, by formulating the stiffness and the carryover moment matrices using the various Hysteresis models, e.g. elasto-plastic, bilinear and curvilinear models.

3. For more simplification of the problem solution, columns or vertical members not contributing to the resistance of the lateral loads can be included in the floor rotation stiffness and the problem solution will include only the walls or the vertical members that actually contribute to the resistance of the lateral loads.

4. For more optimization of the analysis, the stiffness of the floor can be calculated by using simplified rules instead of calculations by finite elements, e.g. for slabs with beams construction considering the properties of the equivalent T and L sections.

5. For flexible supports, the rotational and axial stiffness of the supports may also be incorporated in the analysis.

6. Columns shortening in reinforced concrete and composite tall buildings due to time-dependant creep, shrinkage and elastic modulus could be also analyzed.

References

1- ACI 318-14 (2014), American Concrete Institute, *"Building Code Requirements for Structural Concrete"*, Farmington Hills, Mich.

2- Abdur Rahman, Fancy Saiada Fuadi and Bobby Shamim Ara, (2012), *"Analysis of drift due to wind loads and earthquake loads on tall structures by programming language c"*, International Journal of Scientific & Engineering Research, Volume 3, Issue 6, June-2012, ISSN 2229-5518, IJSER © 2012, http://www .ijser.org

3- Akis Tolga (2004),*"Lateral Load Analysis of Shear Wall-Frame Structures"*, PhD Thesis Dissertation, The Graduate School of Natural And Applied Sciences of The Middle East Technical University.

4- Albrecht James T., Chan Cy P., And Edelman Alan, (2009) *"Sturm Sequences and Random Eigenvalue Distributions"*, Foundations of Computational mathematics, Volume 9 Issue 4, June 2009, Pages 461-483.

5- Ali Mir M. and Moon Kyoung Sun, (2007), *"Structural Developments in Tall Buildings Current Trends and Future Prospects"* , Structures Division, School of Architecture, University of Illinois at Urbana-Champaign, USA, Architectural Science Review Volume 50.3, pp 205-223.

6- Almeida J.P., Correia A.A. and Pinho R., (2008), *"Development of a 3d Force-Based Beam Element for Nonlinear Analysis of RC Frame Structures Considering Flexure-Shear Coupling"*, The 14th World Conference on Earthquake Engineering October 12-17, 2008, Beijing, China.

7- Aly, Aly Mousaad, Zasso Alberto and Resta Ferruccio, *"Tall Buildings under Multidirectional Winds: Response Prediction and Reduction"*, "Wind Tunnels and Experimental Fluid Dynamics Research", Published online 27, July, 2011.

8- American National Standards Institute, ANSI-A58.1. (1982), *"Minimum Design Loads for Buildings and Other Structures"*.

9- Applied Technology Council, May 2007, *"Proceedings of Workshop on Tall Building Seismic Design and Analysis Issues"*.

10- BS 8110 (1997), British Standards Institution. Structural use of Concrete, Part 1: *"Code of Practice for Design and Construction"*, London.

11- BS 8110 (1997), British Standards Institution. Structural use of Concrete, Part 2: *"Code of Practice for Special Circumstances"*, London.

12- Barbi Jernej, (2012), *"Exact Corotational Linear FEM Stiffness Matrix"*, Technical Report, University of Southern California.

13- Bathe Klaus Jurgen And Wilson Edward L., (1973), *"Solution Methods for Eigenvalue Problems in Structural Mechanics"*, International Journal For Numerical Methods In Engineering, Vol. 6, 21 3-226 (1973), University Of California, Berkeley, California, U.S.A.

14- Bayati Z., Mahdikhani M. and Rahaei A., (2008), *"Optimized Use of Multi-Outriggers System to Stiffen Tall Buildings"*, The 14th World Conference on Earthquake Engineering, October 12-17, 2008, Beijing, China.

15- Berkley, *"STAADProVi8, Structural Analysis and Design Software"*.

16- Bozdogan K.B. and Ozturk D., (2010), *"Vibration Analysis of Asymmetric shear wall structures using the transfer matrix method"*, Iranian Journal of Science and Technology, Transaction B, Engineering, Vol. 34, No B1,PP 1-14.

17- Bozdogan Kanat Burak and Ozturk Duygu, (2010), *"An approximate method for lateral stability analysis of Wall-frame buildings including shear deformations of*

walls", Sadhana Vol. 35, Part 3, June 2010, pp. 241–253.Indian Academy of Sciences, Department of Civil Engineering, Ege University, Izmir, 35040 Turkey, e-mail: kanat.burak.bozdogan@ege.edu.tr

18- Bozdogan Kanat Burak, (2011), *"A method for lateral static and dynamic analyses of wall-frame buildings using one dimensional finite element"*, Scientific Research and Essays Vol. 6(3), pp. 616-626, 4 February, 2011, Available online at http://www.academicjournals.org/SRE , DOI: 10.5897/SRE10.863, ISSN 1992-2248, 2011 Academic Journals.

19- Bozdogan Kanat Burak, (2011), *"Free Vibration Analysis of Wall-Frame Structures by Differential Quadrature Method"*, International Journal of Engineering and Applied Sciences (IJEAS), Vol.3, Issue 4(2011)7-20.

20- *CSI Analysis Reference Manual for SAP2000, ETABS, and SAFE, Computers and Structures, Inc., Berkeley, California, USA, June 2008.*

21- Causevic Mehmed and Mitrovic Sasa, (2010), *"Comparison between non-linear dynamic and static seismic analysis of structures according to European and US provisions"*, Bull Earthquake Eng DOI 10.1007/s10518-010-9199-1.

22- Chan Gordon, (2005), *"Nonlinear Analysis of Multistory Structures Using NONLIN"*, MSc. Thesis dissertation, Faculty of the Virginia Polytechnic Institute and State University.

23- Chandurkar P. P. and Pajgade P. S., (2013), *"Seismic Analysis of RCC Building with and Without Shear Wall"*, International Journal of Modern Engineering Research (IJMER), www.ijmer.com Vol. 3, Issue. 3, May - June 2013 pp-1805-1810 ISSN: 2249-6645

24- Chen Xinzhong and Kareem Ahsan, (2005), *"Coupled Dynamic Analysis and Equivalent Static Wind Loads on Buildings with Three-Dimensional Modes"*,

JOURNAL OF STRUCTURAL ENGINEERING © ASCE.

25- Chopra Anil, K., (2000), solution manual *"Dynamics of Structures - Theory and Applications to Earthquake Engineering"*, Third Edition.

26- Christenson Richard E., (2001), *"Semi-active Control of Civil Structures for Natural Hazard Mitigation: Analytical And Experimental Studies"*, Ph.D. Dissertation, (December 2001), The Graduate School of the University of Notre Dame.

27- Clough Ray W. and Penzien Joseph, (1995), *"Dynamics of Structures"*, Third Edition, Computers & Structures, Inc. University Ave. Berkeley, CA 94704, USA.

28- Coates R. C., Coutie M. G., and Kong F. K., (1990), *"Structural Analysis"*, Third Edition, Chapman and Hall.

29- Coull Alex, Mohammed and T. H., (1983), *"Simplified analysis of lateral load distribution in structures consisting of frames, coupled shear walls, and cores"*, The Structural Engineer, Volume 61B/No. 1/March 1983.

30- Coull Alexander, ASCE F., Bose Bishwanath, and Ahmed Abdulla Khogali, (1982), *"A Simplified analysis of bundled tube structures"*, Journal of the structural division, Proceedings of the American Society of Civil Engineers, © ASCE, Vol. 108, No. ST5, May 1982.

31- Dagnew Agerneh K., Bitsuamalk Girma T. and Merrick Ryan, (2009) *"Computational evaluation of wind pressures on tall buildings"*, 11th Americas Conference on Wind Engineering, San Juan, Puerto Rico, June 22-26 2009.

32- Deierlein Gregory G., Reinhorn Andrei M. and Willford Michael R., (2010), *"Nonlinear Structural Analysis for Seismic Design, A Guide for Practicing Engineers"*, NEHRP Seismic Design Technical Brief No. 4, NIST GCR 10-917-5, October 2010.

33- Ding Kun, Su Ningfen, Chen Xuefeng, Zhou Ying and Lu Xilin, *"Finite Element Analysis and Experimental Verification of A Setback Tall Building"*, 3rd International Conference on Advances in Experimental Structural Engineering, Oct 15-16, San Francisco, USA, State Key Laboratory of Disaster Reduction in Civil Engineering, Tongji University, Shanghai, China.

34- Diotallevi Pier Paolo, Landi Luca and Cardinetti Filippo, (2008), *"A Fibre Beam Column Element for Modelling the Flexureshear Interaction in the Non-Linear Analysis of RC Structures"*, The 14th World Conference on Earthquake Engineering, October 12-17, 2008, Beijing, China.

35- Dobson Richard and Arnott Kenny, (2002), *"A Brief Overview of 2nd Order (or P-Delta) Analysis"*. ,Technical Director for FASTRAK, 3D+ and TEDDS, CSC (UK) Ltd and Product Manager for S-Frame, CSC (UK) Ltd.

36- *Elcentro Earthquake May 18 -1940, North-South Component, www.vibrationdata.com/elcentro.htm*

37- *EN 1992-1-1 (2004) (English): Eurocode 2: Design of concrete structures - Part 1-1: General rules and rules for buildings.*

38- Eads Laura, Miranda Eduardo, Krawinkler Helmut and Lignos Dimitrios G., *"An efficient method for estimating the collapse risk of structures in seismic regions"*, EARTHQUAKE ENGINEERING & STRUCTURAL DYNAMICS 2013; 42:25–41, Published online 30 March 2012 in Wiley Online Library (wileyonlinelibrary.com).

39- Eleni Chatzi, (2012),*" The Finite Element Method for the Analysis of Non-Linear and Dynamic Systems and Dynamic Systems"*, Swiss federal institute of technology Zurich,Lecture 3 - 9 October, 2012.

40- Fukuwa N., Tobita J., Mori M., Koide E. and Hanai T.,(2008), *"Development of*

Vibration Experiment Education Materials for Structural and Soil Dynamics", The 14th World Conference on Earthquake Engineering October 12-17, 2008, Beijing, China.

41- Gavin Henri P.,(2012),*" Structural Element Stiffness Matrices and Mass Matrices"*, Duke University, Department of Civil and Environmental Engineering, CEE 541. Structural Dynamics, Fall 2012.

42- Gavin Henri, (2012), *"Geometric Stiffness Effects in 2D and 3D Frames"*, Duke University,Department of Civil and Environmental Engineering, CEE 421L, Matrix Structural Analysis.

43- Ghali A. and Neville A. M. (1978), *"Structural Analysis – A Unified Classical and Matrix Approach"*, Second edition, New York, Chapman and Hall Ltd.

44- Ghali A., Neville A. M., and Brown T. G., (2009), *"Structural Analysis – A Unified Classical and Matrix Approach"*, Sixth edition, Taylor and Francis, London and New York.

45- Giovanni Rebecchi, (2009), *"Beam Axial Load Identification Using One Vibration Mode Shape"*, PhD Thesis dissertation, Universita Degli Studi Di Ferrara.

46- Gu Ming, (2009), *"Study on Wind Loads and Responses of Tall Buildings and Structures"*, The 7th Asia-Pacific Conference on Wind Engineering, November 8-12, 2009,Taipei, Taiwan

47- Guner Serhan and Vecchio Frank J., (2012), *"Simplified Method for Nonlinear Dynamic Analysis of Shear-Critical Frames"*, ACI STRUCTURAL JOURNAL TECHNICAL PAPER, ACI Structural Journal, V. 109, No. 5, September-October 2012.

48- Gustafsson David and Hehir Joseph, (2005), *"Stability of Tall Buildings"*, M.Sc.

Dissertation, Department of Civil and Environmental Engineering, Division of Structural Engineering, Chalmers University of Technology, Göteborg, Sweden.

49- Hagen Garrett Richard, (2012), *"Performance-Based Analysis of a Reinforced Concrete Shear Wall Building"*, M.Sc. Dissertation, Faculty of California Polytechnic State University, San Luis Obispo, June 2012.

50- Hutt Carlos Molina, (2013), *"Non-Linear Time History Analysis of Tall Steel Moment Frame Buildings in LS-DYNA"*, 9th European LS-DYNA Conference 2013.

51- Ibrahim M. S. (2013), *"Analysis of Tall Buildings using The Moment Transformation Method"*, M.Sc. Thesis dissertation, Sudan University of Science and Technology.

52- Ibrahim M. S. and Mohamed A. E. (2013), *"Analysis of Shear Wall Structures using the Moment Transformation Method"*, Journal of Science and Technology - Engineering and Computer Sciences, Vol. 14, No. 3, June 2013.

53- Ikago Kohju, (2012), *"Dynamic Instability in High-Rise Steel Structures Subjected to Strong Ground Motions"*, 14th U.S. - Japan Workshop on improvement of Structural Design and Construction Practices, 3-5 December 2012. , Tohoku University, Japan.

54- Jaeger G. Mufti A. A. and Mamet J. C. (1973), *"The Structural Analysis of Tall Buildings Having Irregularly Positioned Shear Walls."* ,Build. Sci. Vol. 8, pp. 11-22. Pergamon Press.

55- Jahanshahi M. R., Rahgozar R.,and Malekinejad M., (2012), *" A Simple Approach to Static Analysis of Tall Buildings with a Combined Tube-in-tube and Outrigger-belt Truss System Subjected to Lateral Loading"*, IJE TRANSACTIONS A: Basics Vol. 25, No. 3, 289-299,International Journal of Engineering.

56- Jameel Mohammed, Saiful Islam A.B.M., Hussain Raja Rizwan, Khaleel M. and

Zaheer M. M., (2012), *"The Structural Design of Tall and Special Buildings, Optimum structural modeling for tall buildings"*, Published online in Wiley Online Library (wileyonlinelibrary.com/journal/tal). DOI: 10.1002/tal.1004

57- Jayachandran P. (2003), *"Design of Tall Buildings Preliminary Design and Optimization"*, Ph.D, M.ASCE., Worcester Polytechnic Institute, Worcester, Massachusetts, 01609, USA, jayachan@wpi.edu, International Conference on Tall Buildings and Industrial Structures, PSG College of Technology, Coimbatore, India, Keynote Lecture.

58- Jónsson Örvar,(2014), *"The dynamic behavior of multi-story reinforced concrete building in a seismic and windy environment"*, M.Sc. Dissertation, The School of Science and Engineering at Reykjavík University, January 2014.

59- Kouhia Reijo, (1990), *"Simple Finite Elements for Nonlinear Analysis of Framed Structures"*, Rakenteiden Mekaniikka Vol. 23, No 4 1990, s. 3 – 49

60- Lebofsky Sonia, (2013), *"Numerically Generated Tangent Stiffness Matrices for Geometrically Non-Linear Structures"*, M.Sc. Dissertation, University of Washington.

61- Lee Kang-Kun, Guan Hong and Loo Yew-Chaye (2000), *"Simplified Analysis of Shear-Lag in Framed-Tube Structures with Multiple Internal Tubes"*. Griffith University Gold Coast Campus, Australia.

62- Leung A. Y. T. (1983), *"Low Cost Analysis of Building Frames for Lateral Loads "*Computers & Structures Vol. 11. No. 4. pp. 475-483.

63- Leung A. Y. T. (1985), *"Micro-Computer Analysis of Three-Dimensional Tall Buildings "*, Computers & Structures Vol. 21, No. 4, pp. 639-661.

64- Leung A. Y. T. and Cheung Y. K. (1981), *" Dynamic Analysis of Frames by a Two-Level Finite Element Method "* , Journal of Sound and Vibration 74(l), l-9

65- Leung A. Y. T. and Wong S. C. (1988),*"Local-Global Distribution Factors Method for Tall Building Frames."*, Computer & structures Vol.29, No.3. pp. 491-502

66- Leung A. Y. T. and Zeng S. P., (1994), *"Analytical Formulation of Dynamic Stiffness"*, Journal of Sound and Vibration.

67- Leung Andrew Yee-Tak (1978),*" An Accurate Method of Dynamic Condensation In Structural Analysis"*, International. Journal For Numerical Methods In Engineering. Vol. 12, 1705-1715 (1978).

68- Li B., Duffield C. F. and Hutchinson G. L., (2008),*" Simplified Finite Element Modeling of Multi-storey Buildings: The Use of Equivalent Cubes"*, Electronic Journal of Structural Engineering.

69- Li Guo-Qiang and Li Jin-Jun (2007), *" Advanced Analysis and Design of Steel Frames "* , John Wiley & Sons, Ltd.

70- Li Q. S. and Wu J. R., (2004), *"Correlation of dynamic characteristics of a super-tall building from full-scale measurements and numerical analysis with various Finite element models"*, Earthquake Engineering and Structural Dynamics, Earthquake Engng Struct. Dyn. 2004: 33:1311–1336 (DOI: 10.1002/eqe.405).

71- Liao W.Y., Chen W.H., Ni Y.Q. and Ko J.M., (2008), *"Post-Earthquake Damage Identification of Tall Building Structures: Experimental Verification"*, The 14th World Conference on Earthquake Engineering October 12-17, 2008, Beijing, China.

72- Lodi Sarosh H., Mohammed Aslam F., Khan Rashid A. and Gunay M. Selim, (2011), *"A Practical Guide to Nonlinear Static Analysis of Reinforced Concrete Buildings with Masonry Infill Walls"*, NED University of Engineering and Technology, University of California, Berkeley, Supported by the Pakistan-US Science and Technology Cooperation Program.

73- MacGinley T.J. and Choo B. S. (1990), *" Reinforced Concrete: Design Theory & Examples "*E & FN Spon Second edition.

74- MacLeod, Iain A. (1998), *"Shear Wall-Frame Interaction a Design Aid"*, Portland cement association .1970 reprinted 1998.

75- Manicka Selvam V.K, Bindhu K.R., (2011), *"Split frame method for lateral load analysis of short frames"*, International Journal of Civil and Structural Engineering, Volume 1, No 4, 2011, Research article ISSN 0976 – 4399 835.

76- Marsono Abdul Kadir and Wee. Lee Siong, (2006), *"Nonlinear Finite Element Analysis of Reinforced Concrete Tube in Tube of Tall Buildings"*, Proceedings of the 6th Asia-Pacific Structural Engineering and Construction Conference (APSEC 2006), 5 – 6 September 2006, Kuala Lumpur, Malaysia, A-161,

77- Mathisen Kjell Magne, (2012), *" Solution Methods for Nonlinear Finite Element Analysis (NFEA)"*, Department of Structural Engineering,Norwegian University of Science and Technology, Lecture 11, Geilo Winter School.

78- Matjaž Dolšek., (2013), *"Concept of Risk-Based Seismic Design of Buildings using Methods of Nonlinear Analysis"*, COMPDYN 2013 4th ECCOMAS Thematic Conference on Computational Methods in Structural Dynamics and Earthquake Engineering.

79- Mattacchione Angelo (1991), *"Equivalent Frame Method Applied to concrete Shear walls"*, November l99l lssue of ACI Concrete International.

80- McCormac Jack and Elling Rudolf E., (1988), *"Structural Analysis - A Classical and Matrix Approach"*, Harper and Row, published, 1988.

81- McHugh Peter, (2007), *"Non-Linear Finite Element Analysis: Finite Element*

Solution Schemes I & II", European Society of Biomechanics thematic workshop on Finite Element Modeling in Biomechanics and Mechanobiology, Department of Mechanical and Biomedical Engineering, National Centre for Biomedical Engineering Science, National University of Ireland, Galway.

82- Meftah Sid Ahmed, Tounsi Abdelouahed and El Abbas Adda Bedia, (2007), *"A Simplified Approach for Seismic Calculation of a Tall Building Braced by Shear Walls And Thin-Walled Open Section Structures."* ,Science-direct.

83- Megson T. H. G., (2000), *"Structural and Stress Analysis"*, Butterworth-Heinemann. A division of Reed Educational and Professional Publishing Ltd.

84- Merritt Richard George, (1953), *"Effect Of Foundation Compliance on the Earthquake Stresses In Typical Tall Buildings"*, Ph.D. thesis dissertation, California institute of technology.

85- Moghadam A.S. and Aziminejad A., *"Interaction of Torsion and P-Delta Effects in Tall Buildings"*, 13th World Conference on Earthquake Engineering, Vancouver, B.C., Canada,August 1-6, 2004,Paper No. 799.

86- Mora Rodrigo, Bédard Claude and Rivard Hugues,(2004), *"A Framework for Computer-Aided Conceptual Design of Building Structures"*. International Conference on Computing in Civil and Building Engineering, ICCCBE, 10, 2004.06.02-04, Weimar, Bauhaus-Universitat.

87- NEHRP Consultants Joint Venture, (2013), *"Nonlinear Analysis Research and Development Program for Performance-Based Seismic Engineering"*, Prepared for U.S. Department of Commerce, National Institute of Standards and Technology, Engineering Laboratory, Gaithersburg, MD 20899, A partnership of the Applied Technology Council and the Consortium of Universities for Research in Earthquake Engineering, December 2013.

88- Nakai Masayoshi, Koshika Norihide, Kawano Kenichi, Hirakawa Kiyoaki and Wada Akira, (2012), *"Performance-Based Seismic Design for High-Rise Buildings in Japan"*, International Journal of High-Rise Buildings, September 2012 volume 1 ,No. 3,155-167.

89- Newmark N.M. and Hall W.J., (1982), *"Earthquake Spectra and Design"*, Earthquake Engineering Research Institute.

90- Noor Munaz Ahmed and Seraj Salek M. (1996), *"Comparison of Two and Three Dimensional Analysis of Moderately Sized Tall Building Under Wind Loads"* Journal of Civil Engineering, The Institution of Engineers, Bangladesh Vol. CE 24, no.2.

91- Otani Shunsuke, (1979), *"Nonlinear Dynamic Analysis of Reinforced Concrete Building Structures"*, Department of Civil Engineering, University of Toronto.

92- Pacific Earthquake Engineering Research Center (PEER), (2010), *"Guidelines for Performance-Based Seismic Design of Tall Buildings"*, Developed by the PEER as part of the Tall Buildings Initiative, Report No. 2010/05, Pacific Earthquake Engineering Research Center, College of Engineering, University of California, Berkeley, November 2010.

93- Pank Will and Girardet Herbert and Cox Greg, (2002), *"Tall Buildings and Sustainability"*, Report by Will Pank, Maunsell Ltd, Herbert Girardet, Urban Futures, Greg Cox, Oscar Faber Ltd, Economic Development Office, Corporation of London, March 2002.

94- Parv Bianca R. and Nicoreac Monica P., (2012), *"Global structural analysis of central cores supported tall buildings compared with FEM"*, Acta Technica Napocensis: Civil Engineering & Architecture Vol. 55, No. 3 (2012), Journal homepage: http://constructii.utcluj.ro/ActaCivilEng

95- Paulay T. (1978), *"A Consideration of P-Delta Effects in Ductile Reinforced*

Concrete Frames", Bulletin of the New Zealand National Society for Earthquake Engineering, Vol.11, No. 3, September, 1978.

96- Paulino Madison R, (2010), *"Preliminary Design of Tall Buildings"*, Msc Thesis dissertation, Dept of Civil engineering, Worcester Polytechnic Institute.

97- Petrolito J. and Legge K.A., (2007) , *"General Non-Linear Analysis of Frames"*, 5th Australian Congress on Applied Mechanics ,ACAM 2007, 10-12 December 2007,Brisbane, Australia.

98- Research Engineer International, *"STAADPro2004, Structural Analysis and Design Software"*, California.

99- Reynolds Charles E. and Steedman James C., (2008), *"Reynolds's Reinforced Concrete Designer's Handbook"*, Eleventh edition, Taylor & Francis.

100- Rezaghasemi Hamid, (2012), *"Approximate Analysis of Strength of Tehran's Tall Buildings Reinforced with Spandrel Frame Against Lateral Forces"*, Indian J. Sci. Res. 3(2) : 25-32 , 2012.

101- Samuelsson A. and Zienkiewicz O. C., (2006), *"History of the stiffness method"*, International Journal For Numerical Methods In Engineering, 67:149–157.

102- Sarkar and Manohar C.S.,(1996), *"Dynamic stiffness matrix of a general cable Element"*, Archive of Applied Mechanics 66 (1996) 315-325© springer-verlag.

103- Shi, Weixing, (2000), *"Shaking Table Experimental Study of Reinforced Concrete High-Rise Building"*, 12WCEE 2000.

104- Smith. Bryan Stafford and Coull. Alex. (1991), *"Tall Buildings Structures: Analysis & Design"* John Wiley & Sons ,Inc. 1991 Edition.

105- Swaddiwudhipong S., Lim Y. B. and Lee S. L. (1988),*"An Efficient Finite Strip Analysis of Frame-Shear Wall Tall Building"*, Computers & Structures Vol. 29. No. 6, pp. 1111-1118.

106- Takabatake Hideo,(2012), *"A Simplified Analytical Method for High-Rise Buildings"*, hideo@neptune.kanazawa-it.ac.jp, Department of Architecture, Kanazawa Institute of Technology, Institute of Disaster and Environmental Science, Japan.

107- Taranath Bungale S., (2011), *"Differential shortening of tall steel building columns"*, Professional Development Advertising Section-Bentley Systems, Inc.

108- Taranath, B. S. (1988), *"Structural analysis and design of tall buildings"* New York, McGraw-Hill.

109- Thool Kushal P., Ashok K. Ahuja and Anupam Chakrabarti, (May 2013), *"Effect of interference on Wind loads on Tall Buildings"*, Dept. of Civil Eng., Indian Institute of Technology Roorkee, Roorkee, India., J. Acad. Indus. Res. Vol. 1(12)

110- Timoshenko, S. P. (1948), *"Strength of Materials"*, part II 2nd edition, van Nostrand, New York.

111- Tuan Hiep Pham, (2008), *"Seismic Design Considerations for Tall Buildings"*, M.Sc. Dissertation, (April 2008), Instituto Universitario di studi superiori Pavia.

112- UBC-97, *"Uniform Building Code"*, International Conference of Building Officials, Whittier, California, 1997.

113- Urs Amit (2002), *"Stability Analysis of Frame Tube Tall Buildings"*, MSc Thesis dissertation, Dept of Civil engineering, Worcester Polytechnic Institute.

114- Vafaeihosseini Ehsan, Sagheb Azadeh and Ramancharla Pradeep Kumar, (2011), *"Analysis of High-rise Building using Computational Fluid Dynamics Approach: A*

Case Study on 38-Storey High-rise Building", Structural Engineering World Congress, Report No: IIIT/TR/2011/-1,Centre for Earthquake Engineering, International Institute of Information Technology, Hyderabad - 500 032, INDIA,April 2011.

115- Ventura C.E., Brincker R., Andersen P. and Dascotte E., (2005), *"FEM updating of tall buildings using ambient vibration data"*, Eurodyn 2005 C. Soize and G.I. Schueller, Millpress ,Rotterdam.

116- Ventura C.E., Lord J.F. and Turek M.,(2005), *"FEM Updating of Tall Buildings Using Ambient Vibration Data"*, Structural Dynamics EURODYN 2005: Proceedings of 6th International Conference on Structural Dynamics, Paris, France, 4-7 September 2005.

117- Warden Brandon, Browning Joann P. and Matamoros Adolfo, (2006), *"A simplified Method to estimate nonlinear response with an approximate linear analysis for reinforced concrete structures"*, a report on research sponsored by: structural engineering and materials laboratory, university of Kansas, SM report no. 83.

118- Williams Alan (2009), *"Structural Analysis in Theory and Practice"*, International Codes Council.

119- Wilson Edward , (2000), *"Three Dimensional Static and Dynamic Analysis of Structures"*, Third Edition, Computer and Structures Inc., Berkeley, California, USA

120- Wilson, E. L. and Habibullah A., (1987), *"Static and Dynamic Analysis of Multi-Story Buildings Including P-Delta Effect"* Earthquake Spectra. Vol.3, No.3. Earthquake Engineering Research Institute. May 1987.

121- Wilson, E. L., Dovey, H. H. and Habibullah. A., *"ETABS V13, (2013), Three Dimensional Analysis of Building Systems"*, Computers and Structures Inc., Berkeley, California.

122- Wilson, E. L., Dovey, H. H. and Habibullah. A., *"ETABS, (2006), Three Dimensional Analysis of Building Systems"*, Computers and Structures Inc., Berkeley, California.

123- Wong C. W. and Lau S. L. (1989), *"Simplified Finite Element Analysis of Three-Dimensional Tall Building Structures"*, Computers & Structures Vol. 33, No. 3, pp. 821-830.

124- Yu Chih-Peng and Roesset Jose M., (2001), *"Dynamic Stiffness Matrices for Linear Members with Distributed Mass"*, Tamkang Journal of Science and Engineering, Vol. 4, No. 4, pp. 253-264

APPENDICES

Appendix A1

A Three Segments Cantilever Example

The translations and the rotations of the joint of a cantilever of unit elasticity consists of three segments and subjected to lateral forces as shown in Figure A1.1, were obtained.

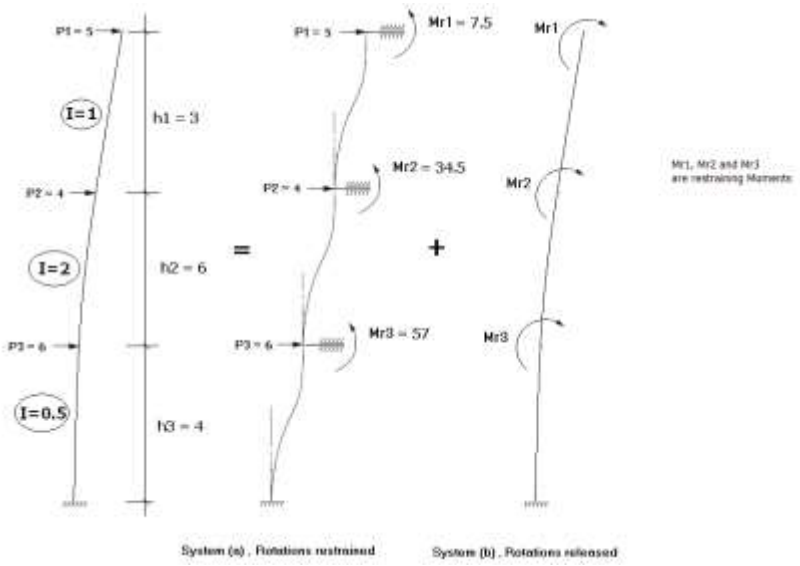

Figure A1.1: Single post example

The translations and rotations of the three free joints of the cantilever are given in shown Tables A1.1 and A1.2. From the two tables, the translations and the rotations of the original structure are equal to the summations of the systems (a) and (b).

Table A1.1: Displacements of the original structure

JOINT#	TRANSLATION	ROTATION
1	9754	940.5
2	6955	918
3	1744	792

Table A1.2: Displacements of the split systems:

System	System(a)		System(b)		System(a) + System(b)	
Joint #	**TRANSLATION**	**ROTATION**	**TRANSLATION**	**ROTATION**	**TRANSLATION**	**ROTATION**
1	252.25	0	9501.75	940.5	9754	940.5
2	241	0	6714	918	6955	918
3	160	0	1584	792	1744	792

Appendix A2

The Moment Distribution Procedure

The moment distribution procedure (ordinary or no-shear Figures A2.1 and A2.2) uses the two loading systems (a) and (b) illustrated previously as follows. The first step in the procedure is by obtaining from the system (a), the fixed-end moments produced from the applied loads and from which the restraining moments at the joints are obtained, then the balancing moments are applied in system (b), the induced carryover moments at the far end of the members are then considered as a fixed moments and are again applied in system (a). This procedure is repeated until the carryover moments become negligible. Then the summations of all the resulting moments in the two systems are obtained and represent the final end moments.

From this illustration it is seen that, the moment distribution procedure is actually equivalent to the two systems (a) and (b) when separately analyzed and the resulting joints moments are superimposed.

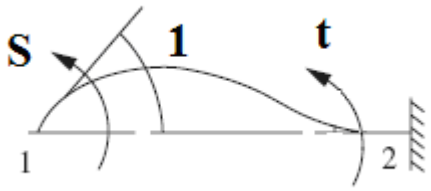

Figure A2.1: Ordinary rotational stiffness of a member

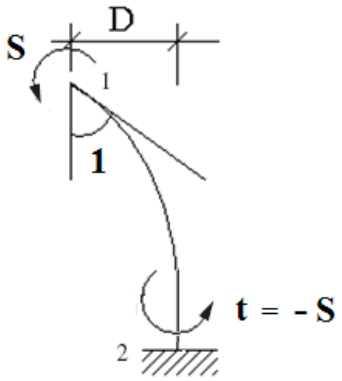

Figure A2.2: No-shear rotational stiffness with translation permitted

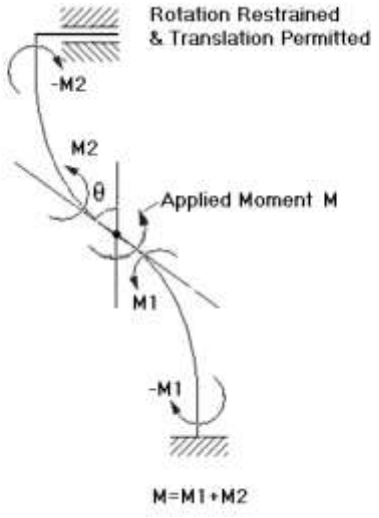

Figure A2.3: No-shear moment distribution between two members

Figure A2.4 shows the split of a continuous beam into the two loading systems (a) and (b):

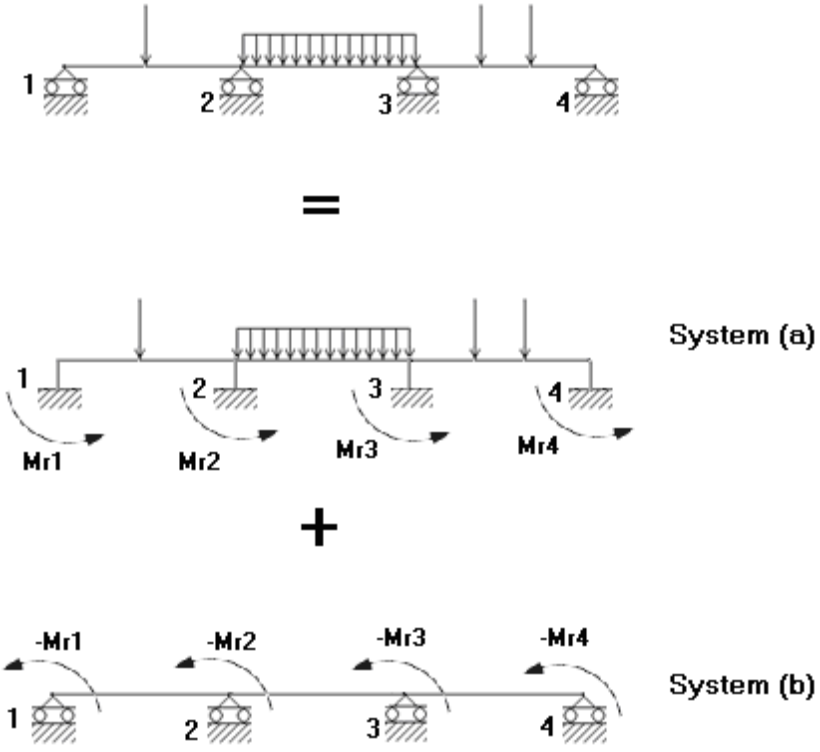

Figure A2.4: Continuous beam model

Appendix A3

The Moment Transformation Procedure

The moment transformation procedure (ordinary or no-shear) can be carried out by considering the two loading systems (a) and (b) described before and also shown in Figure A2.4. In system (a), the fixed-end moments induced from the external applied loads and the restraining moments are obtained then in the system (b) the balancing moment (the reverse of the restraining moment) are applied with special sequence. For example, in joint (1) from which the transformation procedure will be carried out to joint (2), due to the applied moment at joint (1) there will be an induced moment at joint (2).

Superimposing the two systems (a) and (b) will eliminate the moment at joint (1) and produce the equivalent moment at joint (2), then joint (1) will be relieved and will never be considered in the analysis again. Same procedure will be carried out to the next joint (3) until reaching the concerned joint. The transformation will be carried out in the other direction until also reaching the concerned joint. By releasing and balancing the fixed moments at the concerned joint, the rotation of the joint and the final moments in the extremities to the left and to the right of the concerned joint can be calculated using the equivalent stiffness of the connected members. The procedure will be carried out for all the joints of the continuous frame.

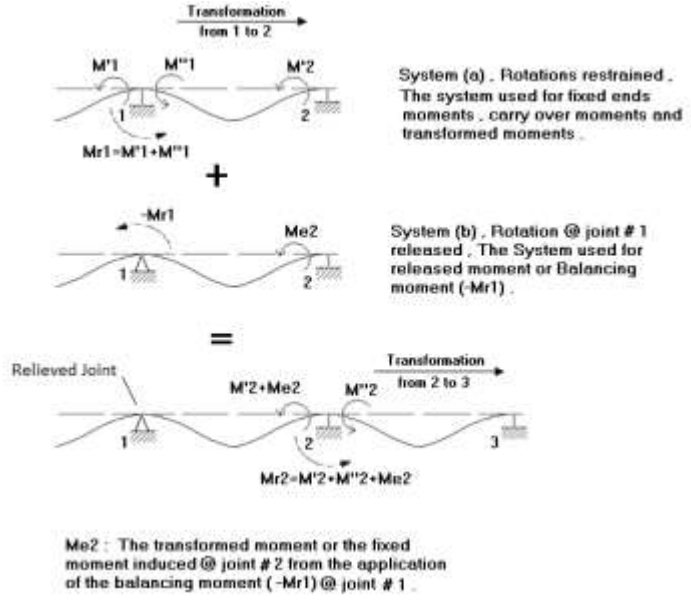

Figure A3.1: Moment transformation of continuous beam

The Figures A3.2 and A3.3 show the moment transformation procedure for structural system subjected to horizontal loads and permitted to side sway at the floor levels. The sway fixed-end moments induced in the vertical members, due to the applied horizontal loads are shown in Figure A3.2.

The illustrated transformation procedure is in the direction from top to bottom. Figure A3.2 shows the transformation from joint (1) to joint (2), and Figure A3.3 shows the transformation from joint (2) to joint (3).

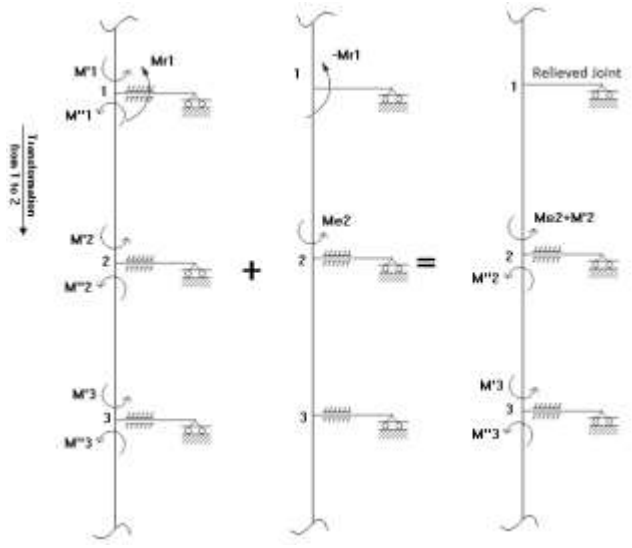

Figure A3.2: Moment transformation from joint 1 to 2 in a single post frame

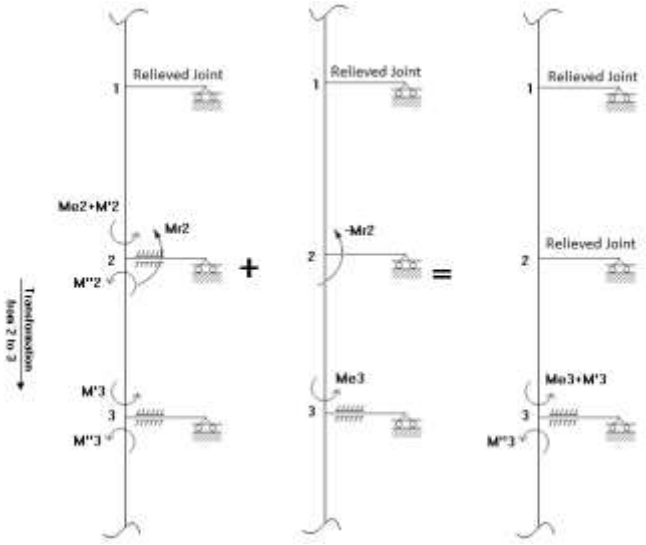

Figure A3.3: Moment transformation from joint 2 to 3 in a single post frame

Appendix A4

A Three Segments Column Example

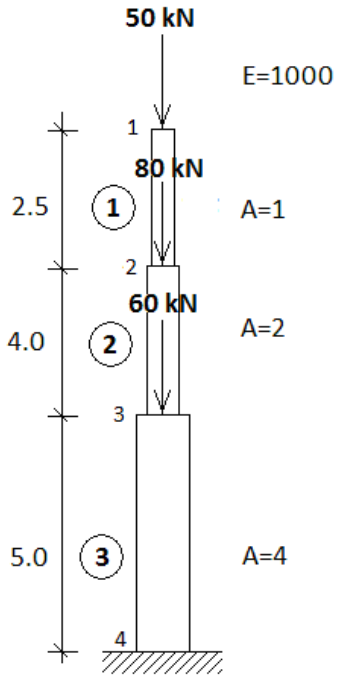

Figure A4.1: Three segments column

The axial translations of the joints are calculated using the force transformation procedure for the shown three columns structural system, with material elasticity, E=1000 kN/m^2, Figure A4.1.

Using equations 3.34 and 3.35, the transformation factors and the axial equivalent stiffness from top to bottom and from bottom to top, are calculated and shown in Tables A4.1 and A4.2:

Table A4.1: Equivalent Stiffness and Transformation Factors from Top to Bottom.

Member	1	2	3
Equivalent Stiffness	0	0	0
Transformation Factors	1	1	1

Table A4.2: Equivalent Stiffness and Transformation Factors from Bottom to Top.

Member	3	2	1
Equivalent Stiffness	800	307.7	173.9
Transformation Factors	0	0.3846	0.5652

By using the transformation procedure illustrated in section 3.6, the axial displacements at the joints are calculated as follows:

Displacement at joint 1:

Total force = [(60*0.3846) + 80]*0.5652+50 = 108.2586 kN

Equivalent Stiffness = (173.9+0) = 173.9 kN/m

D1= 108.2586/173.9 = 0.6225 m

Displacement at joint 2:

Total force =50*1 + 80 + 60* 0.3846 = 153.076 kN

Equivalent Stiffness = (307.7+0) = 307.7 kN/m

D2= 153.076/307.7 = 0.4975 m

Displacement at joint 3:

Total force =50*1 + 80*1 + 60 = 190 kN

Equivalent Stiffness = (800 +0) = 800 kN/m

D3= 190/800 = 0.2375 m

The displacement in the concerned level can also be calculated using the following equation, Taranath (1988):

$$D_n = \sum_{i=n}^{N} \frac{L_i}{A_i.E_i} \sum_{k=1}^{i} P_k$$

Where:

N= total numbers of levels.

n= number of the concerned level.

Displacement at joint 1:

D1= (2.5/1/1000)*(50)+(4/2/1000)*(50+80)+(5/4/1000)*(50+80+60) = 0.6225 m

Displacement at joint 2:

D2= (4/2/1000)*(50+80)+(5/4/1000)*(50+80+60) = 0.4975 m

Displacement at joint 3:

D3= (5/4/1000)*(50+80+60) = 0.2375 m

Appendix A5

Further Optimization of the Transformation Procedure

Based on the subroutines of the transformation procedure presented by Ibrahim (2013), a new faster subroutine was developed and implemented in MFTProgV2. The new subroutine is based on two modifications:

(1) Introducing new indexed variable to store the inverse of the equivalent stiffness of the concerned level.

The equivalent stiffness matrix of the level is calculated as follows:

$$Ktot = KT+KB+KF$$

Where:

Ktot: the total Stiffness of the level.

KT: the equivalent stiffness of the structure part above the floor.

KB: the equivalent stiffness of the structure part below the floor.

KF: the stiffness of the floor.

This modification is very useful and optimizing the computer running time especially in the cases of repeated analysis as in the construction of the global flexibility matrix where the structure is solved for applied unit loads several times, and in the inverse iteration method used in the dynamic analysis.

(2) Introducing new indexed variables used to store the fixed-end moments plus the transformed moments during the transformation procedure in the two directions.

The indexed variable may be calculated as follows:

$$MD1(i)=M1(i)+FT*MDtot(i-1)$$

Where:

MD1(i):the resultant moment vector below level *i.*

M1(i):the fixed moment vector below level *i.*

*FT*MDtot(i-1)*: the transformed moment from level *i-1*.

These indexed variables are calculated only once and may be used several times during the program execution.

Appendix B

Flow Chart of the Conventional Buckling Incremental Method

Based on Figure 3.22, the following notes are made as illustrated by Coates et al (1990):

(1) The input data is very similar to that required by a stiffness analysis, the only difference is the use of the stability functions. The preliminary data must include an initial value for the load factor (*LF*), the increment to be applied to it (*INC*), and the required accuracy in the final result (*ACC*).

(2) *N* is used to count the number of loading cycles and *DET1*, *DET2*, *DET3* are values of the determinant of the stiffness matrix. The axial forces in the members of the structure are not generally known before the analysis begins, and this is unlikely to provide much overall saving in computing time.

(3) A check on *N* might be inserted to limit the number of load cycles in the event of any ill-conditioning preventing convergence.

(4) As the axial forces at each load level are initially only known approximately, a number of solutions (counted by *I*) are performed.

(5) The structure stiffness matrix is set up, but the member stiffness matrices used are those involving the stability functions. The functions are calculated as required using the current estimates of the axial forces.

(6) The repetition of the analysis performed at each load level should be terminated when the terms of the stiffness matrix converge to a steady state at successive cycles. The determinant (*DET2*) is used here as a convenient quantity whose value depends on the stiffness matrix terms- if its values have reach a steady state, it is also likely that the terms of the matrix have done so. The alternative is to check the convergence of the individual displacements.

(7) The repeated analysis is terminated when the proportionate change in determinant is less than 0.1%. This limit is quite arbitrary, but seems to be reasonable in practice. The final value of determinant obtained is stored in *DET3* and its sign is used as the test of positive-definiteness.

(8) When the loading approaches the critical level, the stiffness matrix becomes increasingly ill-conditioned and successive values of the determinant are found to vary widely. In this case there is no virtue in continuing with repeated analyses,

and the chart shows their termination at *I=6*. If this termination is found necessary on the first load level attempted (*N=1*) then obviously the initial loading is too near the critical level for any satisfactory analysis to be performed. In this case the analysis is stopped and must be repeated with a smaller set of loads. Otherwise the load factor can be increased, the axial forces increased by the same ratio as a good initial guess of their new values, and a further load level examined.

(9) When satisfactory convergence is achieved at any load level as described in Step 7 the value of the determinant obtained is compared with that from the previous load cycle. If no sign change is found then the load factor and axial forces are increased by one step and a new load level studied. At the first load level this comparison is impossible, and is bypassed.

(10) If a sign change is found in Step 9, i.e. a change from positive to negative, then the critical value of load factor has been passed. The load factor is then decreased to its previous value, and increased again by smaller steps. If the reduced increment is below some prescribed accuracy and great accuracy is not warranted, then the analysis is ended.

(11) Although output is shown only at this final stage it is generally desirable to trace the progress of the iterations by printing frequent intermediate results.

Appendix C

Buckling of Column Subjected to Axial Load *P*

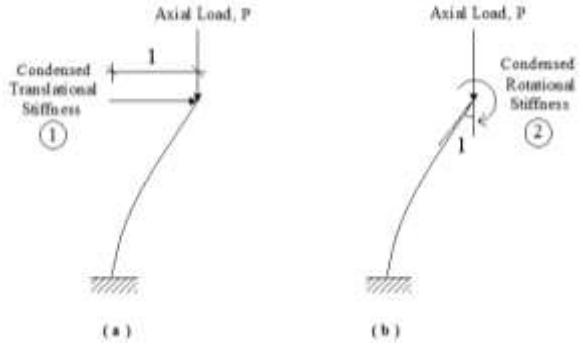

Figure C.1: The condensed translational and rotational stiffnesses

The buckling load for a column subjected to axial load *P*, Figure C.1, is obtained. With linear-deformed shape assumption, the stiffness matrix of the system is as follows:

$$[S] = \begin{bmatrix} \frac{12EI}{L^3} - \frac{P}{L} & \frac{-6EI}{L^2} \\ \frac{-6EI}{L^2} & \frac{4EI}{L} \end{bmatrix}$$

Condensation of the matrix in the translation direction with the rotation of the free joint permitted, yields:

$$S_{11}^* = S_{11} - S_{12}S_{22}^{-1}S_{21}$$

$$S_{11}^* = (\frac{12EI}{L^3} - \frac{P}{L}) - (\frac{6EI}{L^2})^2 / (\frac{4EI}{L})$$

If *P* is the critical buckling load, then, $S_{11}^* = 0$

From which the buckling load $P_{Critical} = \frac{3EI}{L^3}$

Same results can be obtained by condensation of the stiffness matrix in the rotational direction with the translation of the free joint permitted:

$$S_{22}^* = S_{22} - S_{21}S_{11}^{-1}S_{12}$$

$$S_{22}^* = (\frac{4EI}{L}) - (\frac{6EI}{L^2})^2 / (\frac{12EI}{L^3} - \frac{P}{L})$$

For $S_{22}^* = 0$, The buckling load can also be obtained as:

$$P_{Critical} = \frac{3EI}{L^3}$$

Appendix D

StaadPro Buckling Analysis, the basic solver

In StaadPro, a simple procedure has been adopted to incorporate the calculation of the Buckling Factor for any number of primary load cases. The buckling factor is the amount by which all of the loadings in a load case must be factored to cause global buckling of the structure. The procedure followed is: 1) First, the primary deflections are calculated by linear static analysis based on the provided external loading. 2) Primary deflections are used to calculate member axial forces and plate center membrane stresses. These forces and stresses are used to calculate geometric stiffness terms. Both the large delta effects and the small delta effects are calculated. These terms are the terms of the *Kg* matrix which are multiplied by the estimated *LF* (buckling factor) and then added to the global stiffness matrix *K*. For compressive cases, the *Kg* matrix is negative definite. If the buckling factor is large enough, then [[*K*]+*LF**[*Kg*]] will also be negative definite which indicates that *LF* times the applied loads is greater than the loading necessary to cause buckling. 4) STAAD starts an iterative procedure with a *LF* estimate of 1.0. If that *LF* causes buckling, then a new, lower *LF* estimate is used in the next trial. If the *LF* does not cause buckling, then a higher *LF* estimate is used. In STAAD, on the first iteration, if the determinant of the *K* matrix is positive and lower than the determinant of the *K*+*Kg* matrix, then the loads are in the wrong direction to cause buckling; and STAAD will stop the buckling calculation for that case. 5) After a few iterations, STAAD will have the largest *LF* that did not cause buckling (lower bound) and the lowest *LF* that did cause buckling (upper bound). Then each trial will use a *LF* estimate that is halfway between the current upper and lower bounds for *LF* (bisection method). 6) After the default iteration limit is reached or the user specified iteration limit, *MAXSTEPS*, is reached or when two consecutive *LF* estimates are within 0.1% of each other; then the iteration is terminated. 7) Results for this load case are based on the last lower bound *LF* calculated.

Appendix E

Buckling Analysis – the advanced Solver in STAAD package

In STAAD, a second procedure has been adopted to incorporate the calculation of the Buckling Factor for one primary load case. This procedure is an eigenvalue calculation to get buckling factors and buckling shapes.

1) First, the primary deflections are calculated by linear static analysis based on the provided external loading.

2) Primary deflections are used to calculate member axial forces and plate center membrane stresses. These forces and stresses are used to calculate geometric stiffness terms. Both the large delta effects and the small delta effects for members are calculated. These terms are the terms of the *Kg* matrix.

3) An eigenvalue problem is formed. | [*K*] - *LFi**[*Kg*] | = 0 There will be up to 4 buckling factors (*LF*) and associated buckling mode shapes calculated. *LF* less than 1.0 means that the load causes buckling; *LF* greater than 1.0 means buckling has not occurred. If *LF* is negative, then the static loads are in the opposite direction of the buckling load.

Appendix F

Column shortening calculations for reinforced and composite concrete structures (Proposed future study)

This section illustrates briefly a proposal for computing column shortening using the transformation method. The main concept of the calculations is taken from the, Reinforced Concrete Council, Spreadsheet to EC2 Axial Column Shortening to EN 1992-1: 2003

The proposed subroutine is based on the Euro Code, EC2 (prEN 1992-1: 2001) clauses 3.1.3 Elastic deformation (1) and (3) and Annex B (Creep and Shrinkage Strain). It works from the roof down and assumes that time "0" equates to construction of the lowest column. A detailed construction history is input so that time-dependent creep and shrinkage factors may be computed. The proposed program is feed by the materials and dimensional data. Then loads are calculated using the proposed program.

The following physical quantities are used in the proposed analysis:

A- Shortenings between Floors

These are the amounts by which individual column lifts may be reduced in length following construction of the floor immediately above, Figure F.1 (b).

B- Floor Displacements

These are long-term net displacements of floors from the level at which they were constructed; the particular shape of the curve being defined by effects of incremental loading and the assumption that any shortening occurring prior to a floor's construction is compensated for, Figure F.2 (a).

Any differential shortening between connected vertical members will generate a transfer of vertical load. If connecting slabs or beams are stiff and/or short, such load transfer can be substantial and in tall buildings, may even be critical at ultimate limit state.

C- Creep and shrinkage

Creep and shrinkage of the concrete depend on the ambient humidity, the dimensions of the element and the composition of the concrete. Creep is also influenced by the maturity of the concrete when the load is first applied and depends on the duration and magnitude of the loading.

Creep and Shrinkage are time-dependent properties of concrete. Their effects should generally be taken into account for the verification of serviceability limit states. The effects of shrinkage and creep should be considered at ultimate limit states only where their effects are significant, for example in the verification of ultimate limit states of stability where second order effects are of importance.

The total shrinkage strain is composed of two components, the drying shrinkage strain and the autogenous shrinkage strain. The drying shrinkage strain develops slowly, since it is a function of the migration of the water through the hardened concrete. The autogenous shrinkage strain develops during hardening of the concrete: the major part therefore develops in the early days after casting. Autogenous shrinkage is a linear function of the concrete strength. It should be considered specifically when new concrete is cast against hardened concrete.

D- Elastic deformation

The elastic deformations of concrete largely depend on its composition (especially the aggregates). The modulus of elasticity of a concrete with quartzite aggregates, are tabulated in the code and for limestone and sandstone aggregates the value should be reduced by some amount. For basalt aggregates the value should be increased by some amount. The Modulus of elasticity is also varying with time.

Column shortening using the transformation method

In this part, the steps of performing the column shortening in tall buildings are described briefly. The proposed analysis procedure can be summarized in the following steps:

1- For all loaded floors, firstly, with zero prescribed displacements, calculate the supports fixed moments with no rotations permitted.

2- Analyze the frame by distributing the moments only using the moment transformation method, with the axial deformations in the vertical members ignored, Figure F.1, Model (a). The elasticity of the members should be the time-dependant long term elasticity at the time concerned, after the required adjustments. The output results are joints rotations and supports vertical reactions.

Use the no-shear rotational stiffness and the corresponding carryover moment matrices to permit for possible lateral translations. Use the following equations:

Assuming, m = 5 vertical members:

$$[S^*] = \begin{bmatrix} S^*_{11} & S^*_{12} & S^*_{13} & S^*_{14} & S^*_{15} \\ S^*_{21} & S^*_{22} & S^*_{23} & S^*_{24} & S^*_{25} \\ S^*_{31} & S^*_{32} & S^*_{33} & S^*_{34} & S^*_{35} \\ S^*_{41} & S^*_{42} & S^*_{43} & S^*_{44} & S^*_{45} \\ S^*_{51} & S^*_{52} & S^*_{53} & S^*_{54} & S^*_{55} \end{bmatrix}$$

Where

$$D_j = -[\frac{(S+t)}{L}]_j / \sum_{k=1}^{m} [\frac{2(S+t)}{L^2}]_k$$

$$S^*_{ij} = [S]_i + [\frac{(S+t)}{L}]_i D_j \quad \text{for } i=j$$

$$S^*_{ij} = [\frac{(S+t)}{L}]_i D_j \quad \text{for } i \neq j$$

And

$$[t^*] = \begin{bmatrix} t^*_{11} & t^*_{12} & t^*_{13} & t^*_{14} & t^*_{15} \\ t^*_{21} & t^*_{22} & t^*_{23} & t^*_{24} & t^*_{25} \\ t^*_{31} & t^*_{32} & t^*_{33} & t^*_{34} & t^*_{35} \\ t^*_{41} & t^*_{42} & t^*_{43} & t^*_{44} & t^*_{45} \\ t^*_{51} & t^*_{52} & t^*_{53} & t^*_{54} & t^*_{55} \end{bmatrix}$$

Where

$$t^*_{ij} = -S^*_{ij} + (F_i)_{Dj} L$$

$(F_i)_{Dj}$: The interaction force acting on the member *i* due to displacement *Dj*

3- Use the vertical reactions obtained to calculate the time dependent displacements due to the elasticity, creep and shrinkage.

4- Deduct the displacements compensating by the construction of the floor immediately above, using Model (b), Figure F.1. The reactions are calculated by iterations or approximately using the short term Elasticity, but using the force-moment transformation method with the axial deformation in the vertical members considered (no prescribed displacements are applied in this model), use these reactions to calculate the displacements due to creep, shrinkage and elasticity.

5- Again, for all loaded floors and with the prescribed net displacements obtained from 3 and 4, calculate the supports fixed moments with no rotations permitted, the

fixed moments due to the prescribed displacements can be obtained using the matrix equation, $\{F\} = [S]\{D\}$, where $\{F\}$ is the fixed moments and forces, $[S]$ is the floor stiffness matrix and $\{D\}$ is the displacements vector which is contains two parts, one part is zero rotations and the other part is the prescribed displacements.

6- Analyze the frame by distributing the moments as in 2, using the moment transformation method, with the axial deformations in the vertical members ignored. The elasticity of the members should be the time-dependant elasticity at the time concerned, after the required adjustments. Use the no-shear rotational stiffness and the corresponding carryover moment matrices to permit for lateral translations. Obtain the resulting supports vertical reactions, using the new rotations and the prescribed displacements.

7- Repeat the procedures from 3 to 6 until a balance is reached (i.e. residual transfer is close to zero).

NOTE: transfer of loads from the floors to the columns should be damped by a constant factor.

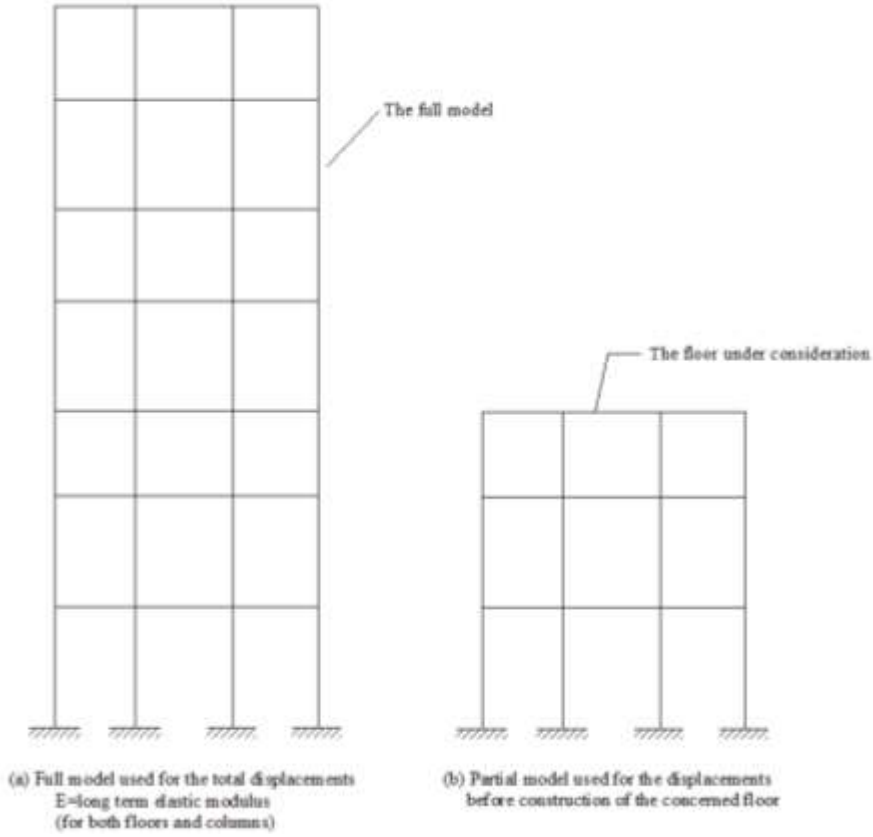

Figure F.1: The proposed analysis two models

APPENDIX G

Manual Check for the Results of the Square Building

A simple manual check for the forces resisted by the four shear walls for the hypothesis square building in Figure 5.3, was carried out, by considering a sample of one floor with the in-plane resistance of the walls considered and the out of plane ignored, and neglecting the effects of the frame action (the flexural rigidity of the floor and the columns lateral stiffnesses). As shown in Figure G.1, the external forces acting on the structure are 50 kN in the *y*-direction at 6 meter eccentricity from the center of the building, and 30 kN in the *x*-direction coincide with the center of the building.

With these assumptions, the twist moment produced from the eccentricity of the force 50 kN, is resisted equally by the four shear walls.

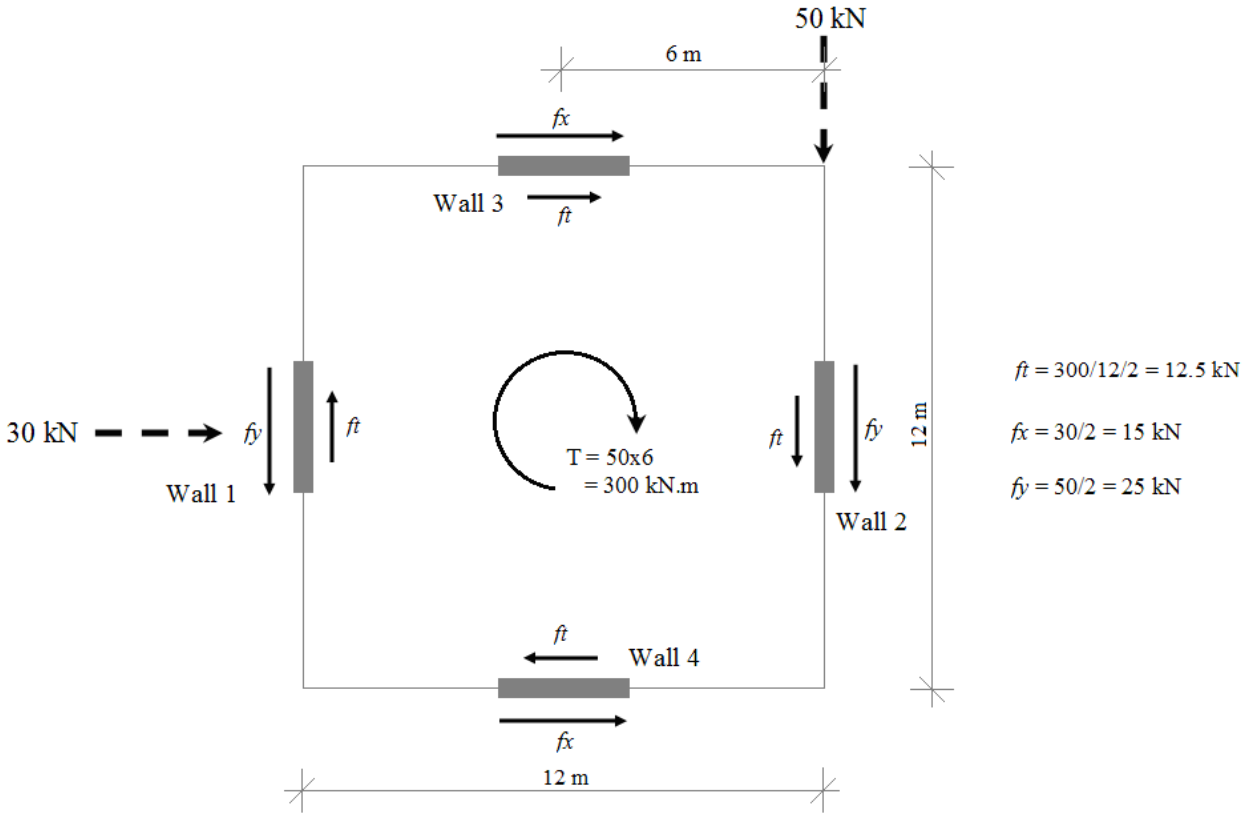

Figure G.1: Simplified sketch of the Square building

The force resisted by each shear wall can be calculated from the following relations:

$$2\,(f_t\,W) = F.e$$

or $$f_t = F.e\,/\,(2W)$$

Where

W is the width of the square building.

f_t = 50*6/(12*2) = 12.5 kN

Therefore, the forces resisted by the shear walls are calculated as follows:

Shear wall 1, $F_1 = f_y - f_t$ = 25-12.5 = 12.5 kN

Shear wall 2, $F_2 = f_y + f_t$ = 25+12.5 = 37.5 kN

Shear wall 3, $F_3 = f_x + f_t$ = 15+12.5 = 27.5 kN

Shear wall 4, $F_4 = f_x - f_t$ = 15-12.5 = 2.5 kN

The calculated forces resisted by the different shear walls show that shear wall #4 is resist very small force compared with the other walls. If considering the effects of the frame action, the force resisted by the wall will be even smaller.

The effect of the different finite elements formulation of the different packages results in small differences in the forces resisted by the different shear walls. The small difference resulted from the different packages may produce a large percentage difference in shear wall 4 due to the already small force resisted by the wall.

In other words, in all the comparisons, the differences are found to be very small for large stresses values (shear forces and bending moments in shear walls 1, 2 & 3), and the largest percentage difference is found in shear wall #4, which resists very small stresses compared with its section. The variations are noticed in the results of all packages as shown in the shear force and the bending moment diagrams of shear wall 4, Figures 5.24 and 5.25.